

---

# An Experimental and Modelling Investigation of Wet Oxidation of Municipal Biosolids

---

Arrian Khan Prince-Pike

School of Engineering  
June 2014

Supervised by:  
Associate Professor David I. Wilson  
Dr John Collins  
Dr Daniel Gapes

A thesis submitted to the Auckland University of Technology in fulfilment of the requirements for the degree of Doctor of Philosophy.

# Abstract

This thesis describes the development and validation of detailed kinetic models describing the wet oxidation of municipal biosolids.

The treatment of municipal biosolids, which are produced by wastewater treatment plants, is becoming increasingly important because current disposal methods are not sustainable. This is driving the focus for alternative treatment processes which address the unique problems that municipal biosolids present, in particular their high water content and the presence of pathogens.

Wet oxidation is particularly suited to treat municipal biosolids as it is a liquid phase process, and therefore does not require water removal prior to treatment. The high temperatures involved, above 200°C, also kill the pathogens present, and sterilise the material. While the wet oxidation process has been around for many years, and has been the focus of numerous studies, there are still relatively few models that describe the kinetic behaviour of the wet oxidation of municipal biosolids. Models that characterise the numerous intermediate and reaction end products are extremely useful for prediction and process optimisation, however most kinetic models available in the literature contain just a single intermediate compound.

An experimental programme was developed and three sets of experiments were performed to characterise the municipal biosolids produced by the Rotorua District Council wastewater treatment plant. Their behaviour under wet oxidation was quantified using standard water quality tests. Computer image analysis of the intermediate liquid samples was also performed to determine whether useful information could be obtained from the series of photographs taken of the liquid samples. This analysis showed that the normalised image intensity index that was computed for each sample closely followed the measured and modelled change in total COD.

Using the concentration results from the experimental investigation, kinetic pathways were proposed as part of a kinetic model to describe the degradation observed under wet oxidation. The developed kinetic model contained the states of the liquid and gaseous intermediate and end products that were of particular interest for this application which were soluble Chemical Oxygen Demand (sCOD), Volatile Fatty Acids (VFAs) and Dissolved Organic Nitrogen (DON). The model compounds were chosen because they represented participating chemical species which have significant influence on the economics and operability of the downstream biological



wastewater treatment process in this study. Without an accurate prediction of these chemical species, the balance of the downstream biological system can be upset. This can cause the microorganisms in the treatment plant to die off, which causes the process to turn septic and stop functioning.

Regressing the kinetic parameters from the experimental data initially produced suboptimal results since the model could not replicate the observed output in response to changes in environmental conditions. However after adding additional constraints, and a careful analysis of the solution process and kinetic pathways, this kinetic model was extended such that it could predict the key compounds of interest under different reaction conditions, as well as the prediction of oxidant consumption.

The developed kinetic model was regressed using experimental data from the lab scale wet oxidation system which used a 600ml stirred batch reactor. Then, the previously regressed model was validated with experimental data from a pilot plant wet oxidation system incorporating the substantially larger 300l bubble column reactor. The model still gave good results using the fitted parameters from the lab scale experiments. The quality of fit for both systems indicates that the kinetic model has successfully captured the reaction kinetics and the effects of important environmental conditions for this specific feed material, with an overall  $R^2$  of 0.925. This was further reinforced by a correlation and statistical analysis which confirmed that the model is statistically significant and not over-parametrised.

The detailed dynamic kinetic model from this research allows the user to establish optimal operation. The model was used to identify optimal operating conditions and showed that for a 2 hour residence time, a temperature of 230°C and 16 bar oxygen partial pressure maximised the concentration of VFAs in the reactor effluent.

# Contents

<b>1</b>	<b>Introduction</b>	<b>1</b>
1.1	The Importance of Solid Waste Management . . . . .	1
1.2	Wet Oxidation Processes . . . . .	3
1.3	The TERAX Process . . . . .	3
1.3.1	Pre-commercialisation Trials . . . . .	4
1.4	Research Objectives and the Thesis Contribution . . . . .	5
1.5	Thesis Outline . . . . .	7
<b>2</b>	<b>A Review of Wastewater Treatment and Wet Oxidation</b>	<b>8</b>
2.1	An Overview of Traditional Wastewater Treatment . . . . .	8
2.1.1	Traditional Wastewater Treatment Processes . . . . .	9
2.1.2	Rotorua District Council Wastewater Treatment Facility . . .	11
2.2	Biosolids and Wastewater Characterisation . . . . .	12
2.2.1	Rotorua Biosolids Characterisation . . . . .	15
2.3	Alternative Strategies to Deal With Biosolids . . . . .	20
2.3.1	Summary of Biosolids Disposal Methods . . . . .	23
2.4	The Wet Oxidation Process . . . . .	23
2.4.1	Process Description . . . . .	25
2.4.2	Influence of Operating Conditions . . . . .	26
2.4.2.1	Temperature and Pressure . . . . .	26
2.4.2.2	Oxidants . . . . .	28
2.4.2.3	Residence Time . . . . .	29
2.4.2.4	Pre-treatment Processes for Wet Oxidation . . . . .	29
2.4.3	The Main Reaction Mechanisms . . . . .	29
2.4.4	Wet Oxidation Reaction Products . . . . .	31
2.4.4.1	Characterisation of Off-gas Products . . . . .	32
2.4.4.2	Characterisation of Liquid Products . . . . .	32
2.4.4.3	Characterisation of Residual Solids . . . . .	32
2.4.5	Typical Process Results for Organic Wastes . . . . .	33
2.4.6	Advantages of Wet Oxidation . . . . .	34
2.5	Historical Uses of Wet Oxidation Processing . . . . .	35
2.5.1	Pulp and Paper Mill Liquor . . . . .	35

2.5.2	Petrochemical Spent Chemicals . . . . .	36
2.5.3	Municipal Biosolids . . . . .	36
2.5.4	Pure Components (Model Compounds) . . . . .	37
2.5.4.1	Glucose . . . . .	37
2.5.4.2	Acetic Acid . . . . .	38
2.5.4.3	Phenols . . . . .	38
2.5.4.4	Ethanol . . . . .	39
2.6	Modelling of Wet Oxidation . . . . .	40
2.7	Kinetic Models for Wet Oxidation . . . . .	41
2.7.1	Kinetic Summary . . . . .	46
2.8	Mass Transfer Considerations . . . . .	47
2.8.1	Summary of Mass Transfer . . . . .	49
2.9	A Review of Shortcomings in the Literature . . . . .	49
<b>3</b>	<b>Experimental Methodology and Development</b>	<b>51</b>
3.1	Prior Experimental Work at Scion . . . . .	51
3.2	Wet Oxidation Experimental Platforms . . . . .	52
3.2.1	Lab Scale Reactor . . . . .	52
3.2.1.1	Sampling and Injection System . . . . .	54
3.2.1.2	Stirrer Modifications . . . . .	57
3.2.2	The TERAX Pilot Plant Reactor . . . . .	58
3.3	Biosolids Feed and Materials . . . . .	62
3.4	Experimental Procedure . . . . .	63
3.4.1	Lab-scale Reactor . . . . .	63
3.4.2	Measuring Reactor Off-gas . . . . .	64
3.4.3	Pilot Plant Experimental Procedure . . . . .	65
3.5	Online Data Acquisition . . . . .	65
3.6	Analysis Procedure and Analytical Techniques . . . . .	66
3.6.1	Suspended Solids . . . . .	66
3.6.2	Chemical Oxygen Demand . . . . .	66
3.6.3	Volatile Fatty Acids . . . . .	67
3.6.4	Nitrogen . . . . .	68
3.6.5	Gas Composition Analysis . . . . .	68
3.7	Experimental Overview . . . . .	68
3.7.1	Liquid and Gas Sampling . . . . .	69
3.8	Modelling Overview . . . . .	70
3.9	Chapter Summary . . . . .	72
<b>4</b>	<b>A Flexible Modelling Environment</b>	<b>73</b>
4.1	Rationale for Developing a Modelling Environment . . . . .	73
4.2	A Review of Kinetic Modelling Environments . . . . .	74

4.2.1	Summary of the Modelling Environments . . . . .	76
4.3	Environment Design and Philosophy . . . . .	76
4.4	Python as a Modelling Environment . . . . .	77
4.4.1	Overview of Developed Models . . . . .	78
4.4.2	The Generic Chemical Reaction Model . . . . .	78
4.4.3	The Continuously Stirred Tank Reactor Model . . . . .	79
4.4.4	The Plug Flow Reactor Model . . . . .	81
4.4.5	An Illustrative Example Demonstrating Use of the Package . .	82
4.4.6	Validation Against Literature Examples . . . . .	83
4.4.7	Environment Use and Discussion . . . . .	85
4.5	Matlab Modelling Environment . . . . .	86
4.6	Chapter Summary . . . . .	87
<b>5</b>	<b>Modelling the Wet Oxidation Process</b>	<b>89</b>
5.1	Presentation of Results . . . . .	90
5.2	Set 1 Experiments: Characterising the Wet Oxidation of RDC Biosolids	91
5.2.1	Experimental Design Programme . . . . .	92
5.2.2	Experimental Results . . . . .	94
5.2.3	Influence of Temperature . . . . .	100
5.2.4	Influence of Oxygen Partial Pressure . . . . .	101
5.2.5	Influence of Stirrer Speed . . . . .	102
5.3	Development of a Kinetic Model . . . . .	103
5.3.1	Preliminary Model Simplifications . . . . .	108
5.3.2	Preliminary Model Results . . . . .	108
5.3.3	Set 1 Experiment Summary . . . . .	112
5.4	Second Set of Experiments . . . . .	114
5.4.1	Possible Reasons for Discrepancies . . . . .	119
5.4.2	Reaction Extent Using Image Analysis . . . . .	121
5.4.3	Stirrer Current Investigation . . . . .	124
5.5	Third Set of Experiments . . . . .	128
5.6	Incorporating Extensions to the Dynamic Kinetic Model . . . . .	134
5.6.1	Model Assumptions and Simplifications . . . . .	136
5.6.2	Extended Kinetic Model Summary . . . . .	137
5.6.3	The Matlab Model Structure . . . . .	141
5.6.4	Model Regression . . . . .	144
5.6.5	A Comparison with Published Kinetic Parameters . . . . .	145
5.7	Chapter Summary . . . . .	148
<b>6</b>	<b>Model Results and Pilot Plant Validation</b>	<b>149</b>
6.1	Kinetic Model Results . . . . .	149
6.2	Effect of Operating Conditions on the Model Results . . . . .	156

6.3	A Statistical Analysis of the Extended Kinetic Model . . . . .	160
6.3.1	A Correlation Analysis of the Model . . . . .	160
6.3.2	An Analysis of Variance of the Proposed Model . . . . .	162
6.3.3	Comparison with Published Kinetic Models . . . . .	166
6.4	Validation against the TERAX Pilot Plant . . . . .	168
6.4.1	Pilot Plant Batch Experiment 1 . . . . .	170
6.4.2	Pilot Plant Batch Experiment 2 . . . . .	171
6.5	Summary of the Model Results . . . . .	173
6.5.1	Exploiting the Developed Model . . . . .	174
6.5.2	Establishing an Optimum Operating Point . . . . .	175
6.6	Chapter Summary . . . . .	177
<b>7</b>	<b>Conclusions and Recommendations for Future Work</b>	<b>178</b>
7.1	Key Achievements . . . . .	178
7.1.1	Kinetic Model Development and Regression . . . . .	179
7.1.2	Pilot Plant Validation . . . . .	179
7.1.3	Characterisation of RDC Municipal Biosolids . . . . .	179
7.1.4	Exploiting the Kinetic Model . . . . .	180
7.1.5	Image Analysis of Intermediate Samples . . . . .	180
7.1.6	Analysis of Stirrer Power Measurements . . . . .	181
7.2	Review of Research Objectives . . . . .	181
7.3	Recommendations for Future Work . . . . .	182
	<b>Bibliography</b>	<b>184</b>
	<b>A Appendix CD Contents</b>	<b>194</b>
	<b>B Experimental Results</b>	<b>195</b>
	<b>C Model Results</b>	<b>205</b>

# List of Figures

1.1	A diagram of the TERAX process. . . . .	3
1.2	The TERAX pilot plant situated at the Rotorua Wastewater Treatment facility. . . . .	5
2.1	Schematic diagram of a typical activated sludge wastewater treatment process. . . . .	10
2.2	An aerial photograph of the RDC wastewater treatment plant . . . .	12
2.3	A diagram of the RDC 5 Stage modified Bardenpho wastewater treatment plant . . . . .	12
2.4	A sample of biosolids from the RDC wastewater treatment plant. . .	16
2.5	Total solids (TSS) content of weekly composite samples over several months. . . . .	19
2.6	Volatile solids (VSS) content . . . . .	19
2.7	Schematic diagram of a typical wet oxidation process . . . . .	25
2.8	A summary of the key factors affecting wet oxidation. . . . .	26
2.9	Preliminary experiments conducted by Scion on the effect of temperature on TSS concentration during wet oxidation . . . . .	27
2.10	Effect of increasing temperature during wet oxidation with a two hour residence time . . . . .	28
2.11	Photograph of samples of suspended biosolids before and after wet oxidation . . . . .	33
2.12	One of the first lumped kinetic models for wet oxidation . . . . .	41
2.13	The widely cited ‘Triangular’ kinetic model . . . . .	42
2.14	Reaction scheme of a model with additional intermediate compounds	43
2.15	Kinetic pathways for wet oxidation proposed by Chacuk <i>et al.</i> . . . .	44
2.16	The gas-liquid mixing scheme as part of the stagewise-backmixing model . . . . .	48
3.1	Schematic diagram of the lab scale wet oxidation system at Scion which was used in the experimental investigation. . . . .	52
3.2	The 4540 Parr reactor and 4848 controller . . . . .	53
3.3	Stirrer, cooling coil and dip tube inside the Parr reactor, with the reactor vessel removed. . . . .	54

3.4	The Parr reactor stirrer . . . . .	55
3.5	The Parr reactor with the added sampling and injection system. . . . .	55
3.6	A close-up of the liquid sampling and flushing system. . . . .	57
3.7	Parr reactor with the replacement stirrer motor fitted. . . . .	58
3.8	A schematic diagram of the TERAX wet oxidation pilot plant bubble column reactor and recirculation systems. (The second reactor is not shown in this figure). . . . .	59
3.9	The TERAX wet oxidation pilot plant feed tank and high pressure feed pump. The feed pump is to the right of the feed tank. . . . .	60
3.10	The main bubble column reactor with the liquid recirculation pump in the foreground. . . . .	60
3.11	The secondary bubble column reactor and discharge tank. . . . .	60
3.12	Reactor off-gas analysis equipment used in this study . . . . .	64
4.1	Schematic diagram of the CSTR model for the reaction of a single compound, $C_A$ . . . . .	79
4.2	Schematic diagram of the PFR model. . . . .	82
4.3	The reactor internal temperature in response to a $\pm 5K$ change in coolant temperature. . . . .	85
4.4	The change in concentration in response to a $\pm 5K$ change in coolant temperature . . . . .	85
4.5	The kinetic model adapted from Li <i>et al.</i> at different temperatures developed in the Python modelling environment. . . . .	86
5.1	Central composite design used for the Set 1 experiments. . . . .	92
5.2	Total COD during the experiment under different reaction conditions . . . . .	95
5.3	The percentage of total COD degradation under different reaction conditions . . . . .	95
5.4	The change in particulate COD during the experiment under different reaction conditions. . . . .	96
5.5	The change in soluble COD during the experiment under different reaction conditions. . . . .	97
5.6	The change in acetic acid COD during the experiment under different reaction conditions. . . . .	98
5.7	The change in VFACOD during the experiment under different reaction conditions. . . . .	98
5.8	The change in DON during the experiment under different reaction conditions. . . . .	99
5.9	Liquid samples taken during a wet oxidation experiment clearly showing the solids reduction achieved over the duration of the 60 minute experiment. . . . .	99

5.10	The influence of temperature increase from 220 to 240°C with a constant O <sub>2</sub> partial pressure and stirring speed. Data from experiments 1 and 2 listed in Table ??.	100
5.11	The influence of oxygen partial pressure on degradation when increased from 20 to 40 bar. Temperature and stirring speed remained constant. Data from experiments 2 and 4.	101
5.12	The influence of increasing stirrer speed from 300 to 500 RPM on the degradation achieved at a constant temperature and O <sub>2</sub> partial pressure. Data from experiments 1 and 5.	102
5.13	The concentration of pCOD from the preliminary kinetic model versus experimental data.	109
5.14	The concentration of sCOD from the preliminary kinetic model versus experimental data.	109
5.15	The concentration of AACOD from the preliminary kinetic model versus experimental data.	110
5.16	The concentration of VFACOD from the preliminary kinetic model versus experimental data.	110
5.17	The concentration of DON from the preliminary kinetic model versus experimental data.	111
5.18	A comparison of the actual measured data compared to the model predictions. (See also Fig. 6.13.)	112
5.19	An illustration of the magnitude of the fast and slow components that make up pCOD in the kinetic model.	113
5.20	Photograph showing the reflux condenser installed on the gas outlet of the Parr reactor and the location of the off-gas sampling line.	115
5.21	Photographs of the the liquid samples taken during the course of the experiment varying the temperature from 180 to 220°C at a constant O <sub>2</sub> partial pressure of 40 bar.	117
5.22	Photographs of the the liquid samples taken during the course of the experiment varying O <sub>2</sub> partial pressure from 16 to 40 bar at 220°C.	118
5.23	Dissolved gasses in the reactor effluent after de-pressurisation at the completion of the experiment	120
5.24	Image analysis of the liquid samples varying O <sub>2</sub> partial pressure from 16 to 40 bar at 220°C and a constant stirring speed of 400 RPM.	122
5.25	Varying the temperature from 180 to 220°C at a constant O <sub>2</sub> partial pressure and stirring speed of 400 RPM.	123
5.26	Stirrer current and viscosity during the warmup phase. The solid dark blue trace is the filtered current measurement.	125
5.27	Log of viscosity versus the normalised stirrer power during the warmup phase.	126



5.28	Stirrer current and environmental conditions from warmup to the completion of an experiment. The solid dark blue trace is the filtered current measurement. . . . .	127
5.29	Gas composition analysis of the off-gas samples performed as part of the Set 3 experiments. The labels on the right axis correspond to the experiment conditions described in Table ?? . . . . .	130
5.30	Lab scale Parr reactor with the pressure measurement system highlighted. . . . .	133
5.31	Gas port for pressure gauge plugged with biosolids material. . . . .	134
5.32	Diagram of the extended kinetic model showing the states, inputs, outputs and parameters. . . . .	138
5.33	Diagram of the extended kinetic model operation including inputs and calculation steps. . . . .	142
6.1	The concentration of total COD from the extended kinetic model in Section ?? versus experimental data from the lab scale wet oxidation system. . . . .	150
6.2	The fraction of total COD remaining, computed from the extended kinetic model in Section ?? versus experimental data from the lab scale wet oxidation system. . . . .	151
6.3	The particulate COD concentration from the extended kinetic model versus experimental data from the lab scale wet oxidation system. . .	151
6.4	The soluble COD concentration from the extended kinetic model versus experimental data from the lab scale wet oxidation system. . . . .	152
6.5	The acetic acid COD concentration from the extended kinetic model versus experimental data from the lab scale wet oxidation system. . .	153
6.6	The VFACOD concentration from the extended kinetic model versus experimental data from the lab scale wet oxidation system. . . . .	153
6.7	The DON concentration from the extended kinetic model versus experimental data from the lab scale wet oxidation system. . . . .	154
6.8	The mass of O <sub>2</sub> remaining in the reactor from the extended kinetic model versus experimental data from the lab scale wet oxidation system.	155
6.9	The mass of CO <sub>2</sub> remaining in the reactor from the extended kinetic model versus experimental data from the lab scale wet oxidation system.	155
6.10	The extended kinetic model output versus the response from the experimental data to an increase in temperature from 220°C to 240°C. The points represent experimental data, while the solid line is the model response. . . . .	157

6.11	The extended kinetic model output versus the response from the experimental data to increasing the oxygen partial pressure from 20 bar to 40 bar. The points represent experimental data, while the solid line is the model response. . . . .	158
6.12	The extended kinetic model output versus the response from the experimental data to an increase in stirrer speed from 300 to 500 RPM. The points represent experimental data, while the solid line is the model response. . . . .	159
6.13	The correlation between model predictions and experimental data . .	161
6.14	The correlation between model and experiment for the individual components from experimental Set 1.(See also Fig. 6.13.) . . . . .	162
6.15	The tCOD prediction from the Li <i>et al.</i> kinetic model versus the extended kinetic model response from this work, and compared with experimental data. . . . .	167
6.16	The AACOD prediction from the Li <i>et al.</i> kinetic model versus the extended kinetic model response from this work, and compared with experimental data. . . . .	167
6.17	The extended kinetic model compared with the first semi-batch pilot plant experiment at 240°C. . . . .	171
6.18	The extended kinetic model compared with the second semi-batch pilot plant experiment at 220°C. . . . .	172
6.19	Results from the extended kinetic model showing the effect of increasing temperature from 220 to 260°C on the concentration of the main components of interest. . . . .	174
6.20	Results from the extended kinetic model showing the effect of increasing the oxygen partial pressure from 20 to 60 bar on the concentration of the main components of interest. . . . .	175
6.21	The concentration of acetic acid, VFA and the combination as predicted from the model at different reaction times, temperatures and pressures. Contour lines show the concentration on a mg/l COD basis.	176
B.1	Experimental results for the compounds of interest from the Set 1 experiments for Run 1. . . . .	195
B.2	Experimental results for the compounds of interest from the Set 1 experiments for Run 2. . . . .	196
B.3	Experimental results for the compounds of interest from the Set 1 experiments for Run 3. . . . .	196
B.4	Experimental results for the compounds of interest from the Set 1 experiments for Run 4. . . . .	197
B.5	Experimental results for the compounds of interest from the Set 1 experiments for Run 5. . . . .	197

B.6	Experimental results for the compounds of interest from the Set 1 experiments for Run 6. . . . .	198
B.7	Experimental results for the compounds of interest from the Set 1 experiments for Run 7. . . . .	198
B.8	Experimental results for the compounds of interest from the Set 1 experiments for Run 8. . . . .	199
B.9	Experimental results for the compounds of interest from the Set 1 experiments for Run 9. . . . .	199
B.10	Experimental results for the compounds of interest from the Set 1 experiments for Run 10. . . . .	200
B.11	Experimental results for the compounds of interest from the Set 1 experiments for Run 11. . . . .	200
B.12	Experimental results for the compounds of interest from the Set 1 experiments for Run 12. . . . .	201
B.13	Experimental results for the compounds of interest from the Set 1 experiments for Run 13. . . . .	201
B.14	Experimental results for the compounds of interest from the Set 1 experiments for Run 14. . . . .	202
B.15	Experimental results for the compounds of interest from the Set 1 experiments for Run 15. . . . .	202
B.16	Experimental results for the compounds of interest from the Set 1 experiments for Run 16. . . . .	203
B.17	Experimental results for the compounds of interest from the Set 1 experiments for Run 17. . . . .	203
B.18	Experimental results for the compounds of interest from the Set 1 experiments for Run 18. . . . .	204
B.19	Experimental results for the compounds of interest from the average of experiment Runs 15 to 18. . . . .	204
C.1	The extended kinetic model results compared with the experimental results for Run 1. . . . .	205
C.2	The extended kinetic model results compared with the experimental results for Run 2. . . . .	206
C.3	The extended kinetic model results compared with the experimental results for Run 3. . . . .	206
C.4	The extended kinetic model results compared with the experimental results for Run 4. . . . .	207
C.5	The extended kinetic model results compared with the experimental results for Run 5. . . . .	207
C.6	The extended kinetic model results compared with the experimental results for Run 6. . . . .	208

C.7	The extended kinetic model results compared with the experimental results for Run 7. . . . .	208
C.8	The extended kinetic model results compared with the experimental results for Run 8. . . . .	209
C.9	The extended kinetic model results compared with the experimental results for Run 9. . . . .	209
C.10	The extended kinetic model results compared with the experimental results for Run 10. . . . .	210
C.11	The extended kinetic model results compared with the experimental results for Run 11. . . . .	210
C.12	The extended kinetic model results compared with the experimental results for Run 12. . . . .	211
C.13	The extended kinetic model results compared with the experimental results for Run 13. . . . .	211
C.14	The extended kinetic model results compared with the experimental results for Run 14. . . . .	212
C.15	The extended kinetic model results compared with the experimental results for Run 15. . . . .	212
C.16	The extended kinetic model results compared with the experimental results for Run 16. . . . .	213
C.17	The extended kinetic model results compared with the experimental results for Run 17. . . . .	213
C.18	The extended kinetic model results compared with the experimental results for Run 18. . . . .	214
C.19	The extended kinetic model results compared with the average of Runs 15 to 18. . . . .	214

# List of Tables

1.1	Current biosolids disposal options in New Zealand and Europe . . . .	2
2.1	Constituents present in municipal wastewater . . . . .	9
2.2	Allowable heavy metal limits for biosolids in New Zealand . . . . .	15
2.3	Wastewater quality metrics used in this study. . . . .	15
2.4	Solids characterisation of the RDC biosolids, with validation from a third party laboratory. . . . .	16
2.5	COD characterisation and measured limits of the RDC biosolids. . . .	16
2.6	Elemental composition of RDC biosolids. All concentrations expressed as % of dry weight. . . . .	17
2.7	Nitrogen analysis across liquid and solid phases. . . . .	18
2.8	Heavy metals present in RDC biosolids. . . . .	18
2.9	Operating conditions in use for wet oxidation systems. . . . .	27
2.10	Typical wet oxidation conversion results for organic wastes reported in the literature. . . . .	34
2.11	Reaction conditions for the wet oxidation of glucose . . . . .	37
2.12	Reaction conditions for the wet oxidation of acetic acid . . . . .	38
2.13	Reaction conditions for the wet oxidation of 4-chlorophenol . . . . .	39
2.14	Reaction conditions for the wet oxidation of ethanol . . . . .	40
2.15	Summary of published wet oxidation kinetic models. . . . .	46
3.1	Characteristics of the municipal biosolids from the RDC wastewater treatment plant used for the experimental investigation. . . . .	62
3.2	System parameters recorded by the data acquisition system ( $\Delta t = 10\text{s}$ )	66
3.3	The range of reaction conditions explored as part of the experimental investigation in this study. . . . .	69
4.1	Summary of the reviewed modelling environments. . . . .	75
4.2	Operating Conditions of the CSTR example . . . . .	84
5.1	The colours used for the following figures given in this and later chapters.	91
5.2	Experimental reaction conditions that were investigated as part of the Set 1 experiments. . . . .	93
5.3	The parameters measured from the analytical analysis. . . . .	93

5.4	Calculated parameters from measured data. . . . .	94
5.5	The measured and derived state variables used in the kinetic model. .	103
5.6	The COD conversion ratio for different measured volatile fatty acids .	104
5.7	Experimental conditions investigated in the Set 2 experiments. . . . .	114
5.8	Results from the Set 2 experiment samples. . . . .	116
5.9	Set 3 experimental conditions. . . . .	128
5.10	A summary of the measured and derived state variables in the ex- tended model. . . . .	135
5.11	Fitted kinetic parameters for the extended model. (See also Table 6.1.)	146
5.12	Fitted component reactivity fractions. . . . .	146
5.13	Overall rate constants using the regressed kinetic parameters from the extended kinetic model for conditions 220°C, 20 bar oxygen partial pressure and 300 RPM stirring speed. . . . .	148
6.1	The fitted model parameters, their associated 95% confidence limits and statistical metrics. . . . .	164
6.2	Overall model fit. . . . .	165
6.3	Nonlinear least-squares analysis of variance. . . . .	166
6.4	Semi-batch pilot plant experimental conditions for the pilot plant experiments. . . . .	170
A.1	Software included on the Appendix CD. . . . .	194

# List of Abbreviations

AACOD	Acetic Acid COD
ANOVA	Analysis of Variance
BNR	Biological Nutrient Removal
COD	Chemical Oxygen Demand
CRI	Crown Research Institute
CSTR	Continuously Stirred Tank Reactor
DKN	Dissolved Kjehldahl Nitrogen
DOC	Dissolved Organic Carbon
DON	Dissolved Organic Nitrogen
GC	Gas Chromatograph
nr	Non-reactive
NZ	New Zealand
pCOD	Particulate Chemical Oxygen Demand
PFR	Plug Flow Reactor
PID	Proportional-Integral-Derivative controller
RDC	Rotorua District Council
RMSE	Root Mean Square Error
sCOD	Soluble Chemical Oxygen Demand
SSE	Sum of Squared Errors
tDS	Tonnes of Dry Solids
TKN	Total Kjehldahl Nitrogen
TOC	Total Organic Carbon
TSS	Total Suspended Solids
VFA	Volatile Fatty Acids
VFACOD	Volatile Fatty Acid COD
VSS	Volatile Suspended Solids
WO	Wet Oxidation

# List of Symbols

Symbol	Description	Units
$\alpha$	Confidence limit	–
$C_A$	Initial $C_A$ concentration	$\text{mol}\cdot\text{l}^{-1}$
$C_{Af}$	Feed concentration	$\text{mol}\cdot\text{l}^{-1}$
$c$	Mixing constant	–
$C_p$	Feed heat capacity	$\text{J}\cdot\text{g}^{-1}\cdot\text{K}^{-1}$
$\Delta H$	Heat of reaction	$\text{J}\cdot\text{mol}^{-1}$
eps	Numerical machine precision, $\text{eps}(1)\approx 2.2 \cdot 10^{-16}$	–
$E_a$	Activation energy	J
GasVolume	Reactor headspace volume	ml or l
$k$	Reaction rate constant	variable
$k_0$	Pre-exponential factor	$\text{s}^{-1} \text{ min}^{-1}$
$k_H$	Henry’s constant	$\text{mol}\cdot\text{kg}^{-1}\cdot\text{bar}^{-1}$
$m$	Reaction order with respect to reactant	–
	Number of observations (§6.3.2)	–
$N$	Stirrer speed	RPM
$n$	Reaction order with respect to oxidant	–
	Number of model parameters (§6.3.2)	–
<b><math>P</math></b>	Covariance matrix	–
$p$	Pressure	bar
$q$	Flow rate of material	$\text{l}\cdot\text{min}^{-1}$
$R$	Universal gas constant	$\text{J}\cdot\text{mol}^{-1} \cdot \text{K}^{-1}$
ReactorVolume	Total reactor volume	ml or l
$\rho$	Feed density	$\text{g}\cdot\text{l}^{-1}$
$s$	Measurement noise estimate	variable



Symbol	Description	Units
$T$	Temperature	K
$T_c$	Coolant temperature	K
$T_f$	Feed temperature	K
$t$	Time	min or s
$\theta$	Model parameters	–
$UA$	HTC times heat transfer area	$\text{J}\cdot\text{min}^{-1}\cdot\text{K}^{-1}$
$V$	Volume	ml or l
$\nu$	Degrees of freedom	–
$X$	Jacobian matrix	–

# Attestation of Authorship

I hereby declare that this submission is my own work and that, to the best of my knowledge and belief, it contains no material previously published or written by another person (except where explicitly defined in the acknowledgements), nor material which to a substantial extent has been submitted for the award of any other degree or diploma of a university or other institution of higher learning.

Arrian Prince-Pike

# Chapter 1

## Introduction

### 1.1 The Importance of Solid Waste Management

Sustainable waste management is increasingly important for economic and environmental reasons. Wastewater is the largest waste product by volume in New Zealand, with approximately 1.5 billion litres of domestic wastewater discharged into the environment daily [1]. In New Zealand, the Waste Minimisation Act was introduced in 2008 to encourage waste minimisation and reduce waste disposal, with a levy of \$10 per tonne introduced on all waste going to landfill [2].

Wastewater treatment plants produce large amounts of organic solids, often referred to as sewage sludge or municipal biosolids. A large percentage of municipal biosolids that are generated by wastewater treatment plants end up in landfills. These organic solid wastes are of particular concern for landfills for a number of reasons. The high moisture content of biosolids makes transportation costs high and increases the likelihood that leachates from these wastes, such as heavy metals and nitrates, can enter and contaminate waterways. Under landfill conditions organic solid wastes typically generate large amounts of methane, which is a greenhouse gas and very difficult to recover in a landfill. Organic wastes such as municipal biosolids are a health risk as they contain harmful pathogens [3].

Despite legislative and economic pressure, most municipal solid wastes in New Zealand end up in landfills. Alternative methods for dealing with solid wastes have so far only been partly successful for a variety of reasons [4–6]. Thermal treatments such as drying and incineration often have poor energy balances, since removing water is expensive and energy intensive. Another reason is the lack of markets for the products resulting from biosolids, such as compost, because of the volumes produced and perceived health hazards. Other methods can have their own particular drawbacks: For example windrow composting can be problematic because of

odour generation, while the characteristics of the biosolids can prevent redirection for alternative uses if the concentration of heavy metals is too high.

Unlike New Zealand, many countries in Europe have alternative methods of dealing with municipal biosolids without resorting to landfill. Table 1.1 illustrates the common disposal options for biosolids in New Zealand and a number of European countries. New Zealand has a comparatively high percentage of landfilling compared to most European countries, where alternative disposal techniques are rapidly developing.

Scion is a New Zealand Crown Research Institute (CRI) that specialises in research, science and technology development. It is primarily focused on the areas of forestry, wood products including wood derived materials, biotechnology, and other environmental technologies [7]. Scion has extensive knowledge in innovative wastewater treatment processing and value recovery which has been developed in response to the increasing challenges of sustainable waste management.

To address these challenges, Scion [8] has partnered with the Rotorua District Council to investigate the feasibility of the wet oxidation process as part of a novel alternative treatment technology to reduce the volume of municipal biosolids going to landfill [4, 9].

Table 1.1: Current biosolids disposal options in New Zealand and Europe, [10].

Country	Landfill (%)	Agriculture (%)	Composting (%)	Thermal Treatment (%)	Other (%)
New Zealand	78	17	0	0	5
European Union	18	45	7	23	7
Germany	6	32	0	37	25
Austria	0	15	50	35	0
Bulgaria	100	0	0	0	0
The Netherlands	0	0	15	85	0
Norway	7	65	0	0	28
Slovenia	30	7	15	47	1
UK	1.5	67	5	19.5	7

The effectiveness of wet oxidation as a treatment process is well known. It is capable of delivering over an 80% reduction in solids volume [11] and oxygen depletion potential [12], often characterised as Chemical Oxygen Demand (COD). Depending on the operating conditions, it enables recovery of useful chemicals from the effluent (such as acetic acid, ammonia and phosphate) which can be used for other applications, such as a feed source for biological processes.

## 1.2 Wet Oxidation Processes

Wet oxidation is a treatment process that is used for treating aqueous wastes. The process involves the oxidation of suspended or dissolved organic compounds in liquid water at elevated temperatures and pressures, using an oxidising agent such as gaseous oxygen. A defining feature of this process is that the reactions only occur in liquid water. Therefore the environmental conditions used must be sufficient to prevent the water boiling. The temperatures used are above the normal boiling point of water, and are typically between 180 to 300°C with the system pressure maintained above the vapour pressure of water at the desired operating temperature. In general, the higher the temperature, the greater the level of oxidation, but corrosion of the reactor vessel can become a problem at temperatures over 300°C [13].

The process has been in use commercially since the 1950's and has been proven to be an effective technology for treating aqueous, non-biodegradable wastes. A review of the process is given in Section 2.4.

## 1.3 The TERAX Process

The TERAX process is a novel organic waste treatment process developed by Scion for treating wet organic solid wastes while delivering maximum volume reduction and value recovery [14]. The TERAX process is a combined biological and thermo-chemical approach to maximise efficiency, effectiveness and the economics of organic solid waste processing and is represented in Fig. 1.1. This process incorporates wet oxidation as part of the treatment process and is specific to this study.

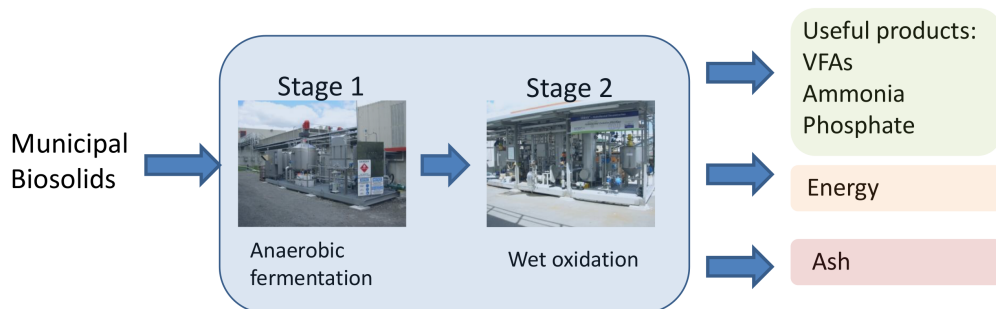


Figure 1.1: A diagram of the TERAX process.

The first stage of the TERAX process uses anaerobic fermentation, which is a biological process to pre-treat incoming organic material. The fermentation process breaks down the organic material, which improves the handling properties and al-

allows easier pumping, a partial reduction in volume and enables energy recovery in the form of methane gas.

The second stage uses wet oxidation to chemically decompose compounds into simple carboxylic acids, while nitrogen and phosphorus containing compounds are converted primarily into ammonia and phosphate. This stage also achieves considerable solids reduction. If the solids concentration is high enough (around 6%) the process is auto-thermal and generates excess heat which can be recovered and used to heat the fermenter, which is the first stage of the TERAX process. The carboxylic or volatile fatty acids produced can be used as a carbon source for Biological Nutrient Removal (BNR) processes, while the ammonia and phosphate can be used as fertilisers.

This thesis is focused solely on the second stage which uses wet oxidation.

### **1.3.1 Pre-commercialisation Trials**

In 2009 Scion conducted trials of the wet oxidation process using fermented biosolids from the Rotorua wastewater treatment plant in a lab-scale reactor. The preliminary results showed that the dual stage process increased the value recovery and waste treatment and was more effective than either stage on its own. In summary, the key results were:

- A 90% reduction in solids
- High conversion of solids to a volatile fatty acid rich carbon source
- Around 75% conversion of total nitrogen to ammonia
- Phosphate concentrated in the residual solids phase (38% by weight)

Based on the encouraging lab scale results, Scion, in conjunction with the Rotorua District Council (RDC), constructed a pilot scale TERAX treatment plant which was completed in mid 2011. Fig. 1.2a and Fig. 1.2b show the fermentation and wet oxidation pilot plants.

During 2012, further experiments were conducted using the TERAX pilot plant which validated the results obtained from the lab scale reactor. The fermentation stage was able to achieve between 20 and 30% solids reduction and produced sufficient amounts of fatty acids that were amenable to wet oxidation. The secondary wet oxidation stage achieved over 90% solids destruction and nutrient conversion targets were achieved.

Based on the results obtained from the pilot and lab scale plants, a full scale production plant is currently being designed to treat all of the municipal biosolids produced



(a) TERAX stage 1: 2000L anaerobic fermentation unit



(b) TERAX stage 2: Wet oxidation unit with two 300L reactors

Figure 1.2: The TERAX pilot plant situated at the Rotorua Wastewater Treatment facility.

by the RDC wastewater treatment plant. Despite the fact that the pilot plant met or exceeded the desired treatment objectives, a number of operating issues were identified:

- Poor oxygen control
- Mass transfer limitations due to poor mixing
- Considerable dead time in the off-gas measurements

The consequences of this were incomplete oxidation of the feed material, producing by-products that were not as amenable to biological treatment, and large amounts of CO. For these reasons it was decided that a systematic approach was required to formally characterise the feed material as well as a detailed kinetic model of the wet oxidation stage to better control and optimise the plant operation.

## 1.4 Research Objectives and the Thesis Contribution

The survey of the literature related to wet oxidation in Chapter 2 shows that wet oxidation can be used successfully to treat municipal biosolids, with a variety of outcomes depending on the reaction conditions. In addition, Scion have conducted studies on a variety of different wastes, including municipal biosolids, to verify its effectiveness using the lab scale reactor and pilot scale wet oxidation facility.

Continuous wet oxidation of municipal biosolids presents a number of challenges. The biosolids feed composition can change from day to day depending on factors such as industry operations, or the amount of rainfall. Based on the composition of the day, certain minimum levels of destruction are required, while simultaneously

maximising the production of desired intermediate products such as VFAs and ammonia, and minimising the production of undesirable reaction end products such as CO.

Despite research in specific fields of wet oxidation, such as reactants, catalysis, reaction conditions and control, a suitable lumped model is not available that can predict key quality indicators required for this project. This means that one cannot efficiently predict performance of the wet oxidation plant and the concentrations of key components, and therefore it is not possible to design an optimal wet oxidation plant.

What has not been investigated is taking a holistic view of the wet oxidation process and amalgamating different modelling strategies. In order to complete the modelling objectives of this research, several key issues need to be addressed. The first is how to define the feed composition for the reactor model, as biosolids are not a component in common chemical process simulators. The second key issue is to characterise and define the likely, or dominant, reaction pathways that are occurring. The third issue is to investigate mass transfer effects, however this has not been investigated and is left as future work.

The overarching objective of this thesis is to characterise, and develop a suitably detailed model of the wet oxidation process that assists the optimal design of experiments, which will then allow the design of an optimal wet oxidation plant. This requires the following key objectives to be met:

1. To investigate the characteristics of biosolids produced by the RDC wastewater treatment plant and their behaviour under wet oxidation.
2. To formulate and validate a kinetic model of the wet oxidation process in order to predict operation and enable optimal bench-scale experimental design.
3. To build sufficiently flexible models to enable the scale up to the design of a full-scale production plant.
4. To show that the developed models can be used as a design aid for future wet oxidation plants.

To achieve these objectives, the author has postulated kinetic models to best fit the phenomena observed from the experimental programme. These models were then regressed to best fit the experimental data. A statistical analysis of the models was then performed to investigate the validity of the model, and finally the usefulness from a design and operation perspective was shown.



## 1.5 Thesis Outline

This thesis is organised as follows: A review of the biosolids disposal problem and the key strategies of wet oxidation is given in Chapter 2. Based on this, an experimental programme, described in Chapter 3, is designed to systematically characterise the behaviour of the RDC biosolids under wet oxidation. Using the experimental data and observations, a model is proposed in Chapter 4 which would provide useful information to address the points given in Section 1.4 above. To regress the key parameters in this model, an experimental computer program is developed in Chapter 4. The model validation and results are given in Chapters 5 and 6. Finally Chapter 7 revisits the key research questions posed in Section 1.4 and discusses future research opportunities.

## Chapter 2

# A Review of Wastewater Treatment and Wet Oxidation

This chapter provides a review of traditional wastewater treatment processes in use, with a focus on the different solid wastes produced by wastewater treatment plants discussed in Sections 2.1 and 2.1.1, and with information specific to the RDC wastewater treatment facility given in Section 2.1.2. Methods and metrics used to characterise wastewater and the treatment process, as well as an overview of the biosolids produced by the RDC wastewater treatment plant are described in Section 2.2. Alternative strategies to deal with biosolids are examined in Section 2.3. A detailed description of the wet oxidation process is given in Section 2.4, and historical uses of the process are reviewed in Section 2.5. Section 2.6 reviews the modelling of the wet oxidation process, and examines the models developed to model the reaction kinetics and mass transfer in Section 2.7 and Section 2.8 respectively. Lastly, Section 2.9 reviews the shortcomings in the literature and thereby justifies this research programme.

### 2.1 An Overview of Traditional Wastewater Treatment

A common definition of wastewater is that it is any water which has been contaminated with undesirable contaminants, typically as the result of human activities [15]. Wastewater can be divided into municipal wastewater from homes, also known as sewage, and industrial wastewater, such as paper pulp mill liquor.

Although the terms sewage and wastewater are often interchanged, sewage refers to wastewater contaminated with human waste. Municipal sewage is water-carried

organic waste, typically containing suspended particles, fibrous materials and dissolved substances such as detergents. The quantity and characteristics of the sewage depend on many factors such as the amount and type of industries present in the area which are connected to the sewage system. This thesis is primarily concerned with municipal biosolids, and wastewater to a lesser degree. It is not concerned with chemical or other industrial wastewater.

The typical constituents of municipal wastewater can be divided into the categories described in Table 2.1. The concentration of the constituents can vary considerably depending on both physical factors, such as the infrastructure connected to the treatment plant, as well as on environmental factors such as the level of rainfall in the area.

Table 2.1: Constituents present in municipal wastewater, table adapted from [3].

<i>Constituent</i>	<i>Contaminants</i>	<i>Environmental Impact</i>
Micro-organisms	Pathogenic bacteria, viruses, protozoa, worms	Risk when swimming
Bio-degradable organic materials	Oxygen depletion	Algal blooms, death of aquatic life
Other organic materials	Detergents, fats and oils, solvents	Toxic effects, bio-accumulation
Nutrients	Nitrogen, phosphorus, ammonium	Eutrophication, toxic effects
Metals	Mercury, lead, cadmium, chromium, copper, nickel	Bio-accumulation, toxic effects
Other inorganic materials	Acids eg $H_2S$	Corrosion, toxic effects
Odour	$H_2S$	Toxic effects

### 2.1.1 Traditional Wastewater Treatment Processes

A number of treatment processes are available to remove or reduce the contaminants present in wastewater. Generally the treatment process produces a large flow of treated water and a smaller flow containing the impurities and solids present, which is often referred to as sewage sludge or municipal biosolids. The biosolids can then be treated further to reduce bacteria levels before disposal, or dumped untreated in landfills, or applied to land as a fertiliser. The treated water is usually discharged into the environment, which can be directly into a river, sprayed onto vegetation, or into a constructed wetland for additional biological purification.

One of the most common wastewater treatment processes in use is the activated sludge process [15]. This is primarily a biological treatment process utilising micro-organisms to digest the contaminants present in the water. Figure 2.1 illustrates the

main stages in an activated sludge treatment process. The first two stages, screening and grit removal, are used to remove material that can be easily separated from the water and which would cause problems by clogging downstream equipment such as pipes and valves. The screening stage removes large debris such as drink cans, branches and plastic material.

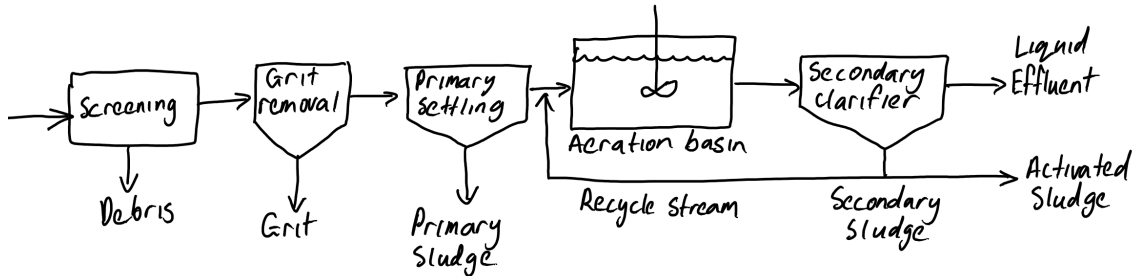


Figure 2.1: Schematic diagram of a typical activated sludge wastewater treatment process.

Following the screening stage the water then passes into a settling basin, which allows grit particles such as sand or small stones to settle to the bottom, where they can be removed before they damage pumps and other plant equipment. The water then passes into the first primary clarifier where the heavy suspended solids settle to the bottom, and fats and oils float to the surface, to be skimmed off by a mechanical surface skimmer. The settled solids and material skimmed from the surface is collected and removed, and is referred to as primary sludge.

The resulting liquid from the primary clarifier passes into the secondary treatment phase where it is subjected to biological oxidation in an aeration basin. The micro-organisms present in the water consume the soluble organic matter along with dissolved oxygen in the water. This process is carried out in an aerated tank to maintain a high dissolved oxygen concentration for the micro-organisms. If the oxygen level falls too low the micro-organisms can die off and the secondary treatment stage becomes septic.

The mixture of sludge and treated water from the aeration basin is then passed into the secondary clarifier. A portion of the sludge that is collected at the bottom of the clarifier is returned to the aeration tank to seed the incoming water with bacteria, while the surplus secondary sludge is removed for further treatment. The secondary sludge, which is often referred to as activated sludge, is then combined with the primary sludge, before being mechanically de-watered by passing through a filter belt press prior to being sent to landfill, or being subject to additional treatment such as fermentation. The liquid removed from the secondary clarifier is then usually passed into a holding tank before being released into the environment or receiving tertiary treatment.

Tertiary treatment is used as a final step to improve effluent quality before discharge into the environment. Common processes include nutrient removal to reduce the nitrogen and phosphorus levels, and disinfection to substantially reduce the level of micro-organisms in the water. Constructed wetlands are increasingly being used as a tertiary treatment step and can be highly effective under the right conditions.

While the activated sludge process is effective at treating large volumes of wastewater, it produces large amounts of organic material in the form of biosolids, (shown as the activated sludge flow in Fig. 2.1) which require appropriate disposal. Effectively treating these biosolids to make them safe enough for disposal is difficult for the reasons outlined in the previous chapter. In addition to legislative pressure, traditional methods for disposal, like landfilling, are no longer viable because of the environmental pollution they cause, which is why alternative methods are being actively investigated. Biological treatment processes also struggle when the incoming wastewater contains recalcitrant compounds which are not easily biodegradable [16].

### **2.1.2 Rotorua District Council Wastewater Treatment Facility**

The Rotorua District Council (RDC) wastewater treatment facility, shown in Fig. 2.2, uses a modified 5-stage Bardenpho process to treat wastewater from the city of Rotorua and surrounding areas. This process is similar to a traditional activated sludge process but has additional biological stages to reduce the nitrogen and phosphorus levels in the water. Fig. 2.3 illustrates the individual treatment stages from the sewage pump stations to effluent disposal as part of the Rotorua treatment plant.

The facility treats on average 18,000m<sup>3</sup> of raw sewage every day generated by a population of around 60,000. Most of the wastewater is generated by domestic use, with around 10% from industry [17]. Around 25 tonnes of biosolids are produced each day, consisting of approximately 40% primary sludge and 60% secondary sludge. Around 10% of the biosolids produced are sent to the on-site composting facility, with the remainder sent to landfill. This represents around 10% of the total landfilled waste produced in Rotorua [18].

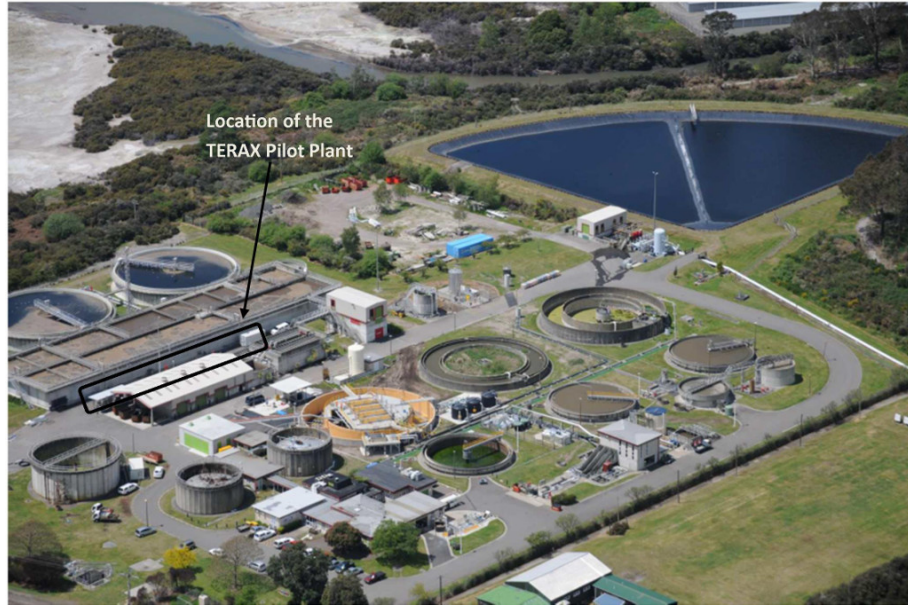


Figure 2.2: An aerial photograph of the RDC wastewater treatment plant [19], showing the location of the TERAX pilot plant.

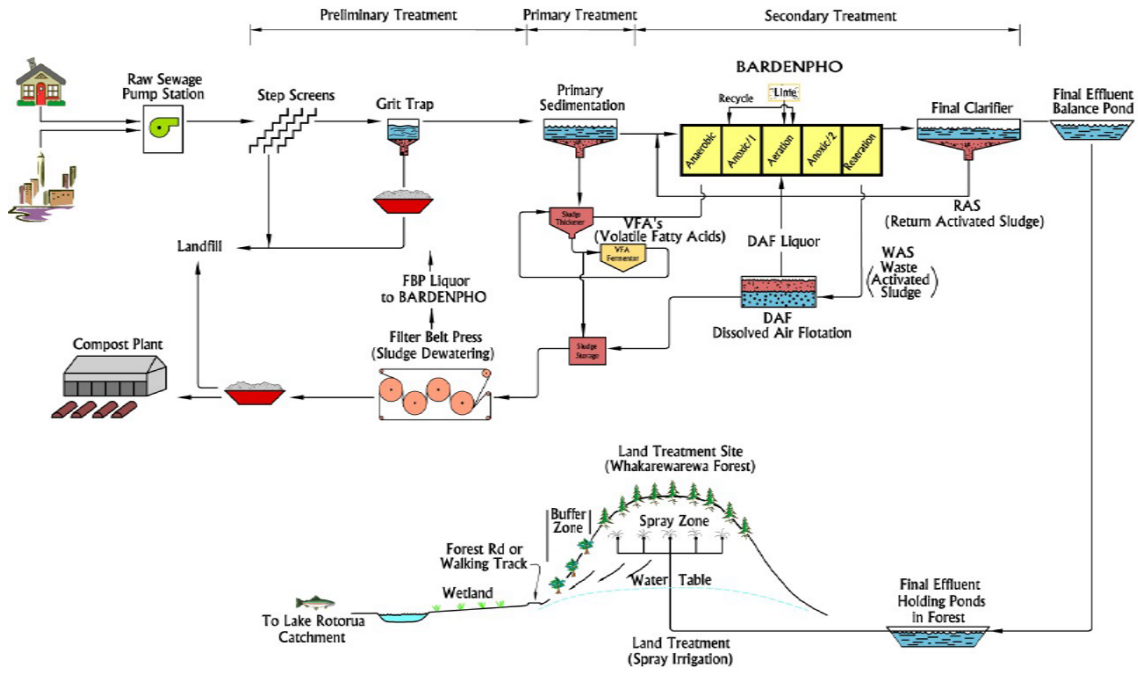


Figure 2.3: A diagram of the RDC 5 Stage modified Bardenpho wastewater treatment plant, diagram from [20].

## 2.2 Biosolids and Wastewater Characterisation

The concentration of contaminants present in wastewater and biosolids can be determined using a number of standard tests and measurements which assess water quality. Standard tests are needed because of the large number of possible com-

pounds present in the water. These tests measure physical, chemical and biological characteristics of the water. The following is a description of the common measurements that are used as wastewater quality indicators as well as those that have been used as part of this research. These quantify and characterise the contaminants present in the feed samples used in the experiments. They can also be used as metrics to assess the effectiveness of the wet oxidation process.

These metrics have been chosen because they describe key intermediate compounds of interest and are surrogates for chemical species. These chemical surrogates or pseudo-compounds are used in the future kinetic modelling work described in Chapter 5. Many of the metrics described below are defined by the standard methods recommended by the American Public Health Association [21].

**Physical Characteristics:** The solids fractions present in wastewater are typically categorised as suspended solids or volatile solids. Total Suspended Solids (TSS) is the dry weight of particles trapped by a standard filter. The liquid sample is first well mixed, before being filtered through a pre-weighed filter paper which is then dried, and subsequently weighed. The solids left on the filter paper represent the TSS of the sample. Measuring Volatile Dissolved Solids (VSS) involves igniting the filter paper in a furnace after the TSS measurement. The weight loss represents the VSS concentration.

**Oxygen Depletion Potential:** One of the most common tests for wastewater involves measuring the Chemical Oxygen Demand (COD). This is a measurement of the amount of oxygen required by oxidisable material present in the water. It quantifies the oxygen depletion effect of the contaminants if the sample was introduced into a body of water. In this study COD was determined using a Scion developed micro-scale method [22] similar to that described in Standard Methods 5220D [21]. Samples were digested with excess of potassium dichromate and COD was determined by estimating the reduced dichromate colorimetrically. Soluble Chemical Oxygen Demand (sCOD) is the COD measurement of the filtrate from the TSS measurement.

The Biological Oxygen Demand (BOD) is another common test for water quality. This test measures the amount of oxygen required by micro-organisms to break down biodegradable organic matter during a standard incubation period. This measurement has not been used as a metric for this research because of the focus on chemical oxidation.

**Carbon:** The carbon content is measured in the form of Dissolved Organic Carbon (DOC) which is a general description of the carbonaceous organic material dissolved in water. Quantitatively it is a measure of all the carbon in the liquid phase which has passed through a standard glass fibre filter. DOC and Volatile Fatty acids are

key indicators for the suitability of the wet oxidation effluent as a potential carbon source for the BNR stage of the waste treatment plant.

**Nitrogen:** Nitrogen is typically measured in the forms of Total Kjeldahl Nitrogen (TKN), Dissolved Kjeldahl Nitrogen (DKN) and ammoniacal nitrogen ( $\text{NH}_4\text{-N}$ ). These parameters are monitored because the difference between DKN and  $\text{NH}_4\text{-N}$  gives the Dissolved Organic Nitrogen (DON) content. DON is undesirable as it may not be able to be separated from the effluent via stripping and its effect on downstream bio-processes is less certain. The fate of nitrogen is important, as the potential load that could be returned to the waste treatment plant from the wet oxidation effluent can be significant [23, 24].

**Phosphorus:** Phosphorus is a nutrient used by micro-organisms and excessive quantities can promote algal blooms causing oxygen depletion in the receiving water body. It is present in wastewater in several forms but the most common is orthophosphate ( $\text{PO}_4^-$ ). Total Phosphorus (TP) is a measurement that quantifies all forms of phosphorus present in water and is used as the metric in this research.

**Volatile Fatty Acids:** Volatile fatty acids are short chain carboxylic acids, usually containing six carbons or less. VFAs are measured as part of the DOC and COD values as they constitute oxidisable dissolved organic carbon. VFAs are produced by the decomposition of organic material in water, and by oxidation reactions under wet oxidation. Research has shown that VFAs can be a suitable carbon source for the BNR stage of a waste treatment plant [25, 26], hence the need to quantify the amount being produced to determine if this is viable.

**Metals:** Heavy metals are of particular concern as they can bio-accumulate when released into the environment. Some heavy metals found in biosolids and wastewater, such as mercury, cadmium and lead, are particularly toxic and most countries have strict limits on the level of heavy metals that may be present. In New Zealand, biosolids are graded according to the level of heavy metals present. This dictates where they can be used, as well as sets maximum allowable limits, which are shown in Table 2.2. Guidelines on the type and amount of metals allowed in municipal biosolids about to be discharged is available in the guidelines published by the New Zealand Water and Wastes Association [27].

For this research, the quality metrics listed in Table 2.3 will be used to characterise the effectiveness of the wet oxidation process. The metrics have been chosen to give insight into the solids reduction, oxygen depletion potential, and specifically the production of intermediate VFAs, nitrogen and phosphorus. Heavy metals have not been measured for the series of experiments described in this thesis, however Scion has conducted previous wet oxidation experiments which revealed that heavy metals are concentrated in the residual solids at the end of the reaction.



Table 2.2: Allowable heavy metal limits for biosolids in New Zealand, adapted from [27].

Heavy metal	Grade A biosolids (mg/kg dry weight)	Grade B biosolids (mg/kg dry weight)
Arsenic	20	30
Cadmium	1	10
Chromium	600	1500
Copper	100	1250
Lead	300	300
Mercury	1	7.5
Nickel	60	135
Zinc	300	1500

Table 2.3: Wastewater quality metrics used in this study.

Parameter	Monitored parameters	Units
Solids	TSS, VSS	mg/l or mg/kg
Oxygen demand	COD, sCOD	mg/l
Nutrients	NH <sub>4</sub> -N, DKN, Total Phosphorus	mg/l
VFAs	Acetic acid, propionic acid, iso-butyric acid, N-butyric acid, pentanoic acid, hexanoic acid	mg/l
Alcohols	Methanol, ethanol	mg/l

### 2.2.1 Rotorua Biosolids Characterisation

To gain insight into the properties and variation in the biosolids produced by the Bardenpho RDC treatment plant, an internal study was conducted over several months in late 2009 by Scion [9]. Daily samples were collected from June 2009 until September 2009 with random grab samples also taken during that time period. These samples were analysed using the metrics described in Section 2.2, as well as elemental, bacteria and detailed carbon and nitrogen analysis. Many of the analyses were performed using in-house methods, while elemental carbon and nitrogen were analysed at Campbell Microanalytical Laboratory in Dunedin. A sample of biosolids from the RDC treatment plant is shown in Fig. 2.4.

As mentioned in the previous section, the typical composition of the biosolids produced by the RDC wastewater treatment plant comprises around 40% primary and 60% secondary sludge. Analysis of the biosolids has showed that carbon was the most prevalent element, followed by oxygen, hydrogen and nitrogen. Heavy metals accounted for 0.08% of the dry weight. Characterisation of the carbon present in the biosolids revealed that around two thirds of the carbon existed as protein and around a quarter as carbohydrates, with cellulose being the most common.



Figure 2.4: A sample of biosolids from the RDC wastewater treatment plant.

### Solids Analysis

Raw primary and secondary solids had a total solids content of between 2 and 3%. De-watering using the belt presses increased the total solids content to 15.1%. The results in Table 2.4 show the solids separation from each of the solid waste streams in the wastewater treatment plant. The results were analysed internally at Scion, as well as Hills Laboratories.

Table 2.4: Solids characterisation of the RDC biosolids, with validation from a third party laboratory.

	Total Solids (Scion) (%)	Total Solids (Hills) (%)
Primary Solids	2.0	2.0
Secondary Solids	2.2	2.4
Mixed Sludge	3.3	2.8
Belt Pressed Solids	15.1	15.0

### COD Analysis

Table 2.5 gives the results of the COD analysis of the raw and filtered feed material. This showed that the majority of the COD exists in the solid phase. The understanding of the COD requirements within a wet oxidation system is important as it provides an indication of the oxygen requirements should the sample be subjected to oxidation.

Table 2.5: COD characterisation and measured limits of the RDC biosolids.

	COD (kg/tDS)	High (kg/tDS)	Low (kg/tDS)
Total COD	1600	1780	1420
Filtered COD	200	300	160

### Elemental Analysis

Table 2.6 shows the common elements present in the biosolids, the most common being carbon, which was expected, followed by oxygen, hydrogen, nitrogen and phosphorus. In total, 38 elements were measured which account for 80 to 97 % of the dry weight. The remaining composition consisted of elements that were not analysed, such as silicon. The percentage of heavy metals was similar between the mixed and belt pressed solids, which indicates that the heavy metals are mostly present in the solid phase and have not solubilised.

Table 2.6: Elemental composition of RDC biosolids. All concentrations expressed as % of dry weight.

Element	Mixed solids (% dry weight)	Belt press solids (% dry weight)
C	28.40	44.90
O	29.90	33.50
H	5.70	6.48
N	5.40	6.42
P	3.50	2.20
K	1.40	0.80
Ca	0.89	0.76
S	0.75	0.56
Mg	0.72	0.47
Al	0.54	0.46
Fe	0.46	0.41
Na	0.35	0.09
Heavy metals	0.10	0.08
Other metals	0.05	0.04

### Carbon Analysis

Analysis of the carbon content ranged from 28 to 45%. This is in line with values reported in the literature of 6.5 to 48% [28]. The majority of carbon exists as solid phase organic carbon.

### Nitrogen and Phosphorus

Nitrogen was quantified by analysing the concentrations of TKN and  $\text{NH}_4\text{-N}$  (ammoniacal nitrogen) and the results were used to determine the fraction of Dissolved Organic Nitrogen (DON) in the liquid phase. The dissolved organic nitrogen was determined using the following equation.

$$\text{Dissolved Organic Nitrogen} = \text{TKN} - \text{Ammonical nitrogen} \quad (2.1)$$

As mentioned earlier, dissolved organic nitrogen is of particular interest. It is an undesirable product as it may not be volatile, and its fate within downstream bio-processing (such as in a BNR plant) is less certain.

Like carbon, nitrogen was primarily present in the solid phase as organic nitrogen, with small amounts of organic and ammoniacal nitrogen present in the liquid phase.

Nitrogen and phosphorus are of particular interest as the liquid effluent from the wet oxidation process will be recycled back into the wastewater treatment plant and the extra nutrient load on the plant needs to be quantified. Table 2.7 shows the distribution of nitrogen across the liquid and solid phases.

Table 2.7: Nitrogen analysis across liquid and solid phases.

Nitrogen component	Nitrogen kg/tDS
NH <sub>4</sub> –N liquid phase	4
Organic–N liquid phase	6
Organic–N solid phase	60

## Heavy Metals

Copper and zinc are the most common heavy metals present and are an order of magnitude greater than other heavy metals. These metals have entered the system primarily through the leaching of domestic plumbing. Analysis of heavy metals has been performed to determine baseline values, as Scion suspects that some metals present may have a catalytic effect under wet oxidation [29].

Table 2.8: Heavy metals present in RDC biosolids.

Compound	Mixed solids (mg/kg dry wt)	Dewatered belt pressed solids (mg/kg dry wt)
Zn	430	380
Cu	420	320
Cr	56	44
Pb	25	23
Ni	11	10
As	11	9.9
Cd	0.96	0.86
Hg	0.69	1.2

## Feed Variability

Scion has conducted an earlier study to investigate the variability of the biosolids feed [9]. Samples of the belt pressed solids were collected five days per week from June 2009 until September 2009 and were combined to create a weekly composite sample for analysis. Random grab samples were also taken from June to October 2009. These samples were analysed for solids content, volatiles, carbon, nitrogen and heavy metals.

Fig. 2.5 illustrates the variability of the total solids content over time of primary,

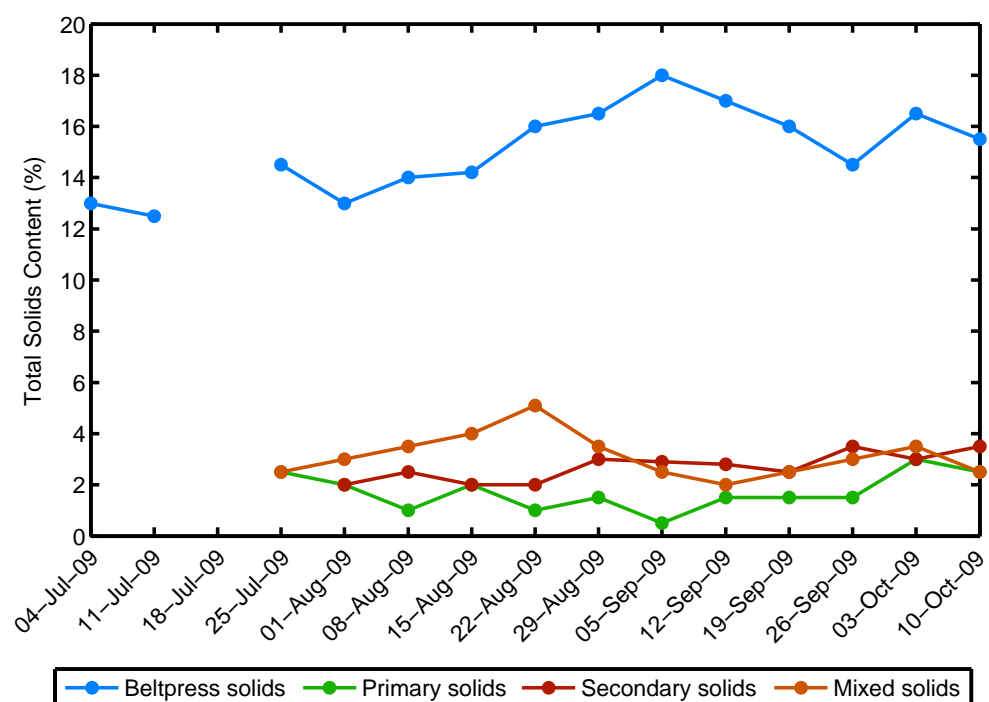


Figure 2.5: Total solids (TSS) content of weekly composite samples over several months.

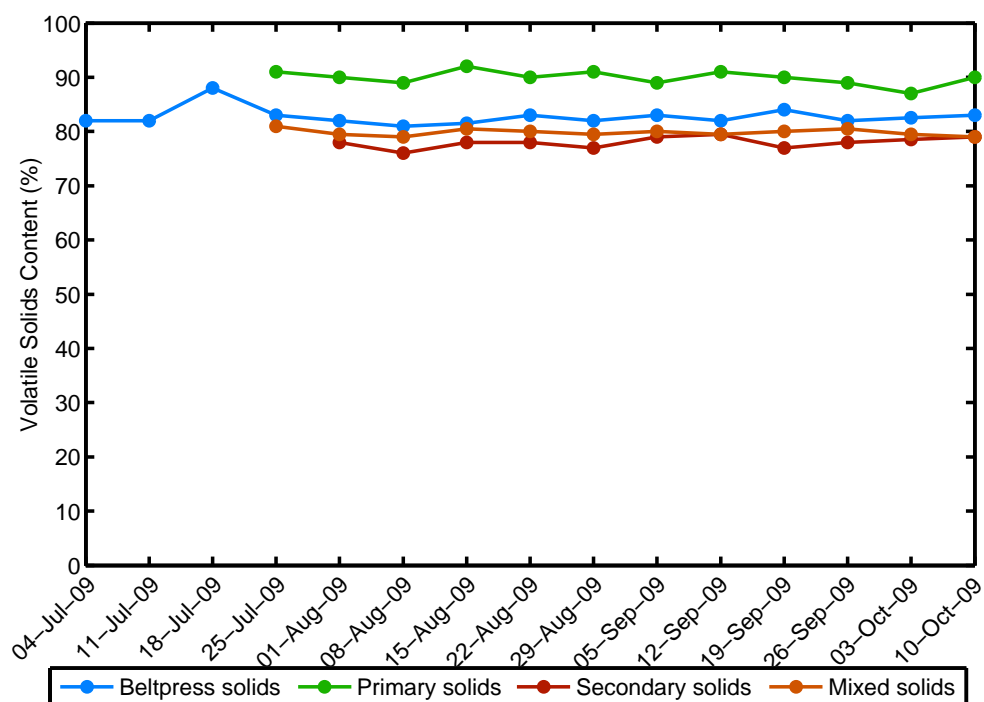


Figure 2.6: Volatile solids (VSS) content of weekly composite samples over several months.

secondary and belt-pressed solids. The de-watering treatment process underwent an operational change during the sampling period around the 4th of August 2009 when it was decided to run the filter belt presses on a continuous basis, rather than accumulate solids in a tank first. This change resulted in a more even distribution of primary and secondary solids which improved the de-waterability. This is illustrated in Fig. 2.5 which shows an increase in the mixed total solids over time. Volatile solids in Fig. 2.6 exhibited much less variability over the same time period.

While the total and volatile solids dry weight measurements were not used in the experiments described later in Chapter 3, they still provide useful insight into the expected variability in the feed material that is likely to be encountered.

## **Bacteria**

Prior analysis has revealed that primary solids contained the highest levels of bacteria with similar levels present in the final belt pressed solids [9]. Secondary solids and mixed solids contained considerably less bacteria which showed that the wastewater treatment process does not reduce the bacteria levels in the solids. An additional advantage of using wet oxidation as a biosolids treatment process is the high temperatures involved in the process mean the resulting liquid effluent and solids are completely sterile.

Bacteria levels have not been measured as part of this series of experiments, however an earlier study demonstrated that the considerable levels of micro-organisms present are completely destroyed by wet oxidation [9], which is of considerable benefit.

## **2.3 Alternative Strategies to Deal With Biosolids**

Disposing of municipal biosolids presents a number of challenges. The high water content creates a number of problems including increased transportation costs, the generation of leachates that can pollute the water table, and difficulties with thermal processes. Despite this, the majority of biosolids in New Zealand (including Rotorua) are sent to landfill.

There are a number of existing strategies to deal with municipal biosolids which are in use around the world. These include digestion, thermal processing, composting, direct land application and traditional landfill dumping. This section reviews alternative disposal methods that are currently available.

**Anaerobic Digestion:** Anaerobic digestion is a bacterial process which is carried out in the absence of air at temperatures of between 35 to 55°C. Bacteria decompose

organic material and produce methane and carbon dioxide gas which can be easily collected and used. Digestion improves the de-waterability of the biosolids and produces a reduction in volume and mass of the resulting solids and also reduces the level of pathogens present [30]. However the digester supernatant typically has high levels of BOD and COD and cannot be discharged into the environment without additional treatment [31].

**Aerobic Digestion:** Aerobic digestion is also a bacterial process but is carried out in the presence of oxygen, where bacteria convert organic material primarily to carbon dioxide. This process decreases the BOD and COD of the effluent and reduces the mass and volume of solids and improves de-watering [30]. Aerobic digestion can be energy intensive due to the energy used for pumps and blowers to aerate the process.

**Thermal Processing:** Common thermal biosolids processing techniques include incineration, gasification and pyrolysis. One of the key problems biosolids present is that they generally require substantial de-watering before thermal processing techniques are successful, and these are therefore very energy intensive. These processes can produce significant gaseous emissions and the process sometimes requires an auxiliary firing source, which is typically petroleum-based adding to the cost of processing.

Pyrolysis has been used as a biosolids treatment technology for many years and been the focus of several studies [32, 33]. Pyrolysis involves heating organic material to high temperatures ranging from 300 to 900°C in an inert atmosphere. Unlike gasification or incineration, pyrolysis is an endothermic process and requires an auxiliary heating source. Despite this, it allows additional value recovery in the form of combustible syngas, which is a mixture of hydrogen, carbon monoxide and carbon dioxide, and produces less pollution than incineration [34, 35].

An extensive review of thermal treatment technologies was undertaken by Fytli and Zabaniotou [33] who explored the disposal of biosolids by incineration in cement kilns, in addition to the traditional thermal disposal strategies described earlier. Although alternative thermal technologies like pyrolysis and gasification are a considerable improvement over regular incineration, a common concern raised by the author was the amount of gas treatment required for each of the technologies, such as flue gas in the case of incineration, pyrolysis and cement manufacture and syngas production from gasification. The heavy metals present in the biosolids were a particular focus for the author. While the majority of the metals remained in the solid char or ash residue, some, particularly mercury, were volatile and were present in the gas exhaust streams. Air pollution is also a common theme in other reviews of thermal treatments conducted by other researchers [36, 37].

Gasification has traditionally been used to produce syngas from wood or solid fossil fuels such as coal and peat, however gasification is now being investigated as an alternative biosolids treatment technology. Uses for syngas include combustion in an internal combustion engine for electricity production, as a source of heating, as well as a feedstock for chemical processes such as synthetic fuels.

Samolada and Zabaniotou [38] assessed the viability of incineration, gasification and pyrolysis as treatment technologies for municipal biosolids. They conclude that pyrolysis was the most favourable process with the major downside being the required level of de-watering needed. Gasification and incineration were the least favourable for a variety of reasons, including air pollution, ash disposal, extensive de-watering and considerable gas cleaning required for the gas to be used.

An overview of gasification technology for municipal solid waste was provided by Kerester [39]. In this article, municipal solid waste refers to material that is traditionally sent to landfill, such as biosolids, but also includes household refuse and industrial waste. A conversion rate of carbon to syngas of 70 to 85% was reported, which is in line with the literature. Contrary to other gasification reviews, the author states that scrubbing the syngas of heavy metals and other impurities is relatively straightforward and mercury removal rates of up to 95% are stated. However no data was provided to support this claim.

A review of the environmental and economic factors of four biosolids disposal options was conducted by Lundin *et al.* [40] who reviewed land application, co-incineration, incineration with combined phosphorus recovery and fractionation with phosphorus recovery as disposal options. They conclude that there is no preferred treatment method as each of the reviewed disposal options had significant drawbacks.

**Composting:** Composting is a commonly used biosolids treatment practice around the world. Biosolids are combined with organic material such as sawdust or wood chips which provide to facilitate aeration. The composting process kills most pathogens due to the heat produced by the bacteria, however heavy metals remain in the resulting material. Disadvantages of this process are the large amounts of land required and the potential for undesirable odours [41].

**Land Application:** The application of biosolids to land can be a successful disposal option and is very common. Applications include land reclamation and the direct application as a fertiliser. Biosolids which are intended for land application are often categorised as Class A biosolids if they have been treated to reduce bacteria levels, and Class B if untreated. In New Zealand the classification also sets limits on heavy metals that may be present [27]. If applied correctly, land applications such as forest spraying can be effective. Problems that may arise when biosolids are applied directly to land are pathogens such as *E. coli* entering waterways, and heavy metals



and other nutrients such as nitrogen leaching into the ground and contaminating the water-table [41, 42].

**Landfill:** Sending biosolids directly to landfill is a common practice in New Zealand and around the world. Leachates from biosolids, due to the high water content can contaminate waterways and large amounts of methane are generated that is difficult to capture under typical landfill conditions [27, 41].

### 2.3.1 Summary of Biosolids Disposal Methods

The following description is a summary of the key points of each of the common biosolids treatment techniques.

- **Digestion:** Enables methane generation and recovery. Minimal volume reduction.
- **Thermal Processing** (incineration, gasification, pyrolysis): Biosolids require substantial de-watering before thermal processing is successful. Significant gaseous emissions. Usually requires an auxiliary firing source which is typically petroleum based.
- **Composting:** Commonly used practice around the world. The composting process kills most pathogens, however heavy metals remain. A lack of markets due to the perceived risk of handling biosolids.
- **Land application:** Presence of contaminants such as heavy metals and pathogens are problematic.
- **Landfill:** Leachates from biosolids can contaminate waterways. Large amounts of methane which can be difficult to capture are generated under typical landfill conditions.

## 2.4 The Wet Oxidation Process

The wet oxidation process was developed in 1912 as an alternative method for treating spent liquor from pulp and paper mills [6]. However the first commercial success of wet oxidation was the manufacturing of vanillin, the main compound in artificial vanilla flavouring and produced from lignosulfonic acids present in pulp and paper mill waste in the 1930's [43].

Wet oxidation, also known as wet air oxidation, or hydrothermal treatment, involves the oxidation of chemical compounds. These are dissolved, or suspended, in an

aqueous solution using an oxidant, which is usually oxygen, air or hydrogen peroxide, at elevated temperature and pressure. Owing to the high temperatures involved, hydrolysis reactions also occur. Depending on the desired level of treatment, for example improved de-watering and sterilising, an oxidant may not be necessary [44].

Soluble or suspended oxidisable compounds in the water are oxidised by dissolved oxygen. The reactions take place in the liquid phase at temperatures above the normal boiling point of water (100°C) but below the critical point (374°C). As the water must be kept in a liquid state, the system pressure is maintained above the boiling point of water at the desired temperature. Typical reaction conditions use temperatures between 150 and 300°C, 20 to 90 bar pressure, and residence times of 15 to 120 minutes [45].

Traditionally, the main objective of wet oxidation was total destruction of all organic compounds to CO<sub>2</sub> and water, which necessitated high temperatures in excess of 300°C and, subsequently, high pressures to maintain the water in a liquid state. However, it is now recognised that production of intermediate VFAs at lower temperatures is beneficial as they are a suitable carbon source for BNR processes at wastewater treatment plants [25, 46].

Catalysts are able to considerably improve the performance of wet oxidation by providing alternative, lower activation energy pathways, therefore increasing the reaction rate at the same temperature and pressure. Catalytic wet oxidation reactions have been investigated by several authors [47–49], showing that the use of a catalyst improved the level of oxidation, and enabled the use of lower temperatures and pressures. At this stage, Scion has elected not to use a catalyst because of uncertainty surrounding the recovery of the catalyst and its effect if the effluent is recycled into the wastewater treatment plant. Depending on the catalyst used, it could increase the concentration of certain heavy metals shown in Table 2.8. Consequently the focus of this research was on non-catalytic wet oxidation.

There have been several comprehensive reviews on wet oxidation and catalytic wet oxidation [6, 49–52] which have covered many aspects of the process in detail. However, there is still a knowledge gap surrounding the dynamic modelling of the intermediate products produced from biosolids under wet oxidation. At the time of writing there is no model which takes into account the oxidant consumption in addition to the liquid and gaseous reaction end products produced.

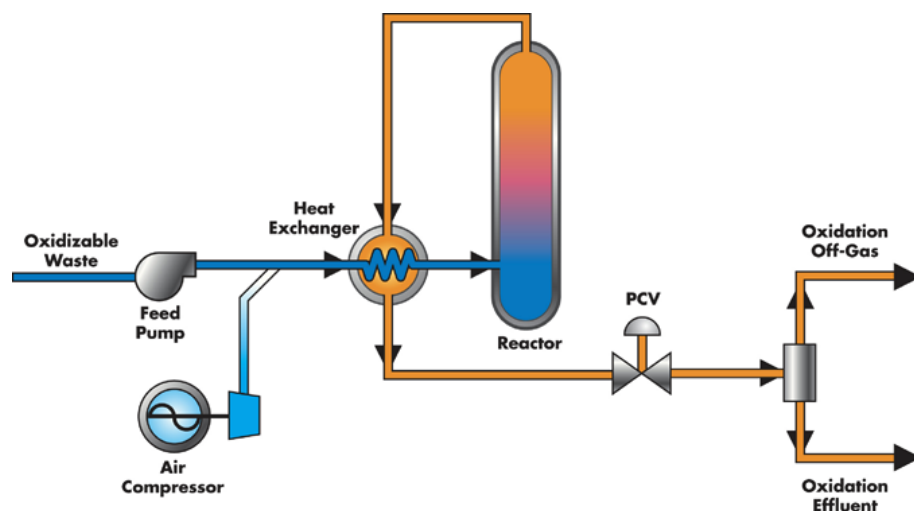


Figure 2.7: Schematic diagram of a typical wet oxidation process, from [45].

### 2.4.1 Process Description

Fig. 2.7 illustrates a basic process flow diagram of a continuous wet oxidation plant. The waste feed is pumped under high pressure where it is mixed with an incoming stream of oxidant, typically oxygen, before being preheated by a heat exchanger which is heated from the reactor discharge, before flowing into the reactor. The reactor vessel is usually either a bubble column or CSTR, designed to promote mixing between the gas and liquid phases to minimise mass transfer resistance. The waste remains in the reactor for a period of time which is governed by the level of degradation required.

The oxidant mass flow required is governed by the COD of the waste. Wastes with a high COD require a high mass flow of oxidant in order to achieve complete oxidation. Otherwise partial oxidation will occur and can result in the production of undesired compounds such as CO, which was discovered during the experimental programme described in Chapter 5. Usually wet oxidation operates with a stoichiometric COD to oxidant ratio or with a slight excess of oxidant.

On start-up, the reactor requires heat input. However once operating temperature is reached, the heat generated by the oxidation reactions is often sufficient to maintain system temperature and balance the heat required to vaporise water [53]. Cooling of the reactor may be required for high COD loadings [24], but for low COD or particularly dilute feeds, additional heat may be required to maintain temperature.

After the material has remained in the reactor for the required residence time, the reactor discharge passes through the recovery heat exchanger, where it heats the incoming feed, before passing through a pressure control valve which maintains the system pressure at the desired set point. The effluent then flows into a flash vessel which separates the off-gas products from the liquid effluent.

The off-gas stream may undergo further processing, such as passing through a scrubber or catalytic converter to remove any CO and other volatiles that may be present. Water vapour in the form of steam makes up the largest percentage of the off-gas. Unlike traditional combustion, the off-gas has negligible amounts of NO<sub>x</sub>, SO<sub>x</sub> and fine particulates to be filtered out [45]. The oxidation effluent is liquid with a small amount of suspended solids in the form of a high phosphate ash which is separated out. The remaining liquid undergoes further biological treatment before discharge into the environment to remove the high levels of VFAs.

## 2.4.2 Influence of Operating Conditions

The level of oxidation achieved, or desired, is heavily dependant on the process operating conditions, mainly temperature, oxidant concentration, system pressure and residence time. The following sections discuss the effect of each operating parameter on the level of oxidation and the typical ranges used in the literature. While different reaction conditions have been described in the literature, few have systematically characterised the effect of the easily manipulated variables shown in Fig. 2.8 and therefore, suitably detailed models which take these variables into account are not available.

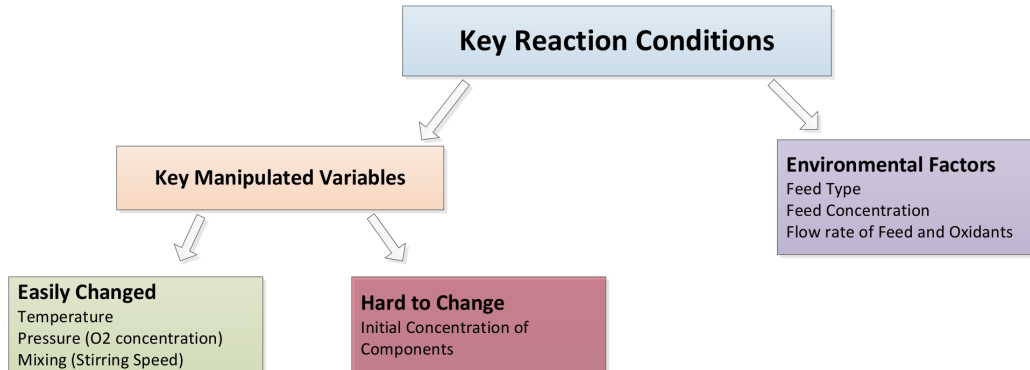


Figure 2.8: A summary of the key factors affecting wet oxidation.

### 2.4.2.1 Temperature and Pressure

It well known, and has been clearly demonstrated, that temperature has the most significant effect on wet oxidation. The higher the temperature, the greater the observable reduction in total COD as well as solids volume [11, 43, 54–56].

The results in Fig. 2.9 illustrates the effect of increasing temperature on the total suspended solids content. It is clear that raising the temperature increases not only the rate at which the solids are reacted but also the final concentration. This is also

demonstrated in the photograph of the resulting effluent at different temperatures in Fig. 2.10. Table 2.9 summarises some of the suggested operating temperatures and pressures used by other researchers.

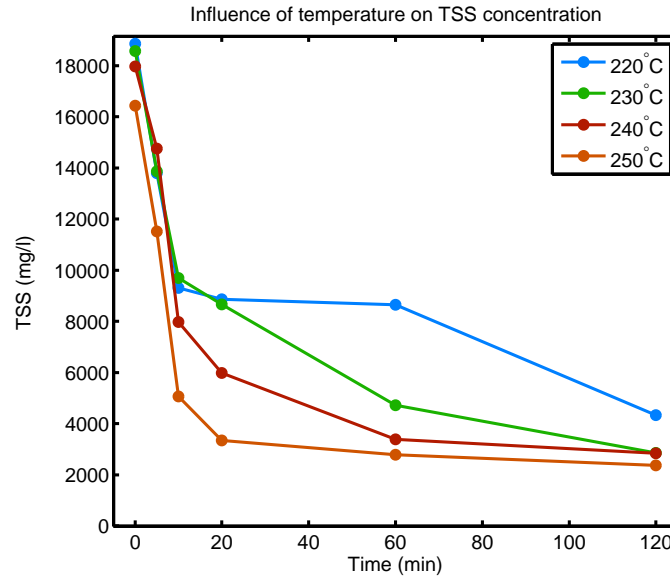


Figure 2.9: Preliminary experiments conducted by Scion on the effect of temperature on TSS concentration during wet oxidation, data from [9].

Table 2.9: Operating conditions in use for wet oxidation systems.

Researchers	Temperature (°C)	Pressure (bar)
Li <i>et al.</i> [57]	150–350	20–200
Debellefontaine [53]	200–325	150
Fousard <i>et al.</i> [58]	197–327	20–200
Mishra <i>et al.</i> [6]	125–320	5–200
Chung <i>et al.</i> [59]	180–240	40–60
Baroutain <i>et al.</i> [60]	220–240	20–40

In addition to the level of solids reduction, the operating temperature also influences the type and concentration of recalcitrant intermediate products produced under wet oxidation. Baroutian and Gapes [56] showed that the yield of acetic acid is strongly linked to the operating temperature, although there is a maximum level of production which begins to decline as the temperature is increased further.

In general, higher temperatures increase the level of conversion achieved. However scale build-up and severe corrosion of the reactor has been documented when the operating temperature is above 300°C [13]. The reasons have been suspected to be due to the formation of highly corrosive chlorides.

The system pressure should always be maintained well above the saturation pressure at the desired operating temperature to prevent boiling, as the oxidation reactions occur in liquid water. Maintaining a high system pressure also prevents excessive

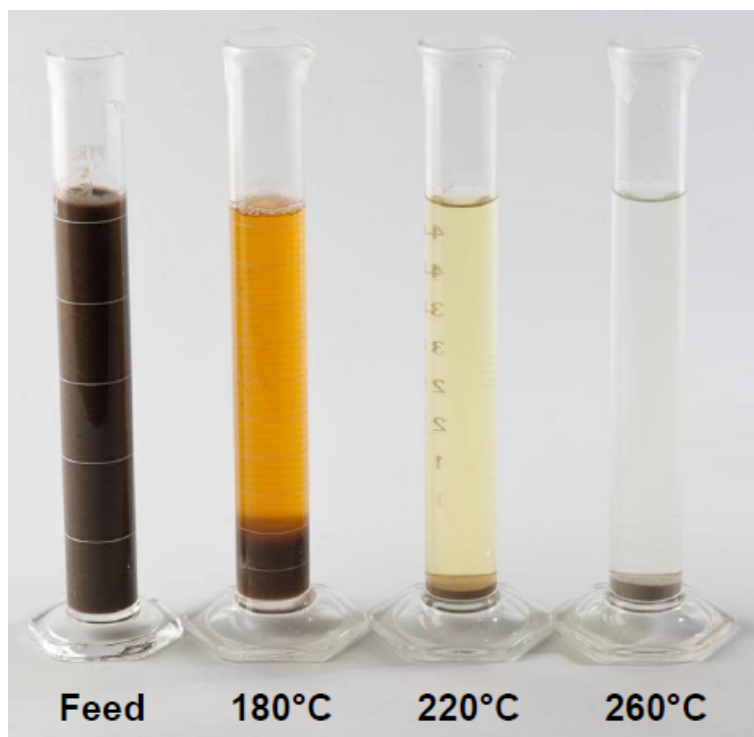


Figure 2.10: Effect of increasing temperature during wet oxidation with a two hour residence time. Photograph from [18].

water evaporation and subsequent energy loss. When the wet oxidation process was in its infancy, it was thought that the pressure had little effect on the process results [61], however it has been shown that increasing the pressure also results in increased oxidation effectiveness [59]. Increasing the system pressure increases the solubility of oxygen in water, and the concentration of dissolved oxygen has been shown to influence the rate of oxidation [62].

#### 2.4.2.2 Oxidants

Oxygen and air are the most common oxidants used for wet oxidation, however ozone and hydrogen peroxide have also been used in some studies [63]. Several researchers have found that hydrogen peroxide was more effective than oxygen and could achieve the same level of conversion at lower temperatures and pressures [53, 64, 65]. Because hydrogen peroxide is a liquid, this eliminates gas-liquid mass transfer limitation that can occur when using gaseous oxidants.

Scion has performed tests with hydrogen peroxide as part of their preliminary study [9], described in Section 1.3.1, but did not observe enough of an improvement in destruction to justify the extra expense of hydrogen peroxide, so it will not be covered further in this research.

#### 2.4.2.3 Residence Time

Common residence times for wet oxidation range from tens of minutes to around two hours. The residence time has a significant effect on the process results. Rose *et al.* [12] noticed a 17% increase in COD removal by increasing the residence time from 60 to 90 minutes, using a temperature of 256°C and a system pressure of 6 MPa. Increasing the residence time can allow the desired COD removal to occur at lower temperatures and pressures, which can reduce the complexity and cost of designing equipment rated for higher temperatures and pressures.

#### 2.4.2.4 Pre-treatment Processes for Wet Oxidation

There are several treatment processes which can be used to pre-treat aqueous wastes, with the aim of improving the efficiency of the wet oxidation process. Thermal hydrolysis is a common processing technique and using this as a pre-treatment process has been investigated by several authors [11, 55, 60, 66]. The results show that higher temperature pre-treatment conditions reduce the COD removal of wet oxidation. It is believed that this is due to the production of refractory intermediates under thermal hydrolysis that resist subsequent oxidation. These intermediate compounds are only oxidisable under extreme conditions (over 310°C) [58, 67]. Apart from thermal hydrolysis, there has been little research on other pre-treatment techniques to improve the performance of wet oxidation.

Scion has investigated the performance of a fermentation pre-treatment process for wet oxidation [11]. The aim of the fermentation stage is to partially decompose the organic material to produce VFAs. Because VFAs, in particular acetic acid, are recalcitrant, it reduces the oxidant requirements for the wet oxidation stage and thus reduces running costs for the same VFA yield. This is in contrast to the work described in the literature as Scion is trying to maximise VFA production, rather than maximise the total COD reduction. Methane gas is also produced, but this is not the primary objective of the fermentation process.

### 2.4.3 The Main Reaction Mechanisms

There are several different oxidising agents, both gases and liquids, that can be used for wet oxidation, and have been described in Section 2.4.2.2. Even though there are different oxidants, the main reaction mechanisms still work on the same principals, with the generation of hydroxyl radicals which later act as oxidising agents. The following is a description of the main reaction steps when using gaseous oxygen as an oxidant.

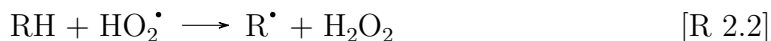
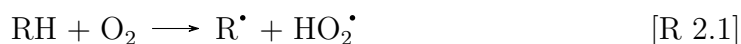
**Oxygen Gas Liquid Transfer:** Oxygen gas diffuses from the gas bulk, through the gas-liquid interface into the bulk liquid. The gas-liquid interface resistance has been documented as an important rate limiting step in wet oxidation [5, 45]. Decreasing the bubble size and improving mixing in the liquid phase helps to reduce this mass transfer limitation.

**Solubilisation of Organic Solids:** Solid particles first solubilise in the water, before they participate in oxidation reactions. The high temperatures promote fast diffusion and the solid-liquid interface is not considered a rate limiting step [5].

**Chemical Reactions:** Wet oxidation reactions take place in the liquid phase between dissolved organic and inorganic matter and dissolved oxygen, resulting in solid, liquid and gaseous product streams. The reaction rates strongly depend on operating conditions and any catalysts present.

According to Li *et al.* and Debellefontaine *et al.* [54, 57], wet oxidation reactions proceed via the production and consumption of hydroxyl radicals. Hydroxyl radicals are highly reactive and act as the primary oxidising agent. The interaction between oxygen, hydroxyl radicals and organic material is generally assumed to proceed via the reaction pathways shown in Reaction R2.1 to R2.5 which were illustrated by Li *et al.* and Debellefontaine *et al.* [54, 57].

A radical is a molecule which has unpaired valance electrons, and therefore one or more “hanging” covalent bonds. The presence of these hanging bonds makes radicals highly reactive.



The production of radicals begins when dissolved oxygen ( $\text{O}_2$ ) reacts with the weakest C-H bonds on the organic compounds, (designated RH) and first produces a hydroperoxyl radical ( $\text{HO}_2^\bullet$ ) and an organic radical ( $\text{R}^\bullet$ ). The hydroperoxyl radical subsequently reacts with other C-H bonds, producing more organic radicals and hydrogen peroxide ( $\text{H}_2\text{O}_2$ ). The decomposition of hydrogen peroxide occurs on the surface of the reactor or other heterogeneous or homogeneous species (M) present [5].







It is the decomposition of the hydrogen peroxide molecule which produces the highly reactive hydroxyl radicals ( $\text{OH}^\bullet$ ) which then oxidise the remaining organic material to hydroperoxides, alcohols, ketones and finally low mass carboxylic acids. The acids can be further oxidised to  $\text{CO}_2$  and  $\text{H}_2\text{O}$  under the right conditions.

Reaction 2.2 has been identified as the main rate limiting step with a high activation energy which can be greater than 100 to 200 kJ/mol [45], and is the primary reason the reactions only start to occur above 200°C and become rapid at around 300°C. The time taken for the formation of oxidising hydroxyl radicals has been proposed as the reason for the initial lag before a reduction in COD is detected after a waste sample is injected into the reactor [5].

Once hydroxyl radicals have been produced, the oxidisable material present is oxidised to water,  $\text{CO}_2$  and carboxylic acids, which is mainly acetic acid and generally resists further oxidation. However it is possible to produce complete oxidation to  $\text{CO}_2$  and  $\text{H}_2\text{O}$  at temperatures over 300°C [53]. Organic nitrogen present is typically converted to  $\text{NH}_3$ , while phosphorus and sulphur are usually converted to  $\text{PO}_4^-$  and  $\text{SO}_4$  respectively, and chlorine reacts to  $\text{Cl}^-$ . These conversion reactions are illustrated by Reaction R2.6 to Reaction R2.10, from [6].



**Desorption of Dissolved Gases:** Gaseous reaction products formed during wet oxidation (which is primarily  $\text{CO}_2$ ) transfer from the liquid to the gas phase in the headspace of the reactor. Other gaseous products include CO, water vapour and small amounts of acids and  $\text{NH}_3$ . This mass transfer step is not believed to be rate limiting [5].

## 2.4.4 Wet Oxidation Reaction Products

Wet oxidation generates gaseous, liquid and solid reaction products in varying amounts depending on the feed material and process conditions. The following

section describes the typical characteristics of these streams.

#### **2.4.4.1 Characterisation of Off-gas Products**

The gaseous stream produced by wet oxidation is far more environmentally benign than from other oxidation processes such as incineration. The composition of the gas usually consists of water vapour,  $\text{CO}_2$  and  $\text{O}_2$ . Carbon monoxide, ammonia and VFAs are also present in the off-gas in smaller amounts and the quantity depends on the reaction conditions. Like incineration, an oxygen deficient environment produces incomplete oxidation and results in a higher ratio of CO to  $\text{CO}_2$  being produced. The percentage of ammonia in the off-gas stream has been shown to be proportional to the rate of water evaporation, and is therefore a function of total system pressure [24].

Rose *et al.* [12] were among the few authors to perform gas analysis and take intermediate gas samples from the reactor headspace for analysis. They showed that the majority of gas was  $\text{O}_2$  with up to 4.9%  $\text{CO}_2$  being formed, and furthermore CO was also produced in quantities of up to 0.41%. Analysis of the reactor off-gas obtained in this work from the experimental investigation will be described in Section 5.5.

#### **2.4.4.2 Characterisation of Liquid Products**

The liquid discharge from wet oxidation primarily consists of water, with moderate amounts of VFAs, dissolved  $\text{CO}_2$ ,  $\text{NH}_3$  and sulfates [6]. Acetic acid is the main volatile fatty acid component remaining in the liquid phase, and is responsible for up to 90% of the soluble COD remaining in solution [13, 23]. Organic nitrogen present in the feed is mostly converted to ammonia, with the fraction remaining in the liquid depending on the water evaporation rate [24].

#### **2.4.4.3 Characterisation of Residual Solids**

The residual solids or ash produced by wet oxidation is a fine powder consisting of phosphates, quartz, calcite and a fraction containing the insoluble heavy metals in the form of hydroxides, carbonates and phosphates [46].

### 2.4.5 Typical Process Results for Organic Wastes

As mentioned earlier, wet oxidation has been shown to be highly effective at reducing the total COD in liquid wastes. Reductions of 50% to over 90% of total COD are achievable under the appropriate reaction conditions [11, 12, 57, 68, 69]. Importantly, it can successfully work with difficult to treat compounds, such as dissolved metals, by transferring them to solid compounds which can be separated [46].

In addition to COD reduction, the process is also highly effective at reducing the level of solids found in the feed material, with reductions of over 80% achieved [11]. This is also illustrated in Fig. 2.11 which shows the effectiveness of solids reduction by the wet oxidation process.

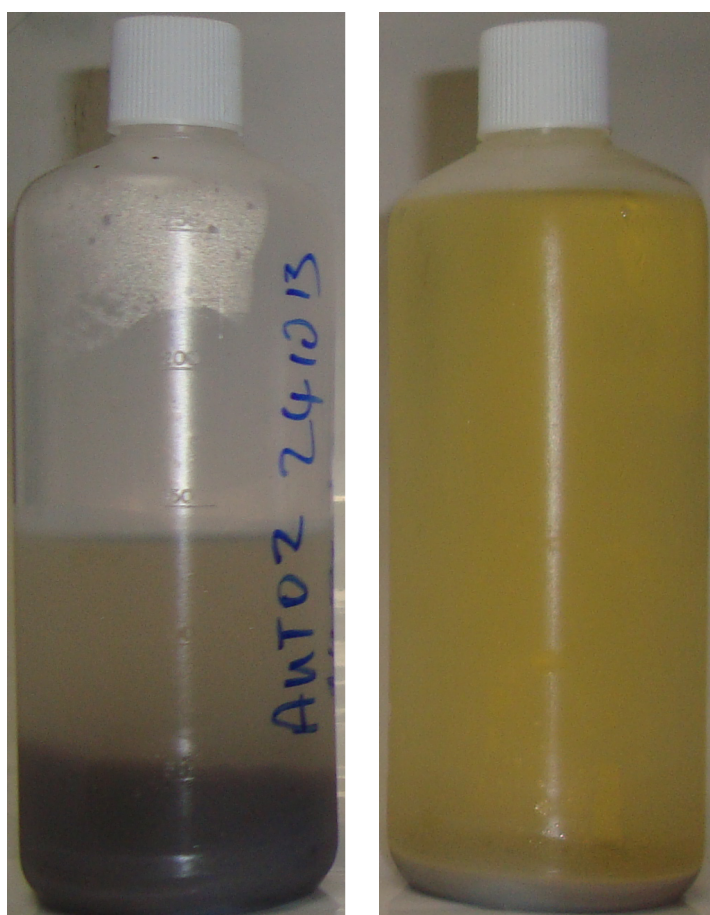


Figure 2.11: Photograph of samples of suspended biosolids before and after wet oxidation. The samples shown are from experiments conducted as part of the experimental programme in Chapter 5.

Low mass carboxylic acids, primarily acetic acid, are major refractory intermediates and are only oxidised under extreme conditions [58]. Therefore they are the dominant intermediate compounds formed and limit the level of COD removal under wet oxidation. Table 2.10 summarises the conversion efficiencies discovered in the literature for the wet oxidation of organic wastes, where (t) designates total system

pressure and (p) designates partial pressure.

Table 2.10: Typical wet oxidation conversion results for organic wastes reported in the literature.

Author	Waste type	Temp (°C)	Pressure (bar)	COD removal	Solids -
Teletzke <i>et al.</i> [61]	Primary	250	-	81%	-
Van Amstel and Rietema [68]	Activated	290	95 (t)	90%	-
Debellesfontaine <i>et al.</i> [54]	Activated	320	150 (t)	89.9%	-
Chung <i>et al.</i> [59]	-	240	60 (p)	66.9%	74.4%
Lendormi <i>et al.</i> [70]	Primary	300	110 (t)	80%	-
Rose <i>et al.</i> [12]	Activated	256	90 (t)	86%	-
Strong <i>et al.</i> [11]	Activated	220	20 (p)	-	83%

## 2.4.6 Advantages of Wet Oxidation

The inability of the standard waste treatment processes described in Section 2.3 to treat the organic material in biosolids without producing new forms of pollution highlights the need for alternative treatment processes which can deal with the unique challenges that biosolids present.

In summary, wet oxidation has been shown to be a highly effective treatment technology and has many advantages which are listed below.

- **Resource Recovery:** Under the right reaction conditions, up to 90% of the soluble COD present can be converted to low weight carboxylic acids can be produced which can be used for other processes such as a carbon source in a BNR plant [13, 26, 46]. Nitrogen is typically converted into ammonia under wet oxidation conditions, and can be separated out with the appropriate equipment. Phosphorus is typically converted into phosphates and is concentrated in the solid phase [46].
- **Volume Reduction:** Solids volume reductions of over 90% have been reported [4, 11] which means less material going to landfill. Fig. 2.11 illustrates the effectiveness of wet oxidation in the volume reduction of biosolids.
- **Sterilisation:** The high temperatures and pressures involved destroy all micro-organisms present, making the effluent much safer to handle.
- **Self Contained:** No atmospheric emissions of NO<sub>x</sub>, SO<sub>2</sub>, dioxins and ash. Only around 10% of the gas volume discharged by wet oxidation compared to incineration [71].

- Improved De-watering: Research has demonstrated that the residual solids left over from wet oxidation are considerably easier to de-water than the original biosolids [4].
- Water Removal: No need for water removal prior to treatment as it is a liquid phase process, therefore represents a considerable saving in energy compared to thermal processes which require low moisture contents in order to be successful.
- Treatment ability: Wet oxidation is capable of treating high-strength industrial wastewater which is not amenable to biological treatment [72–74].

The results presented later in Chapter 5 and Chapter 6 of this thesis reinforce the effectiveness of wet oxidation as a treatment technology for municipal biosolids.

## 2.5 Historical Uses of Wet Oxidation Processing

Wet oxidation was originally developed to treat spent pulping liquor from paper mills in 1912 [55]. It has since been applied to a variety of industrial waste streams that are not amenable to traditional biological treatment. This section describes the main waste streams that wet oxidation has been applied to, and discusses the important observations relevant to this study.

### 2.5.1 Pulp and Paper Mill Liquor

The pulp and paper industry is one of the largest industrial users of water and produces a variety of wastewater streams which are harmful to the environment. The resulting effluent contains toxic and non-biodegradable organic compounds such as sulfur compounds, organic acids, chlorinated lignins, pulping chemicals and other inorganic compounds [5, 43, 44, 75].

These compounds, in particular lignins, resist degradation by conventional biological wastewater treatment. However it was discovered that the dissolved and suspended compounds could be combusted in liquid form using high pressure air at an elevated temperature. Using temperatures of around 300°C resulted in a 95% destruction of organic material [54]. Pulp and paper mill effluents have been the focus for many researchers and it has been widely demonstrated that wet oxidation is a very effective treatment process [44, 47, 75, 76]. Before wet oxidation, pulp mill liquor was often discharged untreated, or de-watered, before being fed into an incinerator [77].

### 2.5.2 Petrochemical Spent Chemicals

Ethylene spent caustic is a caustic by-product from the refinery industry generated by the production of ethylene. It is produced from scrubbing hydrocarbon gases with aqueous sodium hydroxide to strip hydrogen sulphide and carbon dioxide from the gas stream. The caustic effluent can be successfully treated with wet oxidation to destroy the sulphides by converting them to sulphuric acid which helps to neutralise the high pH of the effluent. This process typically operates at a temperature range of 120 to 220°C. Wet oxidation is considered state-of-the-art for ethylene spent caustic treatment and most ethylene plants have a wet oxidation facility on site [43].

Another difficult to treat effluent is the spent caustic streams from petrochemical refineries. These wastewaters are typically laden with sulfides and naphthenic acids depending on the process. Wet oxidation is considered to be a highly successful process for treating refinery spent caustic [43].

While these waste streams are not going to be encountered in this research, it demonstrates that wet oxidation is an effective and very universal treatment technology for wastes which are not amenable to biological treatment.

### 2.5.3 Municipal Biosolids

Wet oxidation was first applied to municipal biosolids in the 1950's. Initially wet oxidation was used at low temperatures and pressures to condition the biosolids which improved de-watering [61]. However at higher temperatures and pressures it was discovered that organic material present can be oxidised into low weight carboxylic acids and CO<sub>2</sub> [68]. Wet oxidation has been shown to be an effective biosolids treatment process and there are now several commercial installations around the world for treating biosolids.

Scion has conducted its own studies using locally available biosolids to investigate its suitability [9], and the results reinforce those described in the literature. As well as a biosolids treatment process, Scion wants to maximise the recovery of useful chemicals from the wet oxidation effluent. This includes ammonia, phosphates and using the carboxylic acid by-products as a carbon source for the BNR stage of the Bardenpho wastewater treatment plant. BNR treatment plants were not widespread when authors such as Ploos van Amstel [55] were investigating wet oxidation and therefore the original aim of the research was maximum destruction, not value recovery.

Kinetic models for wet oxidation are available in the literature (discussed in Section 2.6), but they usually characterise the reaction in terms of one or two lumped

global parameters, usually measured in terms of COD. At the time of writing, models which predict the concentration of a suite of intermediate liquid and gaseous reaction products are not available.

## 2.5.4 Pure Components (Model Compounds)

A number of pure compounds have been subjected to wet oxidation, in order to characterise the reaction pathways and associated kinetics that proceed under wet oxidation as they are convenient to study. These compounds include acetic acid, glucose, phenol, and ethanol and are briefly discussed in the following section.

### 2.5.4.1 Glucose

Van Amstel [55] performed experiments using a glucose solution as a model sludge under a variety of conditions listed in Table 2.11 to obtain insight into the wet oxidation process. Glucose was chosen as a biosolids substitute, as it represented the carbohydrate fraction found in municipal biosolids.

Table 2.11: Reaction conditions for the wet oxidation of glucose by [55].

Reactor type	CSTR and bubble column
Experiment type	Semi-batch and continuous
Oxidant	Air
Pressure	50 bar
Temperature	170–260°C

Because of the large number of potential reaction products and pathways that are possible during glucose oxidation, the COD of the solution was tracked instead of every intermediate component. As shown in Moreno *et al.* [65], the reaction pathways that occur are very complex, and show why it is not realistic to monitor every intermediate product. An interesting observation was that upon injecting glucose into the reactor, it took several minutes for noticeable oxidation to take place. It is suspected that this lag is due to the time needed for radicals to form. The published results by Moreno *et al.* [65] demonstrate that temperature has the greatest influence on the rate and extent of COD reduction over other process variables such as oxygen pressure.

Investigation into the effect of preheating the feed material showed that there is an optimum level of preheating which increases COD removal. Too much pre-heating reduced the COD removal and it was theorised that this was due to refractory intermediates being formed by hydrolysis reactions occurring in the pre-heater, which

then resisted subsequent oxidation.

#### 2.5.4.2 Acetic Acid

It has been demonstrated that low mass carboxylic acids are the common refractory compounds formed by wet oxidation of organic wastes [78], with acetic acid being the most dominant. Shende and *et al.* [67, 79] performed wet oxidation of acetic and formic acids at a variety of operating conditions shown in Table 2.12.

Table 2.12: Reaction conditions for the wet oxidation of acetic acid as investigated by [79].

Reactor type	CSTR
Oxidant	Oxygen
Pressure	25–60 bar
Temperature	300–320°C
Experiment duration	180 minutes

Their results show that acetic acid oxidation produced no intermediate compounds, and is oxidised directly into  $\text{CO}_2$  and  $\text{H}_2\text{O}$ . At the conditions investigated, approximately 20% of the acetic acid was oxidised to  $\text{CO}_2$  with the remainder remaining in solution. This demonstrates the difficulty in its chemical oxidation. Other studies at higher temperatures have shown that it is possible to degrade acetic acid, but extreme temperatures and pressures are required [79]. Although this would appear to be a significant problem, acetic acid is readily degraded by micro-organisms, so alternative biological process can be used for its removal. The activation energy and kinetic expression reported were similar to other published work by Li *et al.* [57].

The study of acetic acid is of particular importance as it is the dominant refractory compound. Unlike typical wet oxidation scenarios where the objective is complete oxidation, the objective of this study is to maximise acetic acid production, as in this application it is a desired product, hence it is important to know the conditions in which it is formed and oxidised.

#### 2.5.4.3 Phenols

Phenols have been studied in detail in the context of wet oxidation as they are present in many difficult-to-treat aqueous wastes [80, 81]. 4-Chlorophenol is a by-product of the bleaching process in paper mills, and a result of disinfecting water through chlorination.

Molina [5] investigated the degradation of 4-chlorophenol and several other chlorophe-



nols under a variety of conditions, using oxygen and hydrogen peroxide as oxidants. Wet oxidation and wet peroxide oxidation were shown to be extremely effective at treating effluents containing 4-chlorophenol with complete removal obtained. It was shown that hydrogen peroxide was more effective and was able to effect complete removal at the lowest temperature and concentration, while oxygen needed a minimum temperature of 160°C to achieve the same result.

Table 2.13: Reaction conditions investigated by [5] for the wet oxidation of 4-chlorophenol.

Reactor type	CSTR
Oxidant	Oxygen and H <sub>2</sub> O <sub>2</sub>
Pressure	5, 7.5, 10 and 15 bar
Temperature	100, 150, 160, 175 and 190°C
Experiment duration	90 minutes

Above the minimum of 150°C, the temperature increased the rate of reaction, as did increasing the partial pressure from 5 to 10 bar. Increasing the partial pressure in the reactor above 10 bar did not change the rate of reaction. Interestingly, they also observed an initial lag before appreciable oxidation took place, which has been documented by other authors [55] despite the fact that they were oxidising different compounds. This initial lag may need to be accounted for in the developed kinetic models.

Although chlorophenol oxidation is not directly relevant to this research, the comparison between gaseous and liquid oxidants and subsequent issues with mass transfer is interesting because it implies that mass transfer limitations encountered could be potentially overcome by changing to a liquid oxidant such as hydrogen peroxide.

#### 2.5.4.4 Ethanol

Koido [82] studied wet oxidation of ethanol under both subcritical and supercritical reaction conditions. Koido demonstrated that acetaldehyde and acetic acid were the main intermediate compounds and the gas phase products were primarily CO and CO<sub>2</sub>.

A set of four consecutive reactions was proposed as a reaction pathway to adequately describe the behaviour of the wet oxidation of ethanol, which was modelled as a set of Arrhenius rate expressions. Ethanol and other alcohols are of particular interest because they have been identified as potential intermediates in the oxidation of biosolids, and therefore their behaviour under wet oxidation is of interest. As identified by Koido, ethanol oxidation is highly exothermic, and the heat of reaction

Table 2.14: Reaction conditions used by [82] for the wet oxidation of ethanol.

Reactor type	CSTR
Oxidant	Oxygen
Experiment type	Continuous
Pressure	25 bar
Temperature	260–350°C
Residence time	20.1 to 119.5s

of this occurring may need to be specially taken into account in the models developed as part of this research.

## 2.6 Modelling of Wet Oxidation

Municipal biosolids contain a complex mix of organic compounds and their composition and concentration can vary day to day. The reaction pathways that occur are often unknown or very complex. It has been shown that even the wet oxidation of a pure substance such as phenol or glucose decomposes via numerous reaction pathways [48, 65] and therefore it is necessary to use a simplified kinetic model which includes only the dominant pathways and using lumped components.

The primary objective of the wet oxidation stage in the TERAX process is to break down organic and inorganic waste compounds into VFAs, ammonia and phosphate and maximise the reduction in solids volume. Unlike many previous studies on wet oxidation kinetics, where the objective is maximising the total COD reduction, this research aims to maximise, quantify and predict the production of intermediates. The result of this means that there will be less reduction in total COD and an increase in soluble COD. For this reason, an understanding of the likely reaction mechanisms will be required for kinetic model development. These will be used for state and parameter estimation to enable efficient experimental design, optimal operation, and assist in the design of a production-scale TERAX plant.

The specific aims of kinetic modelling for the wet oxidation stage of the TERAX process are to predict:

1. Lumped parameters pCOD, sCOD and acetic acid
2. Ammonia concentration
3. Off gas composition (CO, CO<sub>2</sub> etc)  
and also if possible
4. The fate of other VFAs
5. Oxygen mass transfer limitations

The following section discusses simplified kinetic models available in the literature and their suitability in modelling the kinetics for this process. These will be further developed in Chapter 5.

## 2.7 Kinetic Models for Wet Oxidation

One of the first to propose a simplified model of biosolids degradation was Takamatsu *et al.* [83]. Their research focused on the thermal degradation stage of the sludge which occurs before an oxidant is added to the reactor. They proposed that sludge consisted of four basic components; solid matter (waste), soluble non-evaporative matter at 120°C, soluble evaporative matter at 120 °C and water. The weight and COD of the three components were regarded as the state variables in the model, and the reaction pathway is shown in Fig. 2.12.

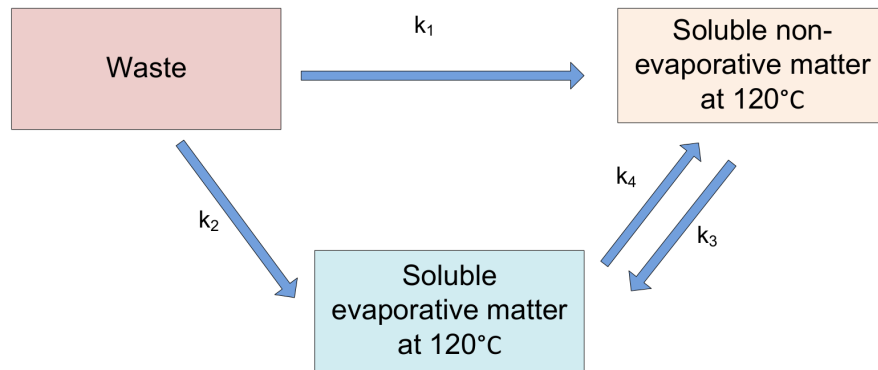


Figure 2.12: One of the first lumped kinetic models for wet oxidation, proposed by [83].

Instead of using real biosolids, this study used artificially created biosolids using a mixture of peptone, glucose, potassium chloride, sodium phosphate and manganese sulfate. One noted limitation is that soluble matter was divided into two groups because of limitations in experimental technique rather than because of any physical significance, however it was assumed that the soluble evaporative matter would contain the reaction products. Despite the fact that this study focused purely on hydrothermal treatment with no oxidant, the proposed kinetic model is important as hydrolysis reactions occur during the warm-up phase as well as during the oxidation process itself.

Van Amstel *et al.* [68] studied the kinetic behaviour of wastewater sludge undergoing oxidation using wastewater from seven different municipal wastewater treatment plants. They characterised the sludge into three components: high reactivity, intermediate reactivity and no reactivity. Their model included several additional modelling assumptions: that the chemical reaction only occurs in the liquid phase,

there were negligible hydrolysis effects, a mass transfer limitation existed around the gas bubbles, and there was a first order chemical reaction for sludge as well as oxygen. It was noted by Mishra *et al.* [6] that the non-reactive fraction that was observed was due to the sub 300°C temperature range which promotes the formation of difficult to oxidise carboxylic acids.

Interestingly, their results for the oxidation of sludge from different wastewater treatment plants demonstrated that there was little variation in COD reduction. They also showed that temperature has a significant effect on COD reduction, while changes in pressure have less of an effect.

Foussard *et al.* [58] also performed kinetic studies using municipal wastewater. Owing to the elevated temperatures used in their study, which ranged up to 327°C (600K) they did not observe the non-oxidisable fraction observed by Van Amstel *et al.* [68]. Because of this, their model only included two states, which were characterised as easily oxidised components, and not easily oxidised components. These were modelled as two parallel first order reactions, with the easily oxidised compounds forming 60% of the feed and not easily oxidised components forming the remaining 40%.

One particular kinetic model which has been the basis for many future studies on wet oxidation was developed by Li *et al.* [57] who proposed a more generalised model for wet oxidation. It is based on a simplified reaction scheme similar to Takamatsu *et al.*, involving the formation and destruction of rate controlling intermediate compounds. Research on wet oxidation has shown that short chain carboxylic acids, aldehydes and alcohols are major intermediates, with acetic acid being the primary intermediate compound. Based on this work, Li *et al.* proposed the reaction pathways that are illustrated in Fig. 2.13;

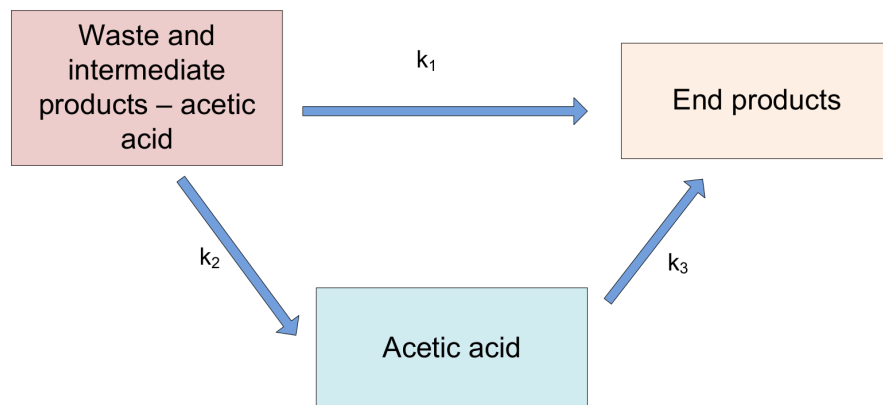


Figure 2.13: The widely cited ‘Triangular’ kinetic model proposed by [57].

where  $k_1$ ,  $k_2$  and  $k_3$  are the overall reaction rate constants, and the concentrations for each compound in this model are expressed in terms of COD.

Li *et al.* show that the generalised kinetic model is a reasonably good approximation of the reaction kinetics occurring in wet oxidation of wastewater sludge and this has been verified independently, [49, 54].

For the majority of wet oxidation reactions, complete oxidation is never achieved, as the operating temperature is not sufficient to oxidise acetic acid to carbon dioxide and water since the activation energy for  $k_3$  in Fig. 2.13 is very high. Near complete oxidation is typically only achieved over 300°C.

Many researchers who have investigated wet oxidation of sludge have focused on determining the pathways and reaction conditions which result in total destruction of the sludge. However Khan *et al.* [69] investigated the transformation of raw sludge into its intermediate components, not total destruction, in order to maximise the effectiveness of downstream biological treatment.

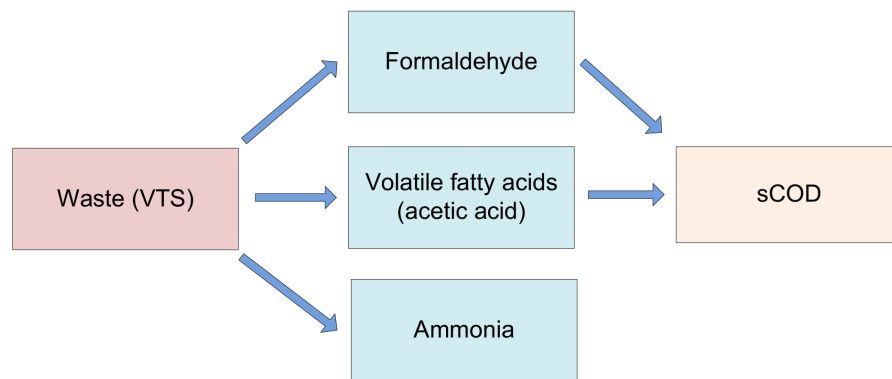
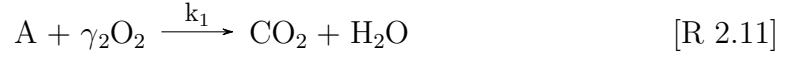


Figure 2.14: Reaction scheme proposed by [69], who first developed a model with additional intermediate compounds.

Because the focus of their work was on making the wet oxidation effluent amenable to further biological processing, additional intermediate components were included in their model. The components selected for evaluation were Volatile Total Solids (VTS), ammonia, soluble COD, acetic acid and formaldehyde. This study was the first to include both real chemical compounds as well as lumped components in their model, and the reaction pathways are shown in Fig. 2.14.

Their research also demonstrated that ammonia was an important product in wet oxidation with ammonia production increasing with higher temperatures. Acetic acid production was shown to be strongly temperature dependant, making up around 20% of VFA at 200°C and 90% at 300°C. They also importantly noted that wet oxidation is a flexible, but predictable, treatment process.

Zhang *et al.* [48] investigated the effectiveness of the wet oxidation process on paper mill effluent with the addition of a catalyst. They proposed a simple model which consists of two parallel first order reactions which are shown in Reaction R2.11 and Reaction R2.12.



All the compounds present in the wastewater are lumped together into compound A, while B represents intermediates formed during the wet oxidation process. The concentrations of A and B are expressed in terms of Total Organic Carbon (TOC). Their results show reasonable fit to the experimental data, however all model results asymptote to a limiting finite value, whereas the experimental data shows a slow but steady reduction in TOC.

Interestingly, they state that  $CO_2$  was the only observed gas phase product produced. In comparison, the results obtained for the experimental investigation conducted as part of this thesis and is presented in Chapter 5 contains a number of compounds including  $CO_2$ ,  $CO$ ,  $H_2O$  and  $H_2$ .

Chacuk *et al.* [84, 85] simulated the degradation of wastewater sludge in a continuous flow bubble column reactor. They proposed that sludge degrades via the reaction pathways illustrated in Fig. 2.15. However with a lack of experimental data it is unknown how valid the proposed pathways are.

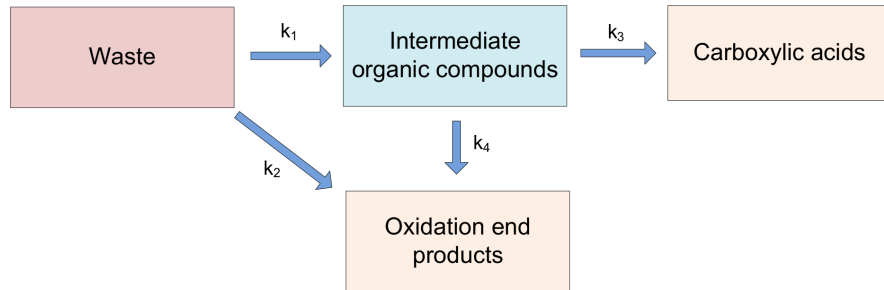
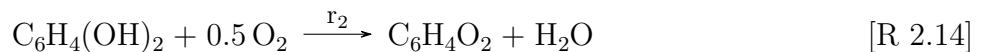
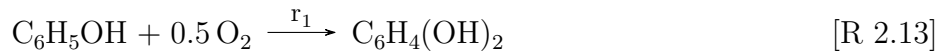
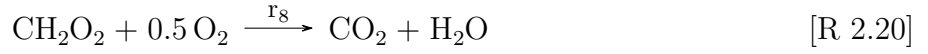
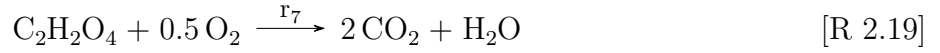
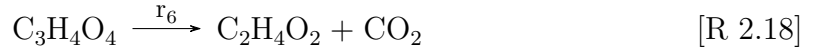
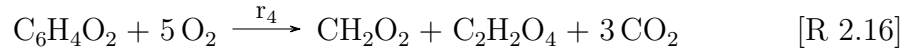


Figure 2.15: Kinetic pathways for wet oxidation proposed by [84].

Eftaxias *et al.* [86] explored the kinetic pathways of catalytic phenol oxidation. Rather than pursue global kinetic expressions or COD based lumped kinetic models like Li *et al.* [57], they proposed a kinetic model which accounts for all detectable intermediate products using air as an oxidant in a trickle bed reactor. Reaction rate constants  $r_1$  to  $r_8$ , shown in Reaction R2.13 to Reaction R2.20, were fitted using experimental data. They demonstrated that their kinetic model gives a 7.8% error on average at different reaction conditions.





The reaction pathways R2.13 to R2.20 clearly show that even for a pure compound such as phenol, there can be a large number of reaction pathways, and intermediate products. With biosolids, it would be unrealistic to track the concentration of all components and reaction pathways owing to the huge range of chemical compounds and concentrations. For these reasons it is likely that some lumping of components, or the use of surrogate compounds, will be necessary to keep the reaction models manageable.

Studies by Shanableh and Jomma [23, 87] have confirmed that under sub-critical wet oxidation, biosolids undergo non-oxidative hydrolysis reactions. These reactions form soluble organic compounds which are subsequently oxidised. However Shanableh explicitly included this non-oxidative reaction step in their kinetic model. Their results show that the hydrolysis reactions are initially faster, which produces an accumulation of soluble organics. This is shown by the initial increase in soluble COD, which then declines as it is removed by oxidation reactions.

The kinetic expressions proposed by Shanableh were Arrhenius expressions in the form of:

$$k_{\text{COD}} = 51280 \exp\left(\frac{-E_a}{RT}\right) \quad (2.2)$$

$$k_{\text{PCOD}} = 9610 \exp\left(\frac{-E_a}{RT}\right) \quad (2.3)$$

$$\text{COD} = \text{COD}_{\text{initial}} \exp(-k_{\text{COD}}t) \quad (2.4)$$

$$\text{PCOD} = \text{PCOD}_{\text{initial}} \exp(-k_{\text{PCOD}}t) \quad (2.5)$$

$$\text{SCOD} = \text{COD} - \text{PCOD} \quad (2.6)$$

Shanableh [88] further investigated the oxidation of biosolids over a wider range of temperatures from 200 to 450°C in a continuous flow tubular reactor. He proposed the same first order algebraic kinetic models shown above to describe the degradation that was observed, but re-fitted the rate coefficients to the model from the experimental data.

While the model showed adequate fit with the experimental data, it is not sufficiently generic for our application. Like many of the models in the literature, it does not

predict nutrient concentrations, nor other intermediate products in sufficient detail.

### 2.7.1 Kinetic Summary

The suite of reaction pathways described in the previous section predict the reduction in total COD, or include the concentration of a single lumped intermediate compound on a COD basis. One of the objectives of this research is to further model the intermediates and the key desirable, and undesirable, end products.

Few of the lumped kinetic models available in the literature model the change in nutrients during wet oxidation (ammonia and phosphate) or off-gas products such as carbon monoxide and carbon dioxide.

The standard first-order Arrhenius expression has been used to model all the reaction kinetics apart from Eftaxias *et al.* [86] who used the Langmuir-Hinshelwood expression because of the use of a catalyst in their experiments.

At the time of writing, the wet oxidation models in the literature do not take into account the easily adjustable experimental parameters such as pressure or mixing which this study will explore, with the majority of models only using temperature as a user changeable parameter. A summary of the kinetic models in the literature is given in Table 2.15

Table 2.15: Summary of published wet oxidation kinetic models.

Investigators	Feed material	Model inputs	Reaction pathways	Validated states
Takamatsu <i>et al.</i> [83]	Mixture of peptone, glucose & metal salts	O <sub>2</sub> , T	3	3
Van Amstel & Rietema [55]	Municipal biosolids	O <sub>2</sub> , T, P	2	1
Foussard <i>et al.</i> [58]	Municipal biosolids	O <sub>2</sub> , T	2	1
Li <i>et al.</i> [57]	Municipal biosolids	O <sub>2</sub> , T	3	1
Khan <i>et al.</i> [69]	Municipal biosolids	O <sub>2</sub> , T	4	4
Zhang & Chuang [48]	Kraft pulp sludge	O <sub>2</sub> , T	2	1
Verenich & Kallas [62, 89]	Pulp mill liquor	O <sub>2</sub> , T	4	1
Shanableh [88]	Municipal biosolids	O <sub>2</sub> , T	2	2
Chacuk & Imbierowicz [84]	Municipal biosolids	O <sub>2</sub> , T	4	0

For this research, the following real and pseudo-components are of particular interest; particulate COD (pCOD), soluble COD (sCOD), ammonia, acetic acid, other dominant volatile fatty acids, oxygen consumption, as well as carbon dioxide and



carbon monoxide production. While not all these compounds will be used in the final kinetic model, they will be recorded to gain insight into the wet oxidation process of real biosolids. To keep the analysis and modelling manageable, a COD basis will be used for all concentrations apart from the gaseous products.

## 2.8 Mass Transfer Considerations

The overall reaction rate in wet oxidation is governed by two steps. The first is the mass transfer of oxygen from the gas to liquid phase, and the second is the reactions occurring in the liquid phase. The other forms of mass transfer discussed in Section 2.4.3, such as the release of dissolved gasses, are usually assumed to be not rate limiting.

Enhancing the oxygen mass transfer from the gas to liquid phase can be performed by increasing the overall mass transfer coefficient  $k_{La}$ , or adjusting the operating conditions to improve the oxygen solubility in the liquid phase. The oxygen solubility is strongly dependant on temperature and pressure, and in general rises significantly with increasing temperature (above 100°C) and pressure [90]. The overall mass transfer coefficient is dependant on physical parameters, such as reactor geometry, stirrer type, gas flow rate and liquid properties and their effect on the system dynamics such as gas-holdup, bubble diameter and flow regime [51, 91, 92].

The overall mass transfer coefficient can also be heavily influenced by compounds present in the reactor. It has been shown that the presence of VFAs, such as acetic acid and various alcohols can increase the overall mass transfer coefficient by up to 300% [93]. It was speculated that the addition of VFAs prevented bubble coalescence.

An interesting observation was made by Van Amstel [55], who discovered that at temperatures of around 180°C, the mass transfer limitations could be neglected, while at 290°C the reaction rate was largely determined by the rate of mass transfer.

The most common approach to modelling the gas liquid mass transfer in bubble column reactors is referred to as the “Stagewise Backmixing” model, originally developed by Debellefontaine *et al.* [94, 95]. This model divides the reactor into two columns of  $n$  cells (between 10 to 30), shown in Fig. 2.16, where each cell is treated as a small CSTR. The input and output of each CSTR are connected to the previous and following CSTRs, with additional axial transfer term between the gas and liquid cells. Owing to its simplicity and ease of implementation, this model is commonly used and has been shown to closely approximate the behaviour of bubble column reactors [64, 84].

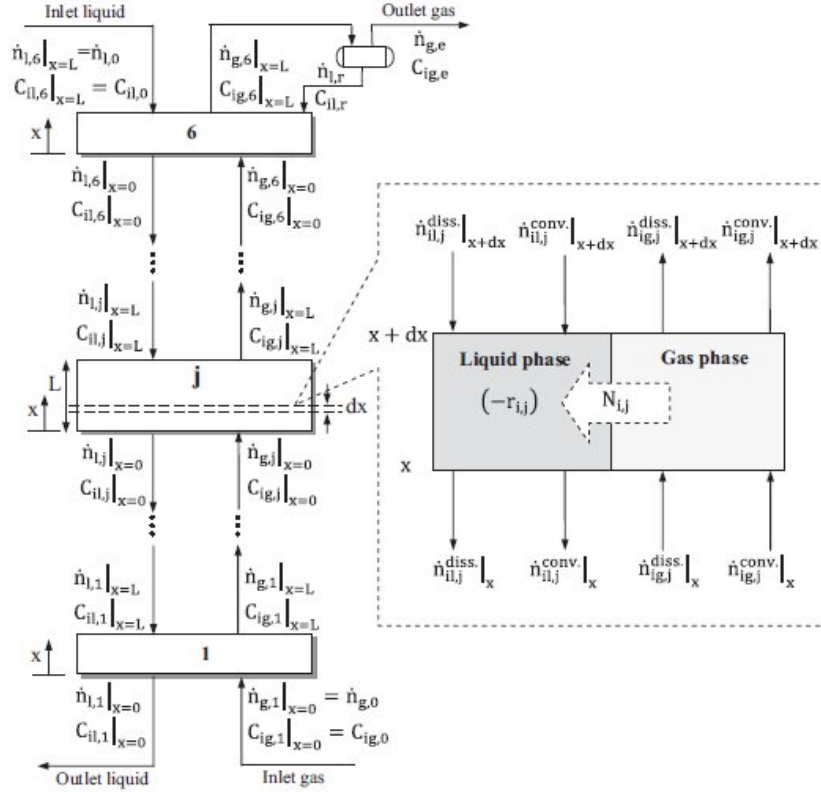


Figure 2.16: The gas-liquid mixing scheme as part of the stagewise-backmixing model, diagram from [64].

Benbelkacem and Debellefontaine [96] studied gas-liquid mass transfer effects on the oxidation of fumaric acid using ozone in a bubble column reactor, with a specific focus on modelling the reactions occurring in the liquid film and liquid bulk. Their model was capable of predicting the fraction of the reaction that was occurring in the film or bulk during the reaction period and was validated against experimental data. Interestingly, at the beginning of the reaction, 90% of the reactions were occurring in the film, while towards the end of the reaction period, almost all of the reactions were occurring in the liquid bulk.

Bubble column, plug flow, and CSTR reactors are the most common reactor types in use for wet oxidation. Bouaifi *et al.* [97] showed that the gas-liquid mass transfer area was higher in bubble column reactors when compared to CSTRs.

Much of the research into mass transfer limitations in wet oxidation has been conducted in bubble column reactors. Mixing models such as stagewise-backmixing have been proposed to account for the effect of mixing parameters [94, 98–100]. However, the effect of stirrer speed on the level of oxidation achieved in a CSTR was investigated by Baroutian *et al.* [60]. While the experiments conducted did not directly include changes to the mass transfer area, the results show that increasing the stirrer speed did increase the reaction rate indicating that the experimental conditions were mass-transfer limited to an extent.

Meille *et al.* [101] investigated the effect of stirrer speed on the mass transfer coefficient  $k_{La}$  in small lab-scale CSTRs using the physical absorption of hydrogen. One of their research aims was to compare correlations from the literature for  $k_{La}$  from larger reactors with the experimentally determined correlations for 25 to 300ml CSTRs. They determined that a power law of the form  $k_{La} = AN^B$  adequately captured the effects of the change in stirrer speed on the mass transfer coefficient, where A and B are fitted constants and N is stirring speed in RPM.

### 2.8.1 Summary of Mass Transfer

Mass transfer models have been investigated for both bubble column and CSTR reactors, which are the most common reactor types used for wet oxidation. Scion has wet oxidation facilities that use both reactor types and the intention is that the models developed as part of this research will be sufficiently flexible so that they can be used for both systems.

While reviewing the literature surrounding mass transfer effects in wet oxidation, it is apparent that many researchers who have studied wet oxidation use an excess of oxidant in an attempt to avoid mass transfer limitations while investigating the kinetic behaviour.

## 2.9 A Review of Shortcomings in the Literature

This literature review is focussed on prior research in the wet oxidation process, including municipal biosolids. The review highlights the knowledge gaps such as a systematic characterisation of biosolids oxidation, and the lack of suitably detailed dynamic models to predict the concentration of the intermediate reaction products under anticipated environmental conditions.

Traditionally, the objective of wet oxidation was complete chemical destruction. However with BNR wastewater treatment plants commonplace, the focus has started shifting towards using wet oxidation to produce a suitable VFA carbon source which can be recycled back into the wastewater treatment plant. This changes the focus for the optimal operation of a wet oxidation system.

The available kinetic models do not adequately predict the concentration of the common intermediate products, in particular VFAs, nor do they include the influence of many of the easily modifiable process parameters. Because of these modelling limitations, optimal experimental design cannot be performed, nor can an optimal wet oxidation plant be designed.

Consequently this thesis will undertake the following: (i) perform a detailed characterisation of the biosolids feed material and the wet oxidation samples, with a specific focus on VFAs to allow better prediction of metrics other than simply total COD, (ii) build a kinetic model which predicts the formation and conversion of the dominant compounds under wet oxidation, which allow the concentration of intermediate VFAs to be determined. Finally, this model will be validated to determine its efficacy and suitability as a design tool.

## Chapter 3

# Experimental Methodology and Development

This chapter covers in detail the overall experimental procedure used as part of this study. Prior experimental work to this thesis performed at Scion is discussed in Section 3.1 and the specifics of the wet oxidation experimental systems used in this investigation are given in Section 3.2. The raw feed materials used in the course of the experiments are listed in Section 3.3 and the experimental procedure used is given in Section 3.4. In order to acquire real-time data from the equipment, a data acquisition system was used and is discussed in Section 3.5. The metrics used to characterise the biosolids and the analytical techniques are listed in Section 3.6. The environmental conditions investigated in the experiments are given in Section 3.7 and an overview of mathematical models used as part of modelling the wet oxidation process is discussed in Section 3.8. A more detailed discussion of the model will be left to Chapters 4 and 5.

### 3.1 Prior Experimental Work at Scion

Beginning around 2009, researchers at Scion began conducting wet oxidation experiments under different process conditions using biosolids obtained from the RDC wastewater treatment plant, in addition to testing other waste sources such as paper pulp mill waste [44, 102]. While different temperatures and pressures had been investigated, no systematic study had been completed using the same batch of feed material and analysing the effect of all the environmental parameters of temperature, oxygen partial pressure and mixing parameters.

In order to develop kinetic and mass transfer models that achieve the objectives of this research, an experimental programme was designed to cover the operating

conditions of interest. The use of historical experimental data, in addition to the recent experiments performed for this study was used where possible for parameter fitting and validation which is discussed further in Chapter 5.

## 3.2 Wet Oxidation Experimental Platforms

Scion currently has two wet oxidation experimental systems available, a lab scale stirred reactor, and a pilot plant employing a 300l bubble column reactor. Because the focus of this research was on developing kinetic models of the wet oxidation process, the majority of the experimental work used the lab scale reactor. This was because of the fast turnaround time for experiments, and ease of use. These are described in Chapter 5. Experiments were then performed using the pilot plant to validate the proposed kinetic models and are described in Chapter 6.

### 3.2.1 Lab Scale Reactor

The lab scale wet oxidation system at Scion uses a high pressure stirred autoclave vessel manufactured by the Parr instrument company (model 4540), combined with a Parr 4848 reactor controller which controls reactor temperature and stirrer speed. The sampling and injection system was custom built in-house to enable batch and semi-continuous experiments, as well as on-line liquid and gas sampling. A schematic diagram of the system is shown in Fig. 3.1, and a photograph of the reactor is illustrated in Fig. 3.2.

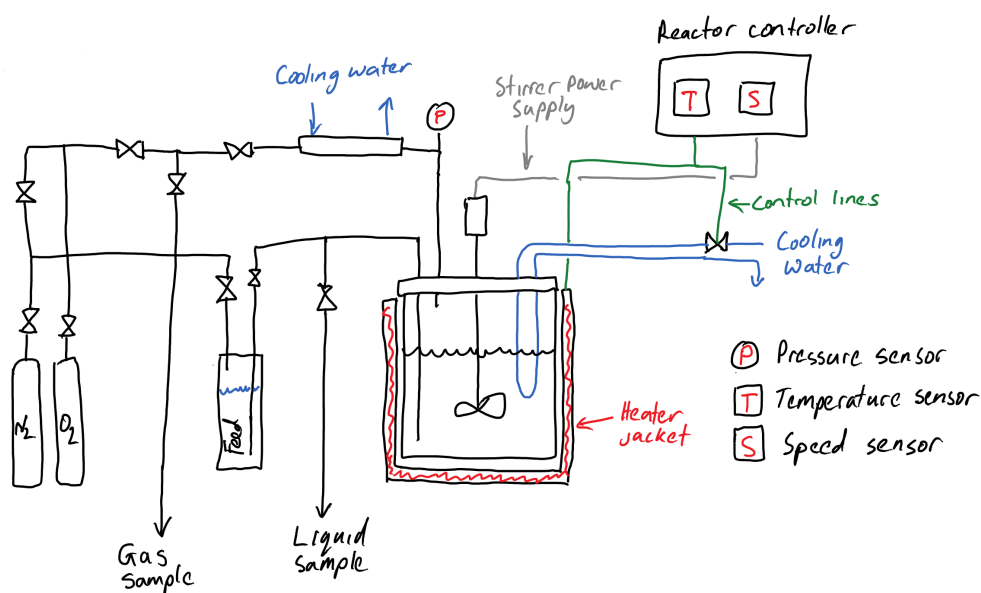


Figure 3.1: Schematic diagram of the lab scale wet oxidation system at Scion which was used in the experimental investigation.



Figure 3.2: The 4540 Parr reactor and 4848 controller (schematic shown in Fig. 3.1).

The Parr 4540 reactor contains a 316 stainless steel reactor vessel of 600ml volume. The maximum operating temperature is 350°C, and pressures up to 345 bar. A magnetically coupled drive is used to connect the stirrer to the drive system outside the reactor. An optional cooling coil has been included which cools the reactor contents using tap water, while heating is provided by an electrical heater jacket. The Parr 4848 reactor controller controls the stirring speed and temperature to the desired set points by operating the heating jacket or a solenoid valve to allow water to flow through the cooling loop.

Fig. 3.3 and Fig. 3.4 show the internal components of the Parr reactor. The adjustable height stirrer impeller is located at the bottom of the shaft next to the liquid dip tube where the feed material is injected, and liquid samples are withdrawn from it to promote fast mixing of the biosolids sample on injection into the



reactor at the beginning of the experiment. It is possible to adjust the height of the stirrer as well as to add multiple impellers to the shaft. Also visible is the cooling coil which is used to cool the reactor contents during the first few minutes of the experiment, as well as cool the reactor contents at the completion of the experiment. The thermowell visible in the background of Fig. 3.3 houses a PT100 thermocouple to sense the temperature of the reactor contents.

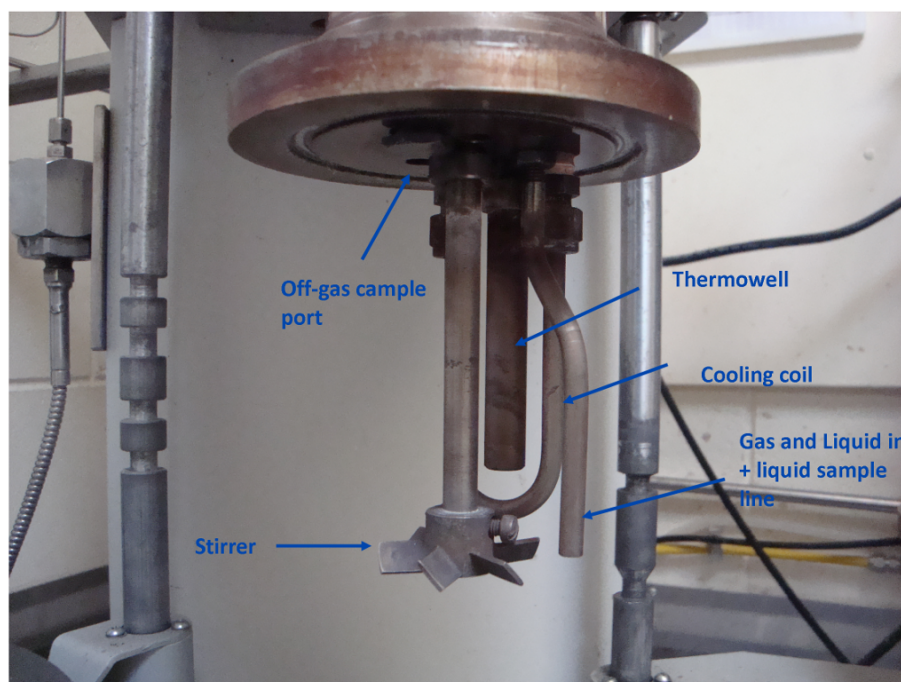


Figure 3.3: Stirrer, cooling coil and dip tube inside the Parr reactor, with the reactor vessel removed.

#### 3.2.1.1 Sampling and Injection System

The gas and liquid sampling and injection system was custom made in-house at Scion to suit the Parr reactor and the types of experiments being performed and is shown in Fig. 3.5. The injection system allows liquid and gaseous reactants to be injected into the reactor vessel during operation. Gases can flow continuously through the reactor system, while liquid material can be injected in discrete amounts in semi-batch mode.

A water cooled reflux condenser has been installed on the gas outlet port of the reactor to condense water vapour and other liquid reaction products out of the gas stream. This allows them to flow back into the reactor under gravity. The reflux condenser's primary job is to prevent water condensing inside the back pressure controller. The gas stream is also heated to 40°C by a heating jacket on the outside of the pipe leading to the back pressure controller as an added precaution against condensation droplets flowing through the controller.



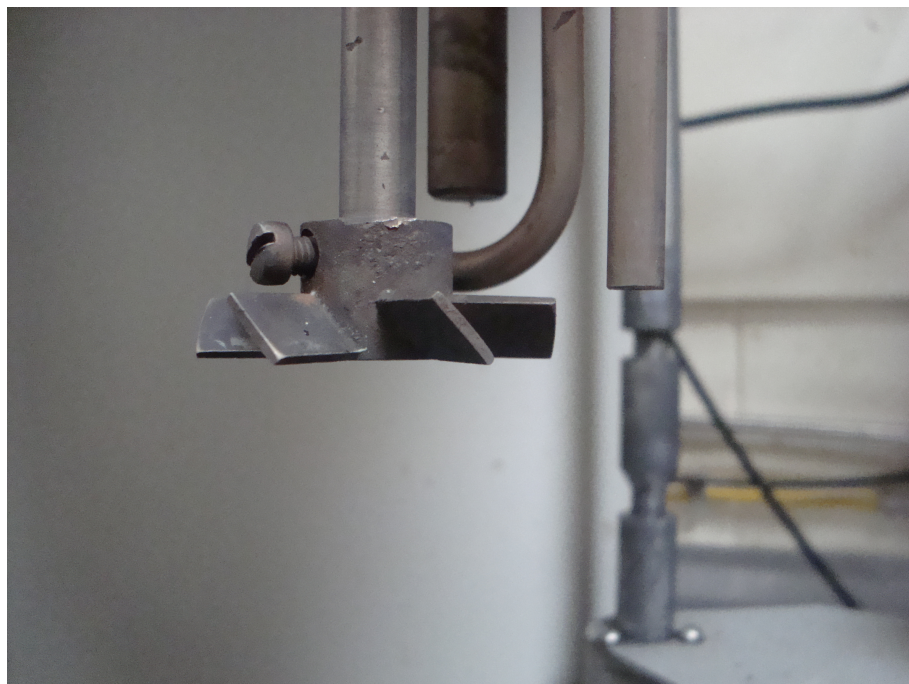


Figure 3.4: The Parr reactor stirrer (detail from Fig. 3.3).



Figure 3.5: The Parr reactor with the added sampling and injection system.

A back pressure controller (Bronkhorst EL-PRESS P-600 Series) is used to control the system pressure in the reactor to the desired set point. A Bronkhorst high pressure mass flow controller (EL-FLOW PN-100 series) is used to control the mass flow of gas (oxygen, nitrogen or air) through the reactor.

Injecting feed material into the reactor involves filling a small autoclave vessel which is used as a holding tank and feed pre-heater. A Berghof HR100 magnetically stirred autoclave of 200ml total volume is used to pre-heat the feed material to 90°C while continuous stirring ensures the mixture is homogeneous. The aim of the pre-heating system is to reduce the temperature gradient inside the main reactor, while the relatively low temperature ensures that hydrolysis reactions do not occur while the feed is being heated. The feed is transferred from the pre-heater to the main reactor via pressure differential using dry nitrogen approximately 10 bar above the system pressure. The Berghof autoclave vessel is fitted with a dip tube which extends to the bottom of the vessel which allows the liquid material to be transferred to the main reactor. A non-return valve prevents material from flowing out of the reactor back into the autoclave. This system can be used to provide batch and semi-batch operation by continually injecting feed samples at the required interval, although it is generally used to inject material only at the start of the experiment.

The Parr 4548 reactor is equipped with a dip tube which extends to the bottom of the reactor vessel to allow liquid samples to be withdrawn. These samples are quenched upon removal via an air cooled sampling loop to stop any further reaction. Incoming gas also flows through this tube, so that when operating in continuous gas mode, gas is bubbled through the reactor contents to improve oxygen mass transfer between the gas and liquid phases.

A sampling port has been used in the reactor head to allow gas in the reactor headspace to be withdrawn, and to allow for gas flow out of the reactor when using continuous flow.

The sampling system shown in Fig. 3.6 has been designed to allow discrete liquid samples to be withdrawn during operation. The system allows the sampling lines to be flushed after each sample with water and dried using dry nitrogen. Withdrawing liquid samples is achieved using a system of Swagelok valves rated for the pressures and type of liquid being used. Opening the first valve fills the sampling coil with fluid from the reactor which has a total volume of 10ml. This allows a fixed volume to be withdrawn, and allows the sample to cool before being withdrawn. The first valve is then closed, and the end valve opened slowly to allow the cooled sample to be collected in a sampling tube. This procedure is repeated to obtain the required 20ml sample.

The lower valve is a two position valve which is used to select between tap water and

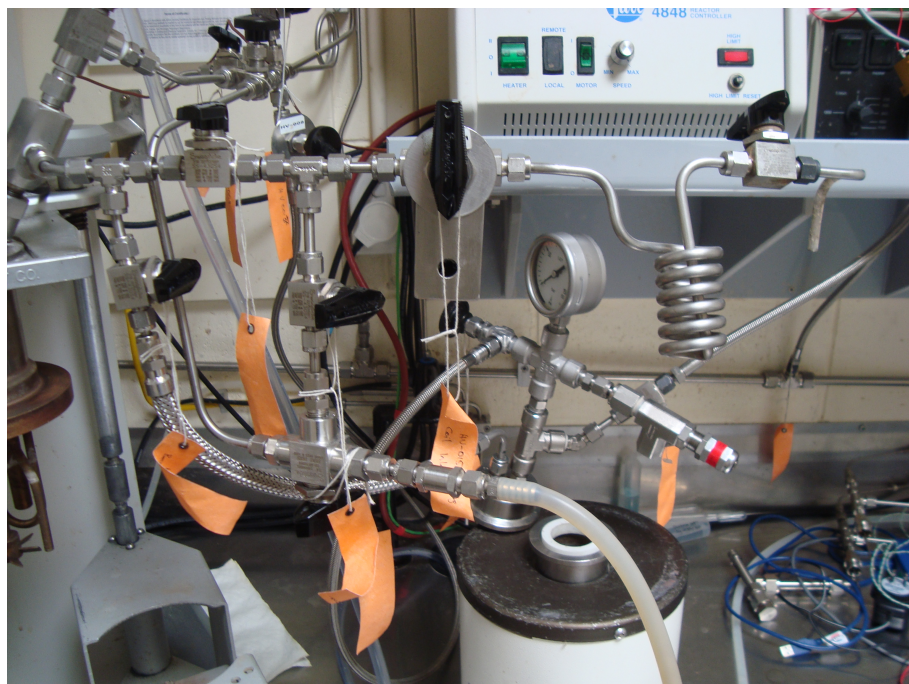


Figure 3.6: A close-up of the liquid sampling and flushing system.

dry nitrogen for flushing the sampling loop. After each sample has been withdrawn, the sampling loop is first flushed with water before purging with dry nitrogen to prevent sample contamination.

Gas samples are withdrawn from a sampling port at the top of the reflux condenser. The sampling port is connected to a high pressure Valco selector valve which fills a sampling loop with gas and cools the sample to 10°C using a temperature controlled peltier cooler. The Valco valve then discharges the gas sample in the sample loop into a Tedlar gas sample bag. This process is repeated several times until approximately 20ml of gas has been collected.

After the reflux condenser was added there was concern that the gas sample present at the top of the condenser was not representative of gas in the reactor headspace. It was therefore decided to only take a gas sample at the end of the experiment when the condenser can be purged and a representative sample obtained. However the reflux condenser was removed for some of the experiments described later in Section 5.5 so that intermediate gas samples could be obtained.

### 3.2.1.2 Stirrer Modifications

An important modification was made during the course of the experimental investigation to the stirrer drive system on the lab scale reactor. The original motor was replaced with a much smaller geared DC motor to allow current measurements to be performed. The motor originally fitted was a 1/4 HP 180V DC motor which





Figure 3.7: Parr reactor with the replacement stirrer motor fitted.

was significantly oversized given the size of the impeller and viscosity of the working fluid, and therefore prevented useful measurements of the change in motor current. The original speed controller also struggled to operate the original motor at low RPM.

The aim of measuring the motor current is to infer information relating to the change in viscosity of the fluid in the reactor during operation. Tests performed using a geared (19:1) brush type 12V DC motor showed that the increase in current drawn by the motor when water was added to the reactor was very small compared to the current required to overcome the friction in the magnetic drive mechanism. As expected there was also considerable electrical noise present in the measurements. Despite this, the current measurements appeared to be repeatable. The reactor equipped with the new stirrer motor is shown in Fig. 3.7.

### 3.2.2 The TERAX Pilot Plant Reactor

Section 3.2.1 described the bench-scale reactor used in this research. However for further studies it was desirable to scale-up this reactor to pilot plant scale.

The second stage of the TERAX pilot plant consists of a wet oxidation stage. The

pilot plant wet oxidation unit was designed by a local engineering firm to Scion's specification. It consists of a pair of 300l bubble column reactors and is capable of operating in batch, semi-batch with continuous gas flow, and fully continuous liquid feed and gas flow. The reactors can be configured in series, or the second reactor can be bypassed, depending on the requirements of the experimental programme. A schematic diagram of the main reactor components is shown in Fig. 3.8.

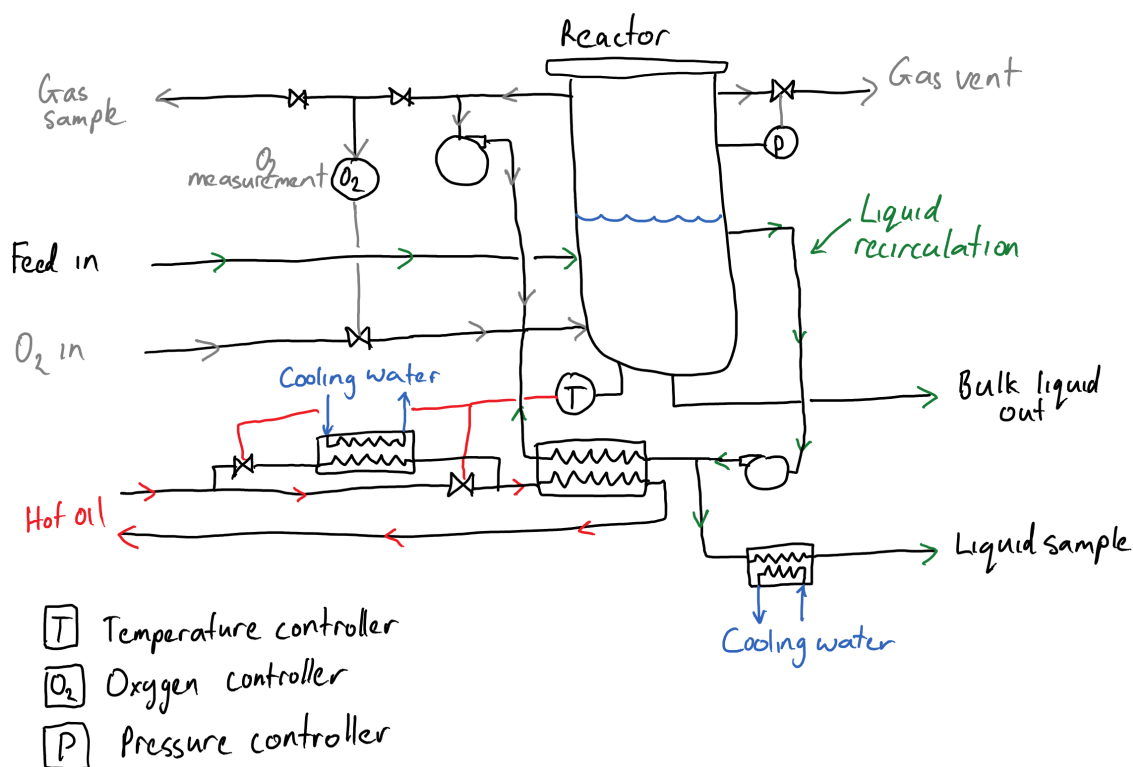


Figure 3.8: A schematic diagram of the TERAX wet oxidation pilot plant bubble column reactor and recirculation systems. (The second reactor is not shown in this figure).

To begin an experiment, the feed tank in Fig. 3.9 is filled with biosolids at the required concentration, and is pumped into the main reactor via a high pressure pump which is capable of operating while the reactor is at operating pressure. An impeller in the feed tank keeps the solids from settling while the main reactor is being filled. Oxygen gas is fed into the reactor from a large high pressure oxygen cylinder through a regulator to an automated valve which is under PID control. This admits oxygen into the system to keep the oxygen concentration in the reactor headspace at the desired set point.

The main reactor, shown in Fig. 3.10, incorporates liquid and gas re-circulation to promote mixing of the two phases, with the gas flow being co-current to the liquid. The re-circulated liquid is passed through a large double pipe heat exchanger. This is used to maintain the operating temperature if the heat released by the oxidation reactions is insufficient, and it is also capable of cooling the system, but at reduced



Figure 3.9: The TERAX wet oxidation pilot plant feed tank and high pressure feed pump. The feed pump is to the right of the feed tank.



Figure 3.10: The main bubble column reactor with the liquid recirculation pump in the foreground.



Figure 3.11: The secondary bubble column reactor and discharge tank.

capacity. The re-circulated gas stream is mixed with the liquid stream before passing into the bottom of the reactor vessel. Oxygen gas, which can be added while the system is operating, is also mixed into this line.

Provisions for removing samples of liquid and gas have been provided in the design of the equipment and can be performed while the system is operating. Liquid samples are withdrawn after the liquid re-circulation pump. Opening a valve fills a sample loop which is in the form of a small double pipe heat exchanger that is cooled with tap water. This quenches the sample to stop any further reactions after it has been removed. After closing the first valve, the end valve can be opened which will release the sample into the sample container.

Fig. 3.11 shows the secondary reactor, which was not used in this research, and the discharge tank which is used by both reactors.

Gas samples are withdrawn from the gas re-circulation line before it passes through the gas re-circulation pump. The gas sample passes through a pressure regulator to drop the pressure to slightly above atmospheric. A provision for attaching a gas sample bag is also available. This low pressure gas line is also connected to the on-line oxygen concentration sensor which forms part of the reactor control system.

The reactor control system has three PID loops which control reactor temperature, pressure and oxygen concentration. Temperature is regulated using a double pipe heat exchanger which is heated with hot oil from a gas fired heater. A smaller heat exchanger, in series with the oil heater, is used cool the system, if needed, with tap water. Both systems are controlled with valves that regulate the flow of oil by the temperature controller. The reactor pressure controller vents gas from the reactor via a scrubber in order to prevent excessive pressure, while pressure can be increased by adding additional oxygen to the system. The oxygen controller works in tandem with the pressure controller, as they both manipulate the flow of oxygen to keep the oxygen concentration at the required set point.

The pilot plant was constructed based on the outcomes from preliminary experiments conducted by Scion. However a number of challenges have been identified in the operation of the pilot plant, with poor reactor oxygen control being a key problem, resulting in the formation of undesirable end products such as carbon monoxide. One of the aims for developing a kinetic model is to improve the oxygen control, as well as to assist in the design of a full scale wet oxidation plant.

While both wet oxidation systems are available, the experiments have primarily been conducted on the lab scale reactor because of ease of use and the short turnaround between experiments. Provided the feed material is the same, the kinetic model developed on the lab scale reactor should be applicable to the pilot plant. However,

the mass transfer effects will be significantly different because of the different reactor type and the large difference in reactor volume. Chapter 6 will test this hypothesis.

### 3.3 Biosolids Feed and Materials

The municipal biosolids feed material used for the experiments was obtained from the RDC wastewater treatment plant. The biosolids consisted of approximately 40% primary and 60% secondary sludge obtained from the belt filter presses at the RDC plant. The biosolids were subsequently fermented in the TERAX 2000l pilot plant anaerobic fermenter at 35°C under pH control of between 5.5 and 6.2. Samples of the fermented sludge were frozen at -20°C until required. The characteristics of the biosolids are shown in Table 3.1.

Table 3.1: Characteristics of the municipal biosolids from the RDC wastewater treatment plant used for the experimental investigation.

Characteristics	(mg/l)
TSS	14872±542
VSS	12082±440
tCOD calculated	24720±901
tCOD measured	19593±839
pCOD	17640±643
sCOD	7080±258
sDOC	1996±72
Acetic acid	1364±50
Propionic acid	664±24
Iso-butyric acid	143±5
N-butyric acid	542±20
NH <sub>4</sub>	470±10
DKN	560±12
TC	7000±100
TN	1200±20

Gases required for the experiments were obtained from BOC NZ. These were oxygen (99.5%), nitrogen (99.7%) and zero grade helium which was a carrier gas for the GC. A calibration gas mixture (BOC NZ) was used to calibrate the gas chromatograph used for gas analysis. The calibration gas consisted of 2% H<sub>2</sub>, 2% CH<sub>4</sub>, 20% CO, 30% CO<sub>2</sub> in N<sub>2</sub>.

The reagents used for the liquid sample analysis were potassium dichromate (99.9%), hydrochloric acid (0.8%), sodium carbonate, formic acid (98%), butan-1-ol (99.5%) sodium nitroprusside (BDH), mercury (II) sulphate and silver sulphate (97% Hopkin & Williams, UK), sulphuric acid (95-97%) acetic acid (>99%), propionic acid (>99%), iso-butyric acid (>99%) (Merck), N-butyric acid (>99%), DCIC sodium



dichloroisocyanurate (96%) (Aldrich), sodium hydroxide (97%) (Univar), sodium citrate dehydrate (Fisher Scientific), disodium ethylenediamine tetraacetate, sodium dodecyl sulphate (H&W), crystalline phenol (>99%) (Sigma), ammonium molybdate tetrahydrate (J.T. Baker) and potassium hydrogen phthalate (Riedel de Haen). All chemicals were of analytical reagent grade. The analysis procedures follows those outlined in [22, 44].

## 3.4 Experimental Procedure

This section describes the experimental procedures for the lab scale and pilot plant wet oxidation systems that were used as part of this research.

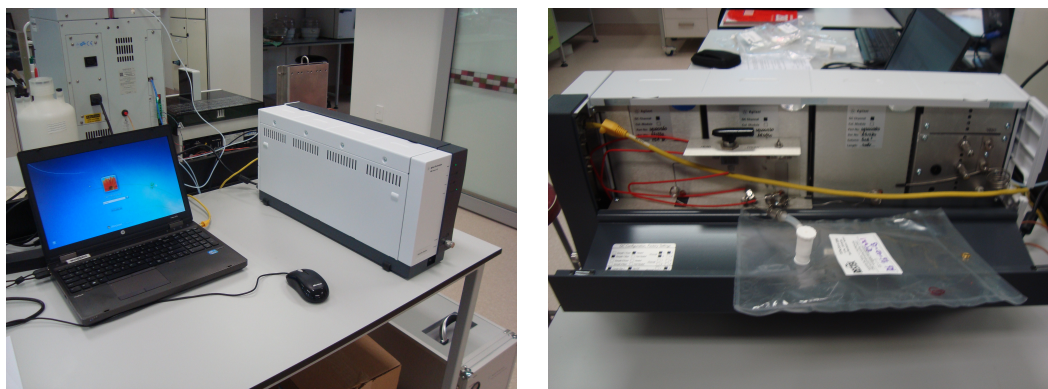
### 3.4.1 Lab-scale Reactor

The frozen biosolids sample was thawed, and kept at 4°C while being homogenised using a magnetically stirred vessel. The 150ml sample was then transferred to the pre-heated feed tank and heated to 90°C while being stirred to keep the solids in suspension. The aim of the pre-heated feed tank is to reduce the temperature gradient in the main reactor upon injecting the sample. Owing to the relatively low temperature it was assumed that no hydrolysis reactions occur during the pre-heating phase. After heating the sample to 90°C, which took around 20 minutes, it was then transferred from the feed tank to the reactor by means of pressure differential using pure nitrogen. Once the system pressure in the reactor had stopped rising the charge valves were closed and the feed tank vented of nitrogen.

The reactor was initially filled with 250ml of water and pressurised to 20 to 40 bar using pure oxygen. It was then heated to the desired temperature (180 to 240°C) before the biosolids sample was injected. After injection, the initial solids concentration in the reactor was approximately 1.5% by weight.

Using the manual sampling system, 20ml liquid samples were taken during operation at the intervals listed in Table 3.3, with the total experiment duration being 60 minutes. The liquid sampling loop had a volume of 10ml, so two samples were taken at each time period to get the required 20ml. The sampling system was flushed with water and purged with dry nitrogen following each sample, while the samples were immediately cooled to room temperature to quench any further reactions. Each sample was labelled with a unique identifier and refrigerated.

While the experiment was in progress, the feed tank was removed from the Berghof unit and weighed before the residual biosolids were rinsed out and the tank weighed



(a) Agilent 490 micro GC

(b) Gas sample bag connected to GC

Figure 3.12: Reactor off-gas analysis equipment used in this study

again. The difference in weight determined the amount of biosolids that was not transferred to the main reactor and this was recorded for each experiment.

This procedure was repeated for each of the experiments.

### 3.4.2 Measuring Reactor Off-gas

Initially, off-gas samples were withdrawn from the head space of the reactor at the end of the experiment ( $t = 60$  minutes). The reflux condenser was purged to ensure that the gas being withdrawn was a representative sample of the gas in the head space before samples were collected. Gas samples were taken using a high pressure Valco selector valve, which directed the gas through a cooler, reducing the temperature of the samples to  $10^{\circ}\text{C}$ . The gas samples were collected in Tedlar gas sample bags for later analysis.

For the earlier experiments, regular gas samples of the head space were not taken owing to poor gas mixing in the reflux condenser. In order to get a representative head space sample, the reflux condenser would need to be purged each time, causing a considerable pressure drop in the reactor. Gas samples were analysed using an Agilent 490 micro GC, shown in Fig. 3.12. However, these preliminary gas samples yielded inconclusive results. All the samples contained high levels of nitrogen, indicating air leaks in the downstream gas sampling equipment, or leaks in the sample bags.

Because of problems with gas sampling with the reflux condenser present, it was removed for the final four experiments, and the Valco gas sampling line was connected directly to the head of the reactor vessel. This enabled intermediate gas samples to be collected at the same time as the liquid samples for later analysis.

### 3.4.3 Pilot Plant Experimental Procedure

While the pilot plant was predominantly used to perform continuous experiments, two batch experiments were performed in order to validate the lab scale experiments. The operating procedure was as follows:

The feed tank in Fig. 3.9 was filled with the required mass of biosolids obtained directly from the TERAX fermenter, which was the same source of feed material for the lab scale experiments. Water was added to dilute the feed to the required concentration of 1.5% solids. Approximately 150kg of biosolids were then pumped into the main reactor, which was then pressurised to the required pressure using compressed air, and the heating and circulation systems were started. After the initial pressurisation, pure oxygen was used to maintain the oxygen concentration in the reactor to between 20 and 25%.

After the temperature had reached the required setpoint, liquid samples of the reactor contents were taken approximately every 15 minutes, while the oxygen concentration was continuously sampled as part of the reactor control system. Other gasses apart from oxygen were not measured on the pilot plant due to equipment constraints. After the required experiment duration had been reached, the reactor cooling was enabled. Once the temperature had dropped below 50°C, the remaining liquid in the reactor was pumped into the discharge tank where the final sample was collected. After this, the system was flushed with tap water and compressed air for cleaning.

## 3.5 Online Data Acquisition

Real time data from the lab scale reactor was recorded using a Scion-developed software application and data acquisition system. This recorded temperature, heater power and stirrer speed from the Parr 4848 controller while the system pressure was sensed using a separate pressure transducer. The system automatically recorded each measurement every 10 seconds while in operation. The ability to measure the current drawn by the stirrer motor was added to the system to investigate whether meaningful data could be obtained that could infer changes in viscosity. The system parameters monitored are summarised in Table 3.2.

Table 3.2: System parameters recorded by the data acquisition system ( $\Delta t = 10\text{s}$ )

Parameter	Range	Units
Temperature	0–350	°C
Pressure	1–400	bar gauge
Stirrer Shaft Speed	0–500	RPM
Stirrer Motor Current	0–1000	mA

## 3.6 Analysis Procedure and Analytical Techniques

The degradation of the biosolids samples undergoing wet oxidation was monitored by analysing the wastewater quality metrics described in Section 2.2, which included solids, COD, VFAs and nutrients (nitrogen and phosphorus). The particular properties of interest were Total Suspended Solids (TSS), Volatile Suspended Solids (VSS), particulate COD (pCOD), soluble COD (sCOD), Ammonia Nitrogen  $\text{NH}_4\text{-N}$ , Dissolved Kjeldahl Nitrogen (DKN), and Volatile Fatty Acids (VFA). The analytical techniques used to determine each of the measurements is described in the following sections.

### 3.6.1 Suspended Solids

Total Suspended Solids (TSS) was determined according to the standard methods recommended by the American Public Health Association and detailed in APHA Standard Methods 18th Edition 2540D [21]. Each sample was mixed and filtered through a pre-weighted  $0.45\mu\text{m}$  glass fibre filter paper, and then dried at  $105^\circ\text{C}$ . The increase in weight of the filter paper represents the total suspended solids.

Volatile Suspended Solids (VSS) was determined following the method described in APHA Standard Methods 18th Edition 2540E [21]. The residue from the total suspended solids measurement is ignited in a furnace to a constant weight at  $500\pm 50^\circ\text{C}$ . The weight loss on ignition represents the volatile suspended solids.

### 3.6.2 Chemical Oxygen Demand

Total Chemical Oxygen Demand (tCOD) and soluble Chemical Oxygen Demand (sCOD) were determined using a Scion in-house micro scale method [22] similar to that documented in APHA Standard Methods 5220D [21]. Samples were digested with an excess of acidic potassium dichromate solution. The amount of reduced dichromate was determined colorimetrically and was used as an estimate of the COD of the sample. Soluble COD was determined by analysing the COD of the

sample after it was filtered through a standard  $0.45\mu\text{m}$  filter. Particulate COD (pCOD) is usually defined as the difference between tCOD and sCOD.

For this investigation, tCOD was instead calculated from the mean from the ratio of pCOD/VSS using the following equations.

$$\text{tCOD} = \text{sCOD} + f_s \cdot \text{VSS} \quad (3.1)$$

where

$$f_s = \frac{\sum_1^n \left( \frac{\text{pCOD}_i}{\text{VSS}_i} \right)}{n} \quad (3.2)$$

and

$$\text{pCOD}_i = \text{tCOD}_i - \text{sCOD}_i \quad (3.3)$$

Where  $n$  is the total number of experiments. This approach was used because of considerable variability in the tCOD measurement of each sample when compared to the TSS, VSS and sCOD measurements. This variation prevented useful analysis of tCOD and frequently resulted in erroneous pCOD values when calculated using the difference of sCOD and tCOD. Using the mean of pCOD/VSS from the experiments resulted in a value of 1.46 which is similar to the value of 1.42 given by Tchobanoglous *et al.* [15].

At the time of writing the reason for the large variability in tCOD remains unknown, although it is believed to be an issue with the difficulty in obtaining a representative sample from the slurry (particularly at the earlier stages of the reaction), and possibly the analytical technique.

### 3.6.3 Volatile Fatty Acids

Volatile Fatty Acid (VFA) concentrations were measured using an in-house method using pH correction with formic acid, followed by capillary gas chromatography with flame ionisation detection (GC-FID). The column used was a nitroterephthalic acid modified polyethylene glycol capillary column DB-FFAP:  $250^\circ\text{C}$   $30\text{m} \times 530\mu\text{m} \times 0.5\mu\text{m}$  ramped from  $40^\circ\text{C}$  to  $180^\circ\text{C}$ . Butan-1-ol solution was used as an internal standard and samples were filtered through a PTFE syringe filter ( $0.22\mu\text{m}$ ) [22].

### 3.6.4 Nitrogen

Ammoniacal nitrogen ( $\text{NH}_4\text{-N}$ ) concentrations were determined based on a colourimetric method using a Skalar segmented flow auto-analyser. The samples were filtered through a PTFE  $0.45\mu\text{m}$  filter and the ammonium compounds reacted with the solution to quantify the dissolved ammoniacal nitrogen. To determine the Dissolved Kjeldahl Nitrogen (DKN) content, the samples were filtered through a PTFE  $0.45\mu\text{m}$  filter and digested according to the Kjeldahl digestion method in APHA Standard Methods 4500-N [21].

### 3.6.5 Gas Composition Analysis

An Aglient 490 micro Gas Chromatograph (GC) was used to analyse the composition of the reactor off-gas samples. The GC was configured to use two calibration profiles using reference gases. The first profile was developed using the calibration gas mixture described in Section 3.3, while the second profile used dry air as a reference.

Using the calibration profiles, the GC was configured to track the concentrations of  $\text{H}_2$ ,  $\text{O}_2$ ,  $\text{N}_2$ ,  $\text{CH}_4$ ,  $\text{CO}$  and  $\text{CO}_2$ . Although the GC had been initially calibrated to track the concentration of  $\text{CO}$ , the concentration reported is influenced by the concentration of  $\text{N}_2$  present in the sample owing to the very similar molecular weights and the use of a TCD detector [29]. In order for the GC to correctly differentiate these components, additional calibrations were required which had not been completed at the time of writing. However the raw data generated by the GC software can be re-analysed once the necessary calibrations have been performed by Scion.

## 3.7 Experimental Overview

The experimental programme consisted of three sets of experiments carried out sequentially, with subsequent experiments characterising and expanding on the phenomenon observed in the previous set. The three sets of experiments are summarised as follows.

**Set 1 Experiments:** The first set of experiments was performed by Dr Saeid Baroutian, a post-doctoral researcher at Scion, between December 2012 and January 2013. The objectives of this set of experiments were to systematically characterise the behaviour of RDC biosolids under wet oxidation. The reaction conditions investigated were determined *a priori* based on the results from preliminary experiments. The effect of temperature, mixing intensity and oxygen partial pressure on

the reaction rates was the primary objective, as well as investigating any possible mass transfer limitations. Set 1 experiments are discussed in detail in Section 5.2.

**Set 2 Experiments:** Based on the results of the Set 1 experiments, the second set of experiments was conducted by the author over a wider temperature range to better characterise the effect of temperature and oxygen partial pressure on the reaction rates and the reaction end products produced and the experiments were part of this PhD programme. This is because the Set 1 experiments demonstrated that these two parameters had the greatest influence on the results. Several repetitions of experiments completed in Set 1 were performed to gauge the variance. The Set 2 experiments were conducted in October 2013 and are discussed in Section 5.4.

**Set 3 Experiments:** The third set of experiments was conducted by the author in December 2013 to capture gas samples from the headspace of the reactor to be analysed on a new GC which had been recently purchased for this purpose. These experiments were carried out to investigate the oxygen consumption, CO<sub>2</sub> and CO production during the duration of the experiments.

The range of reaction conditions investigated by all three sets of experiments are summarised in Table 3.3.

Table 3.3: The range of reaction conditions explored as part of the experimental investigation in this study.

Process variable	Range
Temperature	180–240°C
Oxygen partial pressure	16–40 bar
Stirrer speed	300–500 RPM
Stirrer configuration	Single impeller
Sampling times	0, 2, 5, 10, 20, 60 mins

### 3.7.1 Liquid and Gas Sampling

In order to determine the reaction extent during the duration of the experiments, periodic liquid samples were taken. For the third set of experiments, gas samples were also taken from the reactor headspace at the same time. The initial liquid sample at time  $t = 0$  was prepared outside the reactor. The initial sample was prepared by diluting the feed material by 2.67 times using tap water to obtain a solids content of 1.5%. This is equivalent to the solids content in the reactor after feed injection.

The periodic samples taken at  $t = 2, 5, 10, 20$  and 60 minutes were obtained directly from the reactor at the required intervals using the procedure and sampling equip-

ment described in Section 3.4. At the completion of the experiment and after the reactor had cooled below 50°C and de-pressurised, the remaining liquid was sampled to determine if the cooling down period had any effect on the concentration of the measured compounds.

### 3.8 Modelling Overview

Kinetic models describing the behaviour of the wet oxidation of organic compounds currently available in the literature as reviewed in Chapter 2 typically use a COD basis as a metric for concentration. This is usually the total COD of the solution. However several models factor in the formation and degradation of a couple of intermediate compounds. As discussed earlier in Chapter 2, even the wet oxidation of pure substances can produce many intermediate compounds which degrade via a large number of reaction pathways [86]. Therefore traditional approaches to model wet oxidation are a considerable simplification of the actual process. Better characterisation of the intermediate compounds is needed if more information than just the total COD is required.

The experiments undertaken as part of this research investigated the effect of temperature, oxygen partial pressure and mixing in the form of stirrer speed, on the degradation of biosolids under wet oxidation. As highlighted in Section 2.6, the kinetic models available in the literature do not typically take into account the effect of these operational parameters.

It is common for the reaction rate kinetics to be modelled using a rate expression of the form:

$$\frac{dC}{dt} = -k[C]^m[O]^n \quad (3.4)$$

where the rate coefficient is

$$k = k_0 \exp\left(\frac{-E_a}{RT}\right) \quad (3.5)$$

The rate coefficient is an Arrhenius expression,  $k_0$  is the pre-exponential factor,  $E_a$  is activation energy,  $R$  the universal gas constant,  $T$  is temperature,  $[C]$  is the concentration of the reactant,  $[O]$  is the concentration of the oxidant,  $m$  is the order of the reaction with respect to the reactant and  $n$  is the order of the reaction with respect to the oxidant. For COD based models, this has been demonstrated to be sufficient to capture the effects of changing temperature [57].

Mass transfer is a key component of wet oxidation, and under certain conditions



can be a rate limiting factor. The models developed as part of this research have focused on developing the reaction kinetic pathways, and the main environmental factors which affect them, as opposed to mass transfer models. Because of this, the developed models will need to take into account:

1. Range of variable operating parameters (temperature, O<sub>2</sub> partial pressure, stirrer speed)
2. Changes in liquid volume due to sampling
3. Concentration of dissolved oxygen
4. Batch operation, so dynamic models will be needed

An important factor that needed to be accounted for as part of the model development was the change in liquid volume owing to sampling in the lab scale reactor, although this is not a consideration for the pilot plant reactor due to the larger volume relative to the sample size. At the beginning of the experiment there was approximately 400ml of liquid and 200ml of gas present in the reactor. Over the course of the experiment, five liquid samples were taken of around 20ml volume each. This resulted in an eventual volume change of 25% by the end of the experiment. Because this was a batch process, the change in volume also changed the system pressure, which in turn affected the oxygen solubility in the liquid phase.

The solubility of gasses in water is commonly described using Henry's law which is written as:

$$p = k_H c \quad (3.6)$$

The Henry constant  $k_H$  is only valid at a constant temperature and several equations are available which assess the effect of temperature on the constant, with a common form being:

$$k_H(T) = k_H(T^\theta) \cdot \exp\left(\frac{1}{T} - \frac{1}{T^\theta}\right) \quad (3.7)$$

Because oxygen and water are common compounds, more specific correlations are available for determining the solubility of oxygen in water at elevated temperatures and pressures [90, 103].

Correlations for the mass coefficient  $k_L a$  are available in the literature. However these are typically based on larger reactor vessels than the one used as part of this study. While the coefficient can be determined experimentally, the experiments conducted for this research did not include any changes to the mass transfer area.

As described earlier in Section 2.8, Meille *et al.* [101] investigated the effect of

stirrer speed on  $k_La$  in small CSTRs and determined that a power law in Eqn. 3.8 adequately captured the effects of the change in stirrer speed. This approach has been used to model the effect of the stirring speed in the developed models.

$$k_La = AN^B \quad (3.8)$$

Although the majority of the experimental work was conducted on a CSTR, the modelling environment needed to be flexible enough to model the wet oxidation stage of the TERAX pilot plant, which uses a bubble column reactor.

### 3.9 Chapter Summary

This chapter describes in detail the features of the wet oxidation systems used in this research, which were a lab scale and a pilot scale wet oxidation plant. The experimental procedure for both systems was also discussed, including the specifics of liquid and gas sampling. The sampling was of particular importance due so that the behaviour of biosolids undergoing wet oxidation over time could be studied.

The characteristics of the biosolids used in the experimental programme was shown using standard wastewater quality metrics which were used to gauge the effectiveness of the wet oxidation process.

Furthermore, this chapter gave an overview of the main phenomena in the wet oxidation process which can be modelled, and can be used to describe the wet oxidation process. These kinetic and physical factors will form part of a flexible modelling environment in Chapter 4 which is used to model the wet oxidation of municipal biosolids later in Chapters 5 and 6.

## Chapter 4

# A Flexible Modelling Environment

This chapter discusses the development of a kinetic modelling environment, with the motivation and philosophy for the development being given in Section 4.1. A review of several common modelling environments is provided in Section 4.2, with a focus on the ability to perform reactions with hypothetical or pseudo-components as opposed to true chemical compounds. The ability to perform dynamic simulations and whether they are capable of regressing experimental data is also investigated. The modelling environments developed in the course of this research to perform kinetic studies are discussed in Section 4.4 and Section 4.5.

### 4.1 Rationale for Developing a Modelling Environment

A significant component of this research is the ability to postulate and validate likely kinetic pathways against experimental data, in order to model the behaviour of the chemical compounds of interest. In order to achieve this aim, a suitable flexible modelling environment was required. An obvious choice for this type of problem is a general purpose chemical process simulator such as Aspen Plus, as they usually have the necessary reactor models built in and have large property and thermodynamic databases which can be queried for data. This is in contrast to a generic modelling environment such as Matlab or Python where one would be required to develop many models from scratch, and find a suitable external source of chemical and thermodynamic property data, in addition to the optimisation and regression of the developed models.

The simulation and modelling environment that is used as part of this research will need to meet two main requirements. The first is the ability to perform modelling

tasks that are specific to wet oxidation, and work with the properties of the wet oxidation facilities at Scion. The specific modelling requirements include the ability to postulate and simulate elementary chemical reactions with both real and pseudo-components. The ability to regress parameters for the proposed reaction pathways from experimental data is also important.

The second requirement is that the modelling environment be easily deployable and not be overly restrictive so that the environment can form part of the control and supervisory environment that accompanies the TERAX reactor when it is deployed. This forms part of the future vision for the TERAX process. This requirement will take licensing restrictions and the overall cost into consideration.

## 4.2 A Review of Kinetic Modelling Environments

A number of chemical process simulators and modelling environments are available, both commercial and free-ware. Several environments have been reviewed to establish whether off-the-shelf software packages can solve the key problems of this research. The packages reviewed were VMGSim, Cantera, Simbiology and Aspen Plus. A short comparison of these solutions is given in the following sections.

### **VMGSim** [104]

VMGSim is a chemical process simulator which is primarily geared towards the petrochemical industry. Prior to version 5, it was purely a steady state simulator, although it is now capable of performing dynamic simulations. VMGSim was evaluated using a simplified reactor model performing an oxidation reaction, however it had trouble converging on the test problem.

**Advantages:** Easy to use. Nice PFD and dialogues. Good thermodynamics package.

**Disadvantages:** Computation is slow. It struggled to converge our simplified PFD even in steady state. Not able to regress parameters from experimental data. Only ideal mixing models for reactors.

### **Aspen Plus** [105]

Aspen Plus is a widely used commercial chemical process simulator which has been around for many years. It has a very large component database and thermodynamic library and is capable of modelling electrolyte reactions and dynamic systems.

**Advantages:** Dynamic modelling environment. Mature with many users, and well regarded in the chemicals and hydrocarbon processing disciplines. Electrolyte pack-

age.

**Disadvantages:** Very complex. User interface is not intuitive. Not able to regress parameters to experimental data. Only ideal mixing models for chemical reactors.

### Cantera [106]

Cantera is an open-source software package used for modelling chemical kinetics, thermodynamics and transport processes. It is an application library with interfaces to Python, Matlab and C++.

**Advantages:** Open source (free). Accurate thermodynamics.

**Disadvantages:** Has no GUI, script usage only which makes it more time consuming to develop and test kinetic models. Somewhat sparse documentation. Primarily designed for gaseous combustion and flame propagation with limited support for other phases.

### Simbiology [107]

Simbiology is a toolbox for Matlab provided by the Mathworks for modelling and simulating dynamic systems with a focus on pharmacokinetic and systems biology applications. It enables the user to specify reaction pathways graphically and via the Matlab scripting language.

**Advantages:** Graphical interface allows complex models to be created quickly. Integrates with the Matlab environment. Allows the use of pseudo-compounds.

**Disadvantages:** Less control over the modelling process compared to writing it directly in Matlab. Geared towards modelling of biological systems. Somewhat limited parameter regression.

Table 4.1 summarises key points for the modelling environments reviewed earlier.

Table 4.1: Summary of the reviewed modelling environments.

Chem Simulators	Commercial	Maturity	Thermo	Chem	Reactors	Regression
Aspen Plus	✓	✓✓	✓	✓	✓	×
VMGSim	✓	✓	✓	✓	✓	×
Cantera	×	—	✓	×	✓	×
Simbiology	✓	✓	×	×	×	✓
Matlab	✓	✓✓	×	×	×	✓
Python	×	✓	×	×	×	✓

Although Aspen Plus has short comings, it was initially used in this study for kinetic prototyping as it was able to solve the test problems, and did not require a large

amount of software development to begin with.

However, it was decided that the inability to regress parameters from experimental data in Aspen Plus, and the difficulty in modelling hypothetical reactions because of the restrictive environment was becoming a hurdle to this research and we would have to develop something ourselves.

#### **4.2.1 Summary of the Modelling Environments**

A test of several commercial and free modelling environments was performed, with a specific focus on the modelling of reaction kinetics, and the ability to regress experimental data. This revealed that the commonly available chemical focused modelling environments are quite restrictive when working with custom created pseudo-compounds (such as pCOD) and did not have the ability to easily perform parameter regression. These were subsequently deemed not suitable for use in this research. Because this area is a key component of this thesis, it was decided that off-the-shelf tools were not suitable and the development of custom modelling tools would be required.

Because of this, it was decided to develop our own environment in a modern general purpose programming language and this is discussed in the following section. Although this would involve re-inventing the wheel to some extent, the inability of the off-the-shelf software to meet research requirements meant this was a necessary step. Because this is a fundamental component of this thesis it was decided to develop our own environment.

### **4.3 Environment Design and Philosophy**

The review of common modelling environments earlier in Section 4.2 identified that the ability to work with user defined, or pseudo-components (such as treating pCOD as a chemical component) is an area where many modelling environments are lacking. The ability to perform parameter regression is also an important consideration for any modelling environment.

The focus for this environment is to be able to simulate specific reactions and conditions that are likely to be encountered during wet oxidation, specifically using the wet oxidation facilities at Scion. It is not intended to be a generic chemical process simulator.

The design philosophy adopted for the modelling environment that was developed as

part of this research was to lower the barrier for prototyping of reaction pathways, and to make the process as quick and as easy as possible. It was decided that the optimum solution was to allow the user to enter reactions in a similar manner to sketching the pathways on paper, with the minimum of additional configuration.

The environment should be as modular as possible to make it easy to maintain and expand with new models or improvements to existing ones. One of the advantages of using the Python programming language as the basis for the modelling environment is that the Python environment is open source and free of charge. In addition to this, there is Python programming experience within Scion which will enable the environment to be maintained and expanded.

## 4.4 Python as a Modelling Environment

In order to easily investigate the reaction kinetics, a flexible modelling environment for prototyping hypothesised chemical reaction pathways was required and has been developed as an important component of this research. The modelling environment was developed using the Python programming language [108], because of the large standard library containing high quality scientific, math, and plotting libraries in the form of the `scipy` [109], `numpy` [110] and `matplotlib` [111]. Being a dynamically typed language allows commands to be entered directly into the interpreter with no program compilation. This allows non-programmers to easily work with the programming environment, which is important for model iteration and hypothesis validation.

The Python modelling environment that has been developed in this work makes full use of modern object oriented programming techniques to enable the environment to be flexible and new models to be easily added. It contains classes to perform chemical reactions, as well as CSTR and PFR reactor models. At present, the environment can simulate multiple elementary kinetic reactions, with Arrhenius rates in either CSTR and PFR reactors in series, with heat transfer to the jacket of the reactor. It takes the elementary reactions and automatically generates differential equations which are then passed to an ODE integrator.

The program has been designed with a base simulation class `asim` to which reactions and reactor models are added, while the Python source code for the modelling environment can be found in Appendix A.

### 4.4.1 Overview of Developed Models

The modelling environment constructed for this project contains two main reactor models, a continuously stirred tank reactor (CSTR) and a plug flow reactor (PFR), which are supersets of the underlying base reaction class actually performing the chemical reactions.

### 4.4.2 The Generic Chemical Reaction Model

The chemical reaction model is capable of modelling elementary reactions which have Arrhenius kinetic behaviour, both with or without stoichiometric coefficients as well as reversible reactions. The model computes component balances for the chemical species present, but does not compute the energy balance when solved alone. Only after a reactor model (described in Section 4.4.3) is added to the system is the energy balance solved.

The first step in modelling a chemical reaction is by calling the `reaction` class constructor and adding a reaction:

---

```
import asim # import our simulation environment

rxn = asim.reaction() # Create reaction object

# Next, add a hypothetical reaction
#
# rxn.add(reaction, k, m, E, H, Cp, rho) where the arguments are:
#
# reaction: string, elementary chemical reaction
# k: array, reaction rate constants
# m: array, order of reaction with respect to each component (reactant and
#      oxidant)
# E: double, activation energy (J/mol)
# H: double, heat of reaction (J/mol)
# Cp: double, heat capacity of fluid (J/gK)
# rho: double, density of fluid (g/L)

rxn.add("A -> B", [7.2e10], 1, [5e4], 0.239, 1000) # Add the hypothetical
# reaction
```

---

The call to the `asim.reaction()` routine creates the reaction object `rxn` to which elementary reactions can be added by calling the `add` method. The `add` method takes seven arguments which are the reaction pathway text string, rate constants, reaction orders, activation energy, heat of reaction, heat capacity and density of the liquid in the reactor. Details of these arguments are shown in the above code snippet. Large reaction networks can be modelled by breaking them up into their individual elementary reactions. Internally, the program parses the reaction pathway string argument and determines the reactants and products of the reaction, whether there are any stoichiometric coefficients present and if the reaction is reversible.



Once the reaction string has been parsed, the appropriate Arrhenius rate expressions are generated in the form of a list of coupled ODEs. The heat of reaction and energy balance is only added when a reactor object has been created.

### 4.4.3 The Continuously Stirred Tank Reactor Model

The reaction model described in Section 4.4.2 simply describes how the reactants react. This CSTR model (and the plug flow reactor in Section 4.4.4) describe the physical arrangement of the reactor. The CSTR model is based on the assumption of perfect mixing. This assumes that the contents of the reactor are homogeneous in composition, and in temperature. The composition of the material exiting is identical to that inside the reactor, which is a function of residence time and rate of reaction and is schematically illustrated in Fig. 4.1.

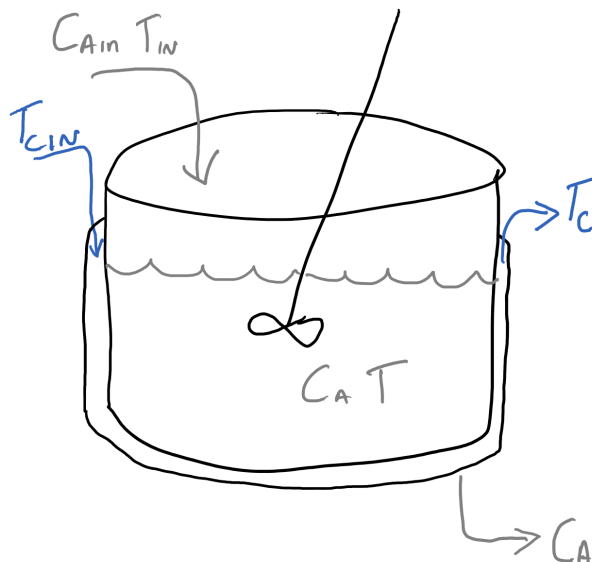


Figure 4.1: Schematic diagram of the CSTR model for the reaction of a single compound,  $C_A$ .

The mathematical model of a jacketed CSTR is given by the mass balances for each of the species contained in the reactor, the energy balances for the reactor contents, and the jacket heating or cooling. Using the conservation of mass, the global mass balance for the dynamic system containing reactions, [112], can be written as

$$\text{Material In} + \text{Production} = \text{Material Out} + \text{Accumulation} \quad (4.1)$$

where the production and accumulation terms can be positive or negative. Since the reactor contents contain more than one component, a system of component balances is more appropriate. For a system containing  $i$  components, applying the conservation of mass to each component in the system results in the following

expression [113]

Rate of flow of $i$ in	Rate of flow of $i$ out	Rate of change of $i$ due to reactions	Rate of change of $i$ in the vessel
$M_w F_{IN} C_{iIN}$	$M_w F C_i$	$-M_w k V C_i$	$M_w V \frac{dC_i}{dt}$

which can be simplified and written as

$$\frac{dC_i}{dt} = \frac{F_{IN}}{V} C_{iIN} - \frac{F}{V} C_i - k C_i^m \quad (4.2)$$

and the reaction rate  $k$  is the Arrhenius expression

$$k = k_0 \exp\left(\frac{-E_a}{RT}\right) \quad (4.3)$$

where

$M_w$  = Molecular weight of  $i$  ( $\text{kg} \cdot \text{mol}^{-1}$ )

$F_{IN}$  = Flowrate into reactor ( $\text{m}^3 \cdot \text{s}^{-1}$ )

$F$  = Flowrate out of reactor ( $\text{m}^3 \cdot \text{s}^{-1}$ )

$C_{iIN}$  = Concentration of  $i$  in feed ( $\text{mol} \cdot \text{m}^{-3}$ )

$C_i$  = Concentration of  $i$  in the reactor ( $\text{mol} \cdot \text{m}^{-3}$ )

$m$  = Order of reaction with respect to reactant

$k$  = Reaction rate ( $\text{s}^{-1}$ )

$V$  = Reactor volume ( $\text{m}^3$ )

$k_0$  = Pre-exponential factor ( $\text{s}^{-1}$ )

$E_a$  = Activation energy ( $\text{J} \cdot \text{mol}^{-1}$ )

$R$  = Universal gas constant ( $8.314 \text{ J} \cdot \text{mol}^{-1} \cdot \text{K}^{-1}$ )

$T$  = Reactor temperature (K)

$t$  = Time (s)

The same approach is used for the energy balance, which can be described as:

$$\frac{dT}{dt} = \frac{F_{IN}}{V} T_{IN} - \frac{F}{V} T - \frac{k C_i \Delta H}{\rho C_p V} - \frac{Q}{\rho C_p V} \quad (4.4)$$

$Q$  depends on the heat removal technique used, but for a jacketed reactor,  $Q$  can be defined as:

$$Q = UA(T - T_c) \quad (4.5)$$

where

$Q$  = Rate of heat removal ( $\text{J}\cdot\text{s}^{-1}$ )  
 $\Delta H$  = Heat of reaction ( $\text{J}\cdot\text{mol}^{-1}$ )  
 $C_p$  = Heat capacity of reactor product ( $\text{J}\cdot\text{kg}^{-1} \cdot \text{K}^{-1}$ )  
 $\rho$  = Density of product ( $\text{kg}\cdot\text{m}^{-3}$ )  
 $T_{\text{IN}}$  = Temperature of feed (K)  
 $T_c$  = Temperature of the cooling jacket (K)  
 $U$  = Heat transfer coefficient ( $\text{W}\cdot\text{K}^{-1}\text{m}^{-2}$ )  
 $A$  = Jacket heat transfer area ( $\text{m}^2$ )

In the cooling jacket, the heat transfer fluid enters the jacket at temperature  $T_{\text{cIN}}$  and leaves the jacket at temperature  $T_c$ . This model makes several assumptions, which include; perfect mixing of the heat transfer fluid in the jacket, constant density of the heat transfer fluid, constant density of the reactor contents and negligible energy input resulting from the stirring mechanism.

While standard SI units have been used in the examples, technically any unit set can be used within the Python environment, as long as it is consistent and each term has units of mass per unit time.

#### 4.4.4 The Plug Flow Reactor Model

The basis for the plug flow reactor model is the assumption that fluid flows through the tubular reactor in a series of infinitely thin slices or “plugs”, each with a uniform composition and temperature, and travels in the axial direction of the reactor. Each plug has a different composition and potentially different temperature from the plugs before and after. The model assumes there is perfect mixing in the radial direction and no mixing in the axial direction.

A common modelling approximation is to treat each fluid plug as a small CSTR, which is schematically illustrated in Fig. 4.2. For computational reasons, the volume of the PFR is divided into 10 to 30 segments. Each is modelled as a CSTR, with the inlet connected to the previous fluid plug and the outlet connected to the inlet of the following fluid plug, and is represented in Fig. 4.2. The process simulator Aspen Plus uses 20 segments in its PFR model by default. In this model, the PFR is divided into 10 segments. This can be changed if required by setting a property in the PFR object.

Configuring the PFR model is similar to the CSTR model except the length and diameter of the reactor are required, and the number of segments to use is optional. Internally, the class checks the arguments to ensure they are valid, such as a non-zero length and diameter, before generating the system of coupled ODEs.

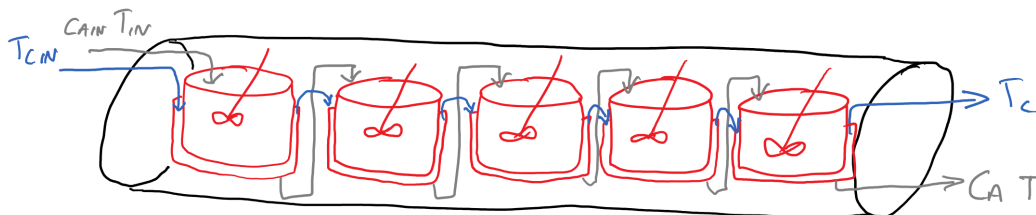


Figure 4.2: Schematic diagram of the PFR model.

#### 4.4.5 An Illustrative Example Demonstrating Use of the Package

In this simple example, we are modelling the irreversible hypothetical exothermic reaction  $A \xrightarrow{k} B$ , where  $k$  is  $k_0 \exp\left(\frac{-E_a}{RT}\right)$ . The following shows the steps and Python code required.

First a reaction object is created, followed by adding the reaction pathway  $A \rightarrow B$  to the `rxn` object, and configuring the reaction parameters. This is shown in the following code snippet. These are in the following order: Arrhenius rate constant ( $k_0$ ), reaction order for reactants ( $m$ ), activation energy ( $E_a$ ), heat of reaction ( $H$ ), heat capacity of the fluid ( $C_p$ ), and the density of the fluid ( $\rho$ ). For this hypothetical example, a rate constant and reaction order of 1 has been chosen, with an activation energy and heat of reaction of  $1000 \text{ J}\cdot\text{mol}^{-1}$ , a heat capacity of  $780 \text{ J}\cdot\text{kg}^{-1}\cdot\text{K}^{-1}$  and density of  $1000 \text{ kg}\cdot\text{m}^{-3}$ . The reactor initially has a concentration of  $1 \text{ mol}\cdot\text{m}^{-3}$  of A, with no B present.

---

```
reaction = asim.reaction() # Create reaction object
reaction.add("A -> B", [1], [1], 1e3, 1e3, 780, 1e3) # Add reaction and
set reaction parameters k0, m, Ea, H, Cp, rho
```

---

Next the initial concentrations of A and B are configured, and the temperature of the material.

---

```
reaction.feedConc = {"A": 1.0, "B": 0} # Initial concentration in
reaction.feedTemp = 350 # Feed temperature
```

---

Following this, a physical reactor is created. For this example, a CSTR is used.

---

```
cstr1 = asim.cstr(reaction, "MainReactor")
```

---

The initial conditions of the CSTR are set, which involves performing the following;

---

```
cstr1.volume = 10 # Volume in
cstr1.flowrate = 10 # Flow in
```

---

---

```

cstr1.initial_conditions = {"A": 0, "B": 0} # Initial concentration of
species
cstr1.initial_temp = 350 # Reactor initial temperatures
cstr1.coolant_temp = 350 # Coolant temperature
cstr1.UA = 5e4 # heat transfer area

```

---

The outlet stream of the CSTR object is copied to a local variable for clarity;

---

```

cstr1_output = cstr1.output()

```

---

Before the timespan is configured and the following code example starts the simulation.

---

```

tf = 10 # Set simulation time
results = asim.sim(cstr1_out,tf) # Perform the simulation

```

---

Internally, the `sim` function evaluates the passed reaction object list by parsing the textual reaction pathway string to determine the number of species in the reaction, the reactants and the products. It then generates ordinary differential equations (ODEs) for each component balance in the system. Evaluating the contained reactor object generates an additional ODE for the energy balance of the reactor and configures the initial conditions and properties of the reactor, such as the volume and initial component concentrations. The ODE equations are encapsulated internally in a Python list object which is solved by the ODE integrator.

#### 4.4.6 Validation Against Literature Examples

To validate the reactor models and automatic ODE generation, a simple hypothetical exothermic reaction of  $A \rightarrow B$  from Henson and Seborg [114, p5] was implemented. The properties of the reaction and reactor are listed in Table 4.2, while the Python code to model this problem is shown below.

---

```

# Create reaction object
reaction = asim.reaction()
# Configure elementary reaction
reaction.add("A -> B", [7.2e10], [1], 72751.88, 5e4, 0.239, 1000)
reaction.feedConc = {"A": 1.0, "B": 0}
reaction.feedTemp = 350 # feed temperature in K

# Add a reactor
reactor_1 = asim.cstr(reaction, "MainReactor")
# Specify reactor volume etc
reactor_1.volume = 100 # volume in l
reactor_1.flowrate = 100 # flow in l/min
reactor_1.initial_conditions = {"A": 0.5, "B": 0} # initial concentrations
in mol/l
reactor_1.initial_temp = 350 # temperature of reactor contents in K
reactor_1.coolant_temp = 300 # coolant temperature in K
reactor_1.UA = 5e4 # heat transfer area J/min K

outflow = reactor_1.output()

# Set simulation time

```

---

```
tf = 10
# Perform the simulation
results = asim.sim(outflow,tf)
```

---

Table 4.2: Operating Conditions of the CSTR example from [114].

Variable	Parameter	Value
Flow	$q$	$100 \text{ l}\cdot\text{min}^{-1}$
Feed concentration $C_A$	$C_{Af}$	$1 \text{ mol}\cdot\text{l}^{-1}$
Feed temperature	$T_f$	$350 \text{ K}$
Reactor volume	$V$	$100 \text{ l}$
Feed density	$\rho$	$1000 \text{ g}\cdot\text{l}^{-1}$
Feed heat capacity	$C_p$	$0.239 \text{ J}\cdot\text{g}^{-1}\cdot\text{K}^{-1}$
Heat of reaction	$-\Delta H$	$5\text{e}4 \text{ J}\cdot\text{mol}^{-1}$
Activation energy	$E_a$	$72751 \text{ J}$
Rate constant	$k_0$	$7.2\times 10^{10} \text{ min}^{-1}$
Heat transfer area	$UA$	$5\text{e}4 \text{ J}\cdot\text{min}^{-1}\cdot\text{K}^{-1}$
Coolant temperature	$T_c$	$300 \text{ K}$
Initial $C_A$ concentration	$C_A$	$0.5 \text{ mol}\cdot\text{l}^{-1}$
Initial reactor temperature	$T$	$350 \text{ K}$

It is possible to view the automatically generated ODEs from the package by calling the overloaded Python `print` function on `reactor.output()` which displays the ODEs. These are integrated when the `sim` function is called. While the output is somewhat cryptic, as it is not intended to be human readable because the expressions are formatted so they can be entered into a Python interpreter, it still provides a useful check and debug tool. The results of simulating the CSTR example above are illustrated in Fig. 4.4.

---

```
>>> print(outflow)
asim reaction object:

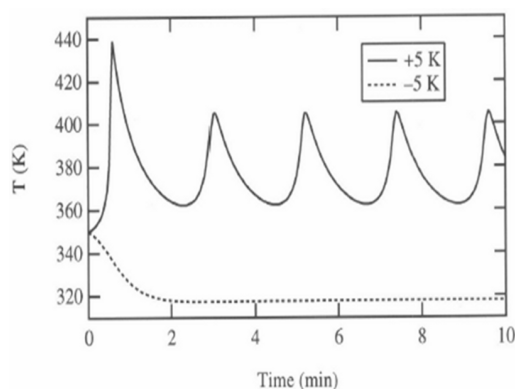
#A -> B
rxn_0 = lambda A, B, k, t : k[0]*math.exp(-72751.88/(8.314*t))* A**1

xdot map:
{'A': 0, 'B': 1}
xdot =([\
    -1*rxn_0(x[0], x[1], k, x[2]) + 1.0*(1.0 - x[0]),\
    +1*rxn_0(x[0], x[1], k, x[2]) + 1.0*(0 - x[1]),\
    +rxn_0(x[0], x[1], k, x[2])*(50000.0/(0.239*1000)) + 1.0*(350 - x\
        [2]) + (50000.0/(0.239*1000*100))*(300-x[2])\
    ])
```

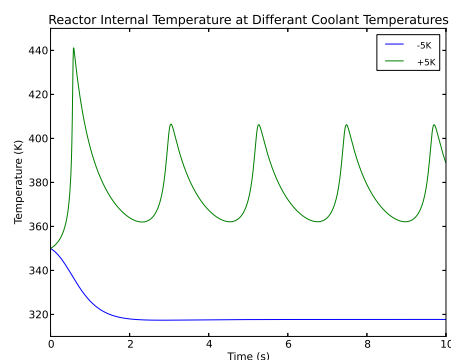
---

The first two entries in `xdot` are the component balance ODEs for species A and B, while the final entry is the energy balance for the system.

Calling the `sim` function integrates the generated ODE expressions using the `odeint` integrator from the `scipy` library. The results for the example from [114] are shown in Fig. 4.3 and Fig. 4.4.

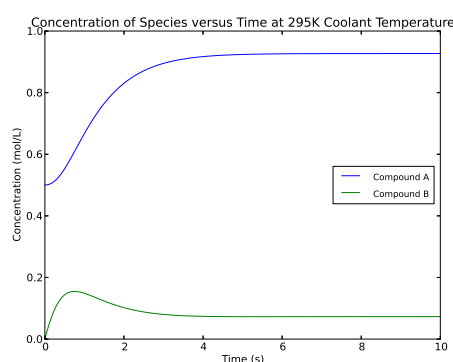


(a) System response from [114].

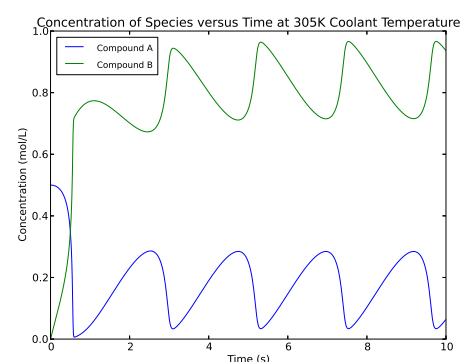


(b) Python environment response.

Figure 4.3: The reactor internal temperature in response to a  $\pm 5\text{K}$  change in coolant temperature.



(a) Concentration of A and B at 295K.



(b) Concentration of A and B at 305K.

Figure 4.4: The change in concentration in response to a  $\pm 5\text{K}$  change in coolant temperature. The change in concentration was not provided in the original reference [114] so the model output is shown for both cases.

This validates the non-trivial ODE system model and automatic ODE generation as shown by the extreme changes in the output which follow the results given in Henson and Seborg [114]. For that reason, the use of this CSTR model is a commonly used benchmark.

#### 4.4.7 Environment Use and Discussion

The Python environment described in Section 4.4 was initially used to prototype reaction pathways which were postulated from the literature and to analyse the experimental data. The generalised kinetic model proposed by Li *et al.* [57] was used as the basis for the kinetic pathway prototyping in the Python environment (because of its extensive use in the literature).

An investigation into the temperature dependence of the generalised kinetic model is shown in Fig. 4.5. The results obtained from the model agree with the results

published by the Li *et al.* [57].

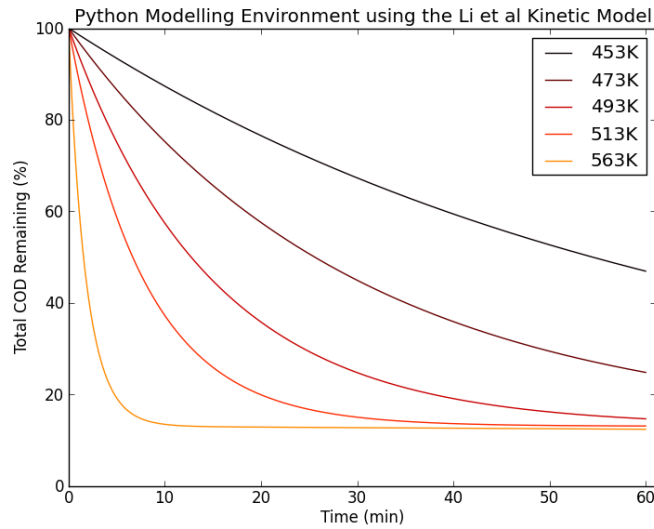


Figure 4.5: The kinetic model adapted from Li *et al.* at different temperatures developed in the Python modelling environment.

While the initial kinetic modelling was performed using the Python environment, it became apparent that it was quicker and easier to perform the modelling and parameter regression in Matlab. This was discovered after beginning the initial parameter regression when the scale and complexity of the problem was realised. Furthermore, the original constraint of using freely available software because of potential commercial requirements was no longer active once the focus of the research moved from software development to wet oxidation model development.

The decision to move the development to Matlab was primarily because of a freely available optimisation toolbox for Matlab, and the ability to leverage experience from the research centre at AUT. In the interests of reduced development time, the majority of the modelling work presented later in this thesis has been completed in Matlab. A description of the Matlab based environment is shown in the following section. However the Python modelling environment still holds many advantages and was used to generate some of the results shown later in Section 6.3.3 and is intended to be further developed in the future.

In principle, the modelling and parameter regression presented later in this thesis could also be accomplished in Python.

## 4.5 Matlab Modelling Environment

The models described in Chapter 5 of this thesis were developed in Matlab R2012b using the Matlab scripting language [115]. The free OPTI optimisation toolbox



[116] developed by AUT PhD candidate Jonathan Currie for Matlab was used as a universal front end to a large variety of optimisers that could be easily interchanged, as the toolbox provided a common front end for all the optimisers.

OPTI presents a common syntax which allows the user to easily select different optimisers from the extensive list (over 25 solvers available) with a single parameter change. This allows the performance of different algorithms to be quickly evaluated. An important feature of the OPTI toolbox is that it is capable of automatically generating derivatives from ODE expressions using the BARON interface. This feature was used as part of the parameter regression for the initial kinetic model described later in Section 5.3.

The Matlab modelling environment consists of a collection of script files which contain initialisation routines, a model of the CSTR, and perform parameter regression. These routines are described in detail as part of the kinetic model development in Section 5.6.3. Because of time constraints, the automatic ODE generation which was created for the Python modelling environment was not implemented in Matlab. The ODEs describing the system were programmed directly in the Matlab scripting language.

After investigation, it was discovered that a derivative free solver was found to give better results because this type of problem has multiple solutions. It was found that unless a close starting guess was given, the derivative solver would converge to a non-optimal solution, and one could improve on the optimised solution by manually adjusting parameters. Owing to this, regressing the parameters for the extended kinetic model in Section 5.6 used a derivative free solver and did not require the automatic derivative generation provided by the OPTI environment.

The Matlab program code for the regression environment and the kinetic models developed in the course of this thesis can be found in Appendix A.

## 4.6 Chapter Summary

This chapter reviews the commonly available simulation and modelling tools which are relevant to modelling chemical reactions and the typical process equipment encountered when performing wet oxidation. The deficiencies of the existing tools were such that a custom modelling environment was needed.

The original aim for the modelling environment is for the practising engineer/scientist to easily develop dynamic models without the need for extensive programming. The modelling environment package should be able to regress experimental data

and allow the statistical comparison of the developed models. Despite the fact that the majority of the modelling work was completed in the Matlab environment as opposed to Python, the Python modelling environment was used to generate the results in Section 6.3.3 and should be expanded as part of future work.

## Chapter 5

# Modelling the Wet Oxidation Process

This chapter analyses a series of wet oxidation experiments that were performed using biosolids obtained from the Rotorua District Council (RDC) wastewater treatment plant. These experiments investigated and characterised the phenomenon observed. The results were analysed and a kinetic model was developed through an iterative design process which enabled the prediction of the concentration of the participating species, based on temperature, oxygen partial pressure and stirring speed. Subsequently, when analysis of the composition of the reactor off-gas became available which allowed oxygen consumption and CO<sub>2</sub> production to be validated, the model was further extended to better account for the oxygen consumption by the oxidation reactions.

The objective of this chapter was to create a detailed model of the process from the experimental investigation in order to improve understanding of the process, to allow optimal experimental design and control of the current wet oxidation facilities, and to assist in the design of further wet oxidation systems.

The experimental investigation was conducted as three sets of experiments. Section 5.2 describes the experimental programme undertaken in the first set of experiments and lists the key findings in Section 5.2.2. Using these results, a simplified kinetic model was proposed in Section 5.3 and compared with results obtained in the first set of experiments as the main factors affecting the process. Section 5.4 details the second set of experiments conducted to further investigate the temperature and pressure dependence, which was highlighted in the first set of experiments. As a result of newly available gas analysis equipment, Section 5.5 examines the results of the third set of experiments, which investigate the composition of gaseous components in the reactor headspace. Using this data, the model described in Sec-

tion 5.3 was expanded to incorporate the effect of the environmental parameters on the wet oxidation process and is discussed in Section 5.6. This extended kinetic model was compared with experimental data from both the lab scale and pilot plant wet oxidation systems in Chapter 6.

The first set of experiments were conducted by Scion post-doctoral researcher Dr Saeid Baroutian [60]. However experiment sets two and three described in this chapter were performed by the author. Sample analysis was performed by Scion laboratory staff and the author, as described in the following sections. The postulation of models, regression, statistical analysis and demonstration of the model was performed by the author.

## 5.1 Presentation of Results

The presentation of the experimental results in this chapter, and the rest of this thesis, follows a deliberate set of basic graphical guidelines.

The graphical design guidelines from [117] and in particular the emphasis for visual clarity from [118, chapter 5] were used to design the form and colours of the plots in this thesis. The colour choices were made deliberately in an effort to add context to the data, but clearly some sacrifices were inevitable given this decision; namely the choice of colour-blind safe palettes and even grey scale safe colour palettes.









The colour and symbol scheme used for the experimental results presented in this thesis is given in Table 5.1. The colours have been chosen to reflect (very approximately) the actual colours of the compounds, or in the case of gases, the standard colour of the industrial gas cylinders (CEN EN 1089-3).

The model results are given by continuous solid lines, while the measured experimental data is plotted as discrete points,  $\bullet$ , in the colours given in Table 5.1. Where duplicates are available, error bars are shown to show the maximum and minimum of the repeats. The exception to this convention is for the first set of experimental results presented in Section 5.2.2 prior to the development of the model, where the data points are joined by a solid line to make the trends easier to interpret.

The main deviation from this colour scheme is for results which directly compare the change in reaction conditions (temperature, oxygen partial pressure and stirrer speed). These plots use dark red for the lower condition, and orange for the high condition (for example, the lower temperature is red and the higher temperature is orange).

The experimental and model results illustrated in this thesis are presented in a

Table 5.1: The colours used for the following figures given in this and later chapters.

Total COD	
Particulate COD	
Soluble COD	
Volatile fatty acids COD	
Acetic Acid COD	
DON	
Oxygen	
Carbon Dioxide	

common format. The centre point of the experimental design programme from Fig. 5.1 is shown with error bars, as well as the results from three other experimental runs which show the effect of high and low temperature, oxygen partial pressure and stirrer speed. The remaining experiments which are not shown are available in Appendix B and C.

The rationale for this decision was to illustrate a selection of results which show the centre point of the design (experiments 15 to 18 in Table 5.2, shown as “Avg” in the plots) as well as three conditions which explore the extremes of the experimental programme in Fig. 5.1 with high temperature, oxygen partial pressure and stirring speed. This has been done for practical reasons for brevity in the body of the thesis. However, all the experimental and model data is given in Appendix B and C, and all the experimental data has been used for model regression described later in Section 5.6.

## 5.2 Set 1 Experiments: Characterising the Wet Oxidation of RDC Biosolids

This section discusses the results obtained from the first set of wet oxidation experiments performed by Scion post-doctoral researcher Dr Saeid Baroutian [60]. The aim of this set of experiments was to characterise the effect of wet oxidation on RDC biosolids. A central composite design strategy was employed to minimise the number of experiments which were required to cover the operating conditions of interest.

### 5.2.1 Experimental Design Programme

The environmental conditions investigated for this experimental programme are shown in Table 5.2. These were the effect of temperature, oxygen partial pressure and stirrer speed on the quality metrics listed in Table 5.3. The centre point of the design was replicated four times (experiment numbers 15 to 18), to gauge the measurement and process error owing to natural variations in the procedure. A diagram demonstrating the factorial experiments is shown in Fig. 5.1.

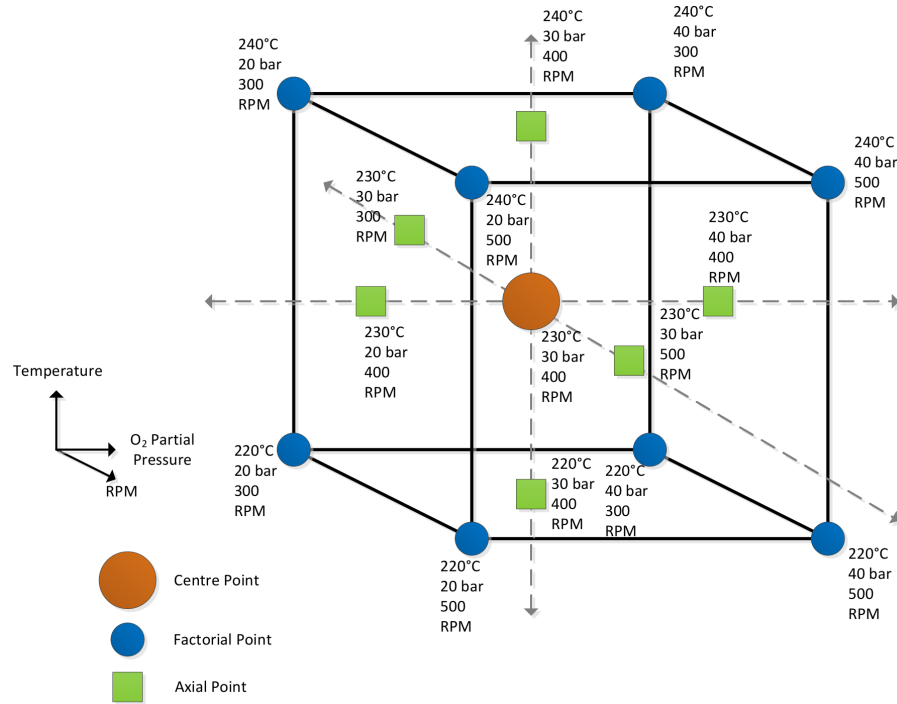


Figure 5.1: Central composite design used for the Set 1 experiments.

The experiment denoted “Avg” in Table 5.2 is not a separate experiment but represents the average of experiments 15 to 18, and this designation features in the results presented later in this thesis. The experiments conducted in this chapter were performed using the laboratory procedure and equipment described in Chapter 3 for the lab scale wet oxidation reactor.

Initiating the experiment at  $t = 0$  involved transferring the preheated biosolids feed sample from the pre-heating vessel to the main reactor, which was at a steady state condition, by means of pressure differential with pure nitrogen. This method of material transfer resulted in a small amount of biosolids remaining in the pre-heating vessel (8 to 27g). The experiments which had less material transferred would subsequently have a higher oxygen-to-biomass ratio, and also have less liquid in the reactor. This in turn resulted in a lower oxygen partial pressure, and subsequently a lower concentration of dissolved oxygen. To account for this dilution, and to enable a fair comparison between different experiments, all the results except the initial  $t = 0$

Table 5.2: Experimental reaction conditions that were investigated as part of the Set 1 experiments.

Experiment Number	Temperature (°C)	Oxygen Partial Pressure (bar)	Stirring (RPM)
1	220	20	300
2	240	20	300
3	220	40	300
4	240	40	300
5	220	20	500
6	240	20	500
7	220	40	500
8	240	40	500
9	220	30	400
10	240	30	400
11	230	20	400
12	230	40	400
13	230	30	300
14	230	30	500
15	230	30	400
16	230	30	400
17	230	30	400
18	230	30	400
Avg	230	30	400

samples, have been scaled by the amount of material transferred to the reactor. The initial  $t = 0$  sample has not been scaled as it was prepared separately outside the reactor. Since not all the pre-prepared material was transferred to the reactor, the other samples were scaled as to have the same biomass to oxygen ratio.

The liquid samples taken were analysed for the chemical and physical properties shown in Table 5.3, using the analytical procedures previously described in Section 3.6, while several of the metrics were calculated according to Table 5.4.

Table 5.3: The parameters measured from the analytical analysis.

Property	Parameter
Solids	TSS, VSS
COD	Soluble COD, Total COD
Carbon	DOC
Alcohols	Methanol, ethanol
VFAs	Acetic acid, propionic acid, iso-butyric acid, n-butyric acid, pentanoic acid, hexanoic acid
Nitrogen	NH <sub>4</sub> -N, DKN
Phosphorus	Total phosphorus

Table 5.4: Calculated parameters from measured data.

Property	Parameter	Calculation method
COD	Particulate COD	$p\text{COD} = \text{VSS} \times 1.46$
COD	Total COD	$t\text{COD} = p\text{COD} + s\text{COD}$
Nitrogen	DON	$\text{DON} = \text{DKN} - \text{NH}_4\text{-N}$

## 5.2.2 Experimental Results

The results obtained from this experimental investigation show that wet oxidation of biosolids is mostly affected by temperature and to a lesser extent oxygen concentration, with stirring speed having the least overall effect. A selection of experiments at the main operating conditions of interest are presented in this section, with the full set of experimental results being left to Appendix B.

Temperature has the greatest effect throughout, affecting the rate and final concentration for all measured components. Changes in mixing intensity appear to mainly affect the initial stage of reaction, and only have a small effect on the level of oxidation achieved. Oxygen partial pressure has the most effect on the final concentration of the components at the end of the experiment. The effects of these environmental factors are illustrated and discussed in Section 5.2.3.

The change in total COD over time is given in Fig. 5.2 and on a conversion basis in Fig. 5.3. Chung *et al.* [59] obtained a COD removal of around 50% at 220°C, which is close to the experimental results obtained in this study, and 67% removal at 240°C. These removal efficiencies are in line with the total COD degradation values shown in Fig. 5.2 and Fig. 5.3 which were between 53 and 61%. This allows comparison with published data which is more commonly in this form, while the trend of total COD removal closely matches published data. The fact that the COD results are in line with published data gives confidence in the experimental and analysis procedure used in this study.

Lendormi *et al.* [13, 24, 70] have performed detailed analysis of the wet oxidation effluent under different reaction conditions. They show that 60 to 67% of total COD removal was achieved at 220°C, with 71% removal at 240°C. An important observation was that the level of COD removal achieved is heavily dependant on the type of waste at lower temperatures, while at 300°C the same removal efficiency was achieved for all investigated waste types.



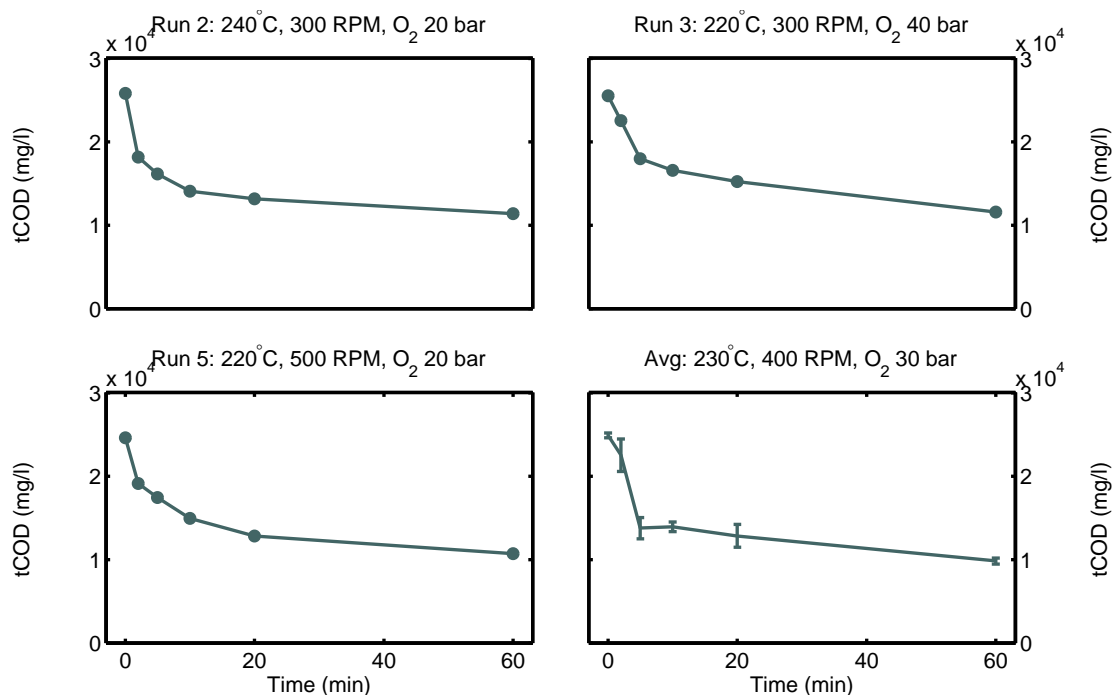


Figure 5.2: Total COD during the experiment under different reaction conditions. This is calculated as the total sum of pCOD and sCOD and is not measured directly.

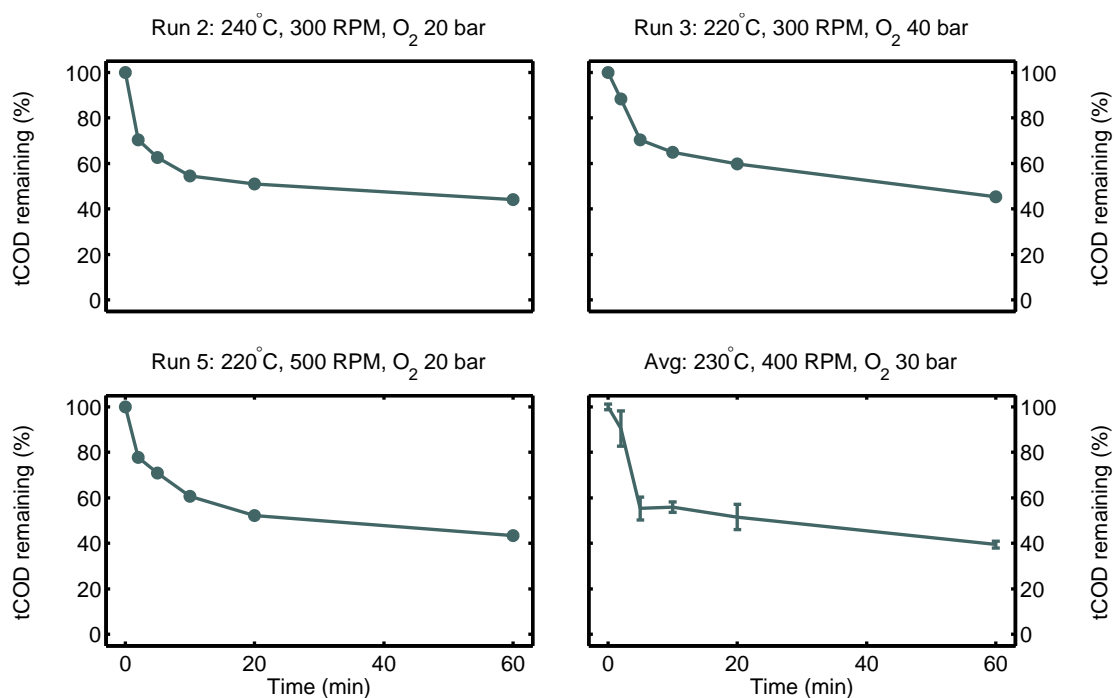


Figure 5.3: The percentage of total COD degradation under different reaction conditions. This is calculated as the total sum of pCOD and sCOD and is not measured directly.

The results in Fig. 5.4 show the degradation of particulate COD during the course of the experiment at different reaction conditions. Particulate COD exhibits a very rapid decline in concentration, with the majority of particulate COD being rapidly

consumed within the first two minutes of the experiment, and then slowly declining after this.

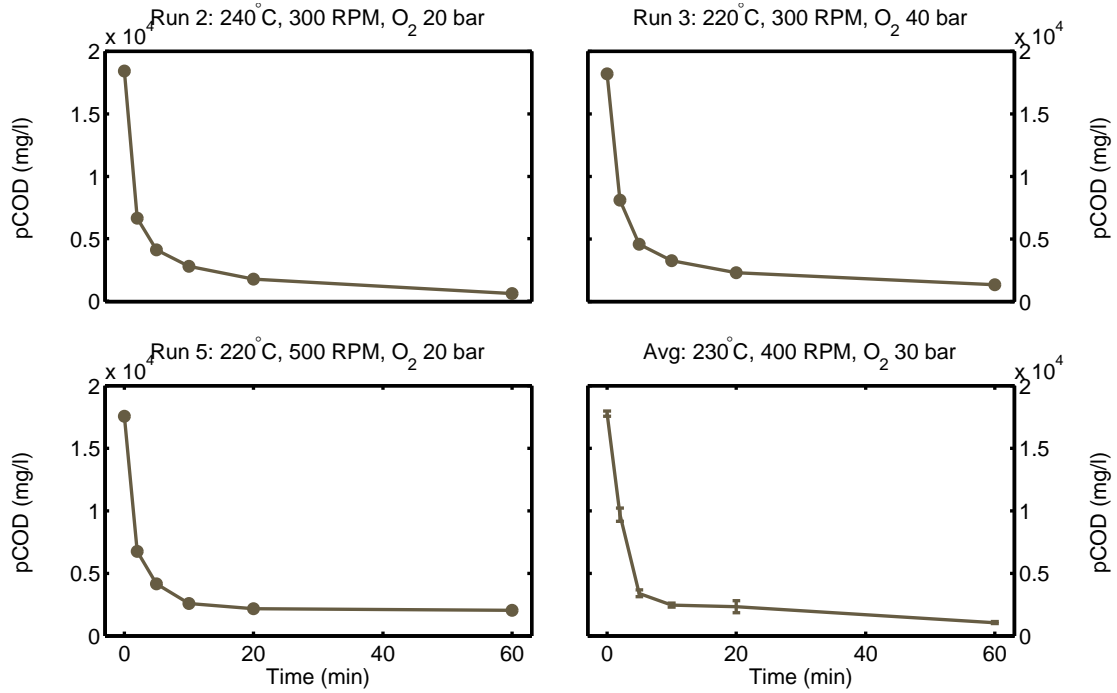


Figure 5.4: The change in particulate COD during the experiment under different reaction conditions.

From a modelling perspective, this behaviour can be approximated by assuming that particulate COD consists of a fast degrading and a slowly degrading fraction. The pCOD concentration profile in Fig. 5.4 suggests that approximately 80% of particulate COD is fast degrading, with the remainder being slow degrading. Shan-ableh [88] also observed this behaviour and suggested the idea of particulate COD consisting of fractions which degrade at different rates, which we intend to explore in the developed models in Section 5.6.4 to validate the slow and fast hypothesis.

The concentration of soluble COD exhibits a rapid rise because of the solubilisation of particulate COD, with the concentration usually peaking at 5 minutes into the experiment in Fig. 5.5. After this, the concentration of soluble COD steadily declines as other reaction products are formed. The experimental error is higher for soluble COD than for particulate COD because of the calculation of pCOD from VSS instead of being measured directly which is due to the reasons described in Section 3.6.2. However, like particulate COD, the error is lowest for the final sample.

It is noted that the sCOD sample taken at  $t = 5$  minutes for the average run in Fig. 5.5 has reduced concentrations. This single anomaly at 5 minutes is also evident for the other compounds for this experiment. This is because two of the four experiments that make up the average run (experiments 17 and 18) exhibited a large drop at this sample. Owing to this, it is suspected that there was a problem with

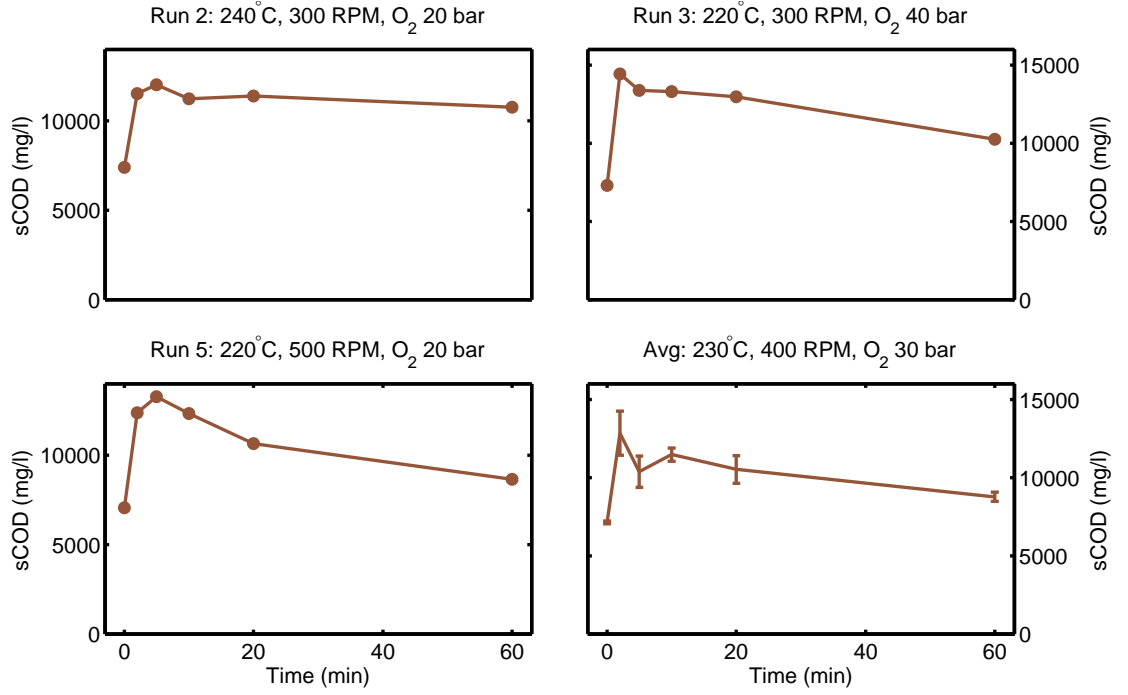


Figure 5.5: The change in soluble COD during the experiment under different reaction conditions.

these experiments as the other experimental runs do not exhibit this behaviour at  $t = 5$  minutes. While the concentrations of sCOD are higher in this work compared (over 10,000 mg/l vs a peak of 4000 mg/l for Chung *et al.*), the trend of sCOD evolution during the experiments was similar to work by Chung *et al.* [59].

The VFA concentration shown in the results presented in this thesis is the sum of all measured VFAs, except acetic acid which was quantified as a separate component because its concentration was much higher than the other VFAs. Of the non-acetic acid VFA components, propionic acid was the most common, followed by N-butyric acid. All acids, except acetic acid, were observed to degrade under all investigated reaction conditions. With the exception of the anomaly at  $t = 5$  minutes for the average run, the degradation trend for AACOD and VFA shown in Fig. 5.6 and Fig. 5.7 is similar to other published results [59].

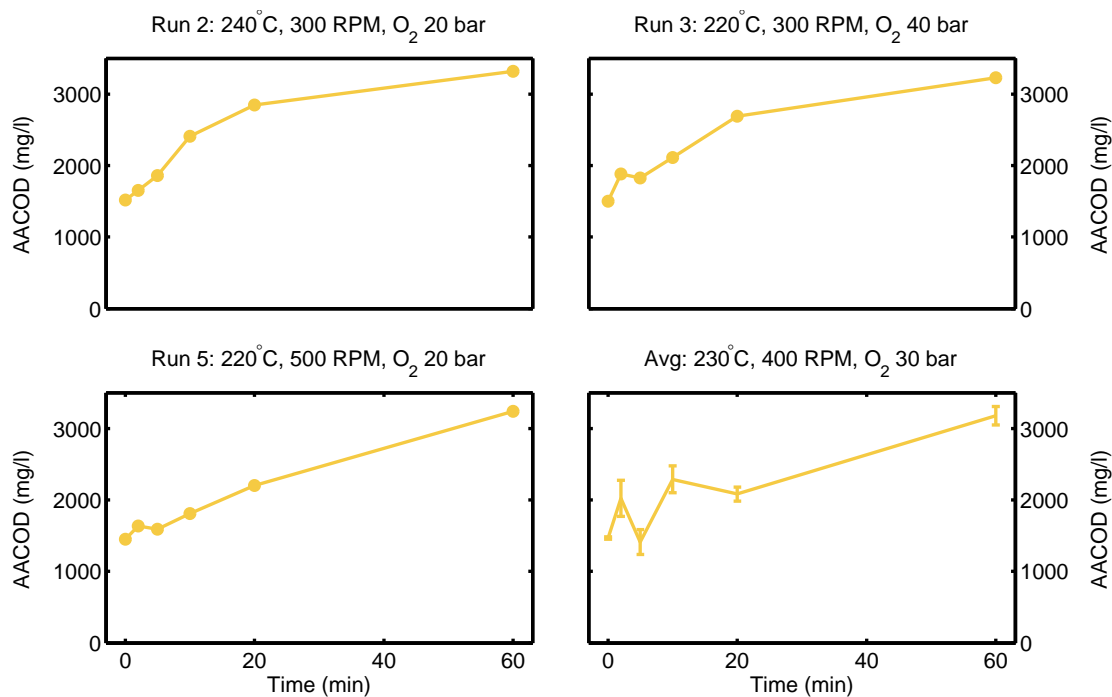


Figure 5.6: The change in acetic acid COD during the experiment under different reaction conditions.

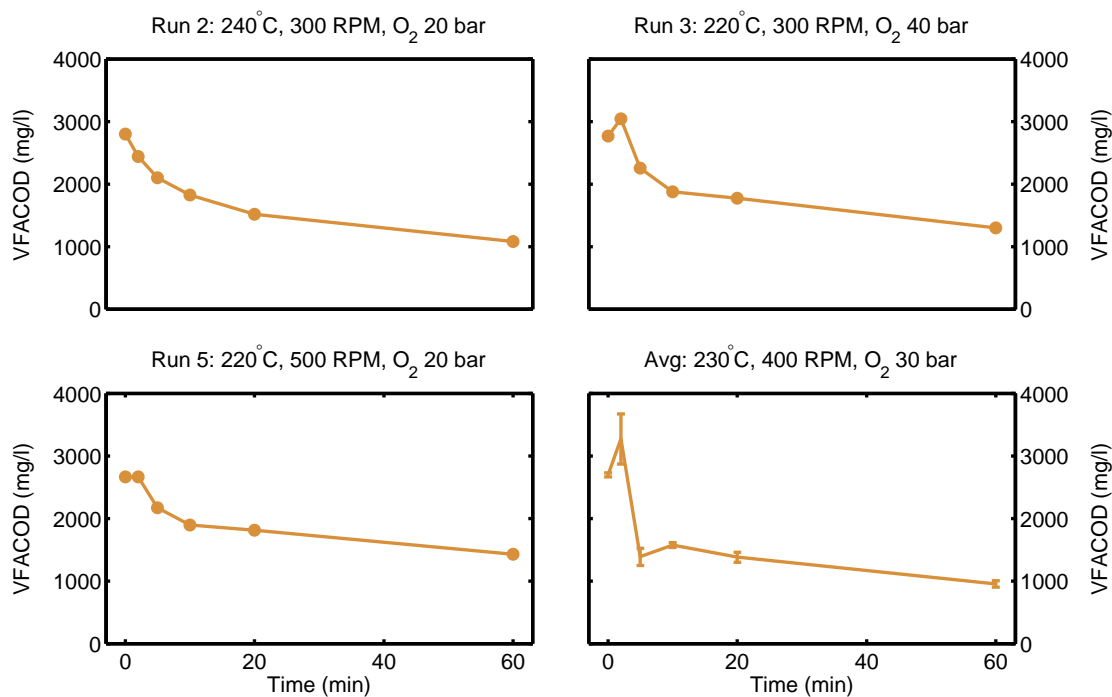


Figure 5.7: The change in VFACOD during the experiment under different reaction conditions.

The dissolved organic nitrogen results for all experiments shown in Fig. 5.8 exhibit considerable variation, with the error bars highlighting considerable uncertainty in these results. This variation is believed to be a problem in the analytical measurement process as all the experiments are affected (including the runs not shown in

this chapter, which are available in Appendix B). Because of this, the observed variation in the DON concentration during the course of the experiments does not appear to be reliable, and the analytical procedure for nitrogen analysis is being reviewed to determine the source of variation in the results. For this reason, it is expected that the regression of model parameters that represent DON are unlikely to be particularly accurate until improved experimental data becomes available.

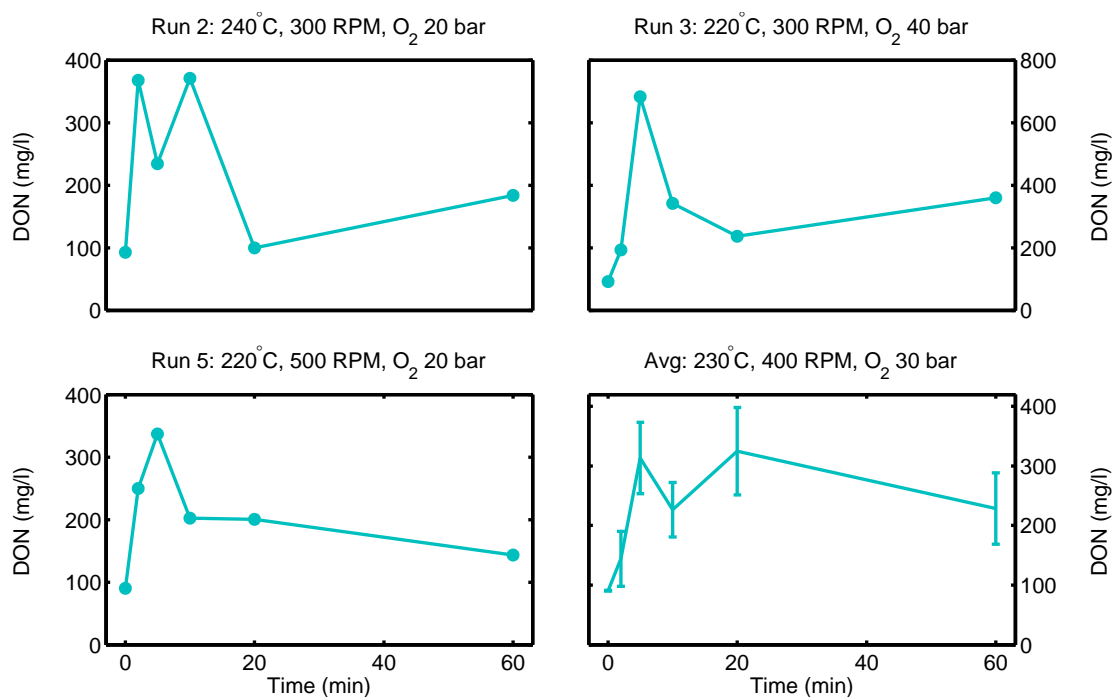


Figure 5.8: The change in DON during the experiment under different reaction conditions.

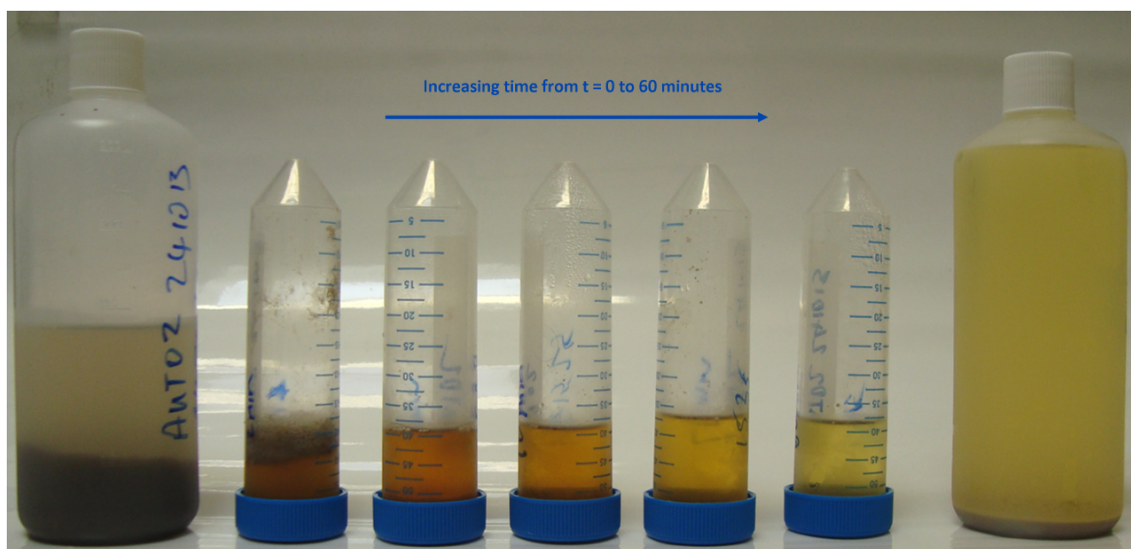


Figure 5.9: Liquid samples taken during a wet oxidation experiment clearly showing the solids reduction achieved over the duration of the 60 minute experiment.

Overall, the error in the experimental results is greatest for the intermediate samples,

with the final sample having the least error as shown by the error bars in the above experimental results. This seems to be due to the somewhat inhomogeneous nature of the initial samples, which subsequently affects the analytical procedures, however this has yet to be confirmed. Fig. 5.9 shows a photo of the full set of sub-samples taken during a wet oxidation experiment, including the feed (left) and final (right) samples, and it is clear that there is a significant amount of particulate matter in the early samples. Scion is investigating ways to make the analytical procedures more robust.

### 5.2.3 Influence of Temperature

Increasing the operating temperature from 220°C to 240°C, shown in Fig. 5.10, results in a faster reaction rate and larger decrease in particulate COD, with a subsequent increase in acetic acid production.

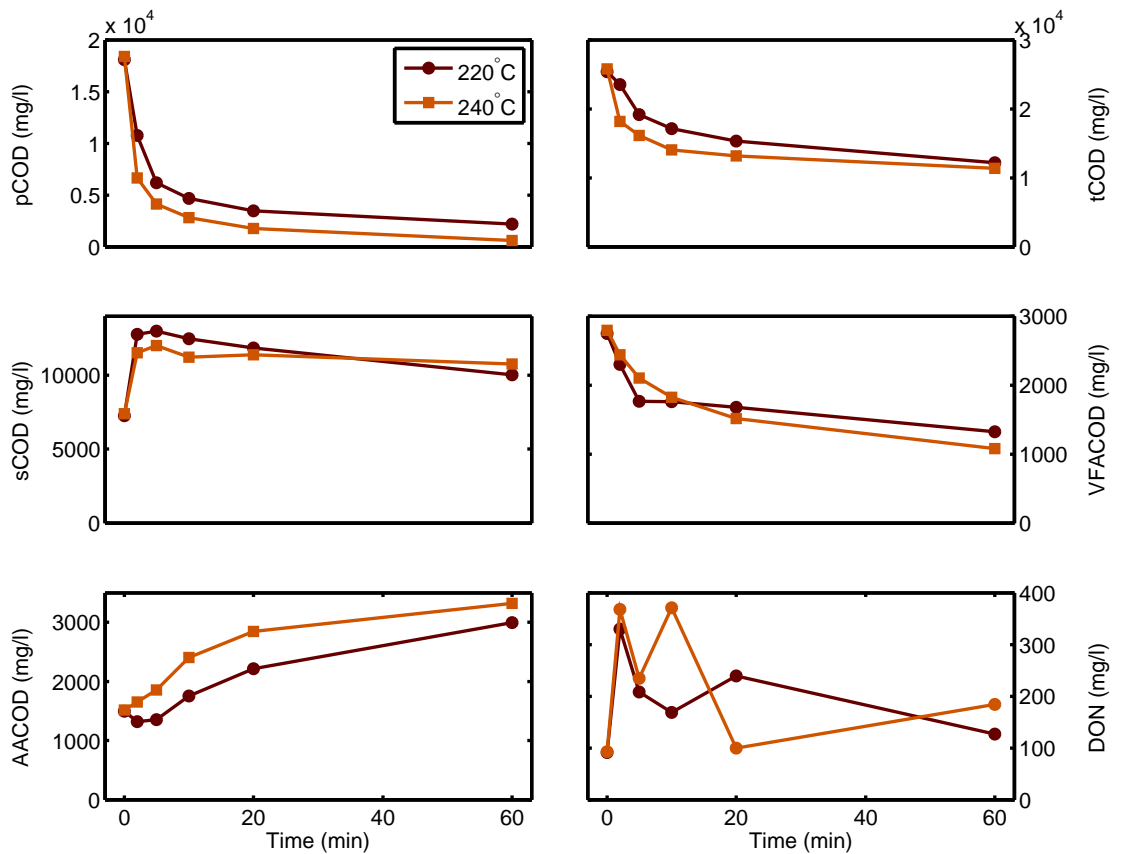


Figure 5.10: The influence of temperature increase from 220 to 240°C with a constant O<sub>2</sub> partial pressure and stirring speed. Data from experiments 1 and 2 listed in Table 5.2.

Chung *et al.* [59] observed similar behaviour when they increased the temperature by the same amount. The concentration of other VFAs decreased at higher tem-

peratures, which suggests that some of the volatile fatty acids that make up the aggregated VFACOD pseudo-compound are degradable under moderate wet oxidation conditions. Importantly, this behaviour was also noted by Jomma [87], and Chung *et al.* [59]. In general, the results show that increasing the temperature increases the rate of conversion to reaction end products.

#### 5.2.4 Influence of Oxygen Partial Pressure

Changing the oxygen partial pressure from 20 to 40 bar, which is shown in Fig. 5.11, resulted in a slight increase in particulate COD conversion, but it increased the rate and final concentration of acetic acid. It also resulted in increased degradation of other VFAs and soluble COD, presumably because of the increased dissolved oxygen concentration. Chung *et al.* [59] observed no change in total COD when increasing the system pressure, although they did observe an increase in acetic acid production, which supports these results.

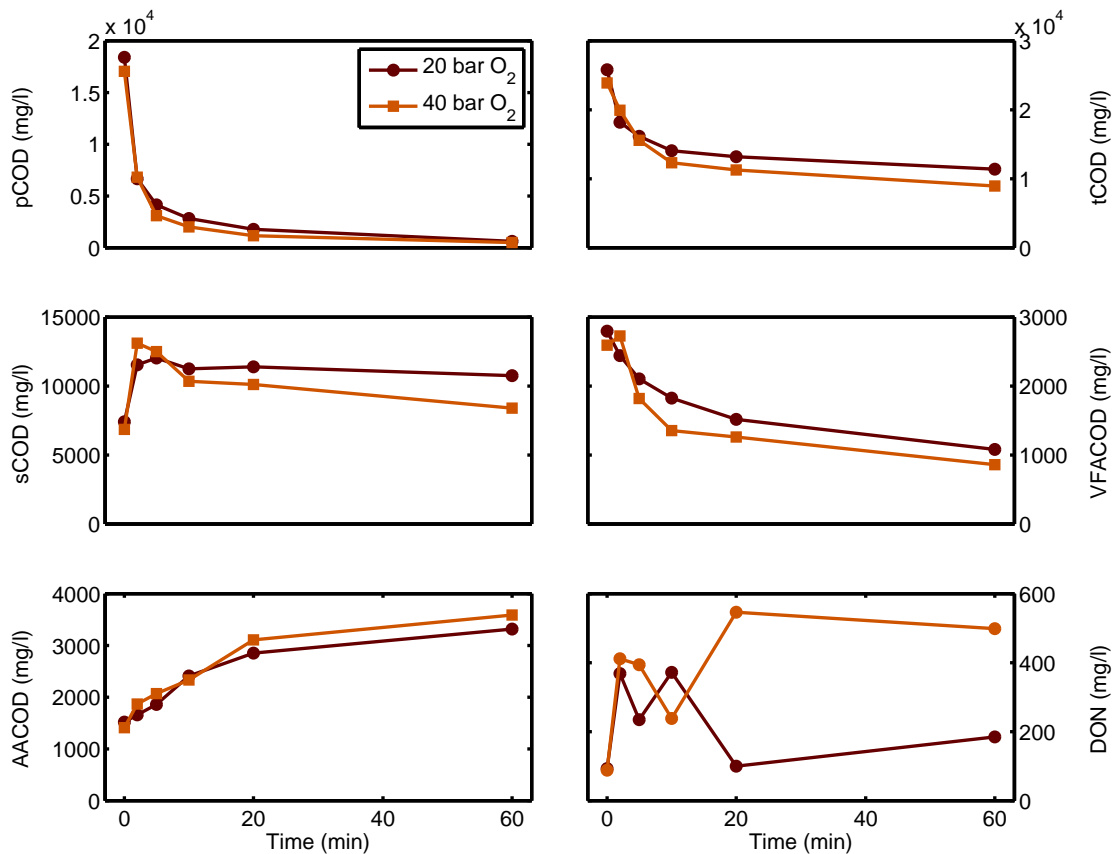


Figure 5.11: The influence of oxygen partial pressure on degradation when increased from 20 to 40 bar. Temperature and stirring speed remained constant. Data from experiments 2 and 4.

It is suspected that the decrease in total COD resulting from an increase in partial

pressure is due to the higher dissolved oxygen concentration reducing mass transfer limitations. This then increases the formation of end products from soluble COD which is mainly responsible for the reduction in total COD.

### 5.2.5 Influence of Stirrer Speed

Increasing the stirrer speed from 300 to 500 RPM resulted in a small increase in the initial rate of degradation for most components, apart from VFACOD, but had the least overall effect. Stirrer speed has the least effect out of the variable environmental parameters on the final level of degradation achieved for the measured components. This observation was also made by Baroutian *et al.* [60] on the same raw data.

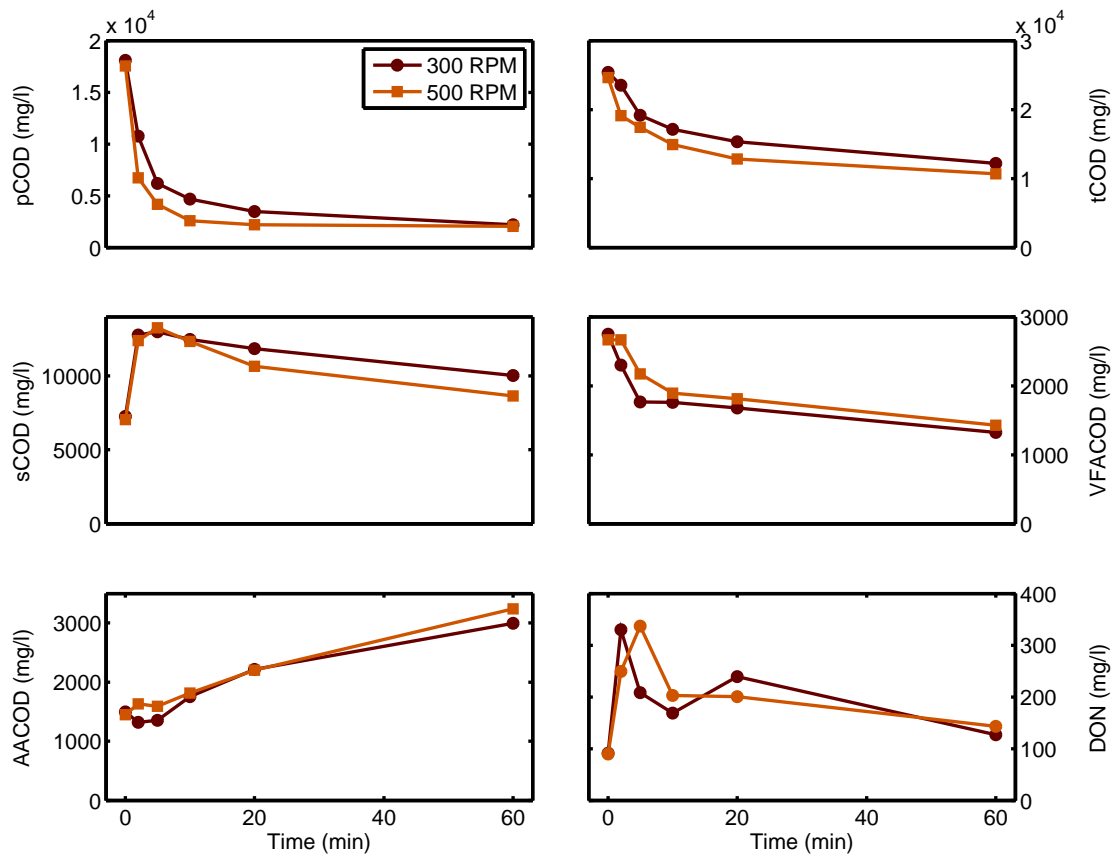


Figure 5.12: The influence of increasing stirrer speed from 300 to 500 RPM on the degradation achieved at a constant temperature and  $O_2$  partial pressure. Data from experiments 1 and 5.



### 5.3 Development of a Kinetic Model

As discussed in Chapter 1, a primary aim of this work is to postulate and develop kinetic models that characterised the degradation of biosolids, with particular focus on the intermediate and end products. The literature review in Chapter 2 showed that wet oxidation reaction pathways are complex and a common simplification is to use lumped components, in addition to a COD basis for concentration. We intend to explore the use of these simplifications to keep the developed kinetic models manageable.

For this study, several COD based pseudo-compounds were postulated to characterise the behaviour observed from the experimental data, with many being common wastewater quality indicators. This is in line with previous work in this area, notably Li *et al.* [57] and Zhang *et al.* [48]. The real and pseudo-components are listed in Table 5.5. Of these, the following components were of particular interest, particulate COD (pCOD), soluble COD (sCOD), acetic acid (AACOD), volatile fatty acids (VFACOD) and dissolved organic nitrogen (DON).

Table 5.5: The measured and derived state variables used in the kinetic model.

State variables	Derived state variables	Measured states
pCODfast pCODslow sCODfast sCODslow sCODnr AACOD VFACOD DON O <sub>2gas</sub> O <sub>2liquid</sub> CO <sub>2</sub>	pCOD = pCODfast + pCODslow sCOD = sCODfast + sCODslow + sCODnr	pCOD sCOD VFA DON AACOD

Acetic acid was modelled as a separate component using a COD basis as AACOD. This was because its concentration was significantly higher than the other acids, and it was of particular interest. The other VFAs shown earlier in Table 5.3 were lumped together and represented by the VFACOD pseudo-component. The concentration for each of the VFAs measured was converted to a COD basis by using the conversion factors listed in Table 5.6.

The soluble COD measurement quantifies all dissolved oxidisable material, and as such it includes the concentration of the acetic acid and VFA components. It was decided that the model should represent soluble COD as the non VFA soluble COD, which is the difference between the measured soluble COD, and total sum of VFAs,

Table 5.6: The COD conversion ratio for different measured volatile fatty acids. Data from [119].

Compound	COD ratio (mgCOD/mgAcid)
Acetic acid	1.067
N-butyric acid	1.818
Propionic acid	1.514
Pentanoic acid	2.039
Hexanoic acid	2.207

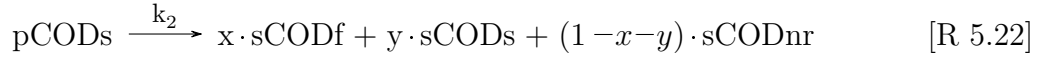
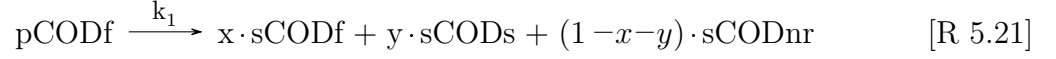
rather than use soluble COD directly. Characterising the components in this manner enabled COD balances to be closed, because the same component was not being quantified multiple times by the sCOD, AACOD and VFACOD components. Soluble COD (sCOD) in the model is therefore the remaining non-VFA soluble COD in solution.

As discussed earlier in Section 5.2.2, the rate of change observed in the experimental data suggests that both particulate and soluble COD consist of at least two fractions that degrade at different rates. Van Amstel [55] previously discovered that biosolids consisted of fractions which degrade at different rates, and proposed that it consisted of fractions of high reactivity, intermediate reactivity and no reactivity. However they applied this classification to the biosolids as a whole, rather than to the intermediate reaction compounds that are formed. This phenomenon was also noted by Shanableh [88] who denoted the fractions of both particulate COD and soluble COD as “difficult to degrade” and “easy to degrade”.

In this study, these components have been divided into fast reacting and slow reacting fractions, while soluble COD also has a non-reacting remainder. These fractions have been denoted as pCOD<sub>f</sub>, pCOD<sub>s</sub>, sCOD<sub>f</sub>, sCOD<sub>s</sub> and sCOD<sub>nr</sub> where f, s and nr correspond to the fast, slow and non reactive fractions. This hypothesis was used because it was found that it was not possible to describe the concentration profile for these compounds with a single reaction and rate constant. The fractions of fast and slow reacting particulate soluble COD were regressed to best fit the experimental data. It is recognised that the value of these fractions will likely depend on the range of operating conditions in use, particularly temperature, as Foussard *et al.* [58] did not observe a non-reactive fraction when they used temperatures over 300°C.

The reaction network proposed in Reaction R5.35 to Reaction R5.48 assumes the following kinetic behaviour:

Particulate COD first solubilises into soluble COD, which is represented by Reaction R5.21 and Reaction R5.22.



where pCOD represents

$$\text{pCOD} = \text{pCODf} + \text{pCODs} \quad [\text{R } 5.23]$$

Particulate COD is assumed to have fast and slowly solubilising fractions, and it is also assumed that this reaction does not consume oxygen. Soluble COD then degrades into the reaction intermediate and end products, which is shown below from Reactions R 5.24 to R 5.30.



while sCOD comprises of the summation of the fast, slow and non-reactive components

$$\text{sCOD} = \text{sCODf} + \text{sCODs} + \text{sCODnr} \quad [\text{R } 5.30]$$

The fast reacting fraction of soluble COD is assumed to oxidise to AACOD, DON, VFA and  $\text{CO}_2$  while slowly reacting soluble COD reacts to AACOD, VFA and  $\text{CO}_2$ , with the reaction pathways being structured to best fit the experimental data. It is assumed that oxygen is only consumed in the reactions which generate  $\text{CO}_2$ . VFACOD is oxidised into  $\text{CO}_2$  to account for the degradation observed in the experimental data. These are represented by Reactions R5.31 to R5.33.

It has been shown that dissolved nitrogen can be further oxidised to nitrogen gas with the appropriate catalyst [120], however the focus of this study was non catalytic wet oxidation. Therefore a degradation pathway for ammonia has not been included, as the uncatalysed reaction rate is too slow. A reaction to degrade DON was included, as DON on average appears to degrade somewhat towards the end of the experiment.

It is assumed that DON is subsequently converted to  $\text{NH}_3$ .



Admittedly the evolution of DON is not strictly chemically correct as shown in Reactions 5.31 to 5.33, and in a modified form in the extended kinetic model in Section 5.6. However, the pathways used were chosen as a compromise to best match the observed behaviour from the experimental data. For example there is no explicit nitrogen on the left hand side of Reaction R5.32, however it is assumed that nitrogen is originally part of the soluble COD, and then disassociates itself. In the modified reaction pathway postulated in Section 5.6, it is assumed that the nitrogen hydrolyses from the particulate COD which is a more reasonable assumption.

Oxygen transfer from the gas to liquid phase has been included as part of the model. The initial concentration of dissolved oxygen is computed using Henry's law, described in Section 3.8, at ambient temperature and pressure. Oxygen is assumed to affect all reactions in an attempt to account for any unmodelled effects caused by the higher oxygen partial pressure, however the oxidant order  $n$  may be zero.

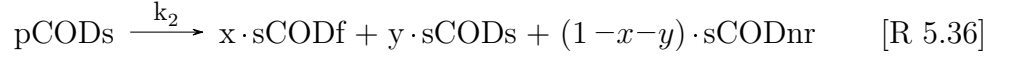
The mass of oxygen present in the reactor headspace after pressurisation is then calculated using the ideal gas law. The mass of dissolved oxygen at the operating temperature is then calculated using the previously determined headspace mass of oxygen to give the mass of dissolved oxygen at the  $t = 0$  point for the experiment.

For this initial model, oxygen transfer from the liquid to the gas has been modelled as a pseudo-reaction in Reaction R5.34, as opposed to a true mass transfer model for simplicity, as the aim of the initial model was to prototype the likely kinetic pathways.



In summary, the full set of reaction pathways shown below in Reaction R5.35 to Reaction R5.48.





It is generally agreed that wet oxidation reactions follow the standard Arrhenius based relationship shown in Eqn. 5.1 [57]. Where  $[C]$  is the concentration of the compound of interest,  $[O_{2(aq)}]$  is the dissolved oxygen concentration,  $m$  and  $n$  are the reaction orders with respect to the reactant and oxidant respectively and  $k$  is the reaction rate constant;

$$\frac{dC}{dt} = -k[C]^m[O_{2(aq)}]^n \quad (5.1)$$

and  $k$  is of the form

$$k = k_0 \exp\left(\frac{-E_a}{RT}\right) \quad (5.2)$$

where  $k_0$  is the pre-exponential factor,  $E_a$  is the activation energy,  $R$  is the universal gas constant, and  $T$  is the reactor temperature.

The reaction network was implemented as a series of ordinary differential equations (ODEs) using the Matlab environment described in Section 4.5, although in principle the Python environment in Section 4.4 would also work.

### 5.3.1 Preliminary Model Simplifications

The focus for the initial model was to postulate and validate the likely reaction pathways occurring during the wet oxidation process. The kinetic model was then expanded to include the environmental effects of interest, and is described later in Section 5.6.

A number of simplifications have been made as part of the preliminary modelling work to reduce the number of parameters required, and simplify the already complex numerical regression problem. These simplifications will be removed in the more detailed model regressed in Section 5.6. The Arrhenius temperature relationship has been replaced by a constant, and interactions due to mixing have not been included. A review published by Li *et al.* [57] contains an extensive list of reaction rate constants and shows that the reaction orders with respect to the reactant and oxidant are typically 1. Based on this, the reaction orders  $m$  and  $n$  have been fixed at 1 initially. Finally, the reaction rates for the fast and slow reactions for both acetic acid and VFA, ( $k_3$  and  $k_6$  in reactions R5.35 to R5.48) were assumed the same for this initial parameter fitting exercise.

Rather than fit the rate constants for all experiments, each experiment has been fitted separately to test the model structure. The simplified rate expression for each reaction therefore becomes the following

$$\frac{dC}{dt} = -k[C][O_{2(aq)}] \quad (5.3)$$

The initial version of the kinetic model did not take into account the change in volume caused by liquid sampling. This is clearly a simplification, as the amount of dissolved oxygen is strongly dependent on the temperature and partial pressure of oxygen in the reactor vessel. This was factored into the extended kinetic model to be described later in Section 5.6.

These simplifications have been performed to ease the initial prototyping of the kinetic pathways. Once the reaction pathways were established, the environmental effects were incorporated in Section 5.6.

### 5.3.2 Preliminary Model Results

A series of ODEs for each of the reaction pathways described in the previous section was implemented in the Matlab modelling environment described in Section 4.5.

Each of the model states represents the concentration of each of the model components. The model was regressed using the OPTI toolbox, [121], described in Section 4.5, to best fit the experimental data and the model results are compared in Fig. 5.13 to Fig. 5.17 against the same experimental runs shown in Section 5.2.2. The results for all experiments conducted are presented in Appendix B.

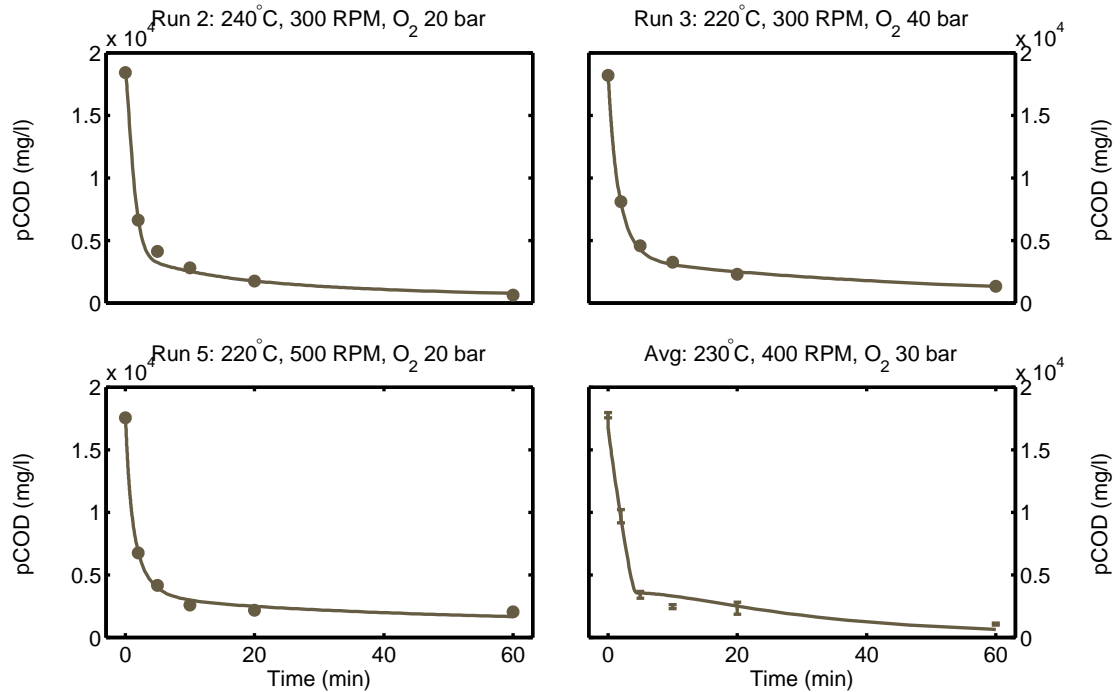


Figure 5.13: The concentration of pCOD from the preliminary kinetic model versus experimental data.

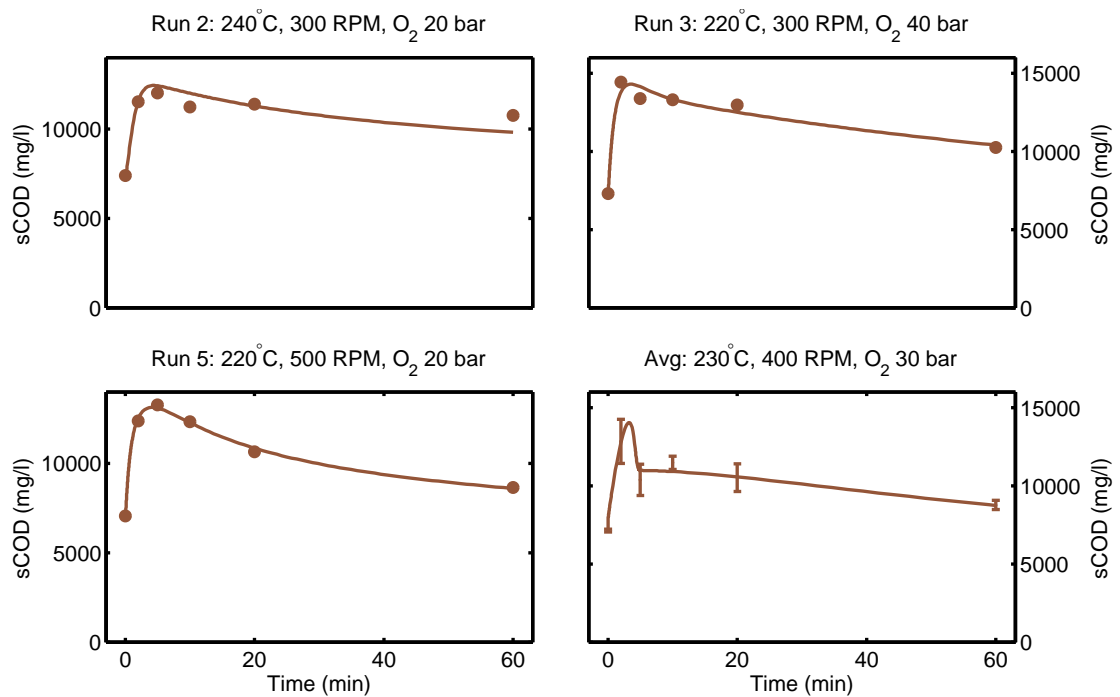


Figure 5.14: The concentration of sCOD from the preliminary kinetic model versus experimental data.

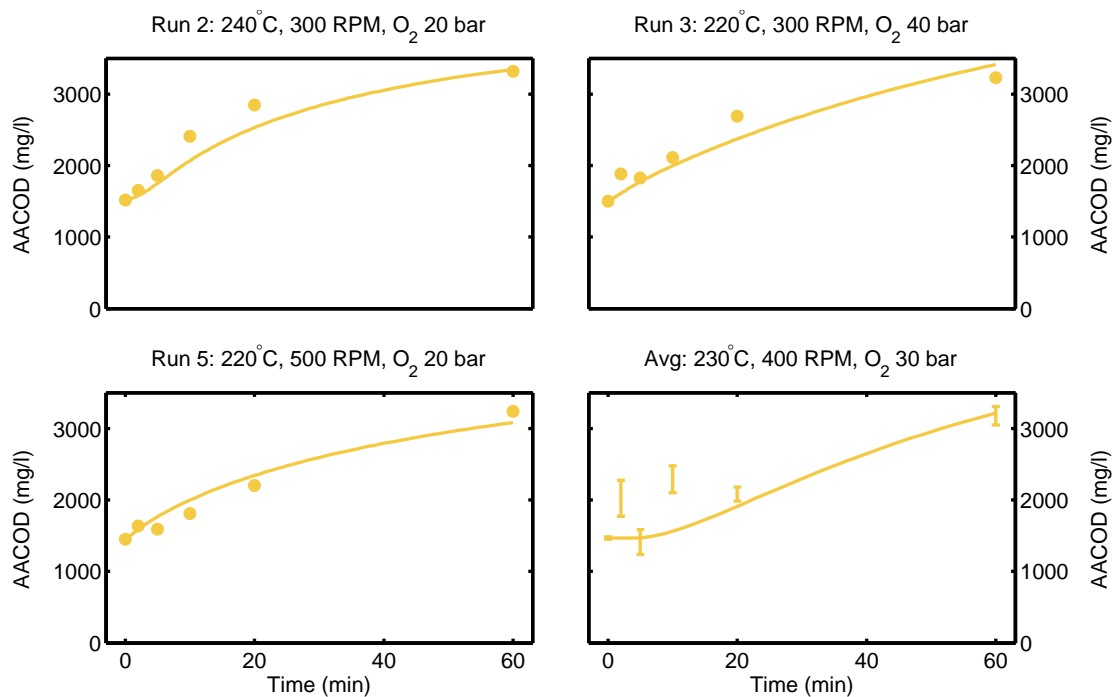


Figure 5.15: The concentration of AACOD from the preliminary kinetic model versus experimental data.

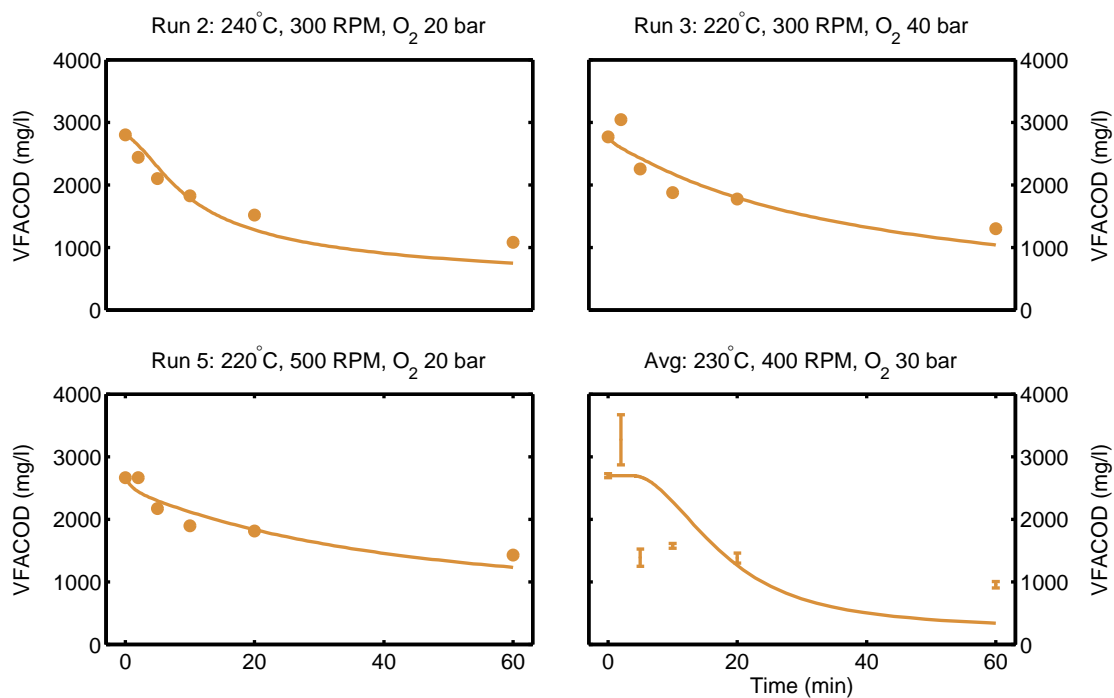


Figure 5.16: The concentration of VFACOD from the preliminary kinetic model versus experimental data.



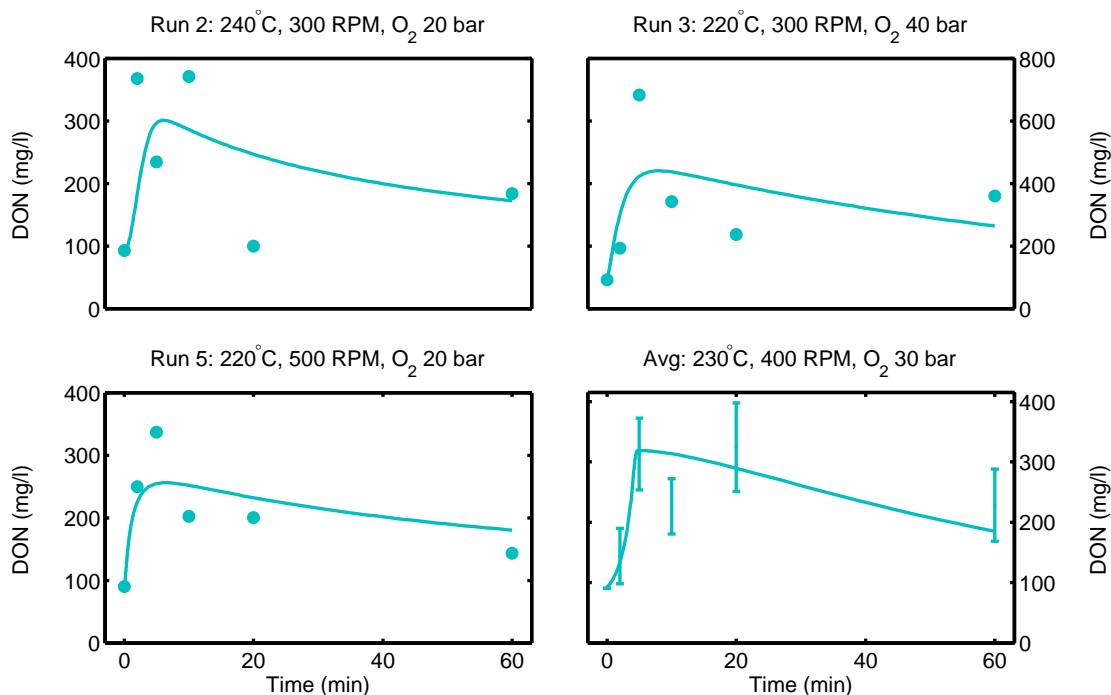


Figure 5.17: The concentration of DON from the preliminary kinetic model versus experimental data.

In general, the model is shown to closely follow the experimental data for each of the measured components. This suggests that the effect of the dominant reaction pathways have been captured in the kinetic model. The next stage is to incorporate the effect of the environmental conditions, namely temperature, oxygen partial pressure, and stirring speed into the model and regress these parameters. This is performed later in Section 5.6.

The correlation between the model and the measured output shown in Fig. 5.18 gives an indication of the quality of this preliminary model. Since some of the measured data at  $t = 0$  was used as an initial condition in the model, these, by definition, have no residual, so were *not* included in the computation of the correlation coefficient. The calculation of the overall correlation coefficient was  $R^2 = 0.983$  which suggests that the model fits the experimental data well.

A more detailed statistical analysis of the extended kinetic model is given later in Section 6.3.

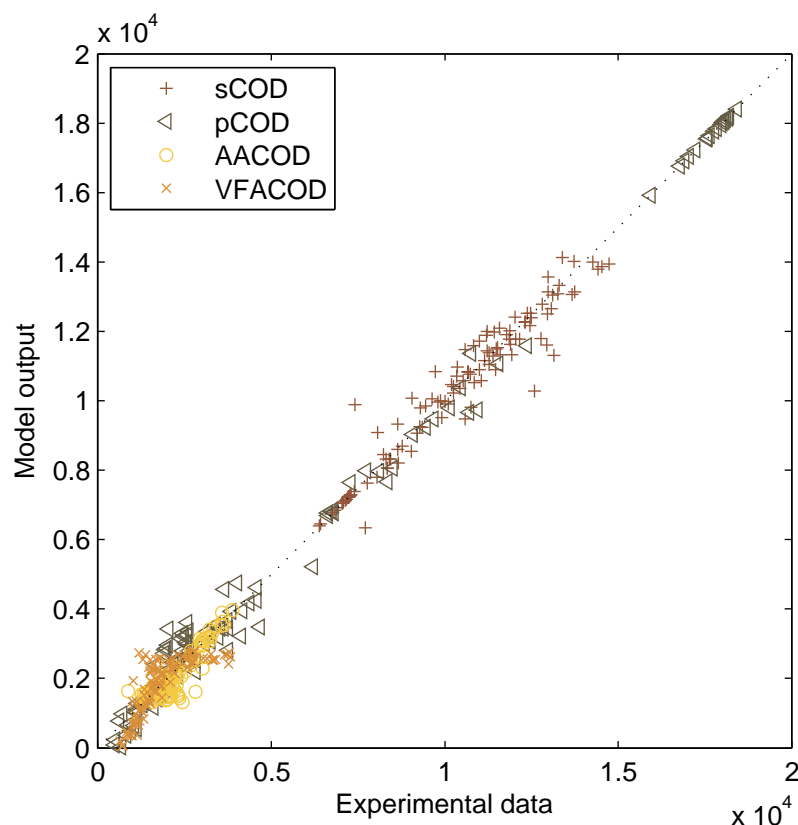


Figure 5.18: A comparison of the actual measured data compared to the model predictions. (See also Fig. 6.13.)

### 5.3.3 Set 1 Experiment Summary

The experimental results show that each of the environmental variables (temperature, oxygen partial pressure and stirring speed) affects the level of degradation achieved, with temperature having the greatest effect. The results also confirm the hypothesis that several of the aggregated compounds need more than one reaction rate constant for an adequate description of the conversion. This fact is illustrated below in Fig. 5.19 for pCOD. This highlights the fact that the trend of pCOD, for example, which exhibits an initial rapid decline followed by much slower decay, cannot be obtained with a single rate expression as it will either asymptote to the incorrect value, or not correctly capture the dynamics in the early phase of the reaction.

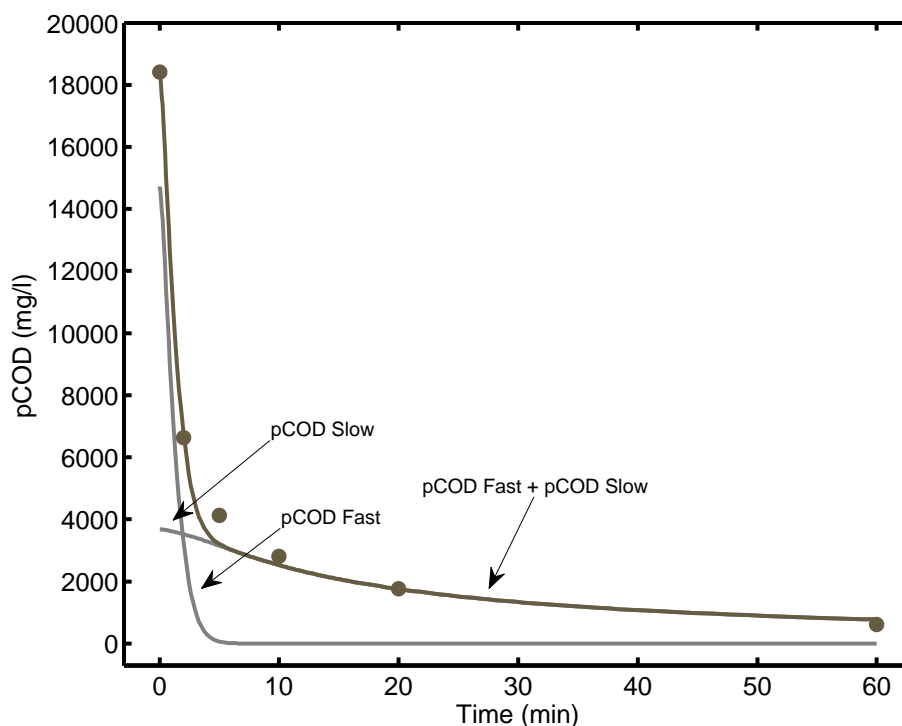


Figure 5.19: An illustration of the magnitude of the fast and slow components that make up pCOD in the kinetic model.

Overall, the kinetic pathways appear to closely follow the experimental data, which suggests that they are representative of the kinetic behaviour of biosolids oxidation. However, one of the problems encountered was that the model regression was very sensitive to the initial guess for the rate parameters, and often had trouble converging. Extreme sensitivity is well known in chemical reaction parameter regression [122]. The next phase will involve adding the environmental effects, and refining the reaction pathways.

The centre point of the factorial design (experiments 15 to 18) demonstrates that the acetic acid and VFA results exhibit considerable variation, particularly for the early samples, while the final ( $t = 60$ ) sample consistently has the least variation. This is due to significant variation in Runs 17 and 18 (shown in Appendix B) which skew the average and result in the large error bars. Because of the lack of variation in the other experiments for these compounds, it is suspected there was a problem with these two experiments. However, the DON concentration results show significant variation across all experiments, and it is not expected that the model will be able to predict the concentration of this component with any certainty without improved experimental data.

## 5.4 Second Set of Experiments

The first set of experiments was used to characterise how RDC biosolids degrade under wet oxidation so that reaction pathways could be postulated. The first set of experiments reinforced the sensitivity that has been described in the literature of wet oxidation to the effect of temperature, and to a lesser extent, oxygen partial pressure. Because of this, it was decided that further investigation was needed into the dependence of these operating conditions.

Preliminary experiments performed at Scion suggested that wet oxidation reactions begin to happen at around 200°C and there was interest in how the production of VFAs was affected at lower temperatures. To explore this hypothesis, a series of experiments was conducted over a wider range of temperatures and oxygen partial pressures to further investigate the effect of these parameters on the degradation rate. The reaction conditions investigated in this second set are listed in Table 5.7. Stirrer speed was kept constant at 400 RPM for all experiments in this set as it was shown to have the least effect on the results.

Table 5.7: Experimental conditions investigated in the Set 2 experiments.

Condition	Range
Temperature	180–220°C
Oxygen partial pressure	16–40 bar
Stirrer speed	400 RPM

One important difference in this set of experiments was that the samples used were non-fermented biosolids directly from the filter belt presses from the RDC wastewater treatment plant (shown in Fig. 2.2) as opposed to being fermented. This was due to the fermenter being shut down for an extended period of time during the second experimental programme. Because of this, the feed samples are likely to have a higher levels of pCOD and lower levels of VFAs.

There were also important equipment and procedural changes that occurred between the Set 1 and Set 2 experiments. Firstly, a reflux condenser was installed on the gas outlet of the reactor, which is shown in Fig. 5.20. The aim of the condenser was to dry the gas stream leaving the reactor when operating in continuous gas flow mode and to prevent vapour condensing inside the back-pressure controller downstream of the reactor. Because of the position of the isolation valves, the presence of the condenser effectively increased the volume of the reactor headspace.

The second major change was that the reactor could no longer be purged with pure oxygen owing to safety concerns about pure oxygen flowing into the gas discharge line. Instead, the reactor was purged with nitrogen, before being sealed and pres-



Figure 5.20: Photograph showing the reflux condenser installed on the gas outlet of the Parr reactor and the location of the off-gas sampling line.

surised with oxygen to the desired pressure. This meant there was now a small amount of residual nitrogen present in the reactor in each experiment.

Liquid samples were collected in the same manner as the Set 1 experiments, but because of economic reasons, only the initial and final samples were analysed. The remaining samples were frozen so they could be analysed at a later date. The samples were analysed for solids content (TSS and VSS) and COD (total and soluble COD). VFA, nitrogen and phosphorus analysis were not performed for economic reasons.

The experiments were performed using the same procedure as the Set 1 experiments, apart from the oxygen purge, and the results from the sample analysis are shown in Table 5.8.

Table 5.8: Results from the Set 2 experiment samples.

Sample ID	Time (min)	Temperature (°C)	O <sub>2</sub> (bar)	TSS (mg/l)	VSS (mg/l)	tCOD (mg/l)	sCOD (mg/l)	pCOD (mg/l)
AUT01	0	220	16.4	11711	1488	14811	2055	2173
AUT01	60	220	16.4	2932	855	8495	5977	1169
AUT02	0	220	32	10174	1237	18084	1904	1805
AUT02	60	220	32	2128	705	7266	5276	945
AUT03	0	220	40	10235	1319	17889	2124	1926
AUT03	60	220	40	2301	807	7524	5745	1085
AUT04	0	200	40	10965	1432	13871	2136	2090
AUT04	60	200	40	3532	837	9766	6646	1222
AUT05	0	180	40	11212	1349	12766	2260	1970
AUT05	60	180	40	3473	679	13333	7248	992
AUT06	0	210	40	10650	1342	13366	2263	1960
AUT06	60	210	40	3465	1009	9896	6830	1473

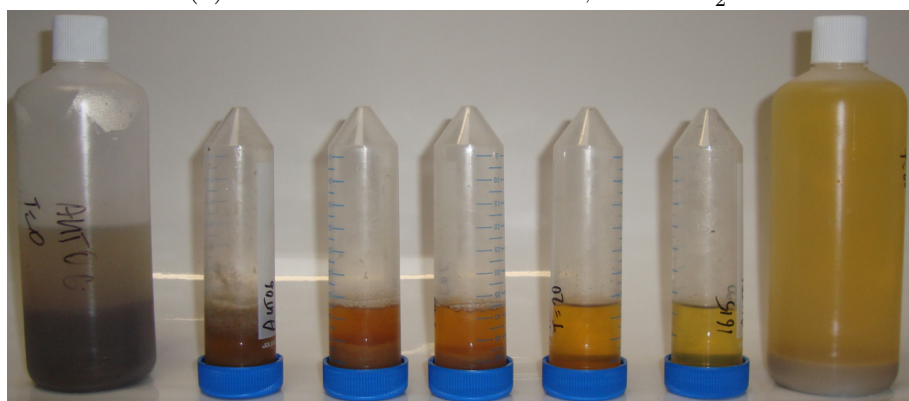
Fig. 5.21 shows photos of the liquid samples taken with varying the temperature from 180 to 220°C. What is immediately apparent is that temperature has a major effect on the level of residual solids, with the volume of solids roughly halving from 180 to 210°C, and halving again from 210 to 220°C. The liquid also has a much lighter colour which suggests that there is more oxidation happening, as opposed to thermal hydrolysis.

A series of photos of the liquid samples taken with a varying oxygen partial pressure and constant temperature of 220°C are shown in Fig. 5.22. It is clear from the photographs that lower oxygen partial pressures result in a much darker colour, which is assumed to be the result of Maillard reactions which are known to form under low or non-oxidative conditions and are highly coloured [123, 124]. It is interesting that even the lowest oxygen concentration resulted in good solids reduction, with a similar amount remaining in each of the final sample bottles at 220°C.

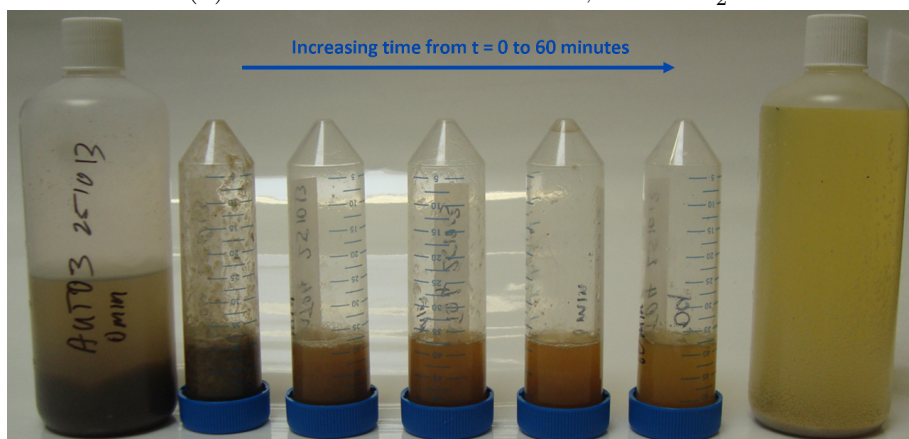




(a) Reaction conditions: 180°C, 40 bar O<sub>2</sub>.



(b) Reaction conditions: 210°C, 40 bar O<sub>2</sub>.

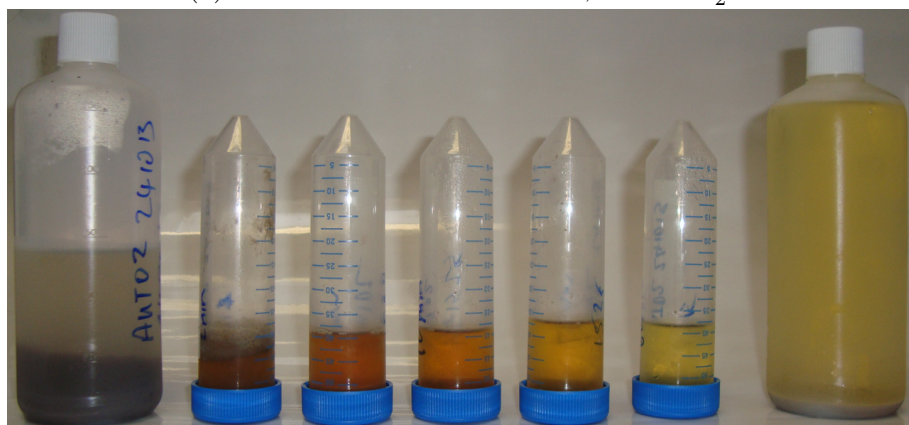


(c) Reaction conditions: 220°C, 40 bar O<sub>2</sub>.

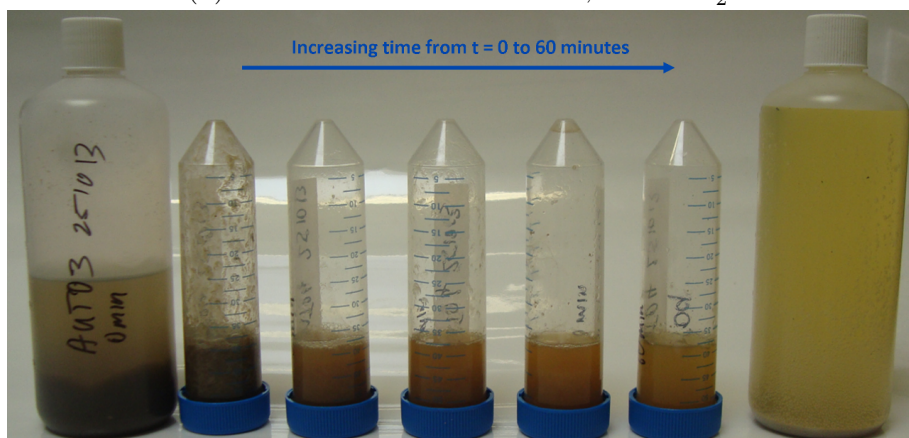
Figure 5.21: Photographs of the the liquid samples taken during the course of the experiment varying the temperature from 180 to 220°C at a constant O<sub>2</sub> partial pressure of 40 bar.



(a) Reaction conditions: 220°C, 16 bar O<sub>2</sub>.



(b) Reaction conditions: 220°C, 32 bar O<sub>2</sub>.



(c) Reaction conditions: 220°C, 40 bar O<sub>2</sub>.

Figure 5.22: Photographs of the the liquid samples taken during the course of the experiment varying O<sub>2</sub> partial pressure from 16 to 40 bar at 220°C.



Comparing the solids and COD results with those obtained in Set 1 highlighted significant differences between some of the components. The initial concentrations of TSS were lower on average than the Set 1 experiments (average TSS of 14878 mg/l), however the trend for the conversion of TSS was quite similar to Set 1. This suggests a potential problem with the feed preparation, such as an error in the dilution of the biosolids feed samples. The dilution was performed to achieve a nominal solids concentration of 1.5% by weight in the reactor.

The final TSS value for the experiments generally increased with decreasing temperature, which was expected. This is clearly illustrated by the photographs of the samples in Fig. 5.21 which show the initial suspended solids have been almost completely removed. However, TSS is not a component in the kinetic model since the solids reduction of wet oxidation is well known, and the primary focus of this study is on the soluble and gaseous intermediate and reaction end products. A similar behaviour was expected for pCOD, however this was not observed in the above results with the final pCOD concentration bearing little correlation to the operating conditions. This was not observed in the Set 1 experiments.

The initial values for VSS and soluble COD were also much lower than the Set 1 experiments, although the final values appear plausible. Unfortunately, without the analysis of the intermediate samples, it is unclear if the results follow the same trend over time.

#### 5.4.1 Possible Reasons for Discrepancies

While there is not a definitive reason for the significant discrepancy between Set 1 and Set 2 experiments, there were a number of changes that occurred during the Set 2 experiments;

**Sample Analysis:** The solids measurements (TSS and VSS) were performed by the author instead of the analytical lab staff at Scion because of time constraints. However the COD analysis was performed by Scion analytical lab staff.

**Feed type:** The use of non-fermented biosolids would affect the initial levels of dissolved COD. However Scion have performed experiments in the past with non-fermented biosolids and this does not account for the magnitude of the discrepancy observed. Fermenting the belt press biosolids reduces the ratio of VSS/TSS from 80 to 90% to 60 to 80% after fermentation. The VSS/TSS ratio for this set of experiments is around content 12 to 13%. VFAs and sCOD have been shown to change by around 20% in earlier experimental work at Scion. The magnitude of the discrepancy of VSS/TSS in these experiments compared with earlier research

suggests that the lack of fermentation is not the cause of the error.

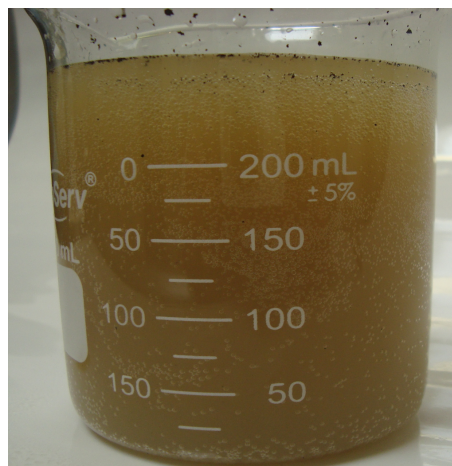
**Equipment Change:** The installation of the reflux condenser may affect the results due to the extra gas volume, but the initial sample, which has the most error, was prepared outside the reactor and therefore would be unaffected by this change.

**Procedure Change:** The removal of the oxygen purge would decrease the dissolved oxygen concentration by a small amount, but not affect the initial sample, which has the most error, as it was prepared outside the reactor.

It is apparent that the results obtained from this set of experiments are significantly different from the results obtained in the first set of experiments. The measured COD concentrations are greatly reduced, in addition to the VSS concentration. The only parameter that is close to the results from the first set of experiments is TSS, but this is not a component in the kinetic model. Although a number of changes have taken place, there is no clear explanation for the considerably different results. However, it is likely that the error is due to a sample preparation or analysis error. As discussed above, experiments have been conducted in the past at Scion with non-fermented biosolids and the results were of similar range to Set 1, therefore it is not believed that this is the cause of the discrepancies.



(a) Dissolved gasses coming out of solution.



(b) Gas bubbles still visible after several minutes.

Figure 5.23: Dissolved gasses in the reactor effluent after de-pressurisation at the completion of the experiment

An interesting observation was that there were considerable amounts of dissolved gasses still present in the liquid effluent, even after the reactor had been de-pressurised. The gasses came out of solution when the reactor contents were emptied into a beaker and fizzed violently. Gas bubbles were still appearing even after the beaker had been left to stand for several minutes. It is believed that the gas is mostly  $\text{CO}_2$ , although it was not measured at the time. This phenomenon was observed for all the experiments undertaken.

Because of the size of the discrepancy between the Set 1 and Set 2 results it was decided not to use the data for parameter regression in the model at this time. The intermediate liquid samples have been frozen and can be re-analysed for verification at a later date.

### 5.4.2 Reaction Extent Using Image Analysis

Because of the poor results obtained from the analytical analysis of the liquid samples, and the lack of intermediate data, it was decided to investigate the possibility of whether useful information could be obtained from the series of photographs that were taken for each set of samples. The series of images earlier in Fig. 5.21 and Fig. 5.22 appear to show a relationship between the reaction extent and the reaction conditions. The hypothesis to be tested is whether the image intensity information from each sample correlates to either the concentration of a component or combination of components of interest in the model.

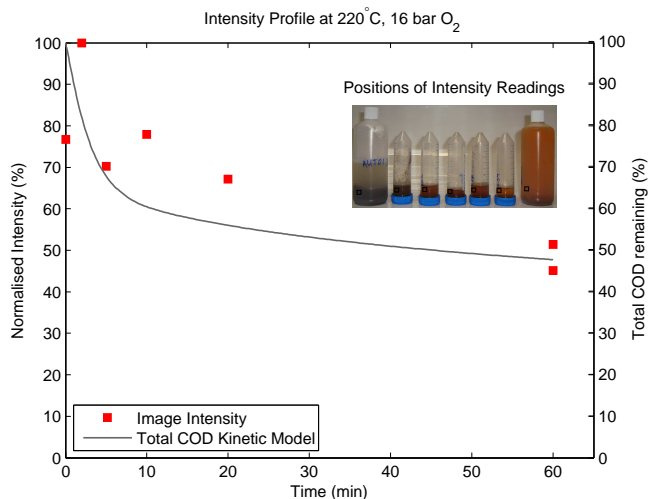
To investigate this, the images were analysed using the image processing tools in Matlab. The images were first imported into Matlab and a group of pixels were selected manually from approximately the same position from each test tube in the liquid fraction, except for the  $t = 0$  sample where the settled solids were selected. Although this is not a scientific way of sampling, this exercise was intended as a proof-of-concept rather than a rigorous scientific study and as a way of making the best use of the data available from the second set of experiments.

The **rgb** colour values for the selected groups were extracted from the image, and the mean value was computed to represent an intensity index. This was normalised about the  $t = 0$  sample, and the normalised intensity results were recorded. It was discovered during testing that the mean of the **rgb** values gave better results than using the Matlab function **rgb2gray**, which converts the image to gray-scale using a weighted sum of the red, green and blue components based on human colour perception.

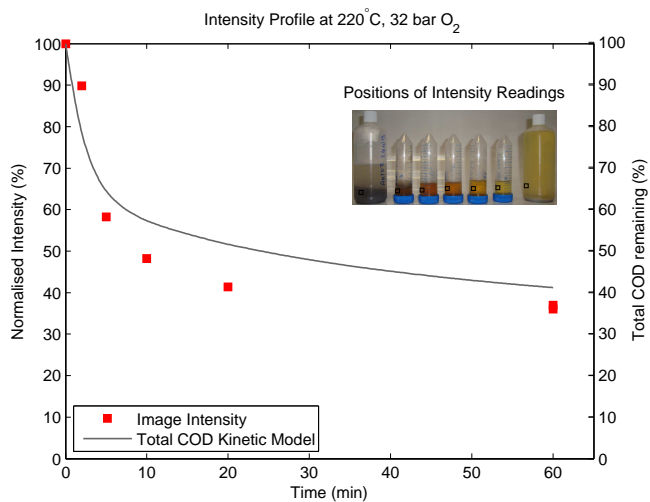
By observation, the trend for the change in intensity appears to be similar to the change in total COD illustrated in the experimental data. To test the image analysis hypothesis described earlier, the results for total COD from experimental Run 7 in Section 5.2 were plotted against the normalised image intensity in Fig. 5.24c and Fig. 5.25a, which was the only experiment with the same operating conditions as those covered in this investigation.

The results for the sets of images are displayed in Fig. 5.24 which shows the change in oxygen partial pressure at constant temperature, and Fig. 5.25 shows the change

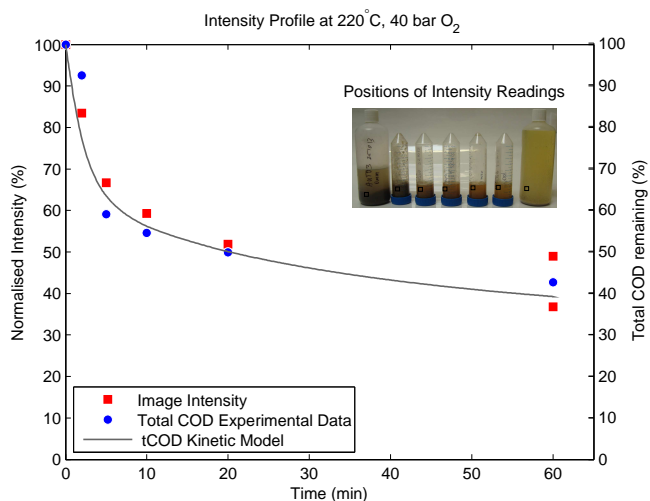
in temperature at a constant oxygen partial pressure.



(a) Reaction conditions: 220°C, 16 bar O<sub>2</sub>

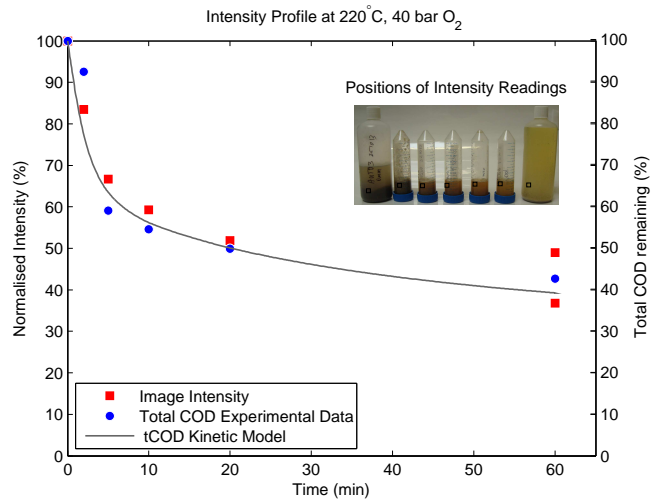


(b) Reaction conditions: 220°C, 32 bar O<sub>2</sub>

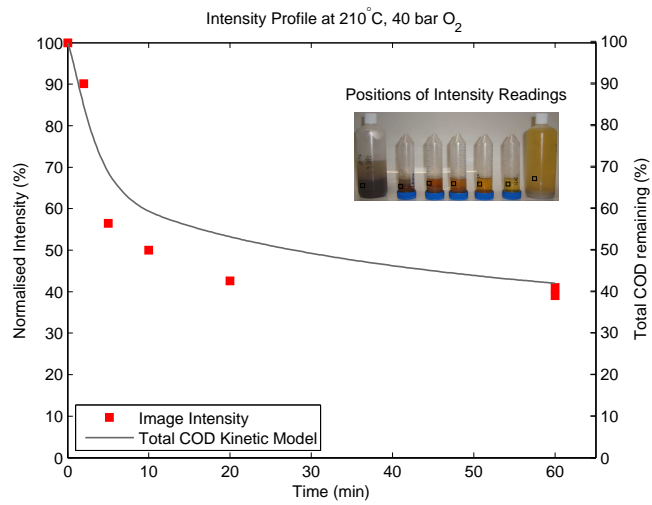


(c) Reaction conditions: 220°C, 40 bar O<sub>2</sub>

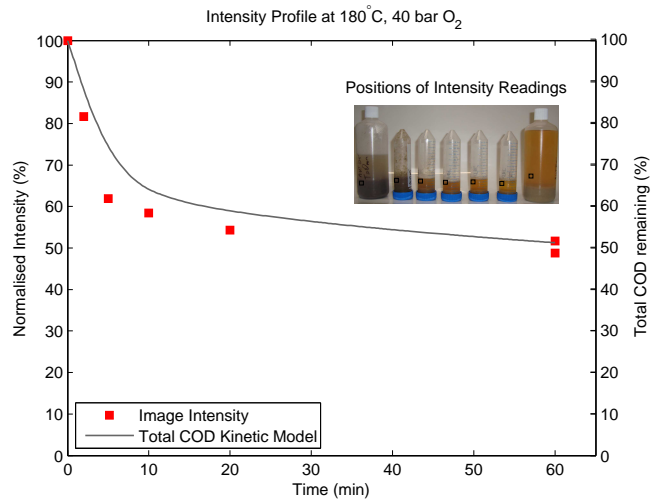
Figure 5.24: Image analysis of the liquid samples varying O<sub>2</sub> partial pressure from 16 to 40 bar at 220°C and a constant stirring speed of 400 RPM.



(a) Reaction conditions: 220°C, 40 bar O<sub>2</sub>



(b) Reaction conditions: 210°C, 40 bar O<sub>2</sub>



(c) Reaction conditions: 180°C, 40 bar O<sub>2</sub>

Figure 5.25: Varying the temperature from 180 to 220°C at a constant O<sub>2</sub> partial pressure and stirring speed of 400 RPM.

While it is difficult to differentiate the difference between changes in oxygen partial

pressure and changes in temperature, it is apparent from the images embedded in Fig. 5.24 and Fig. 5.25 that an approximation of reaction extent can be determined visually.

It is pleasantly surprising that the change in total COD closely follows the change in intensity for this experiment. For economic reasons, there is only one run from both sets for which experimental data is available. To further explore the relationship described above, the kinetic model that is developed in Chapter 5 was used to simulate the conditions used in the remaining Set 2 experiments, and is compared with the intensity data later in Fig. 5.24 and Fig. 5.25.

The total COD results from the extended kinetic model fit reasonably well with the intensity index, which suggests that images of the intermediate liquid samples could be used as an approximation for the total COD removal of biosolids under wet oxidation.

While this work is very preliminary and requires substantial work to provide treatment of results, it highlights the feasibility of using image analysis to determine useful information from photographs of the intermediate liquid samples. This is very quick and easy to perform and could be an interesting avenue to explore as part of the future research.

### 5.4.3 Stirrer Current Investigation

For the second set of experiments, the stirrer drive system was modified, with the addition of a different motor, to investigate whether changes in viscosity, and potentially reaction extent, could be captured by measuring the current drawn by the stirrer motor. This idea is similar to that of Bhat *et al.*, [125] who investigated whether stirrer power could be used as a soft-sensor to detect changes in polymerisation. The details of the modifications made to the reactor were discussed in Section 3.2.1.

To test this hypothesis, experiments were conducted using tap water to determine whether the change in viscosity of water could be detected by the change in current as the reactor was heated from ambient temperature to 220°C. The results of this investigation are shown in Fig. 5.26, which shows the change in temperature and system pressure over time, and the change in motor current and the calculated viscosity of water. The viscosity was determined from the thermodynamic library `coolprop` [126].

It is apparent that there is significant electrical noise in the current measurement, which is partly due to the use of a brush type motor, and consequently the raw and

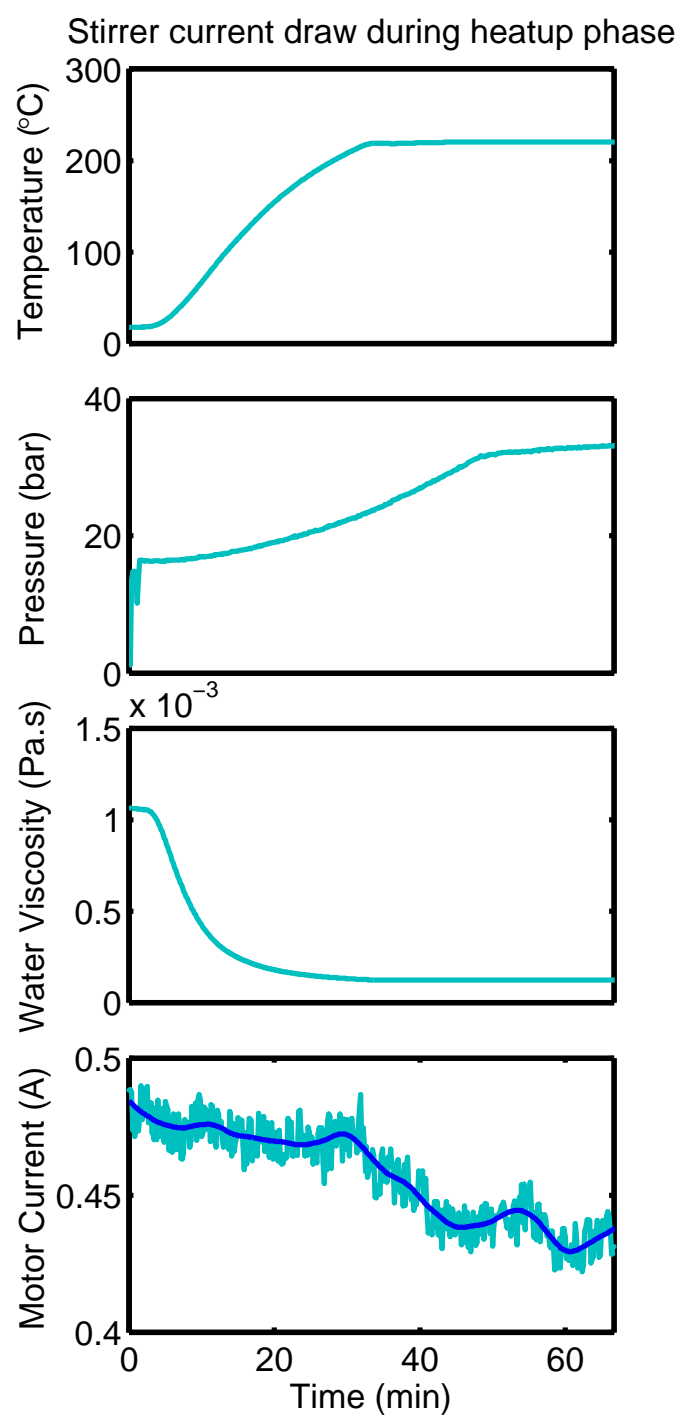


Figure 5.26: Stirrer current and viscosity during the warmup phase. The solid dark blue trace is the filtered current measurement.

filtered current measurements are shown in Fig. 5.26. The current measurement was filtered with the Matlab `smooth` function using the `loess` method. The change in current during warmup period was very small, but it was repeatable over several experiments.

The results show that the change in current does appear to follow the decrease in viscosity, although there is a time lag in the results. This may be due to a hysteresis effect in the magnetic drive coupling which connects the motor to the stirrer inside the reactor, but is otherwise unexplained.

To further explore this relationship, the normalised power required by the stirrer is plotted against the log of the viscosity in Fig. 5.27. Calculation of the correlation coefficient gives an  $R^2$  of 0.6 which confirms that there is a weak relationship between viscosity and the stirrer power requirements, and can be seen in Fig. 5.27. This could be incorporated into the kinetic model as part of future work.

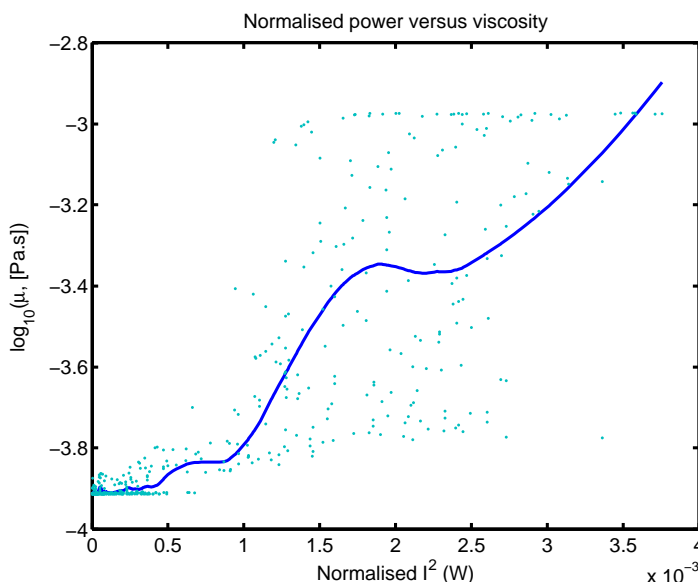


Figure 5.27: Log of viscosity versus the normalised stirrer power during the warmup phase.

A single wet oxidation experiment (run AUT06), including the warmup, reaction and cooldown phases, is shown in Fig. 5.28. It is interesting to note that the final current measurements before the cooldown phase begins are at a higher steady state than before the reaction phase begins. This is promising as it indicates that water, biosolids and final wet oxidation effluent can be differentiated from the stirrer current measurement as shown in Fig. 5.28. This could potentially be used as an online surrogate measurement for reaction extent.

Unfortunately, the data logger terminated recording before the reactor had fully cooled down to ambient temperature so the difference between ambient temperature



water and ambient temperature wet oxidation effluent was not able to be determined.

These results indicate that measuring the power drawn by the stirrer motor could give insight into the reaction extent, and this could be an avenue of further research, and would be a valuable input for the kinetic model.

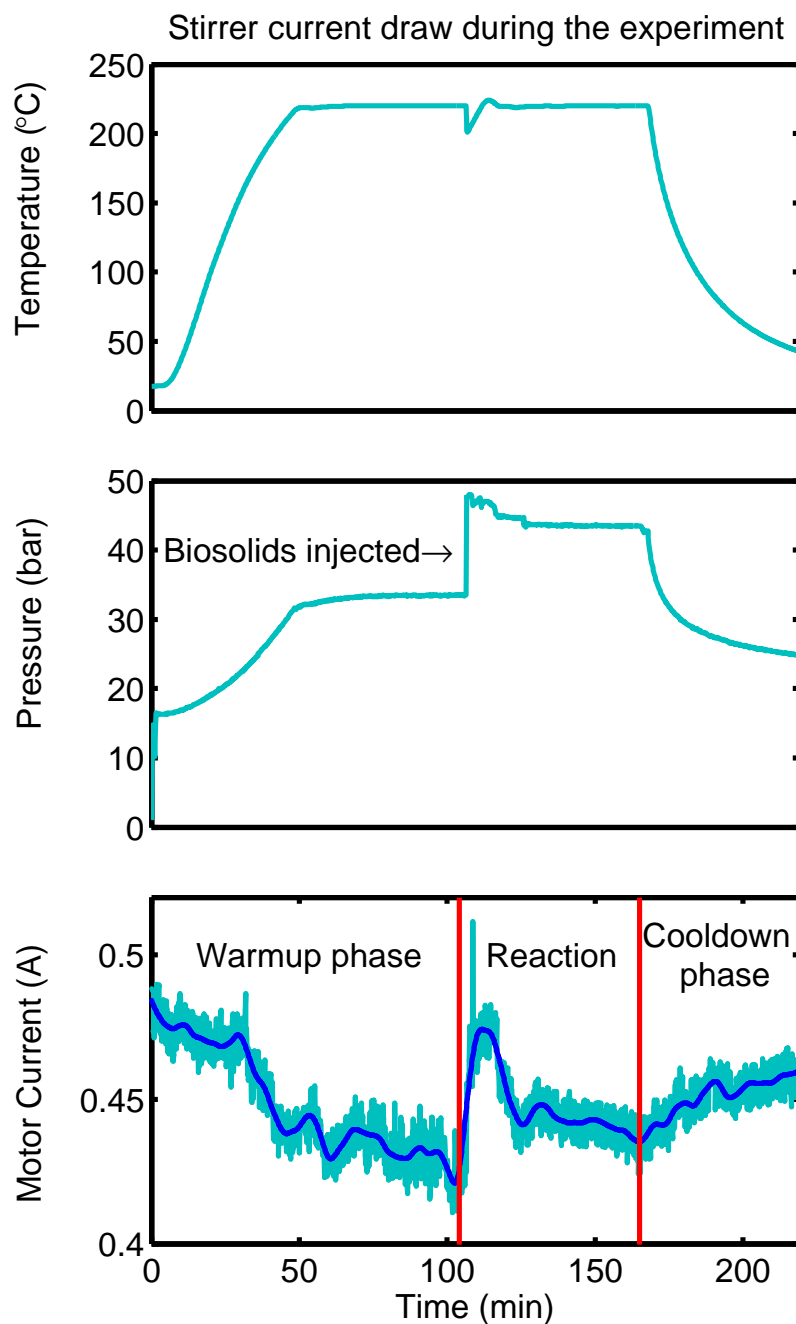


Figure 5.28: Stirrer current and environmental conditions from warmup to the completion of an experiment. The solid dark blue trace is the filtered current measurement.

## 5.5 Third Set of Experiments

Towards the completion of the second set of experiments, a new gas chromatograph (GC) was purchased specifically for analysing gases from the wet oxidation and fermentation experiments that were being performed at Scion by other research groups. One of the main advantages of the new GC was that it was mostly automated and enabled gas analysis to be performed by non-analytical lab staff. To take advantage of this new instrument, a third set of experiments was designed which covered existing operating conditions, to gain insight into the gaseous reaction products produced, and the level of oxygen consumption under the different operating conditions shown in Table 5.9.

Table 5.9: Set 3 experimental conditions.

Experiment ID	Equivalent Set 1 Experiment ID	Temperature (°C)	O <sub>2</sub> (bar)	Stirrer speed (RPM)
AUT07	5	220	20	400
AUT08	6	240	20	400
AUT09	15–18	230	30	400
AUT10	8	240	40	400

Gas and liquid samples were taken at the same intervals as in previous sets of experiments. Like the Set 2 experiments, the liquid samples were not analysed for economic reasons, but were still performed to keep the change in liquid volume the same during the experiments as in the previous sets. The liquid samples were frozen for later analysis if required. The gas samples were withdrawn from the reactor headspace into Tedlar gas sample bags for analysis using the Valco gas sampler described in Section 3.4.2. The GC was configured and calibrated using the methods described in Section 3.6.5.

The reflux condenser that was installed for the Set 2 experiments was removed prior to the commencement of these experiments. This was because the original gas sampling port was located at top of the condenser, and could not be closer to the reactor because of a lack of space required to install the sampling port. This meant there was a significant volume of gas that needed to be purged in order to get a representative gas sample of the reactor headspace. By removing the condenser, the sampling port is very close to the top of the reactor, which enables representative samples to be withdrawn without having to excessively flush the sampling lines and subsequently dropping the system pressure in the reactor. The location of the new gas sampling port is shown in Fig. 5.30.

The results of the off-gas composition analysis are presented in Fig. 5.29. The results show significant changes for all measured components over the duration of

the experiment, apart from nitrogen which is not a participating species in the oxidation reactions. Temperature has a significant effect on the off-gas composition and the experiments AUT07 and AUT08 show that it affects all components.

From Fig. 5.29, it is clear that increasing the temperature has a significant effect on the production of  $\text{CO}_2$ , with fractions of over 50% achieved in addition to greater oxygen consumption. Importantly, the production of  $\text{CO}_2$  is much greater than the batch experiments performed by Rose *et al.* [12] who also analysed the reactor off-gas. However they used compressed air instead of pure oxygen, and as a result had  $\text{CO}_2$  levels of around 5%. Despite this, at the end of their experiments there was still approximately 15% oxygen remaining.

Because of an experimental procedure change during the course of the Set 2 experiments, the reactor could no longer be purged with pure oxygen because of safety concerns. This resulted in a small amount of residual nitrogen remaining in the reactor, which was calculated to be approximately 3.5% at 20 bar partial pressure (dropping to 1.2% at 40 bar), when the reactor is pressurised with oxygen. However, the measured concentration of nitrogen in the gas samples was higher than expected, with levels of nearly 40% detected in Fig. 5.29. The range of nitrogen levels detected indicates that air may have leaked into the gas sampling loop during the sampling procedure, or the sample bags still contained residual gas because of incomplete evacuation, as opposed to nitrogen being produced as part of the oxidation process.

Hydrogen production, in concentrations of up to 0.5% was unexpected and could be a potential hazard in the TERAX pilot plant as well as the full scale wet oxidation plant which is under development. While the GC was capable of measuring the CO concentration, the required calibrations to allow it to correctly differentiate it from  $\text{N}_2$  had not been performed. This calibration is required as CO and  $\text{N}_2$  have very similar molecular weights. If at a later date the calibrations are performed, the raw GC data can be re-analysed and the CO concentration can be determined. This would allow this component to be added as a state variable in the kinetic model.

Because of time restrictions, only four experiments were able to be conducted before the reactor was removed from service. Therefore, a single experiment at the centre point of the factorial design in Set 1 was chosen, as well as three other points which best explored the most common operating conditions. Repeats of the experiments would allow greater understanding of the variability in the process, although this would be at the expense of investigating other operating conditions with the time available.

The primary outcome of the gas analysis was that it would enable the fitting of the kinetic parameters that affect the  $\text{O}_{2(\text{g})}$  and  $\text{CO}_2$  states, as well as allow the validation of the current oxygen uptake in the model. The state variables for the

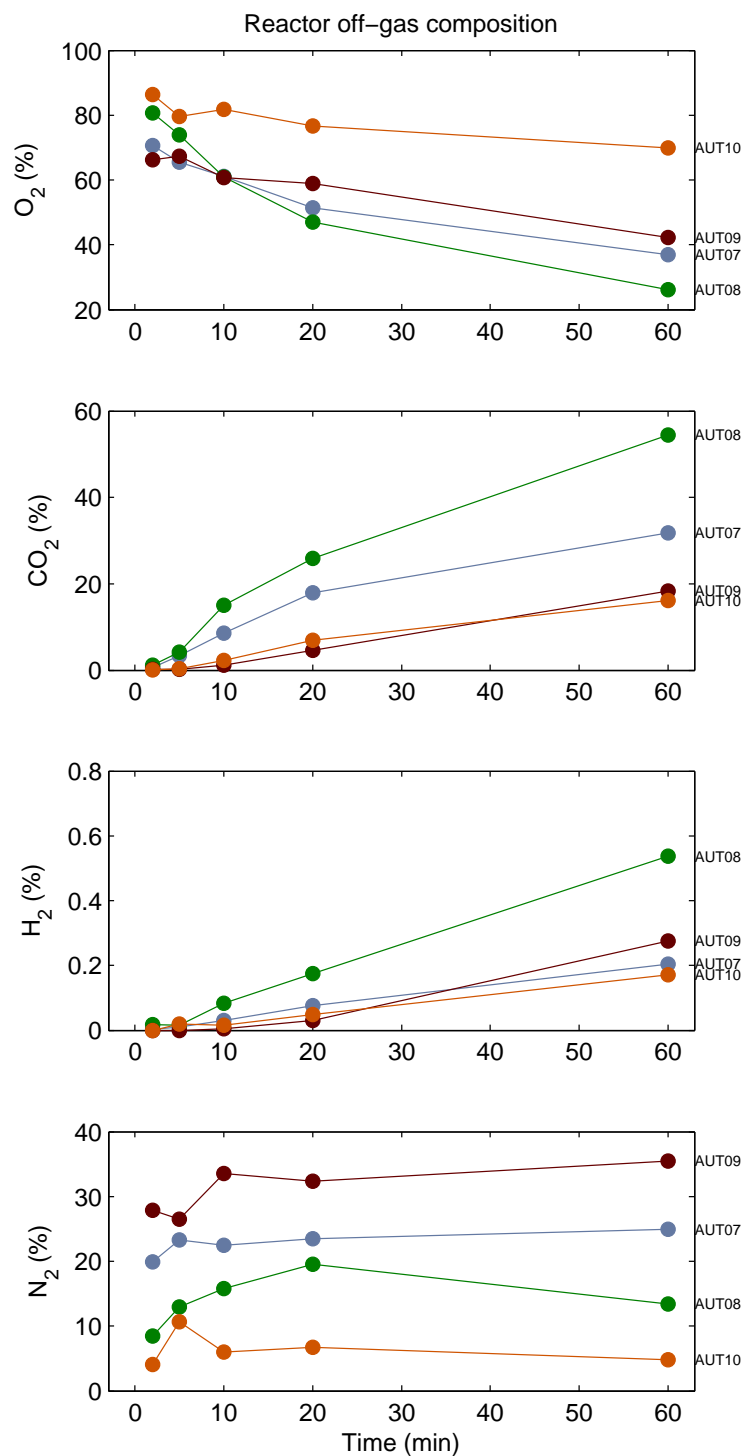


Figure 5.29: Gas composition analysis of the off-gas samples performed as part of the Set 3 experiments. The labels on the right axis correspond to the experiment conditions described in Table 5.9.

gas components present in the model use a mass basis as opposed to concentration. Therefore the component masses need to be calculated from the gas composition data.

It was originally envisaged that using the gas composition results would allow the calculation of the partial pressures for O<sub>2</sub> and CO<sub>2</sub> using the system pressure and Dalton’s law in Eqn. 5.4 to determine the partial pressures,

$$p_i = y_i \cdot p \quad (5.4)$$

where  $p_i$  is the partial pressure of gas component  $i$ ,  $y_i$  is the mole fraction of gas component  $i$  in the gas mixture and  $p$  is the total pressure of the gas mixture.

The mass of each component was initially calculated using the ideal gas law, the previously calculated partial pressure, and accounting for the vapour pressure of water at the current operating temperature. The vapour pressure for water was determined from the thermodynamic property database `coolprop`, [126].

Unfortunately this method of calculation resulted in a significant error as the calculated component masses were much less than expected, with approximately 50% of the calculated O<sub>2</sub> consumed within the first two minutes. An experiment performed with a starting O<sub>2</sub> partial pressure of 20 bar has approximately 9.3g of O<sub>2</sub> in the reactor, however calculations using the mole fractions from the GC and the system temperature and pressure show that 4.3g of O<sub>2</sub> is remaining after the first two minutes, and only 1.1 g was calculated to remain at the end of the experiment. This is despite the fact that the mole fractions from the GC in these experiments show that there is at least 50% O<sub>2</sub> remaining at the completion of the experiment. This suggests an error in the calculations, process or a measurement error. The calculations were repeated using a cubic equation of state instead of the ideal gas law, but the results only changed by 0.2g at 20 bar partial pressure.

To investigate this discrepancy, the next step was to verify that the reactor was not losing pressure during the course of the experiments. The reactor was pressurised to 100 bar with pure nitrogen and left for 24 hours. During this time the pressure remained constant which suggests that the reactor is not leaking and therefore was gas tight.

The system pressure and temperature have considerable effect at elevated temperatures, and therefore the pressure and temperature measurements need to be accurate to allow the gas phase calculations to be completed with reasonable accuracy. Unfortunately, the reactor was dismantled before the sensor calibration could be verified

against reference instruments. However it is suspected that the pressure sensor is the most likely source of error, for several reasons;

1. The pressure transducer was mounted some distance away from the reactor at the end of a long flexible hose. The level of the hose was lower than the reactor, and U shaped, which would trap any condensate in the U shaped portion of the hose, which is highlighted in Fig. 5.30.

It is also likely that biosolid material had condensed inside the tube to the pressure transducer, because when the auxiliary pressure gauge was removed for calibration (shown in the photo in Fig. 5.31), it was found to have a large amount of biosolids condensed inside it.

This would likely affect the operation of the transducer. The reactor was fitted with a mechanical pressure gauge as well as the transducer, however the graduations on the mechanical gauge were very coarse and the potential error in pressure measurement would not have been easily quantifiable on the gauge dial.

2. The reactor temperature sensor consists of a PT-100 type thermocouple mounted inside a thermowell in the reactor. The thermowell is expected to slow the response time of the sensor, but should not adversely affect the steady state measurements.

As a sanity check, the mass of oxygen inside the reactor was calculated at room temperature after pressurisation. The calculation was then repeated using the system pressure and temperature obtained from the data logger after the system had stabilised at operating temperature but *before* the biosolids had been injected. This yielded a much lower oxygen mass compared to room temperature which suggests that the pressure and temperature measurements are likely sources of error, although it is suspected that the pressure transducer measurement is the most likely cause. One alternative observation for the discrepancy in the oxygen partial pressure is due to heat losses from the head of the reactor which mean the system is not in thermal equilibrium yielding a lower pressure than predicted [29]. This hypothesis is still an open question.

For these reasons, the mass for each of the measured gas components has been approximated, by calculating the initial number of moles in the headspace of the reactor after pressurisation but before heating commenced. This data, combined with the mole fractions obtained from the GC results and the molar masses of the components, was used to determine an approximate mass for each sample. If updated sensor calibration data becomes available, then the original approach should be repeated and the results adjusted accordingly.



Figure 5.30: Lab scale Parr reactor with the pressure measurement system highlighted.



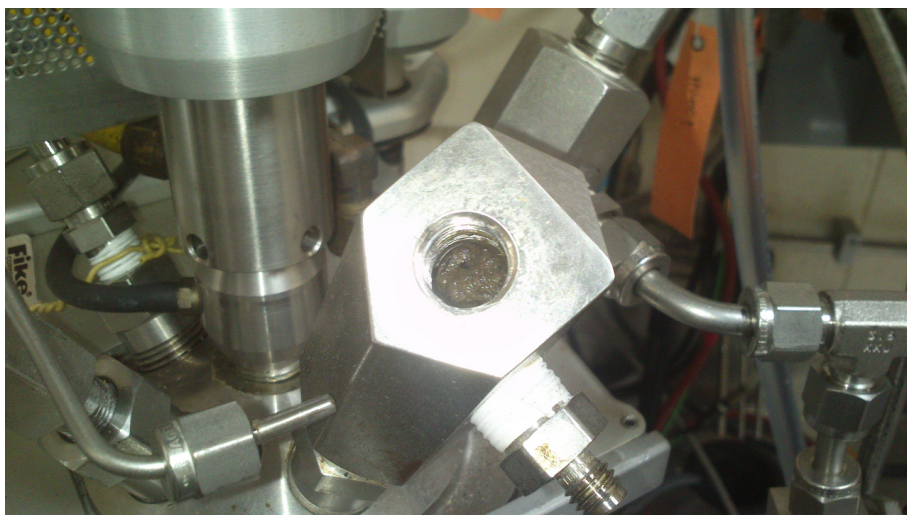


Figure 5.31: Gas port for pressure gauge plugged with biosolids material.

## 5.6 Incorporating Extensions to the Dynamic Kinetic Model

After re-analysing the kinetic model described earlier in Section 5.3 with the newly available gas data, it was apparent that the original model structure hypothesised could be improved upon. In order to improve the model fit with the experimental data, a number of structural changes have been made to the kinetic model to reduce the error between the experimental data and the model, and are discussed in the following section.

A description of the key changes is as follows: The first change is that the VFA component in the original model in Section 5.3 has been split into fast reacting, and slow reacting fractions, shown in Reaction R5.56 and Reaction R5.57. This change enables the model to better account for the observed decay in VFA, since Fig. 5.7 suggests that there is an initial fraction which reacts within the first 5 minutes of the reaction, followed by a fraction which degrades much slower. This results in an extra state variable to account for the VFA fast and VFA slow states, as well as an additional degradation reaction.

The oxygen pseudo mass-transfer reaction was removed and replaced with an algebraic expression using Henry's law, which calculates the dissolved oxygen based on the temperature and oxygen partial pressure in the reactor, using the approach described in Section 3.8. This therefore assumes that the mass transfer happens instantaneously. An additional reaction has been added for AACOD generation from sCOD, to allow for the formation of AACOD at different rates from sCOD fast and sCOD slow.

The availability of the reactor headspace oxygen concentration data revealed that

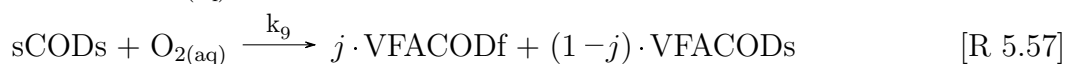
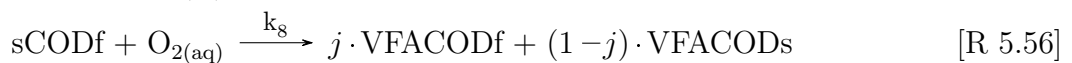


the original model was significantly under-predicting the oxygen consumed by the oxidation reactions. To account for this, oxygen is now consumed by all reactions, except the solubilisation of particulate COD, to better match the oxygen consumption shown in the experimental data. Oxygen is still allowed to affect the solubilisation reaction of particulate COD, to account for non-directly modelled phenomena such as the increase in solubilisation due to increased  $O_2$  partial pressure, although the solubilisation reactions do not consume oxygen.

Based on this, the kinetic model now consists of 12 reactions and 11 state variables, with the measured and derived states incorporated in the model being summarised in Table 5.10. The extended kinetic model reaction pathways are shown in Reaction R5.49 to Reaction R5.60.

Table 5.10: A summary of the measured and derived state variables in the extended model.

State variables	Derived state variables	Measured states
pCODfast (mg/l COD)	pCOD (mg/l COD)	pCOD (mg/l COD)
pCODslow (mg/l COD)	sCOD (mg/l COD)	sCOD (mg/l COD)
sCODfast (mg/l COD)	VFACOD (mg/l COD)	VFACOD (mg/l COD)
sCODslow (mg/l COD)	$O_{2(aq)}$ (g)	DON (mg/l COD)
sCODnr (mg/l COD)		AACOD (mg/l COD)
AACOD (mg/l COD)		$O_{2(g)}$ (g)
VFACODfast (mg/l COD)		$CO_2$ (g)
VFACODslow (mg/l COD)		
DON (mg/l)		
$O_{2(g)}$ (g)		
$CO_2$ (g)		





subject to the following constraints

$$\begin{aligned} \text{sCOD} &= \text{sCODf} + \text{sCODs} + \text{sCODnr} \\ \text{pCOD} &= \text{pCODf} + \text{pCODs} \\ \text{VFACOD} &= \text{VFACODf} + \text{VFACODs} \\ 1 &= x + y, (x, y > 0) \\ 0 &< j < 1 \end{aligned}$$

Where  $x$ ,  $y$  and  $z$  are the fractions of fast reacting, slow reacting and non-reactive soluble COD, and  $j$  is the fractions of fast and slowly reacting VFA. To account for the changes in mixing, a power law based on the work of Meille [101] has been used and incorporated into the rate expression, so that the reaction rate  $r$  in Reaction R5.49 to Reaction R5.60 is of the form;

$$k_i = [\text{C}][\text{O}_{2(\text{aq})}]^n k_i \exp\left(\frac{-E_a}{RT}\right) \text{N}^c \quad (5.5)$$

Where  $[\text{C}]$  and  $[\text{O}_{2(\text{aq})}]$  are the reactant and dissolved oxygen concentrations,  $n$  is the reaction order with respect to oxygen,  $k_i$  is the rate constant,  $E_a$  is the activation energy,  $R$  is the ideal gas constant,  $T$  is temperature in Kelvin,  $\text{N}$  is the stirrer speed in RPM and  $c$  is the mixing constant.

### 5.6.1 Model Assumptions and Simplifications

This section describes the simplifications and assumptions that have been made in the extended kinetic model. One of the difficulties with the proposed reaction set is that they cannot be easily simplified. The concentration of dissolved oxygen is a key component in all reactions which makes the system of reactions difficult to decouple. If reactions are temporarily removed to reduce the number of free parameters in order to make the regression tractable, then it also reduces the overall oxygen consumption in the model as oxygen is used by almost all reactions. As a result of this, the fitted parameters are unlikely to be applicable to the full model.

One of the simplifications performed is that the oxygen pseudo mass-transfer reaction in the first version of the model has been replaced with an algebraic expression based on Henry's law (shown in Section 3.8) to determine the dissolved oxygen concentration, which replaces the  $O_{2(aq)}$  state variable. This removed one reaction and four free parameters from the model.

Because the primary focus of this thesis was investigating the reaction kinetics, and not mass transfer which is another body of work, a detailed mass transfer model has not been included. Hence the simplified power law relationship for mixing has been implemented (described in Section 3.8).

Detailed gas-liquid mass transfer and bubble column reactors have been studied by many researchers [98, 99, 127–129]. These factors have not been incorporated into the developed model at this time. However it is clear that they need to be modelled in detail, and should be added as part of future research.

The effect of pH, salts and dissolved  $CO_2$  on the solubility of oxygen has not been included as part of the solubility calculations.

The reaction order with respect to the reactant variable  $m$  has been removed, and hard coded as 1. This takes account of the work presented by Li *et al.* [57], who provided an extensive summary of kinetic parameters for numerous compounds under wet oxidation, which revealed that the majority had a reaction order with respect to the reactant of 1. Based on this information, the parameter has been removed from the model, reducing the number of fitted parameters by 12.

### 5.6.2 Extended Kinetic Model Summary

This section gives a mathematical summary of the extended kinetic model. The structure of the model is given in Fig. 5.32 which distinguishes between model states,  $\mathbf{x}$ , manipulated inputs,  $\mathbf{u}$ , and model parameters to be regressed,  $\boldsymbol{\theta}$ .

The dynamic component of the model ( $\mathbf{f}(\cdot)$  in Fig. 5.32) implements the kinetic pathways shown above in Section 5.6 after applying the simplifications described in the previous section.

The parameter vector comprises all the reaction rate constants, reaction orders, activation energies, mixing orders and the fractions of fast and slowly reacting sCOD and VFACOD. These are stacked all together into the vector  $\boldsymbol{\theta}$  as

$$\boldsymbol{\theta} \triangleq \left[ \mathbf{k} \quad \mathbf{n} \quad \mathbf{E}_a \quad \mathbf{c} \quad x \quad y \quad j \right]^T \quad (5.6)$$

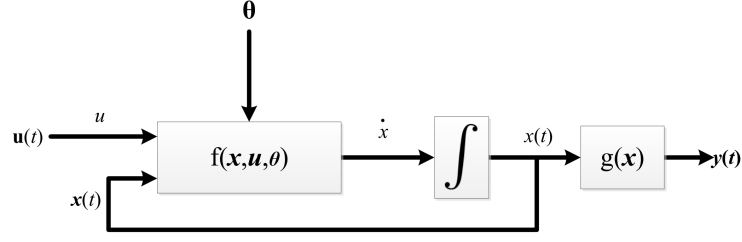


Figure 5.32: Diagram of the extended kinetic model showing the states, inputs, outputs and parameters.

where each variable of  $\theta$  is defined as

$$\mathbf{k} = k_1 \text{ to } k_{12} \quad (5.7)$$

$$\mathbf{n} = n_1 \text{ to } n_{12} \quad (5.8)$$

$$\mathbf{E}_a = E_{a1} \text{ to } E_{a12} \quad (5.9)$$

$$\mathbf{c} = c_1 \text{ to } c_{12} \quad (5.10)$$

$$x = \theta(49) \quad (5.11)$$

$$y = \theta(50) \quad (5.12)$$

$$j = \theta(51) \quad (5.13)$$

The system of ODEs that encapsulate the kinetic pathways is as follows;

$$\frac{dpCODf}{dt} = -[pCODf] \cdot [O_{2(aq)}]^{n_1} \cdot k_1 \exp\left(\frac{-E_{a1}}{8.314 \cdot T}\right) \cdot N^{c_1} \quad (5.14)$$

$$\begin{aligned} \frac{dpCODs}{dt} = & -[pCODs] \cdot [O_{2(aq)}]^{n_2} \cdot k_2 \exp\left(\frac{-E_{a2}}{8.314 \cdot T}\right) \cdot N^{c_2} \\ & - [pCODs] \cdot [O_{2(aq)}]^{n_3} \cdot k_3 \exp\left(\frac{-E_{a3}}{8.314 \cdot T}\right) \cdot N^{c_3} \end{aligned} \quad (5.15)$$

$$\begin{aligned} \frac{dsCODf}{dt} = & x \cdot [pCODf] \cdot [O_{2(aq)}]^{n_1} \cdot k_1 \exp\left(\frac{-E_{a1}}{8.314 \cdot T}\right) \cdot N^{c_1} \\ & + x \cdot [pCODs] \cdot [O_{2(aq)}]^{n_2} \cdot k_2 \exp\left(\frac{-E_{a2}}{8.314 \cdot T}\right) \cdot N^{c_2} \\ & - [sCODf] \cdot [O_{2(aq)}]^{n_6} \cdot k_6 \exp\left(\frac{-E_{a6}}{8.314 \cdot T}\right) \cdot N^{c_6} \\ & - [sCODf] \cdot [O_{2(aq)}]^{n_4} \cdot k_4 \exp\left(\frac{-E_{a4}}{8.314 \cdot T}\right) \cdot N^{c_4} \\ & - [sCODf] \cdot [O_{2(aq)}]^{n_8} \cdot k_8 \exp\left(\frac{-E_{a8}}{8.314 \cdot T}\right) \cdot N^{c_8} \end{aligned} \quad (5.16)$$

$$\begin{aligned} \frac{dsCODs}{dt} = & y \cdot [pCODf] \cdot [O_{2(aq)}]^{n_1} \cdot k_1 \exp\left(\frac{-E_{a1}}{8.314 \cdot T}\right) \cdot N^{c_1} \\ & + y \cdot [pCODs] \cdot [O_{2(aq)}]^{n_2} \cdot k_2 \exp\left(\frac{-E_{a2}}{8.314 \cdot T}\right) \cdot N^{c_2} \end{aligned}$$

$$\begin{aligned}
& - [\text{sCODs}] \cdot [\text{O}_{2(\text{aq})}]^{n_7} \cdot k_7 \exp\left(\frac{-E_{a7}}{8.314 \cdot T}\right) \cdot N^{c_7} \\
& - [\text{sCODs}] \cdot [\text{O}_{2(\text{aq})}]^{n_5} \cdot k_5 \exp\left(\frac{-E_{a5}}{8.314 \cdot T}\right) \cdot N^{c_5} \\
& - [\text{sCODs}] \cdot [\text{O}_{2(\text{aq})}]^{n_9} \cdot k_9 \exp\left(\frac{-E_{a9}}{8.314 \cdot T}\right) \cdot N^{c_9}
\end{aligned} \tag{5.17}$$

$$\begin{aligned}
\frac{d\text{sCODnr}}{dt} &= (1 - x - y) \cdot [\text{pCODf}] \cdot [\text{O}_{2(\text{aq})}]^{n_1} \cdot k_1 \exp\left(\frac{-E_{a1}}{8.314 \cdot T}\right) \cdot N^{c_1} \\
&+ (1 - x - y) \cdot [\text{pCODs}] \cdot [\text{O}_{2(\text{aq})}]^{n_2} \cdot k_2 \exp\left(\frac{-E_{a2}}{8.314 \cdot T}\right) \cdot N^{c_2}
\end{aligned} \tag{5.18}$$

$$\begin{aligned}
\frac{d\text{AACOD}}{dt} &= [\text{sCODf}] \cdot [\text{O}_{2(\text{aq})}]^{n_6} \cdot k_6 \exp\left(\frac{-E_{a6}}{8.314 \cdot T}\right) \cdot N^{c_6} \\
&= + [\text{sCODs}] \cdot [\text{O}_{2(\text{aq})}]^{n_7} \cdot k_7 \exp\left(\frac{-E_{a7}}{8.314 \cdot T}\right) \cdot N^{c_7}
\end{aligned} \tag{5.19}$$

$$\begin{aligned}
\frac{d\text{CO}_2}{dt} &= [\text{sCODf}] \cdot [\text{O}_{2(\text{aq})}]^{n_4} \cdot k_4 \exp\left(\frac{-E_{a4}}{8.314 \cdot T}\right) \cdot N^{c_4} \\
&+ [\text{sCODs}] \cdot [\text{O}_{2(\text{aq})}]^{n_5} \cdot k_5 \exp\left(\frac{-E_{a5}}{8.314 \cdot T}\right) \cdot N^{c_5} \\
&+ [\text{VFACODf}] \cdot [\text{O}_{2(\text{aq})}]^{n_{10}} \cdot k_{10} \exp\left(\frac{-E_{a10}}{8.314 \cdot T}\right) \cdot N^{c_{10}} \\
&+ [\text{VFACODs}] \cdot [\text{O}_{2(\text{aq})}]^{n_{11}} \cdot k_{11} \exp\left(\frac{-E_{a11}}{8.314 \cdot T}\right) \cdot N^{c_{11}}
\end{aligned} \tag{5.20}$$

$$\begin{aligned}
\frac{d\text{O}_{2(\text{g})}}{dt} &= -([\text{sCODf}] \cdot [\text{O}_{2(\text{aq})}]^{n_6} \cdot k_6 \exp\left(\frac{-E_{a6}}{8.314 \cdot T}\right) \cdot N^{c_6} \\
&+ [\text{sCODf}] \cdot [\text{O}_{2(\text{aq})}]^{n_4} \cdot k_4 \exp\left(\frac{-E_{a4}}{8.314 \cdot T}\right) \cdot N^{c_4} \\
&+ [\text{sCODs}] \cdot [\text{O}_{2(\text{aq})}]^{n_5} \cdot k_5 \exp\left(\frac{-E_{a5}}{8.314 \cdot T}\right) \cdot N^{c_5} \\
&+ [\text{sCODs}] \cdot [\text{O}_{2(\text{aq})}]^{n_7} \cdot k_7 \exp\left(\frac{-E_{a7}}{8.314 \cdot T}\right) \cdot N^{c_7} \\
&+ [\text{sCODf}] \cdot [\text{O}_{2(\text{aq})}]^{n_8} \cdot k_8 \exp\left(\frac{-E_{a8}}{8.314 \cdot T}\right) \cdot N^{c_8} \\
&+ [\text{sCODs}] \cdot [\text{O}_{2(\text{aq})}]^{n_9} \cdot k_9 \exp\left(\frac{-E_{a9}}{8.314 \cdot T}\right) \cdot N^{c_9} \\
&+ [\text{VFACODf}] \cdot [\text{O}_{2(\text{aq})}]^{n_{10}} \cdot k_{10} \exp\left(\frac{-E_{a10}}{8.314 \cdot T}\right) \cdot N^{c_{10}} \\
&+ [\text{DON}] \cdot [\text{O}_{2(\text{aq})}]^{n_{12}} \cdot k_{12} \exp\left(\frac{-E_{a12}}{8.314 \cdot T}\right) \cdot N^{c_{12}} \\
&+ [\text{VFACODs}] \cdot [\text{O}_{2(\text{aq})}]^{n_{11}} \cdot k_{11} \exp\left(\frac{-E_{a11}}{8.314 \cdot T}\right) \cdot N^{c_{11}}) \\
&\cdot (\text{ReactorVolume} - \text{GasVolume})
\end{aligned} \tag{5.21}$$

$$\frac{d\text{DON}}{dt} = [\text{pCODs}] \cdot [\text{O}_{2(\text{aq})}]^{n_3} \cdot k_3 \exp\left(\frac{-E_{a3}}{8.314 \cdot T}\right) \cdot N^{c_3}$$

$$- [\text{DON}] \cdot [\text{O}_{2(\text{aq})}]^{n_{12}} \cdot k_{12} \exp\left(\frac{-E_{a12}}{8.314 \cdot T}\right) \cdot N^{c_{12}} \quad (5.22)$$

$$\begin{aligned} \frac{d\text{VFACODf}}{dt} = & j \cdot [\text{sCODf}] \cdot [\text{O}_{2(\text{aq})}]^{n_8} \cdot k_8 \exp\left(\frac{-E_{a8}}{8.314 \cdot T}\right) \cdot N^{c_8} \\ & + j \cdot [\text{sCODs}] \cdot [\text{O}_{2(\text{aq})}]^{n_9} \cdot k_9 \exp\left(\frac{-E_{a9}}{8.314 \cdot T}\right) \cdot N^{c_9} \\ & - [\text{VFACODf}] \cdot [\text{O}_{2(\text{aq})}]^{n_{10}} \cdot k_{10} \exp\left(\frac{-E_{a10}}{8.314 \cdot T}\right) \cdot N^{c_{10}} \end{aligned} \quad (5.23)$$

$$\begin{aligned} \frac{d\text{VFACODs}}{dt} = & (1 - j) \cdot [\text{sCODf}] \cdot [\text{O}_{2(\text{aq})}]^{n_8} \cdot k_8 \exp\left(\frac{-E_{a8}}{8.314 \cdot T}\right) \cdot N^{c_8} \\ & + (1 - j) \cdot [\text{sCODs}] \cdot [\text{O}_{2(\text{aq})}]^{n_9} \cdot k_9 \exp\left(\frac{-E_{a9}}{8.314 \cdot T}\right) \cdot N^{c_9} \\ & - [\text{VFACODs}] \cdot [\text{O}_{2(\text{aq})}]^{n_{11}} \cdot k_{11} \exp\left(\frac{-E_{a11}}{8.314 \cdot T}\right) \cdot N^{c_{11}} \end{aligned} \quad (5.24)$$

In summary, the model can be represented by the 11 state, and 3 manipulated variables,

$$\mathbf{x} = \begin{bmatrix} pCODf \\ pCODs \\ sCODf \\ sCODs \\ sCODnr \\ AACOD \\ \text{CO}_2 \\ \text{O}_{2(\text{g})} \\ DON \\ VFACODf \\ VFACODs \end{bmatrix}, \quad \mathbf{u} = \begin{bmatrix} T(t) \\ \text{O}_2(t) \\ \text{RPM}(t) \end{bmatrix}$$

where the 7 measured variables are

$$\mathbf{y} = \begin{bmatrix} pCOD \\ sCOD \\ AACOD \\ \text{CO}_2 \\ \text{O}_{2(\text{g})} \\ DON \\ VFA \end{bmatrix}$$

Three of the measured variables are summations of other state variables, namely,

$$pCOD = pCODf + pCODs \quad (5.25)$$

$$sCOD = sCODf + sCODs + sCODnr \quad (5.26)$$

$$VFACOD = VFACOD_f + VFACOD_s \quad (5.27)$$

Section 5.6.4 describes how values are regressed to the 51 elements in  $\theta$  to complete the model. In addition, the initial fraction of particulate COD fast/slow is also regressed from the experimental data. This increases the number of regressed parameters to 52.

The discussion around the dissolved organic nitrogen on page 106 has been partially addressed by the extensions to the model proposed in this section. A consequence of the extended model is that we have split the particulate COD into two fractions (slow and fast), and we have assumed the DON resides in the slowly reacting fraction. We take this assumption because it best fits the experimental data as will be seen in Section 6.1.

### 5.6.3 The Matlab Model Structure

The kinetic model developed in the course of this research consists of a collection of Matlab scripts which parse the input data, compute initial conditions, simulate the model, and regress kinetic parameters. The diagram in Fig. 5.33 shows the structure of the model and program flow in the scripts used as part of the modelling environment.

The model first reads the full set of input data. This consists of the initial concentrations of the liquid phase components as well as the environmental parameters, which are temperature, oxygen partial pressure, stirrer speed and liquid volume in the reactor. Additional settings, such as whether continuous gas flow is used, whether liquid samples are taken, and the simulation time, are also specified.

After reading the input data, the main Matlab routine in the model calculates the mass of oxygen in the reactor at the specified partial pressure. If the reactor is not purged with oxygen, the mass of residual nitrogen in the reactor is also calculated.

The mass of dissolved oxygen at ambient temperature is then computed, which allows the total mass of oxygen for both phases in the reactor vessel to be determined. The dissolved oxygen calculation is repeated at operating temperature and the mass of oxygen in the reactor headspace is computed after the biosolids have been injected. This determines the initial condition for the  $O_{2(g)}$  state in the model.

The initial condition and kinetic parameter vectors are subsequently initialised using the values previously calculated. Vectors containing the liquid and gas volume for the duration of the experiment are pre-computed, based on the number and volume of the intermediate samples. This enables the model to take into account changes in

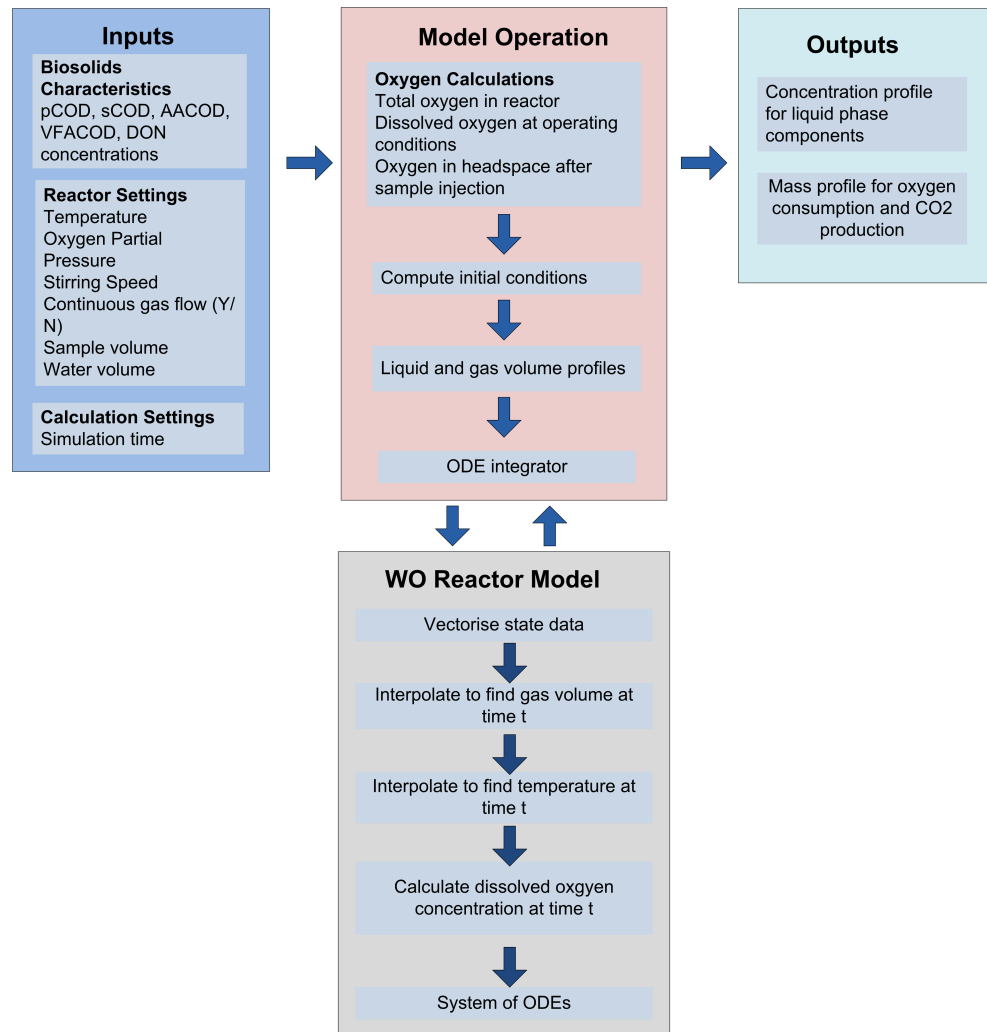


Figure 5.33: Diagram of the extended kinetic model operation including inputs and calculation steps.



volume due to liquid sampling, or the addition of feed material during the simulation.

The Matlab numerical integrator `ode15s` is used internally, to integrate the system of differential equations which makes up the model. A description of the components in the model is presented in the following section.

### **Reactor Model Script**

The reactor model primarily consists of a system of 11 differential equations that represents the change in concentration for each component, while there are 11 corresponding states in the model at present related to chemical equations. The model also contains 3 derived states which are the total sum of pCOD, sCOD and VFACOD respectively.

The script first vectorises the passed input data, and then determines the current temperature and gas volume at time  $t$ . These calculations are required for the next stage, which is to compute the concentration of dissolved oxygen at the current operating condition which is an algebraic relation, as this parameter features in each of the reactions in the model. Once these prerequisites are calculated, the system of ODEs is then integrated.

### **Regression Wrapper Scripts**

To regress the 52 model parameters, the same model structure is used as described above, however two wrapper scripts are used to perform the regression, and these call the above routines during the regression process.

These scripts perform two functions. The main wrapper script constructs, initialises and solves the regression problem, while the other is called by the optimiser to separate and vectorise parameters, run the reactor model, and lastly compute the error between the model and fitting data.

The main script first performs several housekeeping duties, including normalising the fitting data, constructing the fitting and weighting matrices, and creating indexes of states that have fitting data available. Upper and lower bounds on the model parameters are also specified.

The OPTI optimisation toolbox is used as a high level front end to perform the optimisation [116]. The LN\_COBYLA algorithm from the `nlopt` suite of optimisers was selected as the optimiser as it was found by experience to give the most reliable solution. An anonymous function was used to pass the additional parameters such as the fitting data and liquid volume to the internal wrapper script, after which the `solve` method was called to start the optimisation.

One of the reasons for creating the wrapper script is that it was desirable that the

initial fractions of pCODf and pCODs were fitted, as part of the initial conditions for the reactor model. This is because they have a significant effect on the results. The wrapper script is responsible for performing this initial condition regression.

As part of the initialisation routine, the wrapper script registers a callback to the Matlab `odeMaxTime` event to stop the integrator if it is unable to find a solution within 5 seconds. This prevents the regression optimiser from stalling indefinitely. This returns a suitable error if it occurs.

The fitting data and parameters are vectorised and passed to the `ode15s` integrator which calls the reactor model script described earlier. If a solution is found, the norm is computed as the difference between the model results and the fitting data. The difference is then multiplied by the weighting matrix and the solution is returned to the optimiser.

#### 5.6.4 Model Regression

The kinetic model consists of a total of 12 reactions, 11 states, 3 derived states and a number of other parameters which need to be fitted. Each reaction has a total of 4 free parameters. In addition to this, the fractions of fast, slow and non-reactive sCOD, fast and slow VFA, and the initial fraction of fast and slowly reactive pCOD are fitted, which results in a total of 52 free parameters.

In addition to the model parameters, the initial fractions of fast and slowly reacting pCOD are also regressed from the experimental data. This is because it was observed that this fraction has a significant effect on the concentration of downstream products (such as sCOD). This initial condition was added to the parameter vector, but internally the regression wrapper script described in Section 5.6.3 removed it before it was passed to the reactor model itself. The fitted fractions for these components is shown in Table 5.12. Because of this, there are a total of 52 parameters regressed by the Matlab regression environment.

In order to have sufficient fitting data, the data from all experimental runs listed in Table 5.2 was used and fitted simultaneously. One of the complications of this method is that there was only oxygen composition data for 4 of the experiments, which complicates building the fitting data matrix. This results in a total of 266 ODEs, and 52 free parameters. These are solved using the Matlab environment described in Section 4.5, with each iteration taking approximately 5 seconds to solve.

While regressing the model parameters, it became apparent that there is either another non-measured component being formed, or potentially a structural error in

the kinetic model. This is because in order for the model to match the experimental data, it was necessary to make the assumption that only a fraction of the conversion from COD to CO<sub>2</sub> currently produced by the model actually produced CO<sub>2</sub>. This finding needs to be explored further, and is left as future work.

The optimisation problem described in this chapter is sufficiently complex that no numerical optimiser that was tried could automatically find suitable parameters starting from arbitrary conditions. One of the challenges for this type of problem is the presence of multiple solutions, as multiple combinations of  $k_0$  and  $E_a$  can give the same reaction rate constant  $k$ . For this reason, the initial guess for the values of  $k_0$  and  $E_a$  was increased until the expected change due to temperature was observed in the model output and the model regression was repeated. Increasing the value of  $E_a$  in conjunction with  $k_0$  increases the reaction's temperature dependence. This process was repeated for all components.

An increased weighting of 10 has been applied to the  $t = 60$  point of pCOD to further improve the fit because of the large range between the initial and final pCOD concentrations. The  $t = 60$  point for the other components has also been weighted by 1.25 because the experimental results for "Avg" shown in Section 5.2.2 demonstrate that the final sample has the least variation. All other results were weighted with 1.

The regression computations took approximately 4 hours to complete on a modern desktop computer using the LN\_COBYLA algorithm from the `nlopt` package which is part of the OPTI toolbox. Of course such timing metrics are both computer hardware dependent, and their relevance dates rapidly, however these numbers are provided primarily to give the reader a sense of the computational complexity of the problem.

The final values of the fitted kinetic parameters are listed in Table 5.11 and Table 5.12 and are discussed in the following section. The statistical significance of these fitted parameters is discussed later in Section 6.3.

### 5.6.5 A Comparison with Published Kinetic Parameters

There are only a few published sources of rate constants for wet oxidation models available with which to make reliable comparison. One of the few to provide rate constants was Shanableh *et al.* [88]. They determined the kinetic parameters for particulate COD degradation to be  $k_0 = 9.61 \times 10^3 \text{s}^{-1}$  and  $E_a = 8.65 \times 10^4 \text{J} \cdot \text{mol}^{-1}$  compared to the values regressed in this study of  $k_0 = 1.78 \times 10^3 \text{s}^{-1}$  and  $E_a = 4.03 \times 10^4 \text{J} \cdot \text{mol}^{-1}$  for pCOD fast, with  $k_0 = 3.08 \times 10^6 \text{s}^{-1}$  and  $E_a = 1.25 \times 10^5 \text{J} \cdot \text{mol}^{-1}$

Table 5.11: Fitted kinetic parameters for the extended model. (See also Table 6.1.)

	Reaction Reference	Rate constant ( $k$ )	Activation Energy ( $E_a$ ) J/mol	O <sub>2</sub> order ( $n$ ) –	Mixing order ( $c$ ) –
Reaction 1	R 5.49	$1.78 \times 10^3$	$4.03 \times 10^4$	0.30	0.47
Reaction 2	R 5.50	$3.08 \times 10^6$	$1.25 \times 10^5$	0.45	0.74
Reaction 3	R 5.51	$5.91 \times 10^2$	$4.88 \times 10^4$	0.56	0.06
Reaction 4	R 5.52	$1.76 \times 10^3$	$3.53 \times 10^4$	0.30	0.47
Reaction 5	R 5.53	$3.87 \times 10^5$	$1.07 \times 10^5$	0.93	1.18
Reaction 6	R 5.54	$7.40 \times 10^2$	$6.04 \times 10^4$	0.89	0.55
Reaction 7	R 5.55	$2.91 \times 10^2$	$4.79 \times 10^4$	0.25	0.46
Reaction 8	R 5.56	$1.64 \times 10^0$	$1.84 \times 10^5$	0.13	0.02
Reaction 9	R 5.57	$1.26 \times 10^1$	$3.76 \times 10^4$	0.31	0.55
Reaction 10	R 5.58	$8.42 \times 10^2$	$3.52 \times 10^4$	0.37	0.06
Reaction 11	R 5.59	$9.67 \times 10^1$	$4.36 \times 10^4$	0.34	0.40
Reaction 12	R 5.60	$1.21 \times 10^1$	$3.06 \times 10^4$	0.79	0.002

Table 5.12: Fitted component reactivity fractions.

Reacting Fractions	Fraction
pCOD fast	0.84
pCOD slow	0.16
sCOD fast	0.50
sCOD slow	0.30
sCOD non reactive	0.20
VFACOD fast	0.49
VFACOD slow	0.51

for pCOD slow. Although they did not classify particulate COD as fast or slow degrading, the kinetic parameters from Shanableh [88] are of a similar range to those regressed for pCOD fast in this study.

Li *et al.* provide rate constants for their triangular kinetic model which was discussed as part of the literature reviewed in Section 2.7. The values provided for the degradation of total COD were  $k_0 = 1.2 \times 10^4 \text{s}^{-1}$  and  $E_a = 6.70 \times 10^4 \text{J} \cdot \text{mol}^{-1}$ . While the developed model does not directly have a model state for total COD, the values provided by Li *et al.* are of the same order of magnitude as those in Table 5.11.

In addition to a summary of rate constants, Li *et al.* also provided a review of kinetic parameters for the wet oxidation of a wide variety of components. This showed that the reaction order with respect to oxygen can range from 0 to 1, with an order of 1 being the most common found in the study given in [57]. The values for the regressed reaction orders with respect to oxygen in Table 5.11 lie within this range and therefore would appear to be plausible.

The values regressed for the mixing parameter  $c$  are smaller than those published by Meille *et al.* [101], however they investigated the absorption of hydrogen in the hydrocarbon  $\alpha$ -methylstyrene as the liquid for their mass transfer experiments. Interestingly, they point out that the measured mass transfer efficiency was around three times less for water than  $\alpha$ -methylstyrene, which would then be of the same magnitude as the regressed values in this study.

The reaction pathways that have been postulated in the kinetic model designated some reactions as “fast reacting” and others as “slow reacting”. The overall rate constants shown in Table 5.13 are computed at 220°C, 20 bar oxygen partial pressure and 300 RPM stirring speed from the values of  $k_0$ ,  $E_a$ ,  $n$  and  $c$  in Table 5.11.

The extremely small overall reaction rate constant for Reaction 8 shows that this reaction has little effect and suggests that this reaction could be removed from the model. However, it has been left in the model as there are multiple solutions to this problem and re-regressing the model with additional experimental data may lead to a different set of parameters for this reaction. This is an open question and has been left for future work.

It is particularly interesting to note that, in general, the overall rate constants in Table 5.13 agree with this designation, with the rate constants for the fast being greater than the slow reactions. It is important to point out that the regression of the experimental data determined the values for the rate constants and that the numerical regression algorithm was “unaware” of the arbitrary distinction made between “fast” and “slow” reacting components. This supports the hypothesis that these components have fractions that react at different rates.

Table 5.13: Overall rate constants using the regressed kinetic parameters from the extended kinetic model for conditions 220°C, 20 bar oxygen partial pressure and 300 RPM stirring speed.

	Reaction Reference	Reaction Designation	Overall Rate constant	Is Fast Rate Constant > Slow
Reaction 1	R 5.49	Fast	$6.84 \times 10^0$	Yes
Reaction 2	R 5.50	Slow	$1.36 \times 10^{-4}$	Yes
Reaction 3	R 5.51	N/A	$1.07 \times 10^{-1}$	N/A
Reaction 4	R 5.52	Fast	$2.22 \times 10^1$	Yes
Reaction 5	R 5.53	Slow	$1.97 \times 10^{-1}$	Yes
Reaction 6	R 5.54	Fast	$7.23 \times 10^{-1}$	Yes
Reaction 7	R 5.55	Slow	$2.22 \times 10^{-1}$	Yes
Reaction 8	R 5.56	Fast	$1.12 \times 10^{-19}$	No
Reaction 9	R 5.57	Slow	$1.54 \times 10^{-1}$	No
Reaction 10	R 5.58	Fast	$1.51 \times 10^0$	Yes
Reaction 11	R 5.59	Slow	$1.38 \times 10^{-1}$	Yes
Reaction 12	R 5.60	N/A	$4.60 \times 10^{-1}$	N/A

## 5.7 Chapter Summary

This chapter investigated the change in concentration of key components in biosolids undergoing wet oxidation at different reaction conditions. As part of the experimental investigation, a set of reaction pathways was proposed, and a model was developed and regressed to best fit the experimental data.

The experimental results show that the concentrations of all measured components were significantly affected by wet oxidation, and that each of the environmental conditions also influenced the final concentrations achieved. Temperature was shown to have the greatest effect on the results, followed by oxygen partial pressure and stirring speed.

One of the main difficulties with the model is the large number of free parameters to regress. To successfully regress all 52 parameters requires a large amount of fitting data. Considerable computational time is required with so many parameters, with solution times of around 4 hours being typical on a contemporary desktop computer.

In the following chapter, the regressed extended kinetic model is compared with the experimental results from the lab scale reactor. The model, which used the parameters fitted from the lab scale reactor, was also compared to results from the pilot plant. This work is also presented in Chapter 6.

# Chapter 6

## Model Results and Pilot Plant Validation

In this chapter, the accuracy of the dynamic extended kinetic model from Chapter 5 is demonstrated by comparison with data obtained from the experimental investigation on the lab scale wet oxidation system. In addition to this, the validity of the model is reinforced by comparison with data not used for fitting obtained from semi-batch experiments on the pilot plant wet oxidation system.

Comparisons between the model and the data from the lab scale reactor are shown in Section 6.1, which shows the performance of the model against the selected experiments shown earlier in this thesis. Section 6.2 demonstrates the effect of different operating conditions on the model. The performance of the model developed in this research is then compared against models from the literature in Section 6.3.3.

Lastly, the suitability of the dynamic model regressed from the experimental data gathered from the bench scale wet oxidation system from Chapter 5 is compared to the data collected from the full-scale pilot plant described earlier in Chapter 3. As will be shown in Section 6.4 the unmodified model produces a good fit to this new data.

### 6.1 Kinetic Model Results

This section compares the results from the fitted extended kinetic model described in Chapter 5 with experimental data obtained in Section 5.2 in the previous chapter. The model output is presented for the same experimental runs (2, 3, 5 and the averages of 15 to 18) that were illustrated in the previous chapter for validation. The model output for the remaining experiments not shown in this chapter is given in

Appendix C. This section also discusses the discrepancies observed, and differences between the experimental data obtained in this study and data available in the literature.

In the kinetic model, total COD is not a separate model state, but is calculated as the sum of all COD components which are pCOD, sCOD, AACOD and VFACOD. This concentration has been included in Fig. 6.1, and as a percentage of total COD removal in Fig. 6.2, to enable the comparison of the results in this study with those available in the literature, which frequently only show the degradation in terms of total COD.

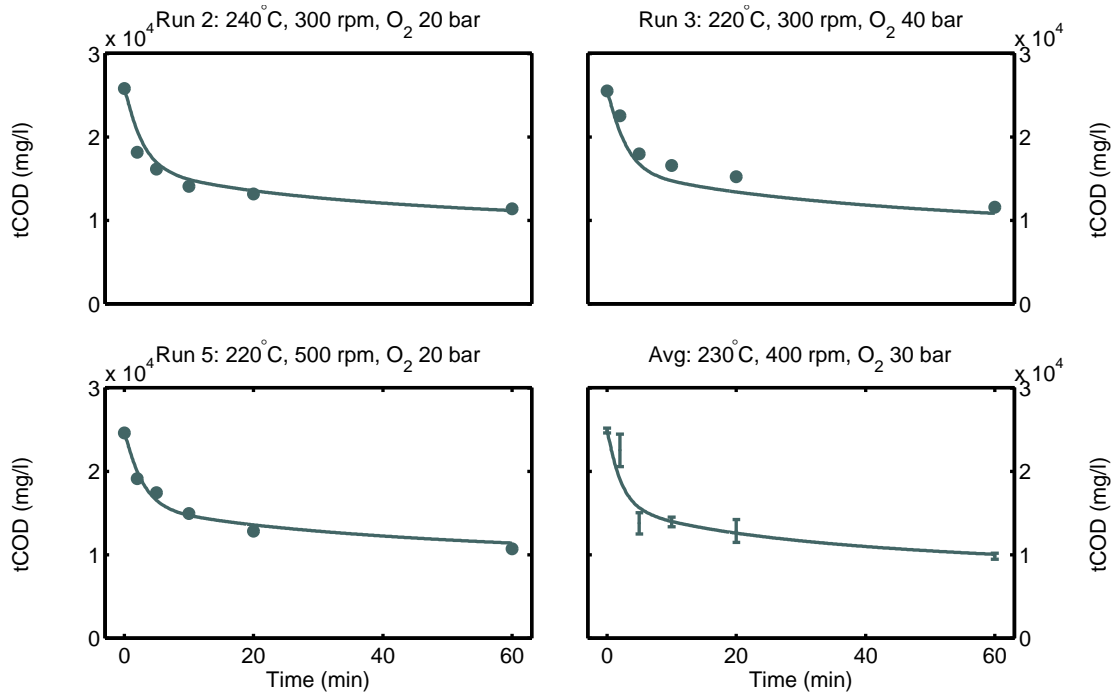


Figure 6.1: The concentration of total COD from the extended kinetic model in Section 5 versus experimental data from the lab scale wet oxidation system.

The total COD concentration results in Fig. 6.1 and Fig. 6.2 show that the model is able to accurately predict the change in total COD over the duration of the experiment. The error between the model and experimental data is low, although the results in Run 3 of Fig. 6.1 show that the effect of oxygen partial pressure could be improved. The percentage of remaining total COD shown in Fig. 6.2 is included to allow comparison with the literature models which are generally given as a percentage of total COD. A comparison of the experimental data from this investigation applied to models from the literature is described later in Section 6.3.3

The particulate COD model results in Fig. 6.3 show remarkably good agreement with the experimental data. While some discrepancy is apparent towards the end of the experiment at the final  $t = 60$  point, the error bars show that it is within the margin of the measurement error.



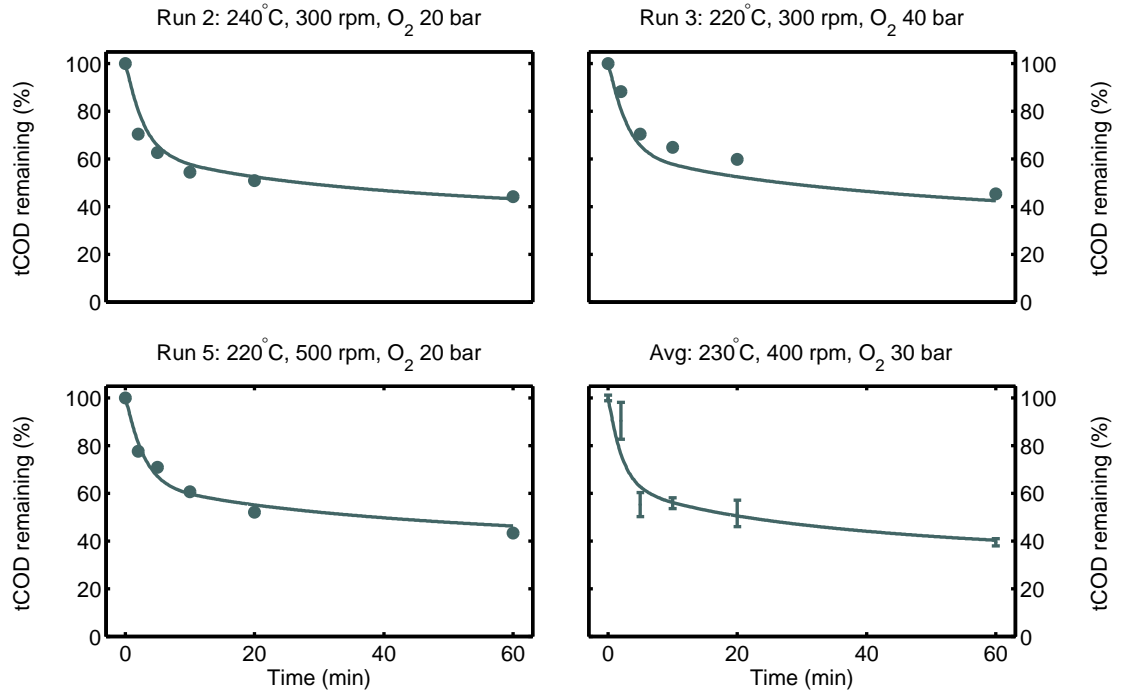


Figure 6.2: The fraction of total COD remaining, computed from the extended kinetic model in Section 5 versus experimental data from the lab scale wet oxidation system.

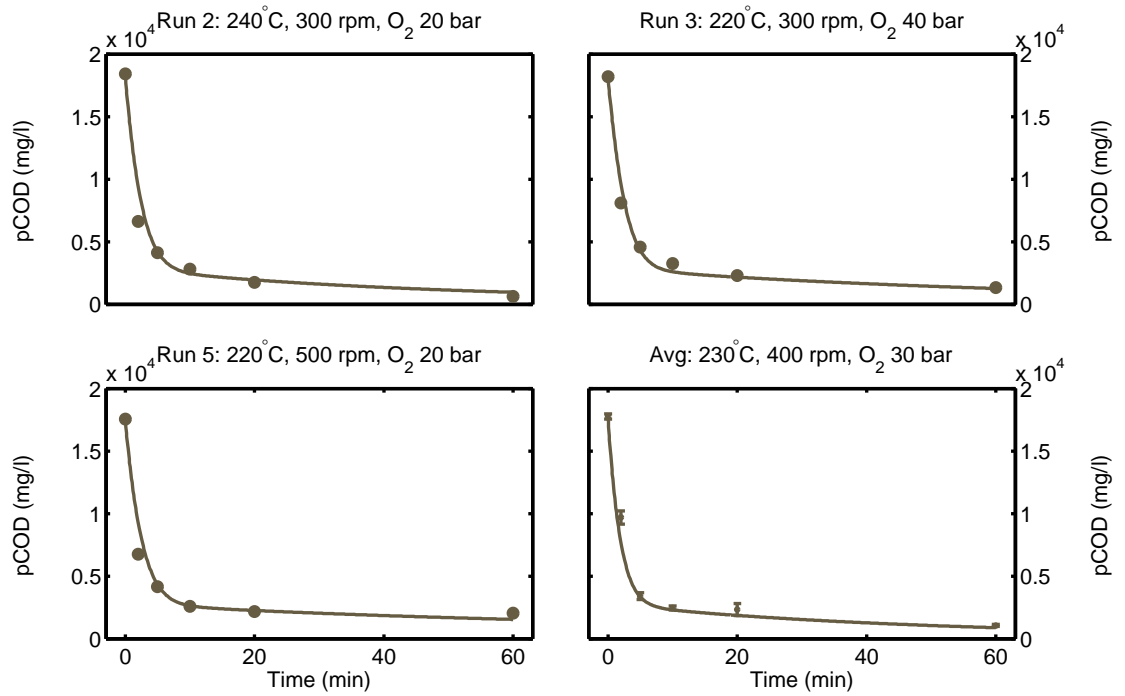


Figure 6.3: The particulate COD concentration from the extended kinetic model versus experimental data from the lab scale wet oxidation system.

However it is apparent that the soluble COD results in Fig. 6.4 exhibit slightly more variation than the particulate COD results, although still reasonable. As previously mentioned in Section 3.6.2, the soluble COD state in the kinetic model represents the remaining non-VFA COD in solution, as opposed to the measured soluble COD. To allow for easy comparison with soluble COD data in the literature, the model results in Fig. 6.4 represent the sum of the model sCOD, AACOD and VFACOD components, and the aggregate of these represent the equivalent measured soluble COD ( $sCOD_{measured} = sCOD_{model} + AACOD_{model} + VFACOD_{model}$ ).

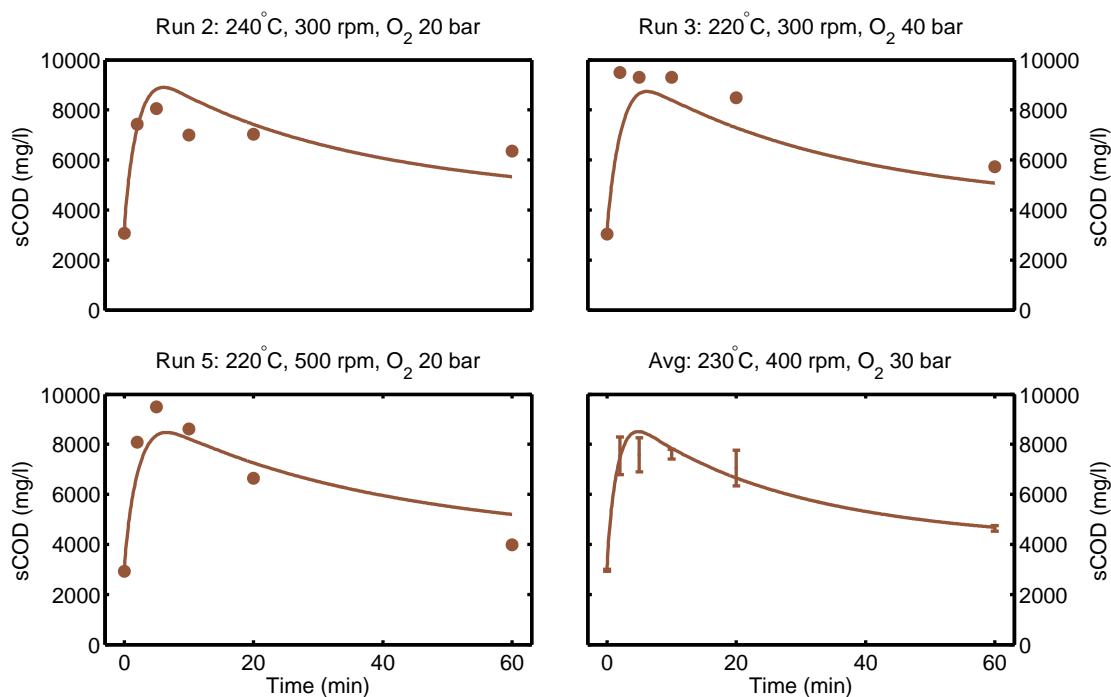


Figure 6.4: The soluble COD concentration from the extended kinetic model versus experimental data from the lab scale wet oxidation system.

One of the key requirements of the model was to predict the production of VFAs, in the form of acetic acid, and other dominant VFAs which were observed under wet oxidation, so that their effect on a downstream BNR plant could be determined. Because of this, it was important that the model was able to predict the VFA production from RDC biosolids with a reasonable level of accuracy. The model results shown in Fig. 6.5 and Fig. 6.6 are excellent compared with the experimental data, and easily achieve this objective.

In addition to VFAs, another modelling requirement was to capture the evolution of DON. However, because of the variation in the DON experimental results shown in Fig. 6.7, which has been discussed earlier in Section 5.2.2, it is hard to produce a convincing model. It is clear that the model does not adequately describe the temperature dependence of DON, but it is believed that the fit achieved for DON is as good as can be expected with the data available.

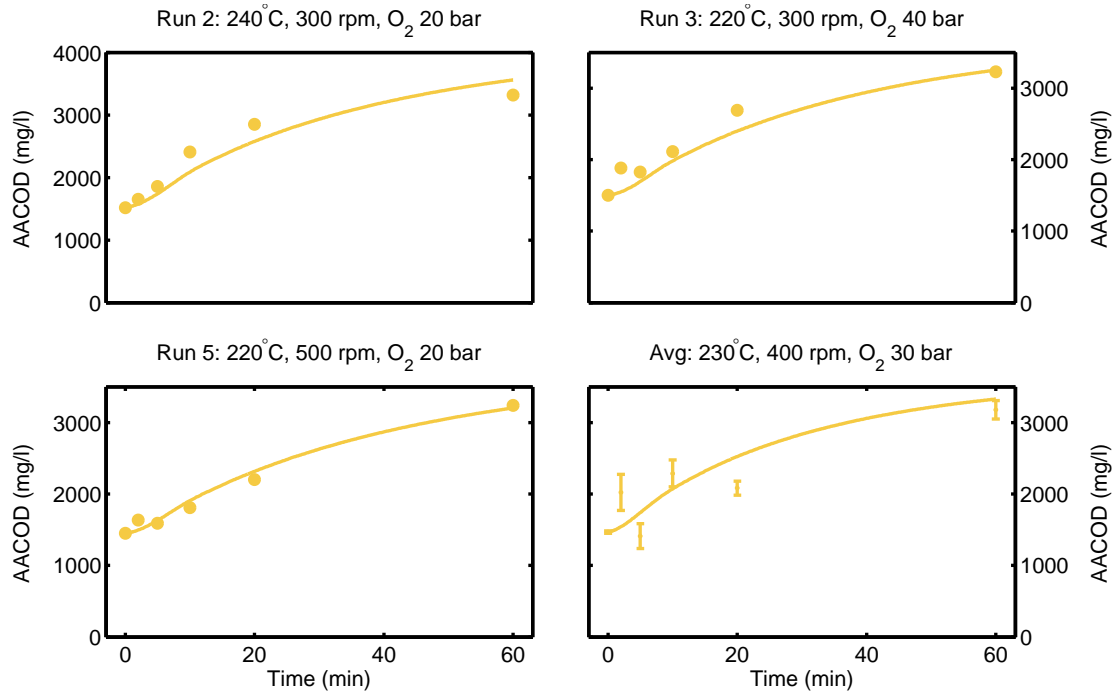


Figure 6.5: The acetic acid COD concentration from the extended kinetic model versus experimental data from the lab scale wet oxidation system.

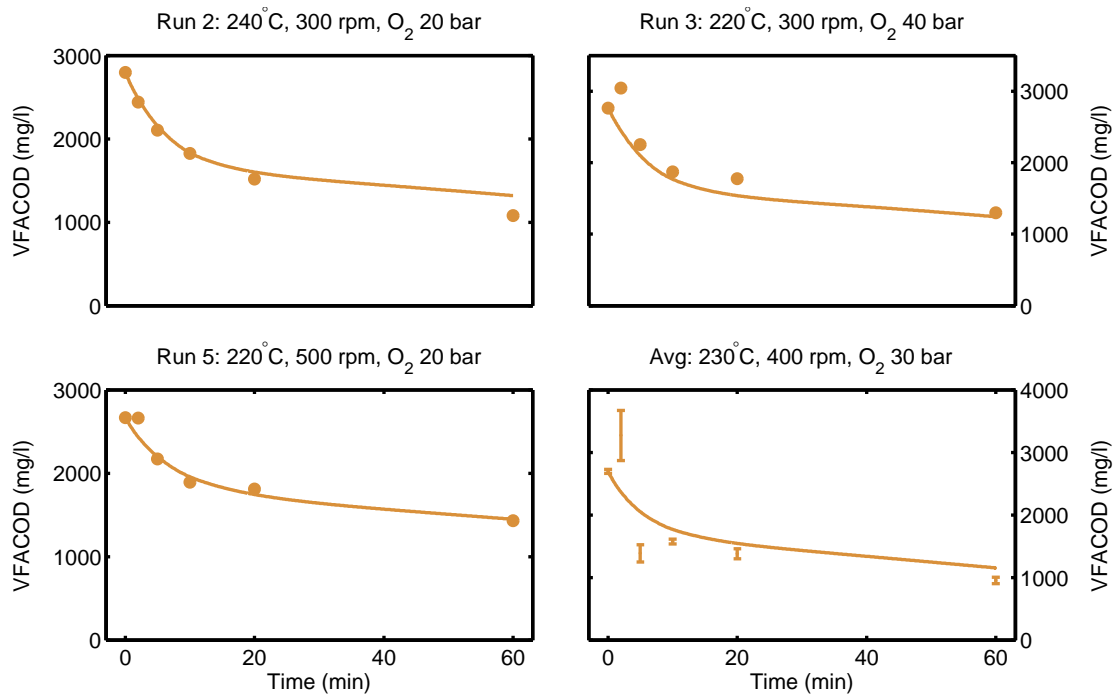


Figure 6.6: The VFACOD concentration from the extended kinetic model versus experimental data from the lab scale wet oxidation system.

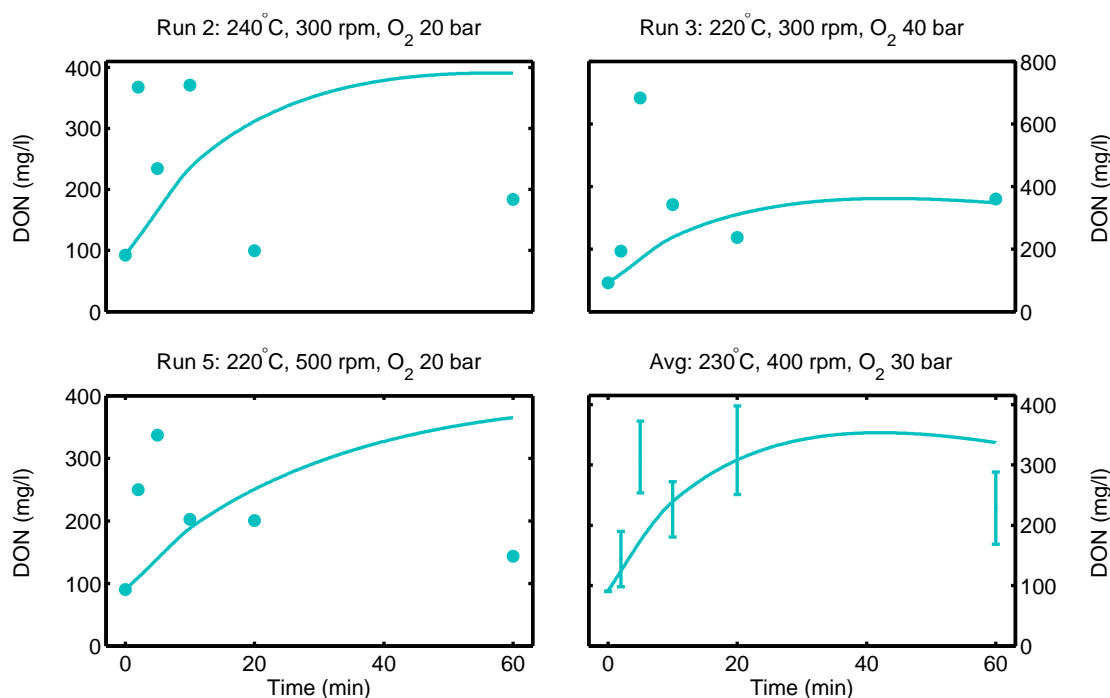


Figure 6.7: The DON concentration from the extended kinetic model versus experimental data from the lab scale wet oxidation system.

The data obtained from the Set 3 experiments allowed the validation of the oxygen uptake in the model. This clearly showed that the simplified model in Section 5.3 was unable to predict oxygen consumption correctly, and far more oxygen was being consumed than was being accounted for in the original model. After allowing all reactions to consume oxygen, apart from the particulate COD solubilisation reactions, the model is now capable of predicting oxygen uptake at a partial pressure of 20 bar with a good level of accuracy. This is shown in Fig. 6.8, although there is still a discrepancy at 30 bar partial pressure. Owing to the lack of repeat gas samples, it has yet to be determined if this discrepancy is due to a sampling problem, or a structural problem in the model. To maintain consistency with the other plots shown in this chapter, the two experiments for which gas composition data was available are shown in Fig. 6.8 and Fig. 6.9, while only the model output is shown in the remaining two experiments.

With the limited measurements of the gas composition data available, the model was able to fit two out of the four experiments which had reactor off-gas composition data well, but the remaining two had large discrepancies, with the model overestimating the oxygen consumption. The extra experiments with gas composition data which are not shown here are given in Appendix C.

Like the fit for oxygen, the model was able to predict  $\text{CO}_2$  evolution well for two runs (experiments 5 and 6) and had a poorer fit for the other two runs (experiments 8 and the averages of 15–18). Fig. 6.9 shows one run with a good fit (experiment 5),

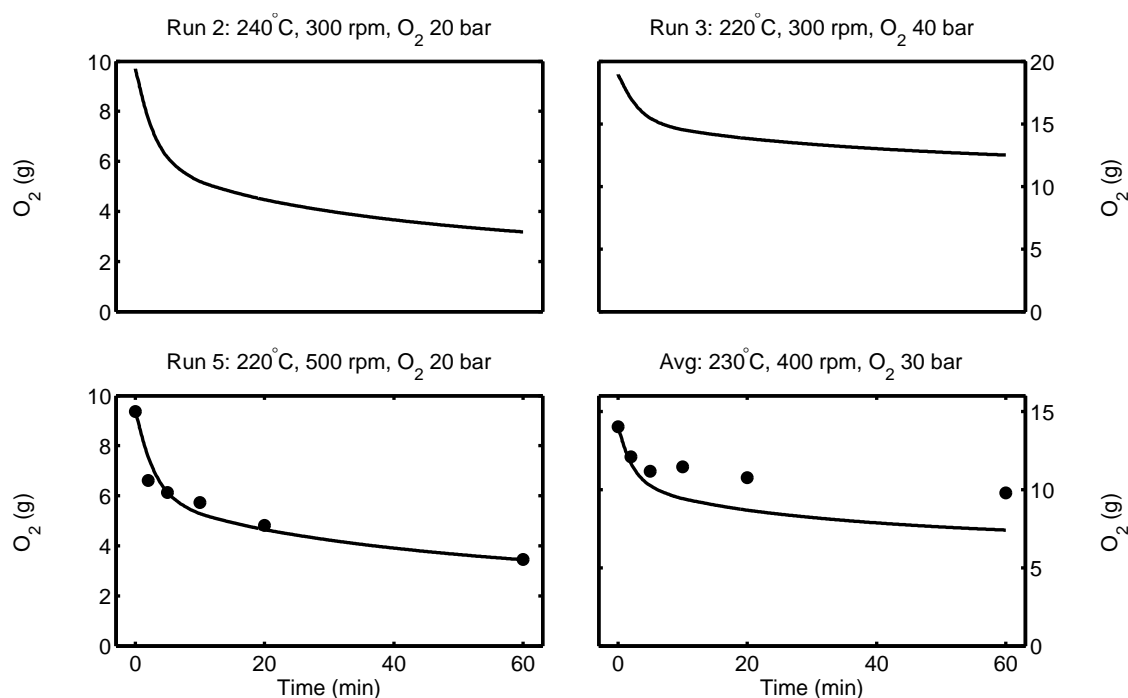


Figure 6.8: The mass of  $O_2$  remaining in the reactor from the extended kinetic model versus experimental data from the lab scale wet oxidation system.

and one with a poor fit (averages of 15–18). Because the same runs had poor fit for both oxygen and  $CO_2$  it is postulated that there is an issue with those gas samples as opposed to a poor model, although this cannot be confirmed without additional data.

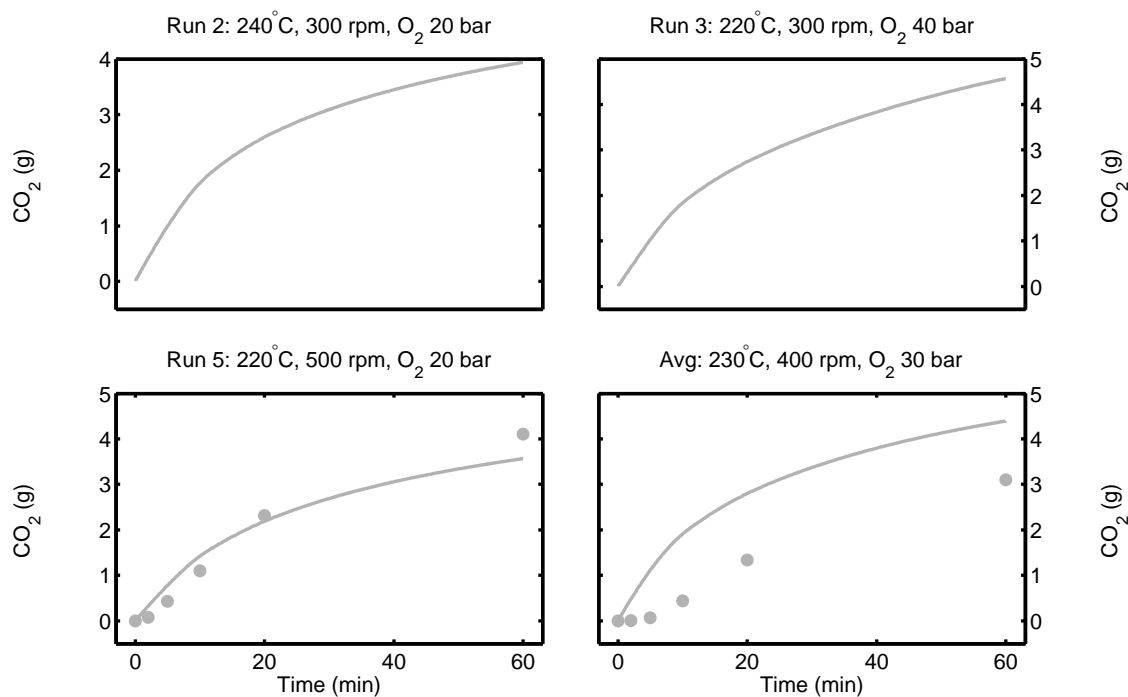


Figure 6.9: The mass of  $CO_2$  remaining in the reactor from the extended kinetic model versus experimental data from the lab scale wet oxidation system.

## 6.2 Effect of Operating Conditions on the Model Results

This section validates the effect of the experimental operating conditions of interest in this study, which are temperature, oxygen partial pressure and stirrer speed, and compares the model results with the experimental data. This is important for the design of future full scale wet oxidation systems.

The results in Fig. 6.10 compare the model's response to the experimental data when the temperature was increased from 220 to 240°C. Apart from the concentrations of DON and CO<sub>2</sub>, which have already been discussed as less reliable than the other components, the model's response is in good agreement with the experimental data.

Experimental results from Lendormi [24] and Chung *et al.* [59] show that increasing the temperature from 220 to 240°C produces an 11 to 17% increase in total COD removal, which is similar to the 10% increase seen in the experimental results, and produced by the extended kinetic model. Their published results on the effect of VFA production reinforce those obtained in these experiments, which is reflected in the model output. One area for future work is to improve the accuracy during the initial phase of the reaction for this component, particularly within the first 20 minutes of the experiment. This is because around 75% of the degradation is achieved in the first 20 minutes.

The model's response to a change in oxygen partial pressure, from 20 to 40 bar is shown in Fig. 6.11. Overall, the model output agrees well with the experimental data and therefore captures the effect of oxygen partial pressure. However, the model's response to the effect of oxygen partial pressure on AACOD could be improved.

Changing the stirring speed produced the smallest effect on the experimental results. The model results in Fig. 6.12 show the model's response to increasing the stirring speed from 300 to 500 RPM. This shows that the model can adequately describe the change in stirring speed, but as in Fig. 6.11, there is generally a greater error in the initial stages of the experiment. It is interesting to note that a simple power law on stirrer speed appears to capture the mixing effects reasonably well without the need for a detailed mass transfer model.

Exploring the likely operating envelope is particularly important for the design of future wet oxidation plants. The more extreme reaction conditions used (higher temperatures and pressures) will require stronger equipment to withstand the additional stresses imposed. However, the results show that higher temperatures and O<sub>2</sub> partial pressures increase the reaction rate. Further results are given in Section 6.5.1.

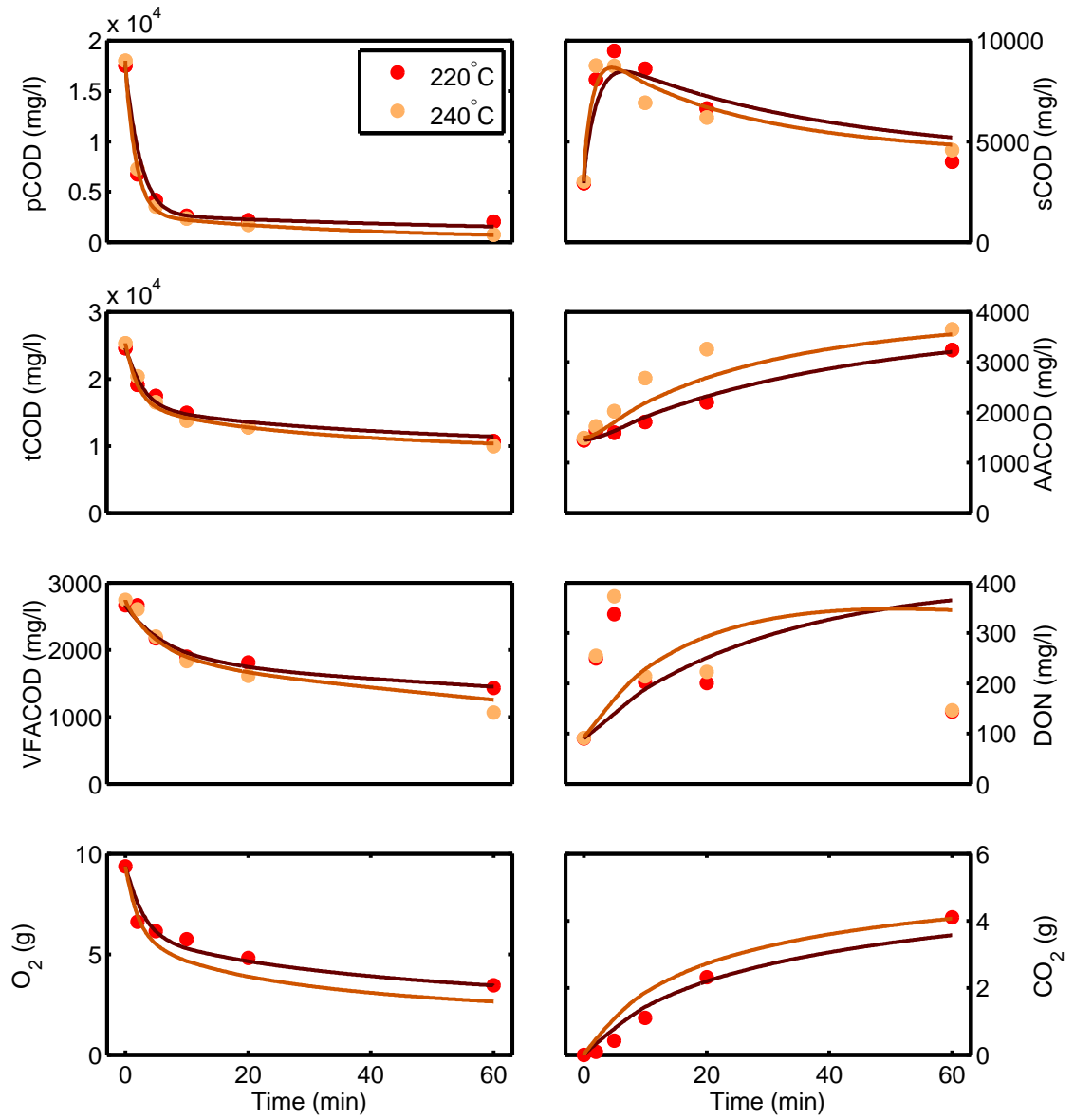


Figure 6.10: The extended kinetic model output versus the response from the experimental data to an increase in temperature from 220°C to 240°C. The points represent experimental data, while the solid line is the model response.

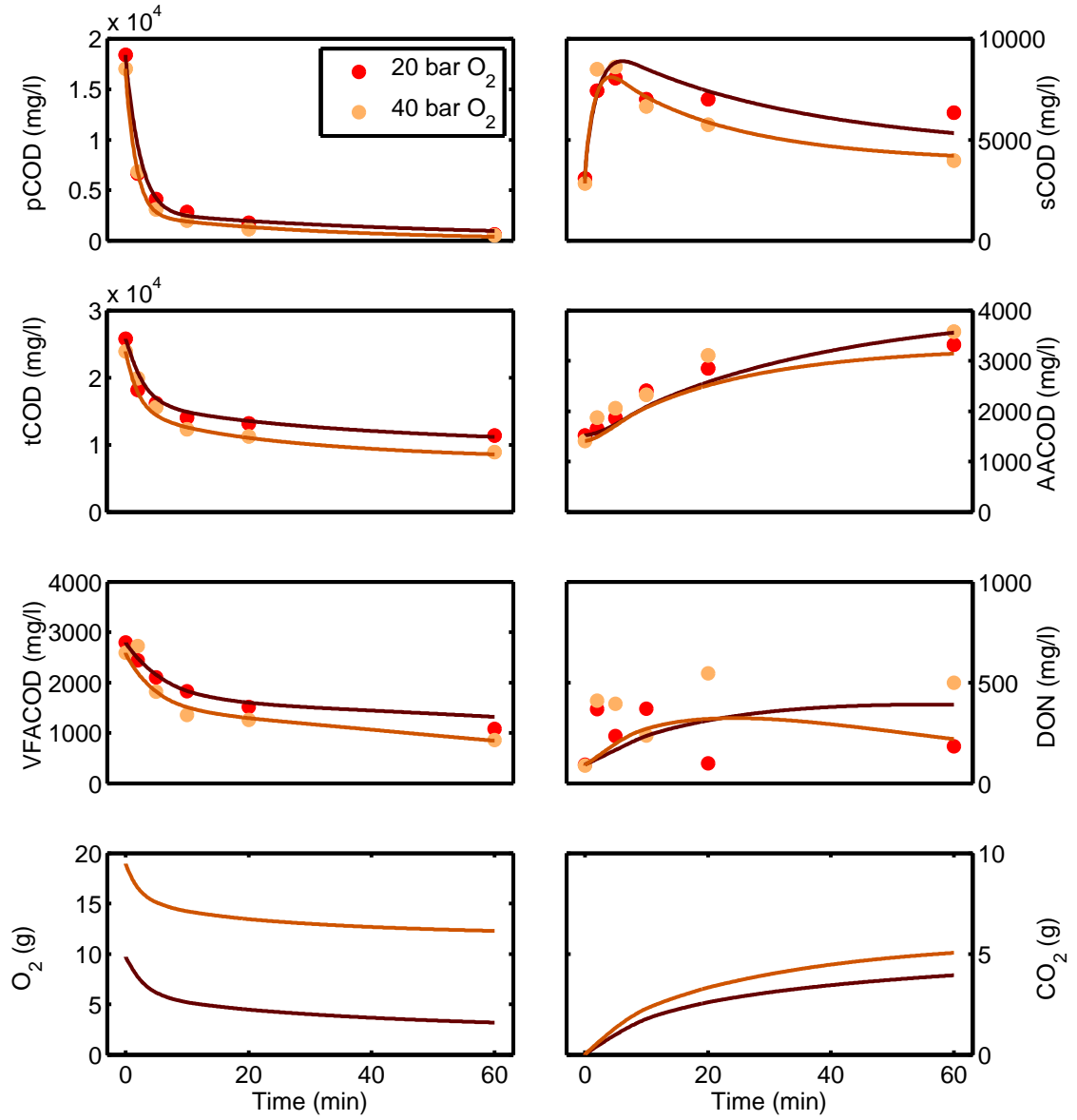


Figure 6.11: The extended kinetic model output versus the response from the experimental data to increasing the oxygen partial pressure from 20 bar to 40 bar. The points represent experimental data, while the solid line is the model response.



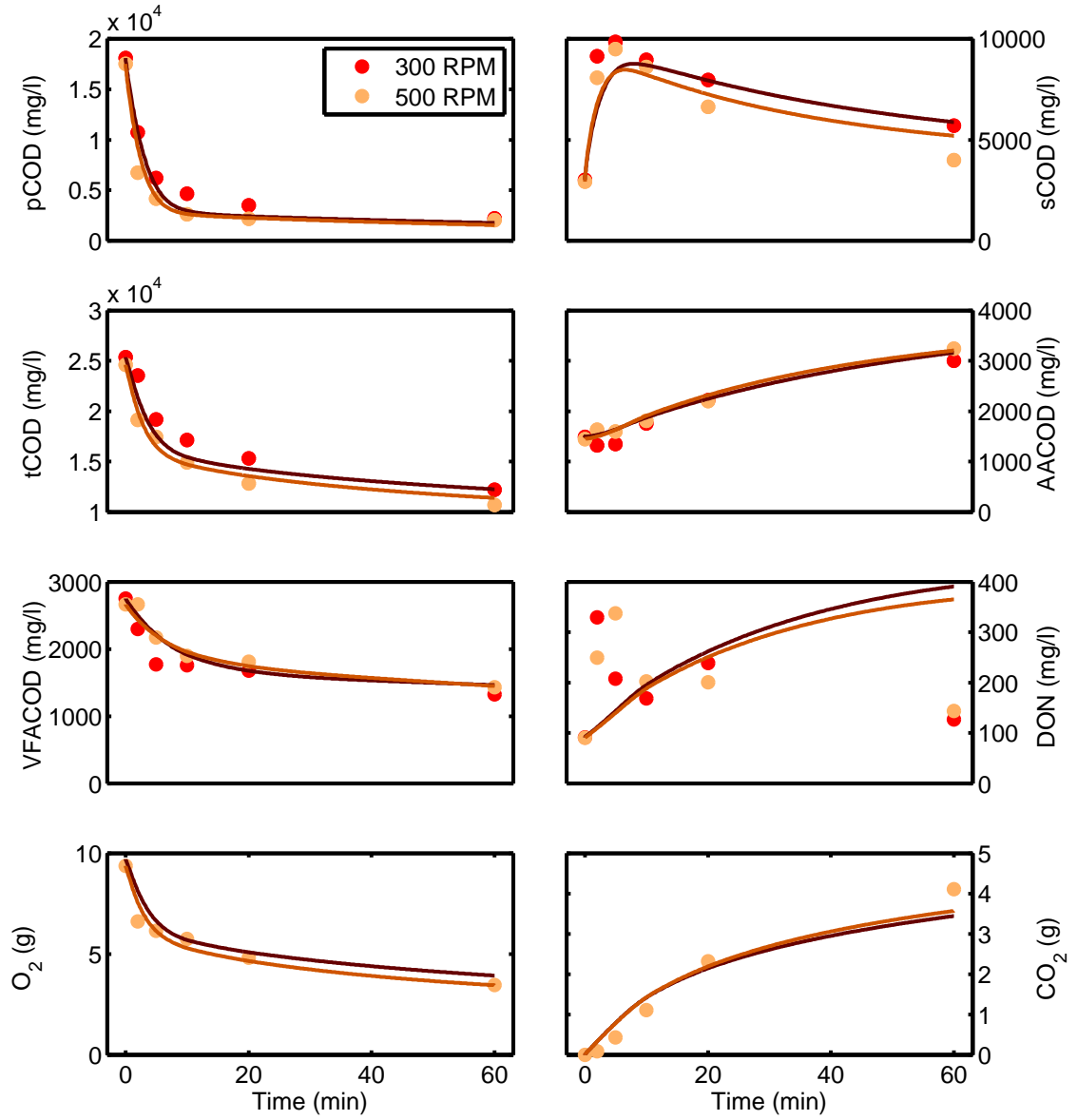


Figure 6.12: The extended kinetic model output versus the response from the experimental data to an increase in stirrer speed from 300 to 500 RPM. The points represent experimental data, while the solid line is the model response.

## 6.3 A Statistical Analysis of the Extended Kinetic Model

A rigorous statistical treatment of the 52 parameter dynamic model is beyond the scope of this thesis. This is partly due to the fact that the regression problem is both highly nonlinear and involves a set of ordinary differential equations to be solved. The nonlinearity destroys the assumption of the underlying Gaussian noise distribution (if any), [130, §6.4, p197], and the ODE component introduces correlation in the independent data as noted again in [130, §4.6, p130] when discussing the analysis of “sampling at intervals of the concentration of a reaction product from a well mixed tank.” The consequence of both these issues is that the analysis of variance described in this section should be treated with some caution.

The statistical calculations for this section were performed in Matlab using algorithms derived for this work employing the statistical distribution routines from the stand-alone maths library, `rmathlib` from the R statistical package, [131]. Standard statistical packages such as R or the Statistical toolbox for Matlab, [132], were not used directly for this analysis because they proved unsuitable for the large-scale ordinary differential equation regression problem. For example, the Statistical toolbox for Matlab formulated the Jacobian using finite differences simply by perturbing all the variables by a constant  $\sqrt{\text{eps}} \approx 10^{-8}$  which suffers from numerical round-off errors in this problem.

However the statistical code written for this work was validated for reduced benchmark problems against the results generated by the Curve fitting toolbox for Matlab, [133], for the parameter confidence limits, and the Statistical Toolbox for the analysis of variance.

Section 6.3.1 describes a simple correlation analysis of the model while Section 6.3.2 calculates confidence limits of the key parameters and other key statistical metrics of the model. Finally in Section 6.3.3, the predictive performance of the proposed model is compared to previously published models.

### 6.3.1 A Correlation Analysis of the Model

A correlation plot between all the experimental data points,  $\mathbf{y}$ , and the corresponding model predictions,  $\hat{\mathbf{y}}$ , from experiment Set 1 is given in Fig. 6.13. Overall, for all the data given in Fig. 6.13, the correlation coefficient,  $R^2$  is 0.925 which is the ratio of the variance explained by the model to the total variance.

However note that the points in Fig. 6.13 that are shaded in red represent the initial

conditions for the fitted dynamic model. In these cases the residual is guaranteed to be zero, so these points were *not* included in the  $r^2$  calculation.

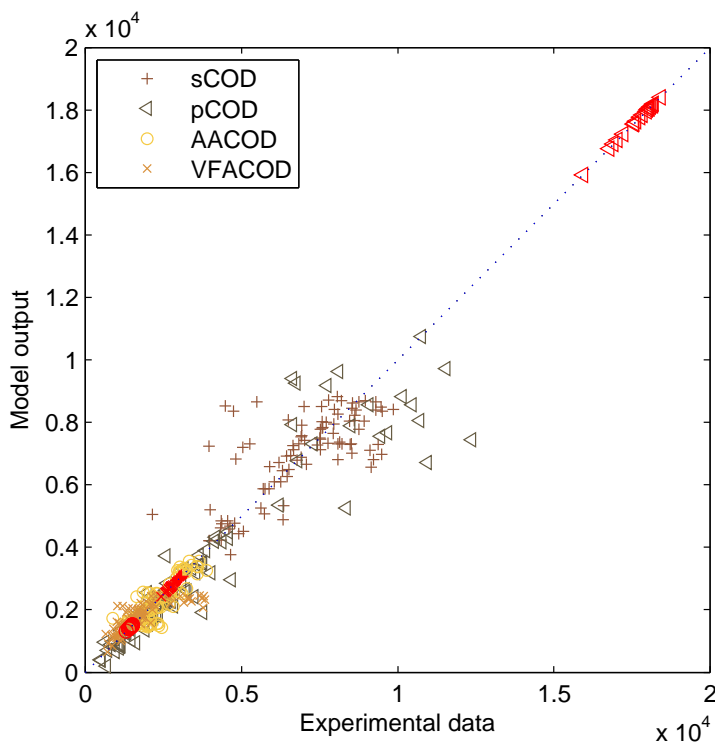


Figure 6.13: The correlation between model predictions,  $\hat{\mathbf{y}}$ , and experimental data,  $\mathbf{y}$ , for all wet oxidation experiments from Set 1. The correlation coefficient is  $R^2 = 0.925$ .

The correlation results in Fig. 6.13 exhibit greater variation than those presented for the initial model correlation in Section 5.3.3, and subsequently a decrease in the correlation coefficient. The reason for this is that for the preliminary model, each experiment was fitted separately as the objective then was to investigate the dominant reaction pathways.

The individual correlations are given separately in Fig. 6.14. In this case the initial conditions are shaded grey (to reduce the visual impact from the red used previously) and again are not included in the calculation for the individual correlation coefficient noted in the subfigures.

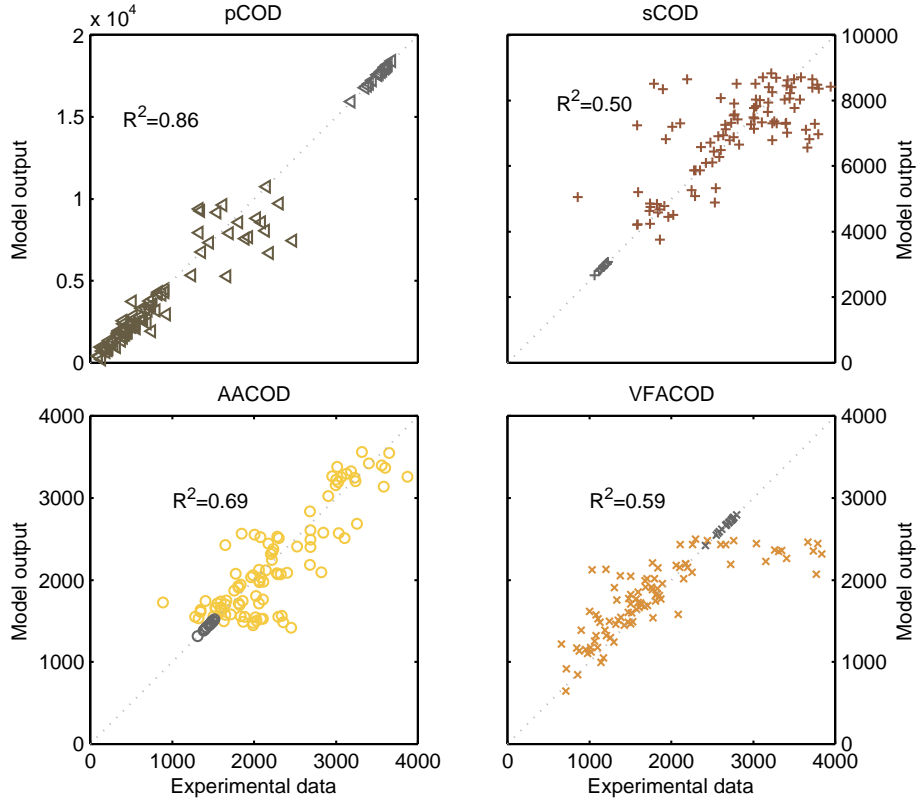


Figure 6.14: The correlation between model and experiment for the individual components from experimental Set 1.(See also Fig. 6.13.)

Overall, the model is shown to predict the likely concentrations of the components of interest with a good level of accuracy, given the variation in the experimental data used for regression.

### 6.3.2 An Analysis of Variance of the Proposed Model

As noted in the introduction to this section, the nonlinearity and dependence of this regression problem means that a standard linearised statistical approach is only ever going to be approximate. Furthermore the extremely high dimension of the fitting problem,  $n(\boldsymbol{\theta}) = 47$  makes visualisation of the confidence ellipsoids problematic. Notwithstanding, the confidence of the fitted parameters can be approximated using a linearised analysis following the strategy given in [134, §3.4.3] or [130, §6.4].

The confidence limits for the parameters at a  $(1 - \alpha)$  level of confidence are given by

$$\theta_i \pm t_{(1-\alpha/2),\nu} s \sqrt{P_{i,i}} \quad (6.1)$$

where  $t_{(1-\alpha/2),\nu}$  is the inverse of the cumulative distribution function of the  $t$ -distribution at  $\alpha$  probability and at  $\nu = m - n$  degrees of freedom. Here,  $\nu$  is sufficiently large that the inverse normal distribution would be a valid approxima-

tion. For this analysis, we have chosen a 95% confidence limit, so  $\alpha = 0.05$  and the  $t$ -statistic is  $t_{1-\alpha/2} = 1.94$ .

The variable  $s$  in Eqn. 6.1 is an estimate of the measurement noise, and is either given by *a priori* knowledge (if known), or in this case approximated by

$$s = \sqrt{\frac{\boldsymbol{\epsilon}^T \boldsymbol{\epsilon}}{\nu}} \quad (6.2)$$

where  $\boldsymbol{\epsilon}^T \boldsymbol{\epsilon}$  is the sum of the squared residuals. The matrix  $\mathbf{P}$  in Eqn. 6.1 is given by

$$\mathbf{P} = (\mathbf{X}^T \mathbf{X})^{-1} \quad (6.3)$$

where  $\mathbf{X}$  is the  $(m \times n)$  Jacobian of the observations with respect to the parameters,

$$\mathbf{X}_{ij} = \frac{\partial y_i}{\partial \theta_j} \quad (6.4)$$

The variable  $y_i$  is the  $i$ th predicted model concentration (of which there are 495 observations), and  $\theta_j$  is the  $j$ th parameter to be fitted. Consequently the dimensions of  $\mathbf{X}$  are  $\Re^{(495 \times 47)}$  and the dimension of the covariance matrix is  $\mathbf{P} \in \Re^{(47 \times 47)}$ .

Numerically the Jacobian is an ill-conditioned matrix, and difficult to construct reliably when the underlying model does not have a closed form (because the ODEs do not have an explicit analytical solution). In this case, the nonlinear optimiser uses internally the well-regarded Intel routine `mk1jac` from [135] for the Jacobian calculation, which can in turn be exported at the solution. Computationally the matrix inverse in Eqn. 6.4 need not be explicitly computed since only the diagonal elements are required in Eqn. 6.1.

The  $n$  optimum parameters  $\boldsymbol{\theta}$  are obtained from the  $m$  experimental observations where in this case  $n = 47$  and  $m = 495$ . The initial condition describing the fraction of the fast versus slowly degrading pCOD was not estimated, nor the parameters to Reaction 8. This gives the  $n = 52 - 5 = 47$  fitted parameters. Regarding the observations, the initial  $t = 0$  observation was not used as it was used as an initial condition to the integrator.

Table 6.1 lists all the parameters and their associated 95% confidence limits calculated using Eqn. 6.1. The fact that none of the uncertainties span zero gives an indication that all parameters are statistically significant. With the exception of one parameter,  $k$  for Reaction 5 at 44%, all uncertainties are usually less than 30% of the nominal value. Confidence limits were not calculated for Reaction 8 because of the limited involvement at these reaction conditions which was discussed earlier in Section 5.6.5, as such it was not included to reduce the number of parameters used.

Table 6.1: The fitted model parameters, their associated 95% confidence limits and statistical metrics.

Reaction		$\theta$ at 95%	Std error	$t$ value	$p$ value
Rxn 1	$k$	$(1.78 \pm 0.46) \times 10^3$	$2.35 \times 10^2$	7.59	$1.82 \times 10^{-13}$
	$E_a$	$(4.03 \pm 0.40) \times 10^4$	$1.90 \times 10^3$	21.26	$7.49 \times 10^{-70}$
	$n$	$0.30 \pm 0.10$	0.05	6.23	$1.10 \times 10^{-9}$
	$c$	$0.47 \pm 0.10$	0.05	9.22	$1.16 \times 10^{-18}$
Rxn 2	$k$	$(3.08 \pm 0.96) \times 10^6$	$4.89 \times 10^5$	6.30	$7.31 \times 10^{-10}$
	$E_a$	$(1.25 \pm 0.08) \times 10^5$	$4.28 \times 10^3$	29.18	$1.16 \times 10^{-105}$
	$n$	$0.45 \pm 0.13$	0.07	6.57	$1.40 \times 10^{-10}$
	$c$	$0.74 \pm 0.31$	0.16	4.59	$5.66 \times 10^{-6}$
Rxn 3	$k$	$(5.91 \pm 2.18) \times 10^2$	$1.11 \times 10^2$	5.33	$1.56 \times 10^{-7}$
	$E_a$	$(4.88 \pm 0.59) \times 10^4$	$2.99 \times 10^2$	16.33	$2.25 \times 10^{-47}$
	$n$	$0.56 \pm 0.17$	0.09	6.44	$3.04 \times 10^{-10}$
	$c$	$0.06 \pm 0.02$	0.01	5.01	$7.86 \times 10^{-7}$
Rxn 4	$k$	$(1.76 \pm 0.49) \times 10^3$	$2.49 \times 10^2$	7.09	$5.38 \times 10^{-12}$
	$E_a$	$(3.53 \pm 0.40) \times 10^4$	$2.03 \times 10^3$	17.37	$4.78 \times 10^{-52}$
	$n$	$0.30 \pm 0.08$	0.04	7.31	$1.26 \times 10^{-12}$
	$c$	$0.47 \pm 0.11$	0.06	8.45	$4.18 \times 10^{-16}$
Rxn 5	$k$	$(3.87 \pm 1.73) \times 10^5$	$8.81 \times 10^4$	4.40	$1.36 \times 10^{-5}$
	$E_a$	$(1.07 \pm 0.08) \times 10^5$	$3.93 \times 10^3$	27.26	$3.65 \times 10^{-97}$
	$n$	$0.93 \pm 0.30$	0.15	6.03	$3.35 \times 10^{-9}$
	$c$	$1.18 \pm 0.26$	0.13	8.94	$1.02 \times 10^{-17}$
Rxn 6	$k$	$(7.40 \pm 1.83) \times 10^2$	$9.31 \times 10^1$	7.94	$1.62 \times 10^{-14}$
	$E_a$	$(6.04 \pm 0.68) \times 10^4$	$3.44 \times 10^3$	17.55	$7.56 \times 10^{-53}$
	$n$	$0.89 \pm 0.23$	0.12	7.57	$2.18 \times 10^{-13}$
	$c$	$0.55 \pm 0.14$	0.07	7.88	$2.47 \times 10^{-14}$
<i>Continued on next page</i>					

Table 6.1 – concluded from previous page

Reaction		$\theta$ at 95%	Std error	$t$ value	$p$ value
Rxn 7	$k$	$(2.91 \pm 0.87) \times 10^2$	$4.43 \times 10^1$	6.57	$1.41 \times 10^{-10}$
	$E_a$	$(4.79 \pm 0.54) \times 10^4$	$2.75 \times 10^3$	17.44	$2.41 \times 10^{-52}$
	$n$	$0.25 \pm 0.09$	0.04	5.66	$2.70 \times 10^{-8}$
	$c$	$0.46 \pm 0.13$	0.07	6.84	$2.61 \times 10^{-11}$
Rxn 8	$k$	$1.64 \times 10^0$	—	—	—
	$E_a$	$1.84 \times 10^5$	—	—	—
	$n$	0.13	—	—	—
	$c$	0.02	—	—	—
Rxn 9	$k$	$(1.26 \pm 0.36) \times 10^1$	0.02	6.91	$1.69 \times 10^{-11}$
	$E_a$	$(3.76 \pm 0.60) \times 10^4$	$3.03 \times 10^2$	12.42	$1.27 \times 10^{-30}$
	$n$	$0.31 \pm 0.10$	0.05	5.97	$4.89 \times 10^{-9}$
	$c$	$0.55 \pm 0.22$	0.11	4.84	$1.77 \times 10^{-6}$
Rxn 10	$k$	$(8.42 \pm 3.3) \times 10^2$	$1.66 \times 10^2$	5.09	$5.39 \times 10^{-7}$
	$E_a$	$(3.52 \pm 0.41) \times 10^4$	$2.06 \times 10^3$	17.07	$1.07 \times 10^{-50}$
	$n$	$0.37 \pm 0.14$	0.07	5.23	$2.63 \times 10^{-7}$
	$c$	$0.06 \pm 0.03$	0.02	3.49	$5.33 \times 10^{-4}$
Rxn 11	$k$	$(9.67 \pm 3.30) \times 10^1$	$1.67 \times 10^1$	5.82	$1.10 \times 10^{-8}$
	$E_a$	$(4.36 \pm 0.76) \times 10^4$	$3.88 \times 10^3$	11.25	$5.08 \times 10^{-26}$
	$n$	$0.34 \pm 0.21$	0.11	3.22	$1.37 \times 10^{-3}$
	$c$	$0.40 \pm 0.13$	0.07	6.03	$3.49 \times 10^{-9}$
Rxn 12	$k$	$(1.21 \pm 0.44) \times 10^1$	2.27	5.34	$1.48 \times 10^{-10}$
	$E_a$	$(3.06 \pm 0.68) \times 10^4$	$3.47 \times 10^3$	8.82	$2.55 \times 10^{-17}$
	$n$	$0.79 \pm 0.26$	0.13	5.93	$5.96 \times 10^{-9}$
	$c$	$0.17 \pm 0.07 \times 10^{-2}$	$3.63 \times 10^{-4}$	4.66	$4.26 \times 10^{-6}$

The  $t$  and  $p$  values in the ANOVA analysis in Table 6.1 show that all of the 47 parameters tested were significantly different from zero, which is shown by the  $t$  values being non-zero. The parameters were statistically significant as all  $p$  values were much smaller than the value of 0.05 corresponding to the 95% confidence limit chosen as the cut-off for this analysis.

Table 6.2: Overall model fit.

Statistical metric	Value
$R^2$	0.925
Adjusted $R^2$	0.917
SSE	$3.953 \times 10^8$
RMSE	939.375

Table 6.2 gives the overall fit of the extended kinetic model. The high values for  $R^2$

and the adjusted  $R^2$  show that the model is able to describe the variation observed in the experimental data with a reasonable level of accuracy. The actual values of the sum of squared errors, and the root-mean-square error (RMSE),

$$\text{RMSE} = \sqrt{\frac{\boldsymbol{\epsilon}^T \boldsymbol{\epsilon}}{m}}$$

are scale dependent, but are commonly stated in an analysis of variance.

The extremely small  $p$  value for the ANOVA summary in Table 6.3 demonstrates that it is highly unlikely that all model coefficients are zero.

Table 6.3: Nonlinear least-squares analysis of variance.

Source	Degrees of Freedom	Sum of Squares	Mean Square	$F$ Value	$p$ Value
Model	47	$9.09 \times 10^9$	$1.93 \times 10^8$	244	$1.28 \times 10^{-288}$
Error	448	$3.95 \times 10^8$	$8.82 \times 10^5$		
Corrected total	495	$9.49 \times 10^9$			

The above statistical analysis has demonstrated, (given the already stated provisos of nonlinearity and dependence), that the model is statistically valid, and the fitted model parameters are statistically significant. Therefore the model is not over-parametrised.

### 6.3.3 Comparison with Published Kinetic Models

The kinetic model developed in the course of this research is considerably more detailed than the kinetic models currently proposed in the literature. As part of the model validation, it was decided to compare the performance of the widely cited generalised kinetic model by Li *et al.* [57] against the model developed in this thesis by using data obtained from the experimental investigation. The original parameters provided by Li *et al.* for municipal sludge were used for their model, so it could be argued that since the proposed model in this work was fitted to this data, it is not an entirely fair comparison. The Li *et al.* model was simulated in the Python modelling environment described in Section 4.4.



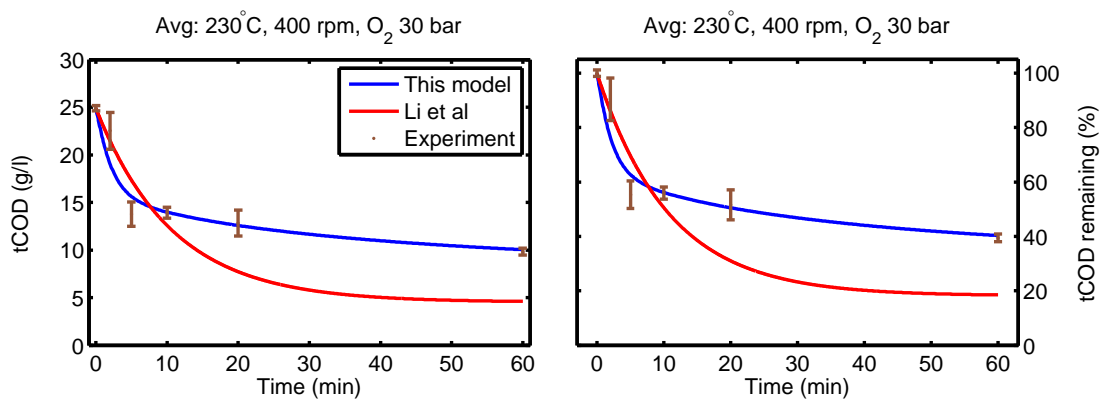


Figure 6.15: The tCOD prediction from the Li *et al.* kinetic model versus the extended kinetic model response from this work, and compared with experimental data.

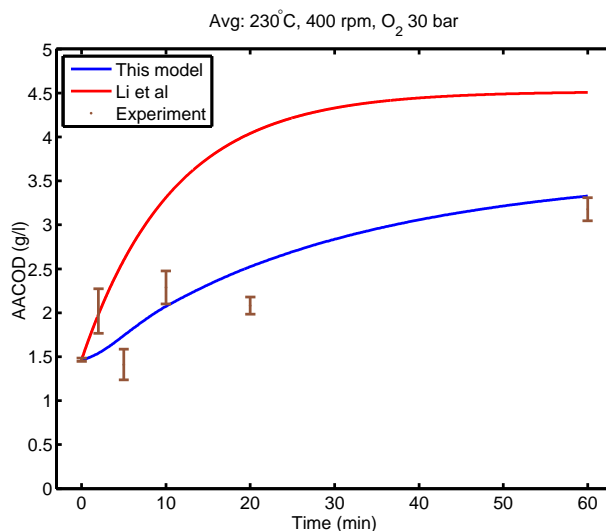


Figure 6.16: The AACOD prediction from the Li *et al.* kinetic model versus the extended kinetic model response from this work, and compared with experimental data.

The results of both models are compared in Fig. 6.15 on a mg/l basis, as well as a percentage basis for comparison with the original results in Li *et al.* [57] which used a percent basis for total COD. The concentration of the acetic acid intermediate product in the Li *et al.* [57] model is shown in Fig. 6.16. It is clear that the Li *et al.* model overestimates the level of conversion of total COD to reaction intermediate and end products.

An important statement by Li *et al.* [57] is that the reaction order with respect to the oxidant is typically zero, or excess oxygen is used and the oxygen terms in the Arrhenius expression can then be assumed to be constants. The model results published by Li *et al.* use a zero order with respect to the oxidant concentration. This is contrary to the kinetic behaviour observed in the experimental and modelling

investigation as part of this thesis, which shows that the oxidant concentration has a significant effect, and that non-zero orders are common.

The experiments performed in the course of this research all used a greater than stoichiometric amount of oxygen in the reactor vessel. However, the dissolved oxygen concentration in the liquid is heavily influenced by the oxygen partial pressure in the reactor, and the experimental results show that oxygen partial pressure clearly affects the concentrations of each of the measured components. This observation suggests that a zero order, (or constant for the oxygen concentration as part of a kinetic model), does not adequately describe the wet oxidation process in a batch reactor and is not an appropriate simplification.

## 6.4 Validation against the TERAX Pilot Plant

To further examine the validity of the kinetic model, the model was configured to simulate the operation of the TERAX pilot plant by using the previously fitted kinetic parameters that were regressed using experimental data from the lab scale experiments. Two semi-batch experiments were conducted using the wet oxidation pilot plant from Section 3.2.2 at 220°C and 240°C with a semi-continuous flow of oxygen. The reaction conditions are listed in Table 6.4.

While the pilot plant system has been previously described in Section 3.2.2, the important differences between it and the lab scale wet oxidation system are summarised below:

- Oxygen control: The pilot plant operates using oxygen control with a semi-continuous flow of oxygen determined by the on-line measurement of the oxygen concentration in the reactor headspace.
- Oxygen concentration: The oxygen concentration is much lower in the pilot plant than the lab scale system. The oxygen concentration set point is typically between 20 to 25% oxygen in the reactor, whereas the lab scale reactor uses an atmosphere of 100% oxygen at the beginning of the experiment.
- Reactor type: The pilot plant uses a co-current bubble column reactor, whereas the lab scale reactor is a CSTR.
- Size: The pilot plant reactor volume is 300l versus 600ml for the lab scale reactor, therefore the pilot plant reactor is 500 times larger.
- Experiment duration: Because of the continuous gas flow, the pilot plant experiment duration was around 4.5 hours versus 1 hour for the lab scale

reactor.

Owing to the use of a semi-continuous gas flow in the pilot plant, the model required modifications to account for the addition of oxygen during the experiment. The pilot plant contains a flow meter on the oxygen feed line which measures the total number of litres that have passed through the meter since the start of the experiment. However, the reactor control system uses a separate PID controller to control the system pressure, and vents to atmosphere when the system pressure rises above the pressure set point. Unfortunately, there is no flow measurement on the vent line which prevented the closing of the mass balance for the gas phase.

As an approximation, the mass of oxygen in the reactor headspace, which the model requires, has been calculated using Daltons's law and the ideal gas law using the on-line oxygen concentration measurement, temperature, pressure and water vapour pressure value from `coolprop` [126] for the duration of the experiment. This oxygen mass profile is then used in the model instead of the gaseous oxygen state variable in the original model.

Clearly the model for mixing will be considerably different for both systems, however the reaction kinetics were the primary focus for this thesis and therefore the CSTR mixing equation has been left in. Ideally, a dedicated bubble column reactor model should be developed incorporating the work of Deckwer *et al.* and Debellefontaine *et al.* [94, 136]. However this has been left for future work.

While the pilot plant is significantly different in configuration, and much larger than the lab scale reactor, it is expected that the reaction kinetics should remain the same provided the same feed material is used. The simplified CSTR mixing model is not expected to be representative, however the pilot plant was run with maximum gas and liquid circulation in order to try and minimise mixing effects.

The pilot plant validation experiments were conducted using the experimental procedure described earlier in Section 3.4.3, and the experiments were commenced once the reactor had reached operating temperature.

It should again be emphasised that the following model results use the kinetic parameters regressed from the lab scale experimental investigation, and have not been re-fitted to the pilot plant data.

Table 6.4: Semi-batch pilot plant experimental conditions for the pilot plant experiments.

Condition	Experiment 1	Experiment 2
Temperature	240°C	220°C
Experiment duration	4.5 hours	4.5 hours
Total oxygen addition	1264 l	2469 l
Gas recirculation speed	100%	100%
Liquid recirculation speed	100%	100%
System pressure	40 bar	40 bar
Liquid volume	150 l	130 l

### 6.4.1 Pilot Plant Batch Experiment 1

The first batch feed experiment was conducted at the experimental conditions listed for Experiment 1 in Table 6.4.

The response from the model derived in Section 5.6 is compared with the experimental data in Fig. 6.17. While the experimental data is reasonable, several discrepancies are noted and are discussed. The large spike in pCOD soon after the experiment commenced is clearly an outlier, possibly caused by sample contamination or an error in the analytical procedure. No biosolids are added once the experiment has commenced and therefore pCOD should never increase as the experiment progresses. The spike in total COD is a result of the spike in pCOD, as the total COD is not measured directly and is computed from the sum of pCOD and sCOD, in the same manner as the lab scale experimental results. Like in Chapter 5, the sCOD results presented in this section are exclusive of AACOD and VFACOD.

There is a simultaneous decrease in AACOD and other VFACOD with an opposite increase in sCOD at the same time midway through the experiment. Interestingly, the excursion lasts for more than one sample. It is likely that this was due to a sampling problem as nothing untoward happened during the course of the experiment that would account for this behaviour.

Overall, the model predicts the concentrations for each of the measured compounds with a good level of accuracy in this experiment, which is significant as this suggests that the reaction kinetics have been adequately captured in the model.

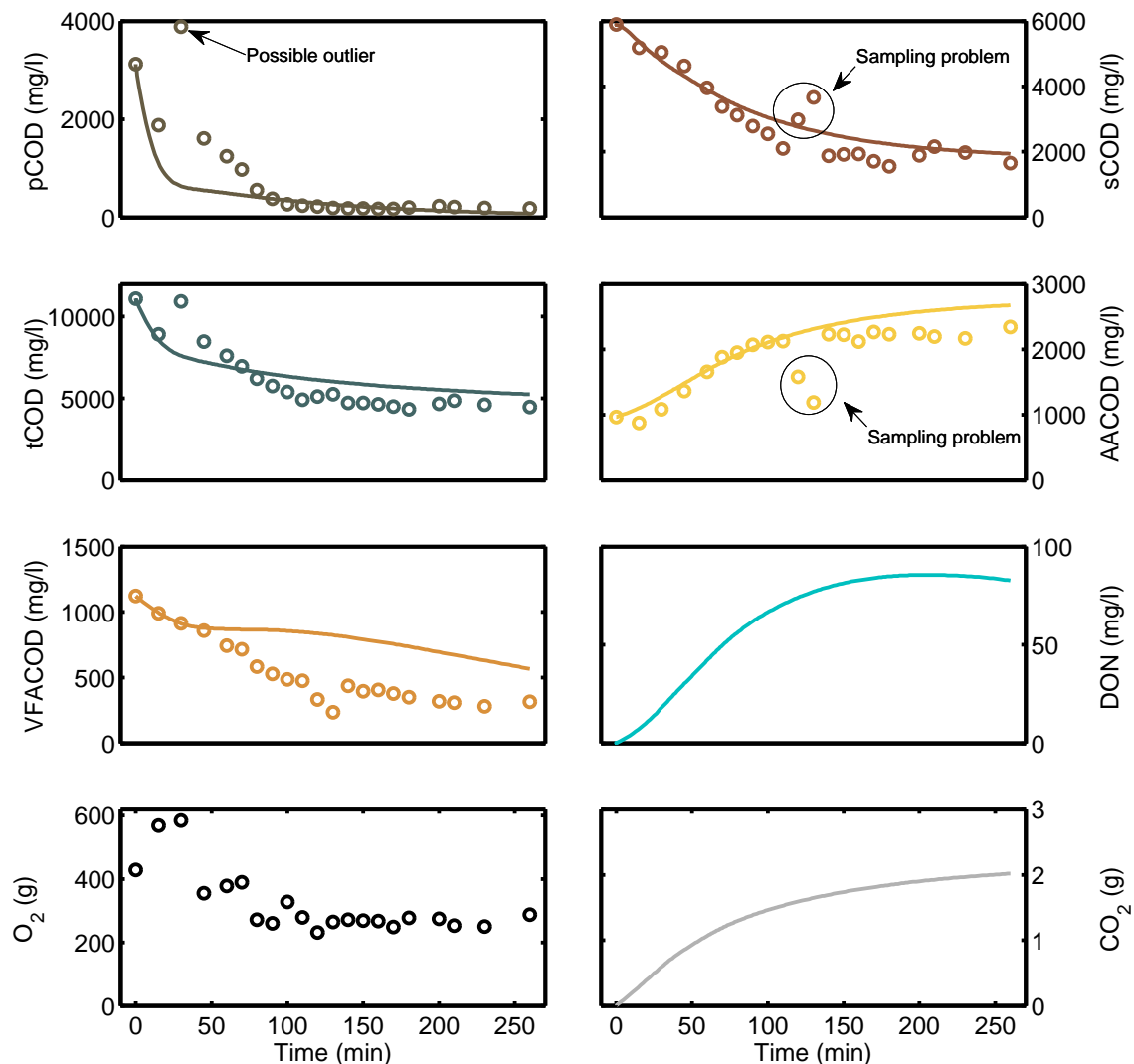


Figure 6.17: The extended kinetic model compared with the first semi-batch pilot plant experiment at 240°C.

## 6.4.2 Pilot Plant Batch Experiment 2

The second batch experiment was conducted at the conditions listed for Experiment 2 in Table 6.4.

The pCOD results in this experiment show an initial lag before degradation begins to occur, which is in contrast to the model results. Importantly, this behaviour was not observed in the previous batch experiment described earlier which suggests that there could have been a problem with the sampling procedure, such as the sample lines were not correctly flushed for the first couple of samples. The limited pCOD data available in this experiment prevents further comparison with the model to see

whether the final concentrations converge.

There are small initial spikes in AACOD and VFACOD which were not observed in the previous experiment, and could potentially be caused by the same problem which affected the initial pCOD measurements.

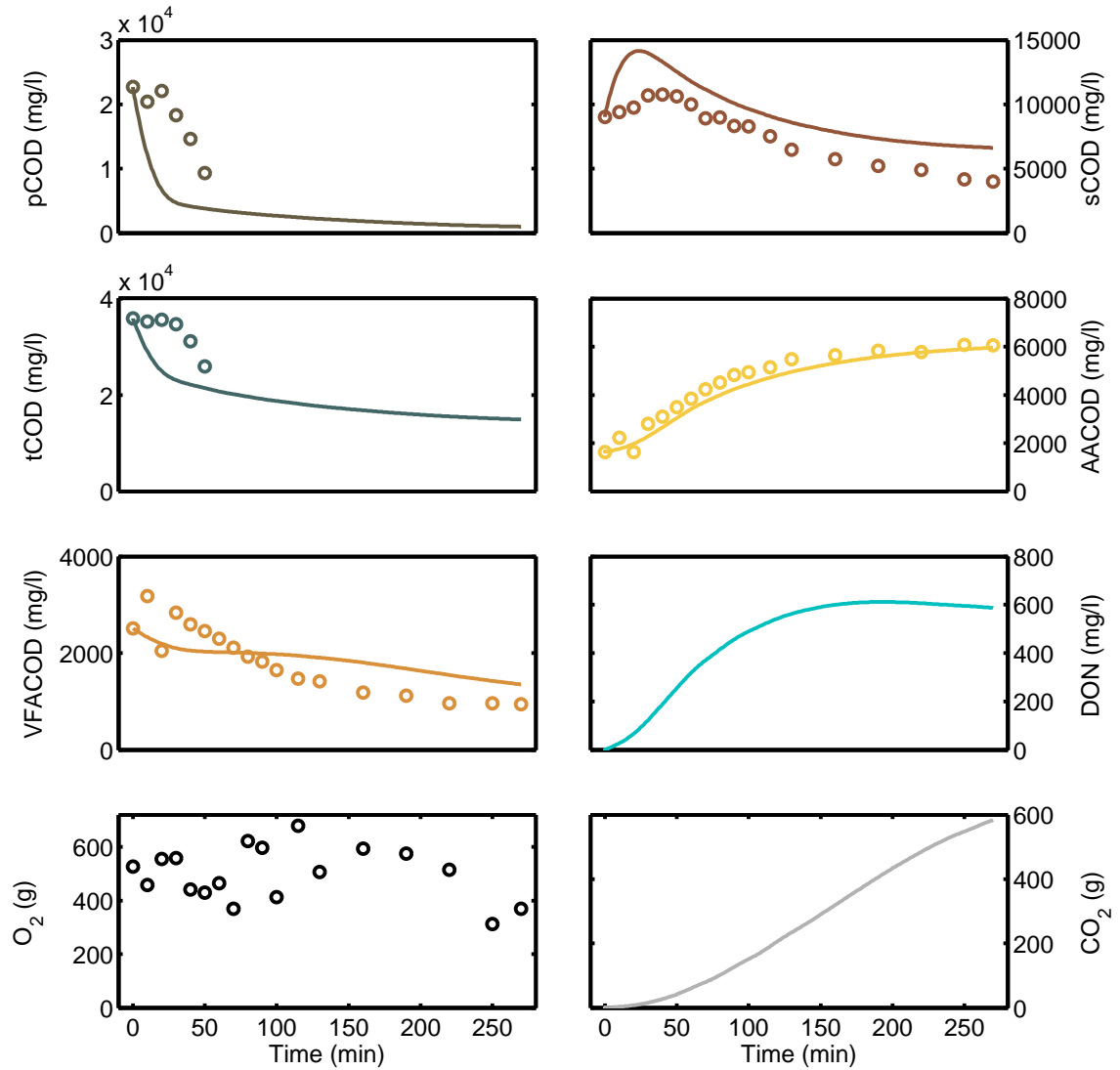


Figure 6.18: The extended kinetic model compared with the second semi-batch pilot plant experiment at 220°C.

Interestingly, the oxygen control was quite unstable over the course of the experiment which did not occur previously. However this does not seem to have adversely affected the experimental results, as the instability occurred after the initial reaction phase.

An important difference between the first and second experiments is that the “strength” of the feed was much higher than in the first experiment, with the initial concentra-

tion of each component being approximately four times greater. This is illustrated in the scales used for Fig. 6.18 compared to Fig. 6.17.

It is important to note that the mass of  $\text{CO}_2$  in the reactor will in fact be lower than predicted by the model because of the unquantified mass flow of gas leaving the reactor during operation owing to the reactor pressure controller.

It is pleasing to note that, overall, the model fits the experimental data from both pilot plant experiments very well. This gives confidence that the kinetic model, and the parameters regressed from the lab scale investigation, are representative of the wet oxidation of RDC biosolids.

## 6.5 Summary of the Model Results

Investigating the behaviour of RDC biosolids under wet oxidation has resulted in the development of an extended kinetic model. This model is capable of predicting the concentrations of a wide variety of liquid and gaseous reaction feed, intermediate, and end products with a high overall level of accuracy.

A number of simplifications have been performed to reduce model complexity and minimise solution time. Solving a single iteration takes 3 to 5 seconds on a modern desktop computer, which is fast enough to allow the simulation of different reaction scenarios. It is pleasing to note that despite the simplifications described in Section 5.6.1, the model exhibits good performance on both wet oxidation systems.

The extended model was capable of predicting the concentration for the measured components from the lab scale wet oxidation system with a high level of accuracy. Improvements to the measurement process have been identified and will result in improved model parameters once they have been implemented and the model refitted.

The developed model consists of 12 reactions, 11 states and 52 parameters which have been regressed from experimental data obtained from the lab scale wet oxidation system. The model has been developed in Matlab, using the regression environment and program structure described in Section 5.6.3.

Results from the wet oxidation pilot plant were used for model validation. This demonstrated that the reaction kinetics have been captured by the model as the fit was very good using the previously regressed parameters from the lab scale wet oxidation system.

The strength of this model is its flexibility to work on both wet oxidation systems

with good accuracy and without the need for separate sets of parameters for each system.

### 6.5.1 Exploiting the Developed Model

One of the key advantages of developing the dynamic kinetic model from Chapter 5 is that it can be used for “what if” studies, such as using a higher temperature, but a smaller reactor and residence time, to achieve the same level of degradation and throughput compared to a larger reactor operating with a lower temperature and longer residence time. This is particularly important as larger equipment is more expensive, with the six-tenths-factor rule often used to quantify the cost of scaling equipment [137].

Using the dynamic model, we can capture the effects of common environmental conditions, and as demonstrated in pilot plant investigation in Section 6.4, show the oxidated result given a wide range of feed concentrations. This allows the user to investigate the effect of changes to the experimental procedure, and within a few seconds, observe the results. This saves the user from potentially wasteful and time consuming experiments that might not have produced the desired outcome.

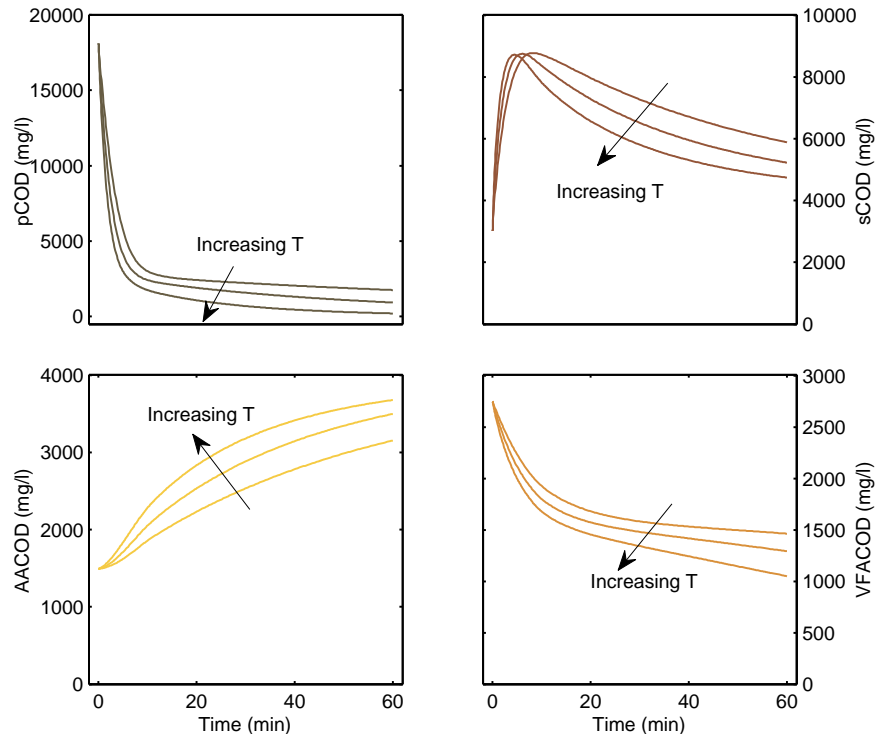


Figure 6.19: Results from the extended kinetic model showing the effect of increasing temperature from 220 to 260°C on the concentration of the main components of interest.



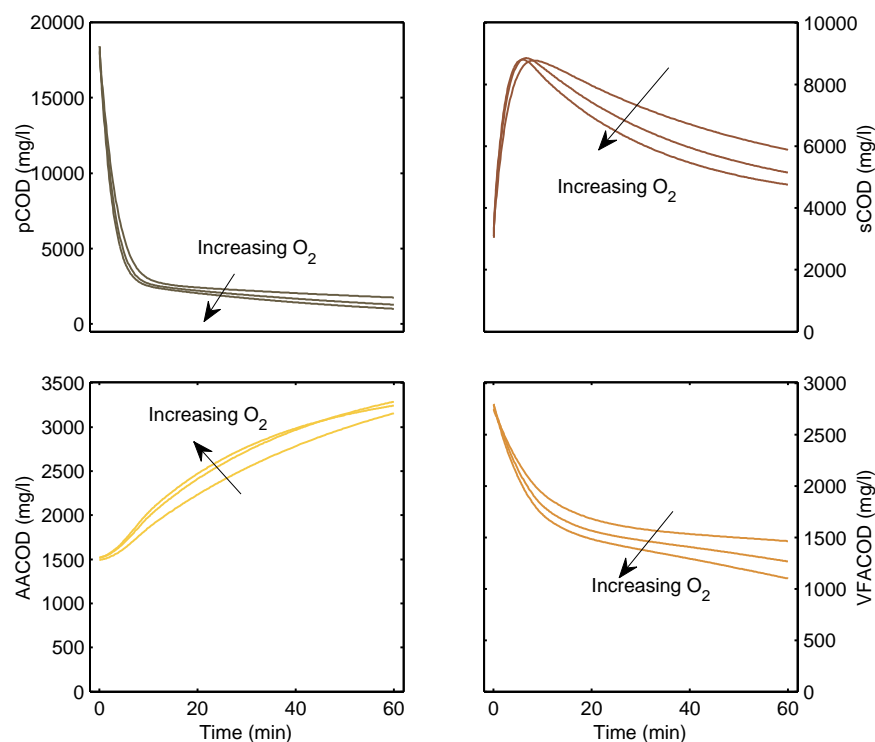


Figure 6.20: Results from the extended kinetic model showing the effect of increasing the oxygen partial pressure from 20 to 60 bar on the concentration of the main components of interest.

In addition to optimal experimental design, the model can be used as a design tool for future wet oxidation plants. The model allows the user to perform “what if” case studies on environmental conditions such as temperatures and pressures, in addition to physical factors such as the reactor volume and flow rates. Figures 6.19 and 6.20 clearly show the effect of temperature and oxygen partial pressure on the main components of interest. Because the developed model is dynamic, it allows detailed studies of these phenomena which can be used to determine the sizing of equipment and optimum operating conditions. This allows degradation levels and cost trade-offs to be explored by the designer.

### 6.5.2 Establishing an Optimum Operating Point

In this application, as noted in Section 2.9, the aim was to produce both acetic acid, and other VFAs for use in a downstream BNR wastewater treatment plant. Fig. 6.21 shows the interrelationships between the three key operational variables: batch reaction time, temperature and pressure. Note that both the plotted temperature range (from 210°C to 260°C) and the plotted oxygen partial pressure range (from 15 to 60 bar) is deliberately extrapolated outside the ranges used during the experiments. The lighter the colour, the higher the concentration and the values on the contour

lines correspond to the concentration in mg/l of COD. The four points in the top left plot indicate the extremities of the experimental program for reference.

The left-hand column of contour plots ((a), (d) & (g)) in Fig. 6.21 show the production of acetic acid after 30 minutes, 60 and 120 minutes residence time. The other two columns are for VFACOD and the sum of acetic acid and VFA.

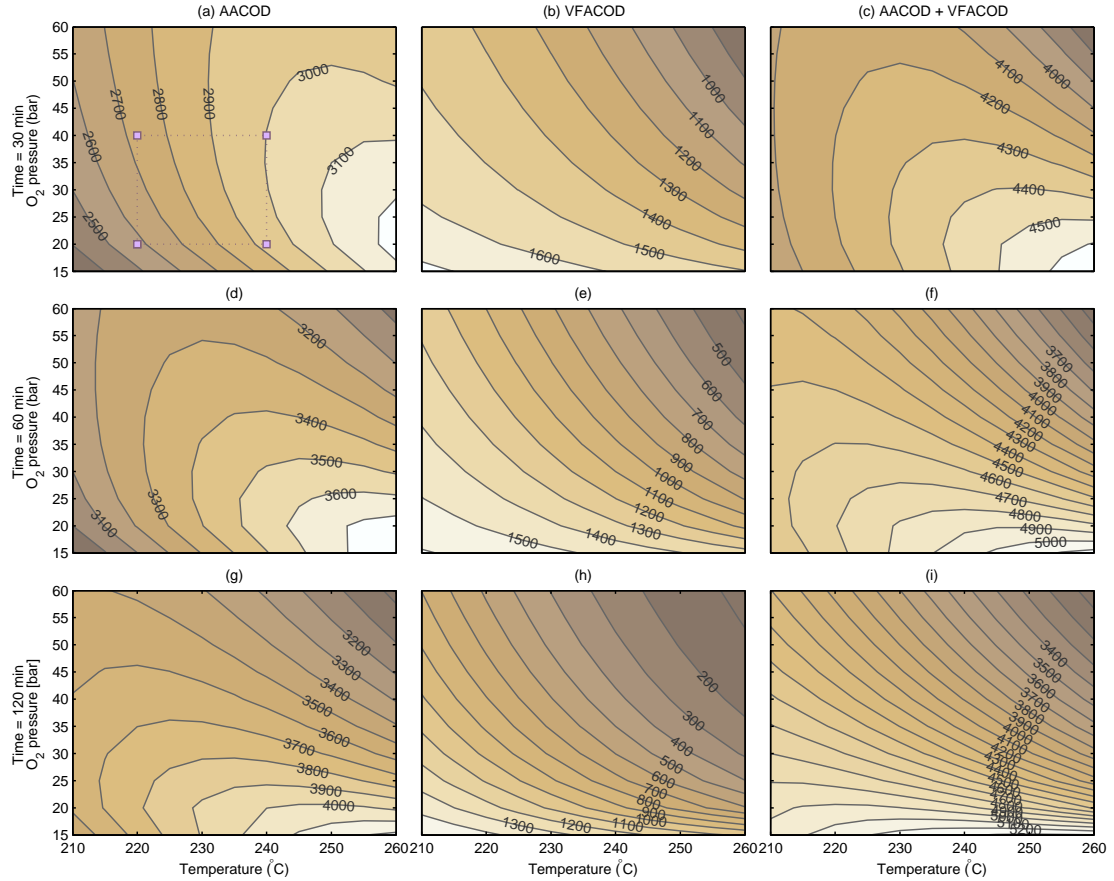


Figure 6.21: The concentration of acetic acid, VFA and the combination as predicted from the model at different reaction times, temperatures and pressures. Contour lines show the concentration on a mg/l COD basis.

Clearly to maximise the acetic acid production, one operates at a high temperature and a oxygen partial low pressure. Of course to avoid the degradation of the acetic acid to a fully oxidised state (which starts to happen around 300°C as noted by [79]), and to avoid corrosion issues, the maximum practical operating temperature is limited. It is interesting to note in subplot (g) of Fig. 6.21 that after 120 minutes at high temperatures, the production of acetic acid drops slightly. Conversely, the production of other VFAs ((b), (e) & (h)) in Fig. 6.21 decreases at higher temperatures and oxygen partial pressures as these are easier to degrade than acetic acid.

Prior to this study, it was hypothesised that an optimum operating temperature

for total VFA production was around 220°C. What is interesting is that this model seems to support this observation, given that the optimum operating point to maximise both the acetic acid and VFA after 2 hours is around 230°C as seen from the maximum point in subplot (i) in Fig. 6.21.

This illustrates the ability of using a dynamic model to highlight optimum operating points which are not always obvious because of the requirement to maximise acetic acid and maximise VFAs which are competing objectives. The ability of the model to suggest an optimal operating point was a key research objective formulated in Section 1.4.

## 6.6 Chapter Summary

This chapter validated the model developed in Chapter 5 against unseen data collected from the pilot plant. A correlation analysis shows that the model is able to confidently predict the concentration of key components. Confidence limits for the parameters derived from a statistical analysis shows that all the parameters are statistically significant. Finally the usefulness of the model is demonstrated by its ability to advise on the operating conditions to maximise the production of acetic acid and VFAs which was a key research objective of this work. It is interesting to note that the optimum point is not perhaps where a naive analysis would suggest.

## Chapter 7

# Conclusions and Recommendations for Future Work

This thesis describes the characterisation of the degradation of municipal biosolids obtained from the Rotorua District Council (RDC) wastewater treatment plant under wet oxidation. This work has been encapsulated in the development of a detailed kinetic model which describes the wet oxidation of municipal biosolids for Scion's wet oxidation system. The model was regressed from data obtained from a lab scale reactor and validated against data obtained from the full scale pilot plant. The model incorporated the main environmental factors, enabling it to predict the change in concentration of components over time for lab and pilot scale wet oxidation systems.

### 7.1 Key Achievements

The following sections highlight the key achievements of this thesis. The first two achievements are concerned with the model development, validation and subsequent use. The third achievement undertook a detailed investigation of the effect of wet oxidation on RDC municipal biosolids. This information, combined with the dynamic model, allowed a user to establish optimal operating strategies as outlined in the fourth achievement. The final two achievements highlight novel measurement strategies that could be used to supplement standard measurement techniques.

### 7.1.1 Kinetic Model Development and Regression

The kinetic model was shown to agree closely with the concentration results obtained from the experimental investigation, with an overall  $R^2$  of 0.925. The model contains a number of simplifications to reduce complexity and the results suggest that, despite these simplifications, the model still accurately captures the effects of wet oxidation. Notwithstanding, the dynamic model is reasonably complex comprising of 52 parameters and a minimum of 14 dynamic equations depending on the amount of experimental data. A statistical analysis of the linearised model indicated that all of the 47 fitted parameters were statistically significant.

The effect of temperature, oxygen partial pressure and stirring speed were investigated and the effects that these parameters have on each of the model components has been captured in the developed kinetic model. Overall the extended kinetic model produces adequate results in response to changes in operating conditions, however the model is not fundamental and would potentially need to be re-regressed if it was used with biosolids from other treatment facilities. A visual comparison shows that the developed kinetic model outperforms previously published model results.

### 7.1.2 Pilot Plant Validation

Applying the proposed kinetic model to subsequently collected experimental data from the wet oxidation pilot plant gave excellent agreement across the modelled components over the environmental conditions investigated. These results were obtained using model parameters that were regressed from the lab scale wet oxidation system, and were then applied to the pilot plant. It should be emphasised that the model was not re-fitted to the pilot plant data but used purely as a validation step. This demonstrates that the reaction kinetics have been adequately captured as part of the kinetic model for the reaction conditions considered.

### 7.1.3 Characterisation of RDC Municipal Biosolids

An experimental investigation consisting of three experiments was undertaken to both characterise the composition of RDC biosolids, and examine the degradation behaviour under wet oxidation with varying reaction conditions. The biosolids characterisation revealed that the incoming biosolids feed composition exhibits some variation over time but is not cause for concern. The concentration of common wastewater quality metrics for the RDC biosolids are consistent with those reported

in the literature.

Regarding the wet oxidation effluent characterisation, the results revealed that temperature had the most effect on the level of degradation achieved. Oxygen partial pressure had less of an effect, while changes in stirring speed had the least effect of the environmental factors. A factorial design was used so that the full range of operating conditions was represented in the results, while minimising the number of experiments required.

The experimental results highlighted possible issues with the techniques used to analyse the samples. The results showed that the intermediate liquid samples had considerably more variation than the initial, and final samples. It was suspected that this was an artefact of the analytical techniques not being suited to the somewhat non homogeneous nature of the intermediate samples, but this has not been investigated in detail and is left as further work. In addition, the dissolved organic nitrogen results exhibited considerable variation. It was believed that this was due to problems with the nitrogen analysis and not the experimental procedure.

#### **7.1.4 Exploiting the Kinetic Model**

The usefulness of the kinetic model was demonstrated by highlighting non-obvious operating points which could maximise the production of VFAs, which have been previously described as being a key product of the process. The effect of residence time was also shown, which allows the user to predict the VFA yield at a given temperature, oxygen partial pressure, stirring speed, after a particular time in the experiment. As an example, the operating point to maximise the total concentration of VFAs for a two hour residence time is 230°C at 16 bar oxygen partial pressure.

#### **7.1.5 Image Analysis of Intermediate Samples**

Photographs of each sample set were taken as part of the Set 2 experimental programme. Computing a normalised intensity index from the images of each sample revealed a strong correlation with the measured change in total COD, when compared with the only experiment which was performed at the same reaction conditions (Run 7) in the first set of experiments. For the remaining Set 2 experiments, the kinetic model was used to simulate the change in total COD at the conditions of interest. This demonstrated the same clear correlation between total COD and the normalised intensity index and is an efficient alternative to a formal COD analysis.

### 7.1.6 Analysis of Stirrer Power Measurements

An investigation into the hypothesis that variations in viscosity, and reaction extent, could be inferred from the stirrer motor current was reviewed during the Set 2 experiments. An analysis of the results revealed a weak correlation between normalised stirrer power and viscosity. Improvements to the measurement process were identified which could be explored for future work. This could form a valuable input in future models as it can be measured online while the reactor is operating.

## 7.2 Review of Research Objectives

This section reviews the research objectives posed in Section 1.4.

1. *To investigate the characteristics of biosolids produced by the RDC wastewater treatment plant and their behaviour under wet oxidation.*

A detailed analysis of biosolids produced by the RDC wastewater treatment plant which were subjected to wet oxidation showed that every measured compound was strongly affected by the wet oxidation process. The concentration of standard wastewater quality indicators of both feed to the WO process and product was in line with literature data.

2. *To formulate and validate a kinetic model of the wet oxidation process in order to predict operation and enable optimal bench-scale experimental design.*

The extended kinetic model developed in Section 5.6 allows the simulation of the wet oxidation process and can predict the concentration of liquid and gaseous reaction intermediate and end products over a wide range of feed concentrations and environmental conditions and matches the experimental data.

3. *To build sufficiently flexible models to enable the scale up to the design of a full-scale production plant.*

Semi-batch experimental data from the wet oxidation pilot plant was then applied to the extended kinetic model and the model results agreed well with the experimental data. This demonstrates that the kinetic model accurately captures the kinetic behaviour of wet oxidation of RDC biosolids, but is also sufficiently flexible to give good results when applied to a different reactor type which is 500 times larger. This also reinforces the suitability of the developed kinetic model for a priori prediction of the concentration of reaction end products and would be suitable for optimisation of the reaction process.

4. *To show that the developed models can be used as a design aid for future wet oxidation plants.*

The extended kinetic model that has been developed in this research is dynamic in nature and is flexible enough to account for batch or continuous wet oxidation. Because of this, the model can be used as a design aid to investigate the effect of different physical design decisions such as changing volumes and flow rates, as well as environmental factors like temperature and pressure, on the reaction end products. This model is therefore a valuable design tool that can be used for the design of future wet oxidation plants.

### 7.3 Recommendations for Future Work

The initial aim of this research was to develop a software platform to support a highly specialised off-gas analyser which had been developed in-house by Scion to analyse gases from wet oxidation and fermentation experiments. However during the preliminary experiments, the research focus of this thesis was changed to the development of a dynamic model which predicted the concentration of key components of interest in biosolids undergoing wet oxidation. This change in research direction was motivated because it was thought at the time to be more critical to study wet oxidation at a pilot scale as opposed to a software platform for their analysis instrument.

Notwithstanding, the need for a flexible model support environment is still very apparent today and a further development of the initiative described in Section 4.4 would be highly beneficial.

Regarding the experimental programme, conducting repeats of the experiments across the full range of experimental conditions used would give a better understanding of the variance as a consequence of the variation in the analytical measurements.

Additional gas composition data in particular would be highly beneficial, as the reactor oxygen concentration is a critical component in the kinetic model as all reactions are influenced by it. Performing the additional calibrations on the gas chromatograph to allow it to correctly differentiate CO would allow this component to be modelled. A survey of the literature in addition to preliminary testing has revealed that it is being produced under wet oxidation. This could have design implications on full scale wet oxidation plants.

Improvements in the analytical techniques, particularly for DON measurement, would greatly improve the model prediction of this component. At present, the fit is as good as can be expected without improved experimental data.



Apart from improved sampling and analysis procedure, this research identified two measurement techniques for wet oxidation which should be further examined.

More rigorous image analysis could be investigated as the work featured in this thesis showed a strong correlation between the calculated image intensity index and change in total COD and it would be a fast and low cost avenue to explore. Further work in this area could lead to an on-line measurement for total COD which would be highly beneficial for on-line kinetic modelling.

Further research into the relationship between the stirrer power requirements and viscosity should be performed as it could form an important part of an improved mass transfer model. Improved current measurement, or a direct torque measurement from the stirrer shaft, would be useful in that one can infer the extent of reaction from a simple, robust transducer.

Wet oxidation experiments could be conducted using municipal biosolids from other wastewater treatment plants around the country which are of a similar size to Rotorua. Results from the experiments could be compared with the model to see how applicable the model is to other biosolid streams.

The developed kinetic model should incorporate a suite of mass transfer models to take into account the CSTR reactor in the lab scale system, and the bubble column reactors that are part of the wet oxidation pilot plant. The bubble column reactor model by Debellefonatine et al [54] has been widely cited in the literature and could be inserted into the extended kinetic model at a later date.

The areas identified for future work, if implemented, will result in an improved model which will be a more powerful design and analysis tool.

# Bibliography

- [1] Anon, “Wastewater,” tech. rep., Ministry for the Environment, 2012.
- [2] Anon, “Waste Minimisation Act 2008,” tech. rep., Ministry for the Environment, 2008.
- [3] M. Henze, *Biological Wastewater Treatment: Principles, Modelling and Design*. IWA Publishing, 2008.
- [4] G. Gielen, S. Love, R. Lei, D. Gapes, P. Strong, K. McGrouther, and T. Stuthridge, “Wet oxidation technology - a potential biosolids management alternative,” *IPENZ Transactions*, vol. 19, 2011.
- [5] V. G. Molina, *Wet oxidation processes for water pollution remediation*. PhD thesis, Universitat de Barcelona, 2006.
- [6] V. S. Mishra, V. V. Mahajani, and J. B. Joshi, “Wet air oxidation,” *Industrial & Engineering Chemistry Research*, vol. 34, no. 1, pp. 2–48, 1995.
- [7] Anon, “About Scion,” tech. rep., Scion Research Ltd, Rotorua, New Zealand, 2014. <http://www.scionresearch.com/general/about-us>.
- [8] Anon, “Scion Research,” tech. rep., Scion Research Ltd, 2013.
- [9] D. Gapes, “Waste to Gold – Biosolids Management Opportunities for the Rotorua District Council,” tech. rep., Scion Research Ltd, 2010.
- [10] A. Aggrey, S. Baroutian, and D. Gapes, “Wet oxidation of municipal biosolids: Scion’s terax process compared to european practices,” *IChemE*, 2011.
- [11] P. J. Strong, B. McDonald, and D. J. Gapes, “Combined thermochemical and fermentative destruction of municipal biosolids: A comparison between thermal hydrolysis and wet oxidative pre-treatment,” *Bioresource Technology*, vol. 102, no. 9, pp. 5520–5527, 2011.
- [12] P. M. Rose, K. J. McKay, S. J. Tallon, O. J. Catchpole, and T. Mollenhauer, “Wet air oxidation of waste water sludge,” in *Chemeca 2012: Quality of life through chemical engineering* (E. Australia, ed.), (Wellington, New Zealand), Engineers Australia, 23–26 September 2012.
- [13] T. Lendormi, C. Prvot, F. Doppenberg, M. Sprandio, and H. Debellefontaine, “Wet oxidation of domestic sludge and process integration: The mineralis process,” *Water Science & Technology*, vol. 44, no. 10, pp. 163–169, 2001.
- [14] Anon, “TERAX : Hydrothermal Deconstruction,” 2013.

- [15] G. Tchobanoglous and F. L. Burton, *Wastewater Engineering*. Metcalf & Eddy, Inc, 4th ed., 2003.
- [16] J. P. Scott and D. F. Ollis, “Integration of chemical and biological oxidation processes for water treatment: Review and recommendations,” *Environmental Progress*, vol. 14, no. 2, pp. 88–103, 1995.
- [17] Anon, “Wastewater Treatment Information,” tech. rep., Rotorua District Council, 2013.
- [18] R. Lei, “Waste 2 Gold Project — One year of WMF,” in *WasteMINZ Conference*, 2011.
- [19] Anon, “Rotorua Wastewater,” tech. rep., Rotorua District Council, 2013. [http://www.boprc.govt.nz/media/295812/rdc-rotorua-wtp\\_lts-ppt-maoricttee300713.pdf](http://www.boprc.govt.nz/media/295812/rdc-rotorua-wtp_lts-ppt-maoricttee300713.pdf).
- [20] Anon, “The Bardenpho Wastewater Treatment Plant,” tech. rep., Rotorua District Council, 2013.
- [21] Anon, “Standard Methods for the Examination of Water and Wastewater,” tech. rep., American Public Health Association, American Water Works Association, Water Environment Federation, 1998. 20th ed.
- [22] Anon, “ERG STANDARD OPERATING PROCEDURES,” tech. rep., Scion Research Ltd, Rotorua, New Zealand, 2013.
- [23] A. Shanableh, “Production of useful organic matter from sludge using hydrothermal treatment,” *Water Research*, vol. 34, no. 3, pp. 945–951, 2000.
- [24] T. Lendormi, C. Prévot, F. Doppenberg, H. Debellefontaine, and R. Pujol, “Application of the wet oxidation process to the treatment of municipal sewage sludge,” *Environmental Technology*, vol. 21, no. 10, pp. 1193–1198, 2000.
- [25] A. Shanableh and S. Jomaa, “Combined Sludge Treatment and Production of Useful Organic Substrate for Recycling – Evidence of Substrate Bioavailability to Support Biological Nutrient Removal,” *Arabian Journal for Science and Engineering*, vol. 30, no. 2C, p. 29, 2005.
- [26] P. Strong, B. McDonald, and D. Gapes, “Enhancing denitrification using a carbon supplement generated from the wet oxidation of waste activated sludge,” *Bioresource Technology*, vol. 102, no. 9, pp. 5533–5540, 2011.
- [27] Anon, “Guidelines for the Safe Application of Biosolids to Land in New Zealand,” tech. rep., New Zealand Water and Wastes Association, Wellington, New Zealand, 2003.
- [28] L. Sommers, “Chemical composition of sewage sludges and analysis of their potential use as fertilizers,” *Journal of Environmental Quality*, vol. 6, no. 2, pp. 225–232, 1977.
- [29] D. Gapes. Private Communication, March 2014.
- [30] M. Davis, *Water and Wastewater Engineering*. McGraw-Hill, 2010.

- [31] J. Mata-Alvarez, S. Macé, and P. Llabrés, “Anaerobic digestion of organic solid wastes. an overview of research achievements and perspectives,” *Bioresource Technology*, vol. 74, no. 1, pp. 3 – 16, 2000.
- [32] L. F. Calvo, M. Otero, B. M. Jenkins, A. I. Garcia, and A. Moran, “Heating process characteristics and kinetics of sewage sludge in different atmospheres,” *Thermochimica Acta*, vol. 409, no. 2, pp. 127–135, 2004.
- [33] D. Fytili and A. Zabaniotou, “Utilization of sewage sludge in EU application of old and new methods—A review ,” *Renewable and Sustainable Energy Reviews*, vol. 12, no. 1, pp. 116–140, 2008.
- [34] S. Yaman, “Pyrolysis of biomass to produce fuels and chemical feedstocks,” *Energy Conversion and Management*, vol. 45, no. 5, pp. 651–671, 2004.
- [35] J. Menéndez, M. Inguanzo, and J. Pis, “Microwave-induced pyrolysis of sewage sludge,” *Water Research*, vol. 36, no. 13, pp. 3261 – 3264, 2002.
- [36] J. Werther and T. Ogada, “Sewage sludge combustion,” *Progress in Energy and Combustion Science*, vol. 25, no. 1, pp. 55 – 116, 1999.
- [37] S. Werle and R. K. Wilk, “A review of methods for the thermal utilization of sewage sludge: The Polish perspective,” *Renewable Energy*, vol. 35, no. 9, pp. 1914 – 1919, 2010.
- [38] M. Samolada and A. Zabaniotou, “Comparative assessment of municipal sewage sludge incineration, gasification and pyrolysis for a sustainable sludge-to-energy management in Greece,” *Waste Management*, vol. 34, no. 2, pp. 411–420, 2014.
- [39] A. Kerester, “Step on the gas,” *The Chemical Engineer*, vol. 867, pp. 33–36, 2013.
- [40] M. Lundin, M. Olofsson, G. Pettersson, and H. Zetterlund, “Environmental and economic assessment of sewage sludge handling options,” *Resources, Conservation and Recycling*, vol. 41, no. 4, pp. 255 – 278, 2004.
- [41] N. Shammass and L. Wang, “Biosolids composting,” in *Biological Treatment Processes* (L. Wang, N. Pereira, and Y.-T. Hung, eds.), vol. 8 of *Handbook of Environmental Engineering*, pp. 669–714, Humana Press, 2009.
- [42] Q. Lu, Z. L. He, and P. J. Stoffella, “Land application of biosolids in the usa: A review,” *Applied and Environmental Soil Science*, p. 11, 2012.
- [43] C. B. Maugans and C. Ellis, “Wet air oxidation: A Review of Commercial Sub-critical Hydrothermal Treatment,” *IT3*, vol. 2, pp. 13–17, 2002.
- [44] S. Baroutian, M. Robinson, A.-M. Smit, S. Wijeyekoon, and D. Gapes, “Transformation and removal of wood extractives from pulp mill sludge using wet oxidation and thermal hydrolysis,” *Bioresource Technology*, vol. 146, pp. 294–300, 2013.
- [45] L. Zou, Y. Li, and Y.-T. Hung, “Wet air oxidation for waste treatment,” in *Advanced Physicochemical Treatment Technologies* (L. Wang, Y.-T. Hung, and N. Shammass, eds.), vol. 5 of *Handbook of Environmental Engineering*, pp. 575–610, Humana Press, 2007.

- [46] M. Djafer, F. Luck, J. Rose, and D. Cretenot, "Transforming sludge into a recyclable and valuable carbon source by wet air oxidation," *Water Science and Technology*, vol. 41, no. 8, pp. 77–83, 2000.
- [47] A. Pintar, G. Bercic, M. Besson, and P. Gallezot, "Catalytic wet-air oxidation of industrial effluents: total mineralization of organics and lumped kinetic modelling," *Applied Catalysis B: Environmental*, vol. 47, no. 3, pp. 143–152, 2004.
- [48] Q. Zhang and K. T. Chuang, "Lumped kinetic model for catalytic wet oxidation of organic compounds in industrial wastewater," *AIChE Journal*, vol. 45, no. 1, pp. 145–150, 1999.
- [49] F. Luck, "A review of industrial catalytic wet air oxidation processes," *Catalysis Today*, vol. 27, no. 1-2, pp. 195–202, 1996.
- [50] S. K. Bhargava, J. Tardio, J. Prasad, K. Föger, D. B. Akolekar, and S. C. Grocott, "Wet oxidation and catalytic wet oxidation," *Industrial & Engineering Chemistry Research*, vol. 45, no. 4, pp. 1221–1258, 2006.
- [51] S. T. Kolaczowski, P. Plucinski, F. J. Beltran, F. J. Rivas, and D. B. McLurgh, "Wet air oxidation: A review of process technologies and aspects in reactor design," *Chemical Engineering Journal*, vol. 73, no. 2, pp. 143–160, 1999.
- [52] L. Oliviero, J. B. Jr., and D. Duprez, "Wet air oxidation of nitrogen-containing organic compounds and ammonia in aqueous media," *Applied Catalysis B: Environmental*, vol. 40, no. 3, pp. 163–184, 2003.
- [53] H. Debellefontaine, M. Chakchouk, J. N. Foussard, D. Tissot, and P. Striolo, "Treatment of organic aqueous wastes: Wet air oxidation and wet peroxide oxidation," *Environmental Pollution*, vol. 92, no. 2, pp. 155–164, 1996.
- [54] H. Debellefontaine and J. N. Foussard, "Wet air oxidation for the treatment of industrial wastes. chemical aspects, reactor design and industrial applications in europe," *Waste Management*, vol. 20, no. 1, pp. 15–25, 2000.
- [55] J. J. A. P. Van Amstel, *The Oxidation of Sewage Sludge in the Liquid Water Phase at Elevated Temperatures and Pressures*. PhD thesis, Technische Hogeschool te Eindhoven, Eindhoven, Netherlands, 1971.
- [56] S. Baroutian and D. J. Gapes, "Non-catalytic subcritical wet oxidation of a wastewater treatment sludge," in *Australian and New Zealand Annual Chemical Engineering Conference, Chemeca*, (Brisbane, Australia), Engineers Australia, 29 Sept–2 October 2013.
- [57] L. Li, P. Chen, and E. F. Gloyna, "Generalized kinetic model for wet oxidation of organic compounds," *AIChE Journal*, vol. 37, no. 11, pp. 1687–1697, 1991.
- [58] J. Foussard, H. Debellefontaine, and J. Besombes-Vailhé, "Efficient elimination of organic liquid wastes: Wet air oxidation," *Journal of Environmental Engineering*, vol. 115, no. 2, pp. 367–385, 1989.

- [59] J. Chung, M. Lee, J. Ahn, W. Bae, Y.-W. Lee, and H. Shim, "Effects of operational conditions on sludge degradation and organic acids formation in low-critical wet air oxidation," *Journal of Hazardous Materials*, vol. 162, no. 1, pp. 10–16, 2009.
- [60] S. Baroutian, A.-M. Smit, and D. J. Gapes, "Relative influence of process variables during non-catalytic wet oxidation of municipal sludge," *Bioresource Technology*, pp. 605–610, 2013.
- [61] G. Teletzke, W. Gitchel, D. Diddams, and C. Hoffman, "Components of sludge and its wet air oxidation products," *Water Pollution Control Federation*, pp. 994–1005, 1967.
- [62] S. Verenich, A. Laari, and J. Kallas, "Parameter Estimation and Sensitivity Analysis of Lumped Kinetic Models for Wet Oxidation of Concentrated Wastewaters," *Industrial & Engineering Chemistry Research*, vol. 42, no. 21, pp. 5091–5098, 2003.
- [63] D. Weichgrebe and A. Vogelpohl, "A comparative study of wastewater treatment by chemical wet oxidation," *Chemical Engineering and Processing: Process Intensification*, vol. 33, no. 4, pp. 199 – 203, 1994.
- [64] J. Behin and T. Shojaeimehr, "Modeling of multistage bubble column reactors for oxidation reaction," *Chemical Engineering & Technology*, vol. 36, no. 5, pp. 819–828, 2013.
- [65] T. Moreno, G. Kouzaki, M. Sasaki, M. Goto, and M. J. Cocero, "Uncatalysed wet oxidation of D-glucose with hydrogen peroxide and its combination with hydrothermal electrolysis," *Carbohydrate Research*, vol. 349, no. 0, pp. 33–38, 2012.
- [66] E. Neyens and J. Baeyens, "A review of thermal sludge pre-treatment processes to improve dewaterability," *Journal of Hazardous Materials*, vol. 98, no. 1–3, pp. 51 – 67, 2003.
- [67] R. V. Shende and J. Levec, "Wet oxidation kinetics of refractory low molecular mass carboxylic acids," *Industrial & Engineering Chemistry Research*, vol. 38, no. 10, pp. 3830–3837, 1999.
- [68] J. J. A. P. Van Amstel and K. Rietema, "Wet-air oxidation of sewage sludge. Part II: The oxidation of real sludges," *Chemie Ingenieur Technik*, vol. 45, no. 20, pp. 1205–1211, 1973.
- [69] Y. Khan, G. K. Anderson, and D. J. Elliott, "Wet oxidation of activated sludge," *Water Research*, vol. 33, no. 7, pp. 1681–1687, 1999.
- [70] T. Lendormi, C. Prevot, F. Doppenberg, J. Foussard, and H. Debellefontaine, "Subcritical wet oxidation of municipal sewage sludge: comparison of batch and continuous experiments," *Water Science & Technology*, vol. 44, no. 5, pp. 161–169, 2001.
- [71] H. Debellefontaine and J. Foussard, "The wet air oxidation process for the treatment of industrial waste and domestic sludge," in *Franco-Thai Symposium "New Advances in Water and Wastewater Treatments"*, (Bangkok, Thailand), 22-24 October 1997.

- [72] S. H. Lin, S. J. Ho, and C. L. Wu, "Kinetic and performance characteristics of wet air oxidation of high-concentration wastewater," *Industrial & Engineering Chemistry Research*, vol. 35, no. 1, pp. 307–314, 1996.
- [73] M. Kindsigo, M. Hautaniemi, and J. Kallas, "Kinetic modelling of wet oxidation treated debarking water," *Proceedings of the Estonian Academy of Sciences*, vol. 59, no. 3, pp. 233–242, 2010.
- [74] F. Stüber, J. Font, A. Fortuny, C. Bengoa, A. Eftaxias, and A. Fabregat, "Carbon materials and catalytic wet air oxidation of organic pollutants in wastewater," *Topics in Catalysis*, vol. 33, no. 1-4, pp. 3–50, 2005.
- [75] A. Garg, V. Narayana, P. Chaudhary, and S. Chand, "Treatment of pulp and paper mill effluent," *Journal of Scientific and Industrial Research*, vol. 63, no. 8, pp. 667–671, 2004.
- [76] Q. Zhang and K. T. Chuang, "Alumina-supported noble metal catalysts for destructive oxidation of organic pollutants in effluent from a softwood kraft pulp mill," *Industrial & Engineering Chemistry Research*, vol. 37, no. 8, pp. 3343–3349, 1998.
- [77] G. Scott and A. Smith, "Sludge characteristics and disposal alternatives for recycled fiber plants," in *1995 Recycling Symposium, Technical Association of the Pulp and Paper Industry (TAPPI), Atlanta, GA*, pp. 239–249, 1995.
- [78] X. Yan, F. Jin, H. Enomoto, T. Moriya, H. Kishida, and H. Higashijima, "A new hydrothermal process for improving acetic acid yield from cellulosic biomass," in *Proceedings of 14th International Conference on the Properties of Water and Steam*, (Kyoto, Japan), pp. 724–728, 2004.
- [79] R. V. Shende and V. V. Mahajani, "Kinetics of wet oxidation of formic acid and acetic acid," *Industrial & Engineering Chemistry Research*, vol. 36, no. 11, pp. 4809–4814, 1997.
- [80] M. E. Suárez-Ojeda, I. S. Metcalfe, J. Font, and J. Carrera, "Calibration of a kinetic model for wet air oxidation (WAO) of substituted phenols: Influence of experimental data on model prediction and practical identifiability," *Chemical Engineering Journal*, vol. 150, no. 2–3, pp. 328–336, 2009.
- [81] H. Joglekar, S. Samant, and J. Joshi, "Kinetics of wet air oxidation of phenol and substituted phenols," *Water Research*, vol. 25, no. 2, pp. 135–145, 1991.
- [82] K. Koido, *Dynamics of Hydrothermal Oxidation*. PhD thesis, Nagoya University, 2011.
- [83] T. Takamatsu, I. Hashimoto, and S. Sioya, "Model identification of wet-air oxidation process thermal decomposition," *Water Research*, vol. 4, no. 1, pp. 33–59, 1970.
- [84] A. Chacuk and M. Imbierowicz, "Mathematical modelling of wet oxidation of excess sludge," *Polish Journal of Chemical Technology*, vol. 9, no. 2, pp. 1–4, 2007.

- [85] A. Chacuk and M. Imbierowicz, *Mathematical modeling of wet oxidation of excess sludge in counter-current bubble columns*, pp. 273–277. CRC Press, 2010.
- [86] A. Eftaxias, J. Font, A. Fortuny, J. Giralt, A. Fabregat, and F. Stüber, “Kinetic modelling of catalytic wet air oxidation of phenol by simulated annealing,” *Applied Catalysis B: Environmental*, vol. 33, no. 2, pp. 175–190, 2001.
- [87] S. Jomaa, A. Shanableh, W. Khalil, and B. Trebilco, “Hydrothermal decomposition and oxidation of the organic component of municipal and industrial waste products,” *Advances in Environmental Research*, vol. 7, no. 3, pp. 647 – 653, 2003.
- [88] A. Shanableh, “Generalized first-order kinetic model for biosolids decomposition and oxidation during hydrothermal treatment,” *Environmental Science & Technology*, vol. 39, no. 1, pp. 355–362, 2004.
- [89] S. Verenich and J. Kallas, “Wet oxidation lumped kinetic model for wastewater organic burden biodegradability prediction,” *Environmental Science & Technology*, vol. 36, no. 15, pp. 3335–3339, 2002.
- [90] D. Tromans, “Oxygen solubility modeling in inorganic solutions: Concentration, temperature and pressure effects,” *Hydrometallurgy*, vol. 50, no. 3, pp. 279–296, 1998.
- [91] N. Kantarci, F. Borak, and K. O. Ulgen, “Bubble column reactors,” *Process Biochemistry*, vol. 40, no. 7, pp. 2263–2283, 2005.
- [92] M. K. Singh and S. K. Majumder, “Theoretical study on effect of operating parameters on mass transfer in bubbly flow,” *Journal of Engineering and Applied Sciences*, vol. 5, no. 2, pp. 163–170, 2010.
- [93] M. D. Gurol and S. Nekouinaini, “Effect of organic substances on mass transfer in bubble aeration,” *Water Pollution Control Federation*, vol. 57, no. 3, pp. 235–240, 1985.
- [94] H. Debellefontaine, S. Crispel, P. Reilhac, F. Périé, and J.-N. Foussard, “Wet air oxidation (WAO) for the treatment of industrial wastewater and domestic sludge. Design of bubble column reactors,” *Chemical Engineering Science*, vol. 54, no. 21, pp. 4953–4959, 1999.
- [95] H. Debellefontaine, F. Cammas, G. Deiber, J. Foussard, and P. Reilhac, “Wet air oxidation: Kinetics of reaction, carbon dioxide equilibrium and reactor design - An overview,” *Water Science and Technology*, vol. 35, no. 4, pp. 111 – 118, 1997.
- [96] H. Benbelkacem and H. Debellefontaine, “Modeling of a gas-liquid reactor in batch conditions. study of the intermediate regime when part of the reaction occurs within the film and part within the bulk,” *Chemical Engineering and Processing: Process Intensification*, vol. 42, no. 10, pp. 723–732, 2003.
- [97] M. Bouaifi, G. Hebrard, D. Bastoul, and M. Roustan, “A comparative study of gas hold-up, bubble size, interfacial area and mass transfer coefficients in stirred gas-liquid reactors and bubble columns,” *Chemical Engineering and Processing: Process Intensification*, vol. 40, no. 2, pp. 97–111, 2001.



- [98] H. Jin, D. Liu, S. Yang, G. He, Z. Guo, and Z. Tong, "Experimental study of oxygen mass transfer coefficient in bubble column with high temperature and high pressure," *Chemical Engineering & Technology*, vol. 27, no. 12, pp. 1267–1272, 2004.
- [99] Y. T. Shah, G. J. Stiegel, and M. M. Sharma, "Backmixing in gas-liquid reactors," *AIChE Journal*, vol. 24, no. 3, pp. 369–400, 1978.
- [100] R. Lau, W. Peng, L. Velazquez-Vargas, G. Yang, and L.-S. Fan, "Gas-liquid mass transfer in high-pressure bubble columns," *Industrial & Engineering Chemistry Research*, vol. 43, no. 5, pp. 1302–1311, 2004.
- [101] V. Meille, N. Pestre, P. Fongarland, and C. de Bellefon, "Gas/liquid mass transfer in small laboratory batch reactors: Comparison of methods," *Industrial & Engineering Chemistry Research*, vol. 43, no. 4, pp. 924–927, 2004.
- [102] P. J. Strong and D. J. Gapes, "Thermal and thermo-chemical pre-treatment of four waste residues and the effect on acetic acid production and methane synthesis," *Waste Management*, vol. 32, no. 9, pp. 1669–1677, 2012.
- [103] D. Tromans, "Temperature and pressure dependent solubility of oxygen in water: A thermodynamic analysis," *Hydrometallurgy*, vol. 48, no. 3, pp. 327–342, 1998.
- [104] Virtual Materials Group Inc., "VMGSim, Version 7.0," tech. rep., 2013. <http://www.virtualmaterials.com/>.
- [105] Anon, "Aspen Plus, Version 7.3.2," tech. rep., Aspen Technology, Massachusetts, USA, 2012. <http://www.aspentech.com/products/aspen-plus.aspx>.
- [106] D. Goodwin, N. Malaya, H. Moffat, and R. Speth, "Cantera: An object-oriented software toolkit for chemical kinetics, thermodynamics, and transport processes, Version 2.1," 2012. <https://code.google.com/p/cantera/>.
- [107] The MathWorks Inc., "Simbiology, Version 4.1," tech. rep., 2012. <http://www.mathworks.com.au/products/simbiology/>.
- [108] Python Software Foundan, "Python Language Reference, version 2.7," tech. rep., 2012. <http://www.python.org/>.
- [109] E. Jones, T. Oliphant, P. Peterson, *et al.*, "SciPy: Open source scientific tools for Python," tech. rep., 2001–2014. <http://www.scipy.org/>.
- [110] T. E. Oliphant, "Python for scientific computing," *Computing in Science & Engineering*, vol. 9, no. 3, pp. 10–20, 2007.
- [111] J. D. Hunter, "Matplotlib: A 2D Graphics Environment," *Computing in Science & Engineering*, vol. 9, no. 3, pp. 90–95, 2007.
- [112] J. Ingham, I. J. Dunn, E. Heinzle, J. E. Prenosil, and J. B. Snape, *Chemical Engineering Dynamics: An Introduction to Modelling and Computer Simulation*, vol. 3. John Wiley & Sons, 2008.
- [113] W. L. Luyben, *Chemical Reactor Design and Control*. John Wiley & Sons, 2007.

- [114] M. A. Henson and D. E. Seborg, *Nonlinear Process Control*. Upper Saddle River, NJ, USA: Prentice-Hall, Inc., 1997.
- [115] The MathWorks Inc, “MATLAB, Version R2012b,” tech. rep., 2012. <http://www.mathworks.com/products/matlab>.
- [116] Industrial Information and Control Centre, AUT University, “Opti Toolbox.” <http://i2c2.aut.ac.nz/Wiki/OPTI/>, 2013.
- [117] N. Yau, *Visualize This: The FlowingData Guide to Design, Visualization, and Statistics*. Wiley, 1 ed., July 2011.
- [118] N. Yau, *Data Points: Visualization That Means Something*. Wiley, 1 ed., Mar. 2013.
- [119] W. Rossle and W. Pretorius, “A review of characterisation requirements for in-line prefermenters: Paper 1: Wastewater characterisation,” *Water SA*, vol. 27, no. 3, pp. 405–412, 2001.
- [120] G. Deiber, J. Foussard, and H. Debellefontaine, “Removal of nitrogenous compounds by catalytic wet air oxidation. Kinetic study,” *Environmental Pollution*, vol. 96, no. 3, pp. 311 – 319, 1997.
- [121] J. Currie and D. I. Wilson, “Opti: Lowering the Barrier Between Open Source Optimizers and the Industrial MATLAB User,” in *Foundations of Computer-Aided Process Operations* (N. Sahinidis and J. Pinto, eds.), (Savannah, Georgia, USA), 8–11 January 2012.
- [122] D. I. Wilson, M. Agarwal, and D. W. T. Rippin, “Experiences implementing the extended Kalman filter on an industrial batch reactor,” *Computers and Chemical Engineering*, vol. 22, no. 11, pp. 1653–1672, 1998.
- [123] J. Dwyer, D. Starrenburg, S. Tait, K. Barr, D. J. Batstone, and P. Lant, “Decreasing activated sludge thermal hydrolysis temperature reduces product colour, without decreasing degradability,” *Water Research*, vol. 42, no. 18, pp. 4699 – 4709, 2008.
- [124] A. Mudhoo, *Biogas Production: Pretreatment Methods in Anaerobic Digestion*. John Wiley & Sons, 2012.
- [125] S. A. Bhat, D. N. Saraf, S. Gupta, and S. K. Gupta, “Use of agitator power as a soft sensor for bulk free-radical polymerization of methyl methacrylate in batch reactors,” *Industrial & Engineering Chemistry Research*, vol. 45, no. 12, pp. 4243–4255, 2006.
- [126] I. H. Bell, J. Wronski, S. Quoilin, and V. Lemort, “Pure and Pseudo-pure Fluid Thermophysical Property Evaluation and the Open-Source Thermophysical Property Library CoolProp,” *Industrial & Engineering Chemistry Research*, vol. 53, no. 6, pp. 2498–2508, 2014.
- [127] Z. Wei-rong, S. Hui-xiang, and W. Da-hui, “Modeling of mass transfer characteristics of bubble column reactor with surfactant present,” *Journal of Zhejiang University Science*, vol. 5, no. 6, pp. 714–720, 2004.

- [128] A. Fadavi and Y. Chisti, “Gas–liquid mass transfer in a novel forced circulation loop reactor,” *Chemical Engineering Journal*, vol. 112, no. 1, pp. 73–80, 2005.
- [129] A. Beenackers and W. Van Swaaij, “Mass transfer in gas-liquid slurry reactors,” *Chemical Engineering Science*, vol. 48, no. 18, pp. 3109–3139, 1993.
- [130] D. M. Himmelblau, *Process analysis by statistical methods*. Wiley New York, 1970.
- [131] R Core Team, *R: A Language and Environment for Statistical Computing*. R Foundation for Statistical Computing, Vienna, Austria, 2013. ISBN 3-900051-07-0.
- [132] Anon, *Statistics Toolbox for use with Matlab*. The MathWorks, Natick, MA, USA, 2003.
- [133] The MathWorks, Natick, MA, USA, *Curve fitting toolbox user’s guide for R2014a*, 2014.
- [134] D. I. Wilson, *Advanced Control Using Matlab or Stabilising the Unstabilisable*. Auckland University of Technology, 3rd ed., 2013. 538pp.
- [135] Intel, “Math Kernel Library v11.1 R0.” <http://software.intel.com/en-us/intel-mkl>, 2013.
- [136] W.-D. Deckwer and A. Schumpe, “Improved tools for bubble column reactor design and scale-up,” *Chemical Engineering Science*, vol. 48, no. 5, pp. 889–911, 1993.
- [137] M. Peters and K. Timmerhaus, *Plant design and Economics for Chemical Engineers*. McGraw-Hill, 4th ed., 1991.

# Appendix A

## Appendix CD Contents

Table A.1 below lists the software included on the attached CD. This is provided to enable further analysis of the examples presented in this thesis and allow the reader to reproduce the simulation results.

Table A.1: Software included on the Appendix CD.

Folder	Description
Experimental Data	Raw experimental data from the three sets of experiments performed for the experimental programme
Kinetic Model Src	Matlab source code for the extended kinetic model
Kinetic Model Data	The full set of results produced by the Matlab extended kinetic model
Python Environment	The source code for the Python kinetic modelling environment described in Chapter 4

# Appendix B

## Experimental Results

This section presents the experimental data obtained for all experiments performed as part of the Set 1 experimental programme.

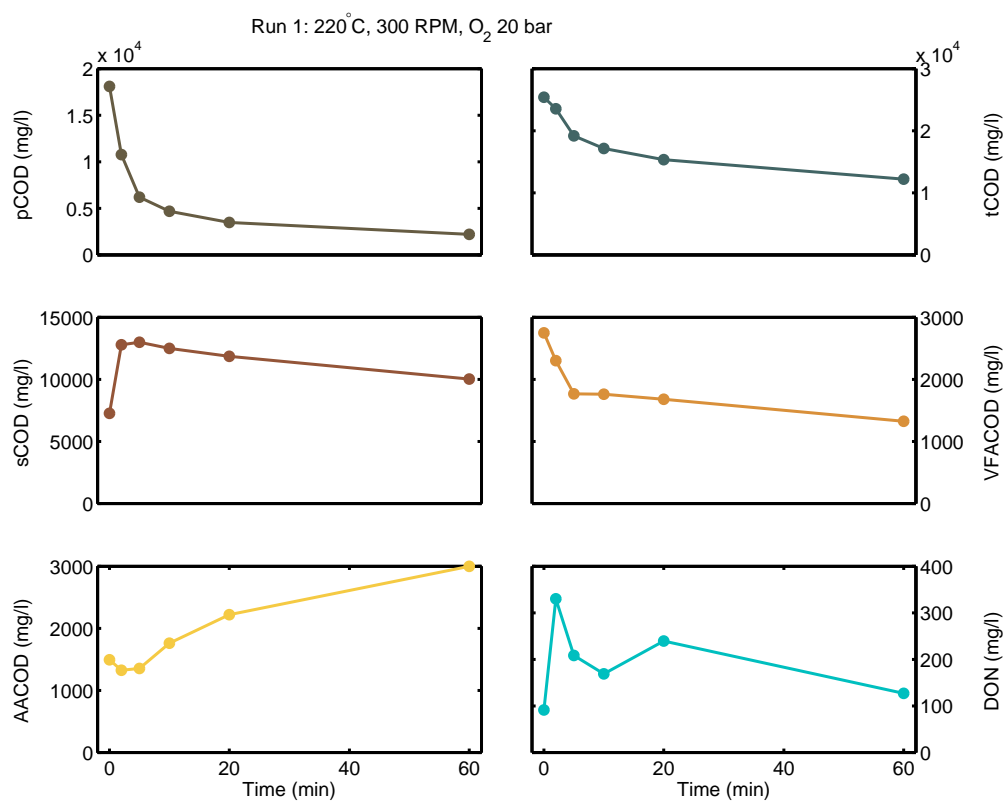


Figure B.1: Experimental results for the compounds of interest from the Set 1 experiments for Run 1.

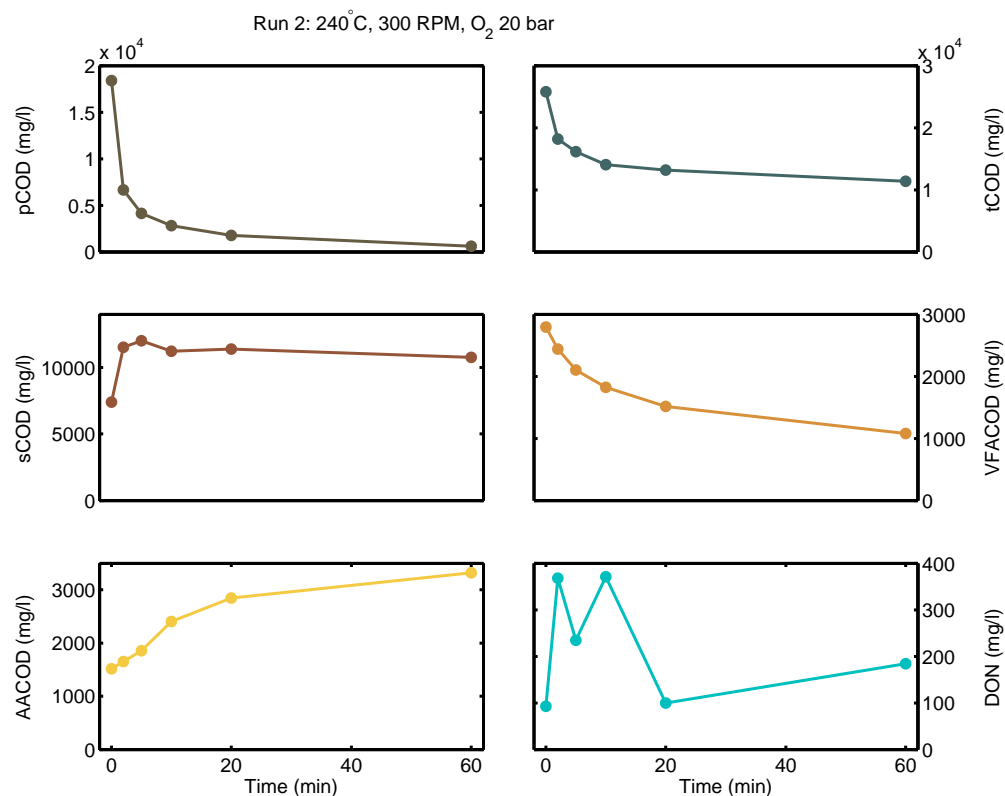


Figure B.2: Experimental results for the compounds of interest from the Set 1 experiments for Run 2.

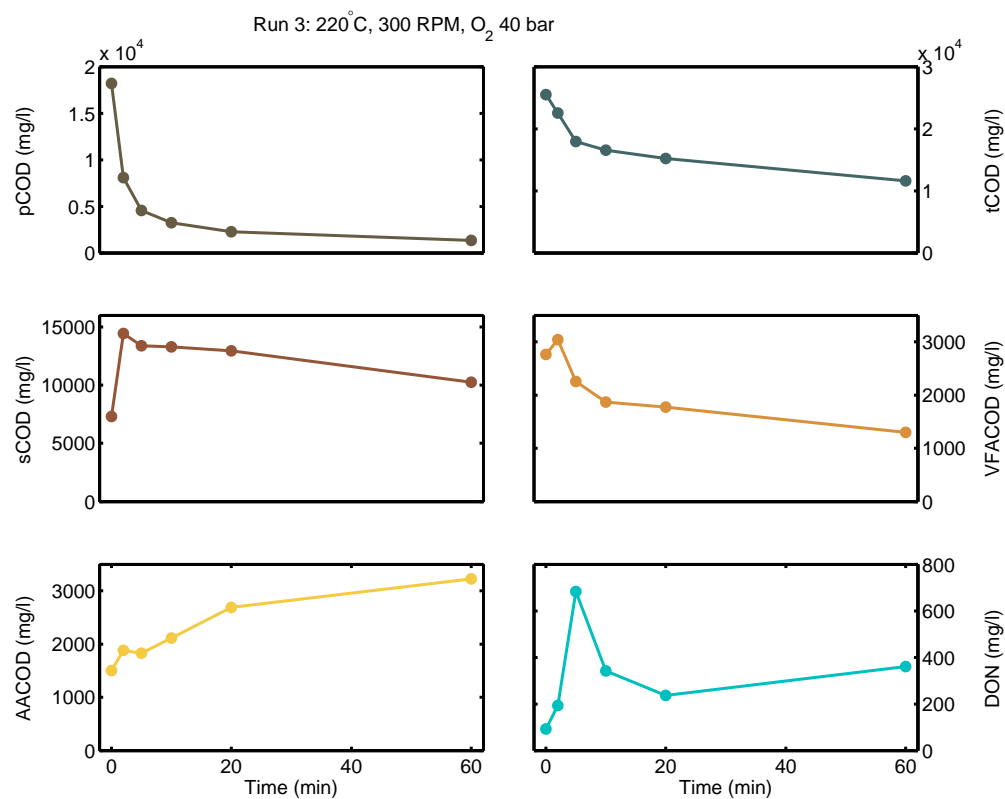


Figure B.3: Experimental results for the compounds of interest from the Set 1 experiments for Run 3.

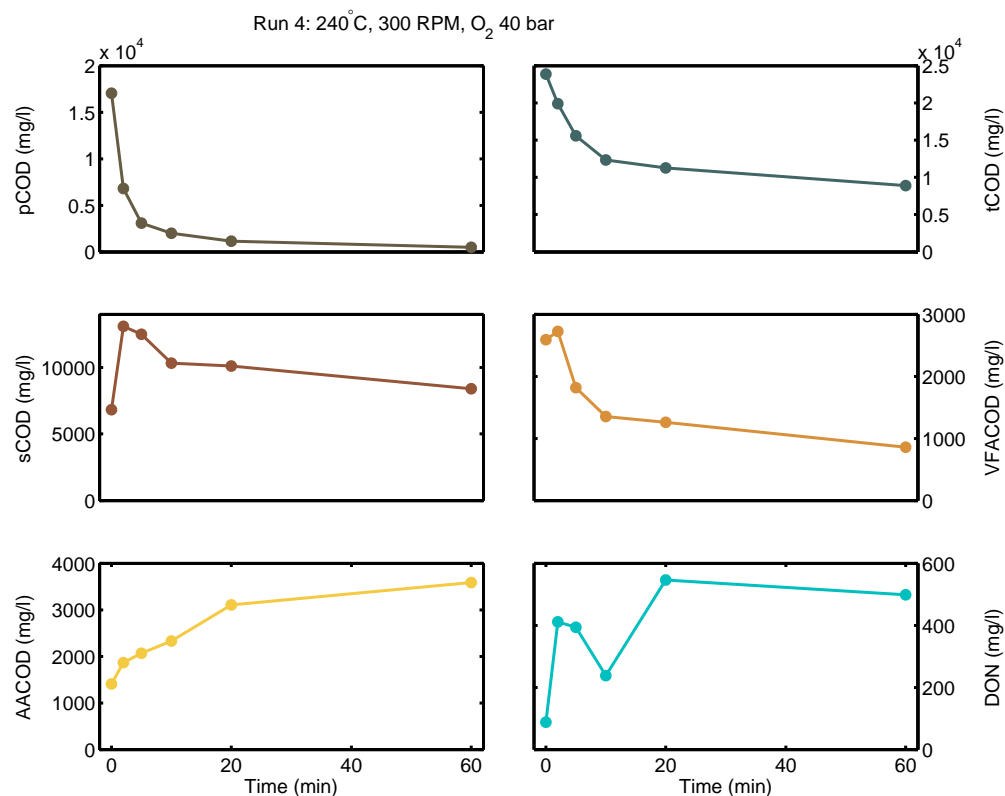


Figure B.4: Experimental results for the compounds of interest from the Set 1 experiments for Run 4.

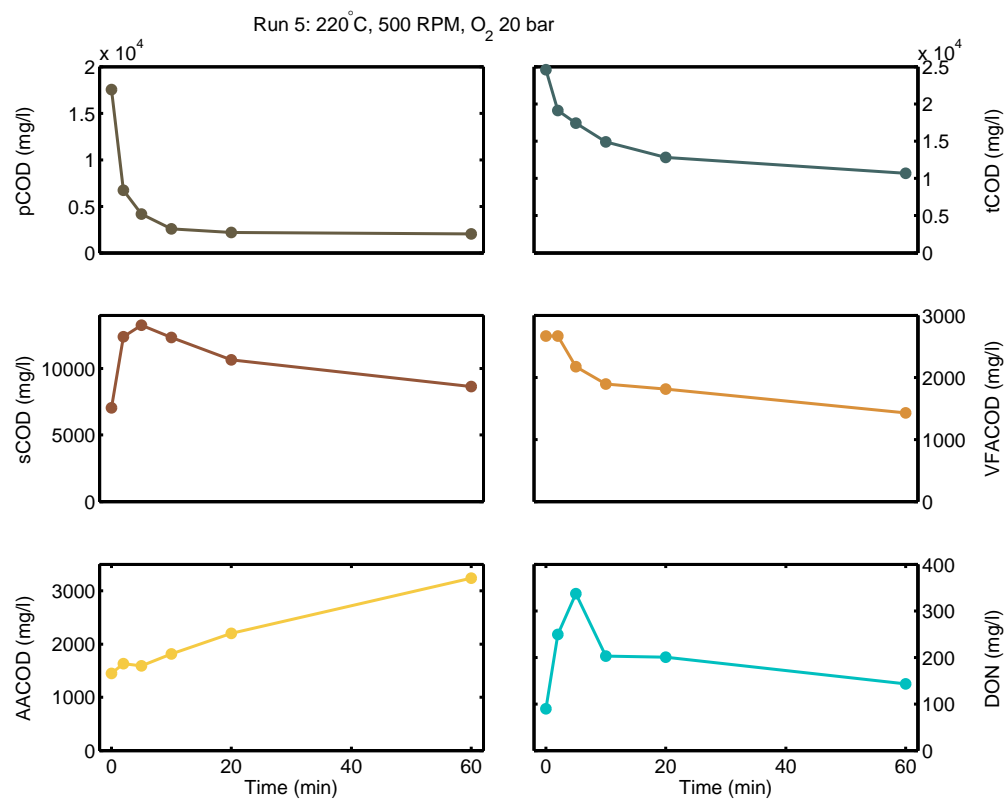


Figure B.5: Experimental results for the compounds of interest from the Set 1 experiments for Run 5.

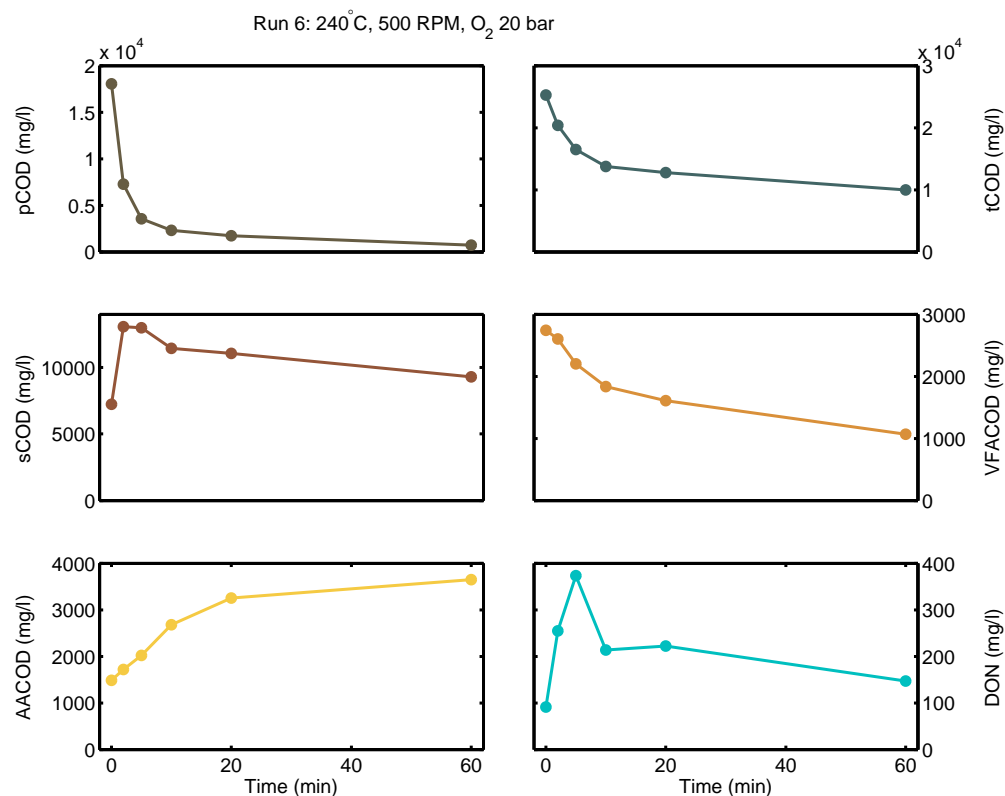


Figure B.6: Experimental results for the compounds of interest from the Set 1 experiments for Run 6.

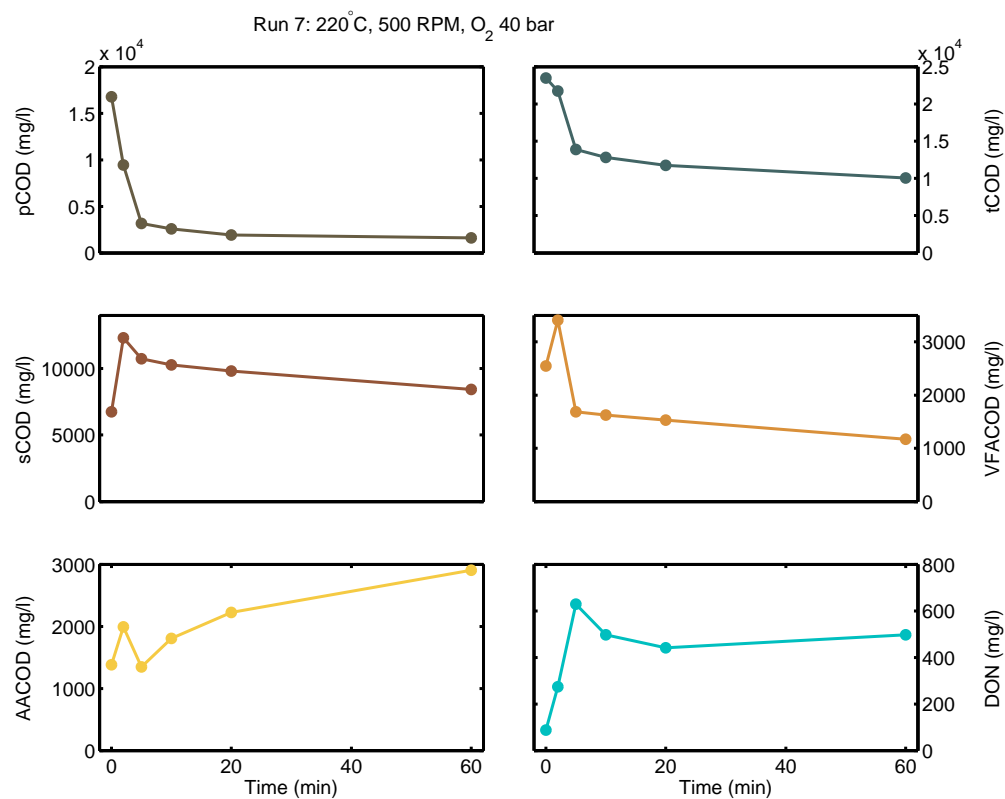


Figure B.7: Experimental results for the compounds of interest from the Set 1 experiments for Run 7.



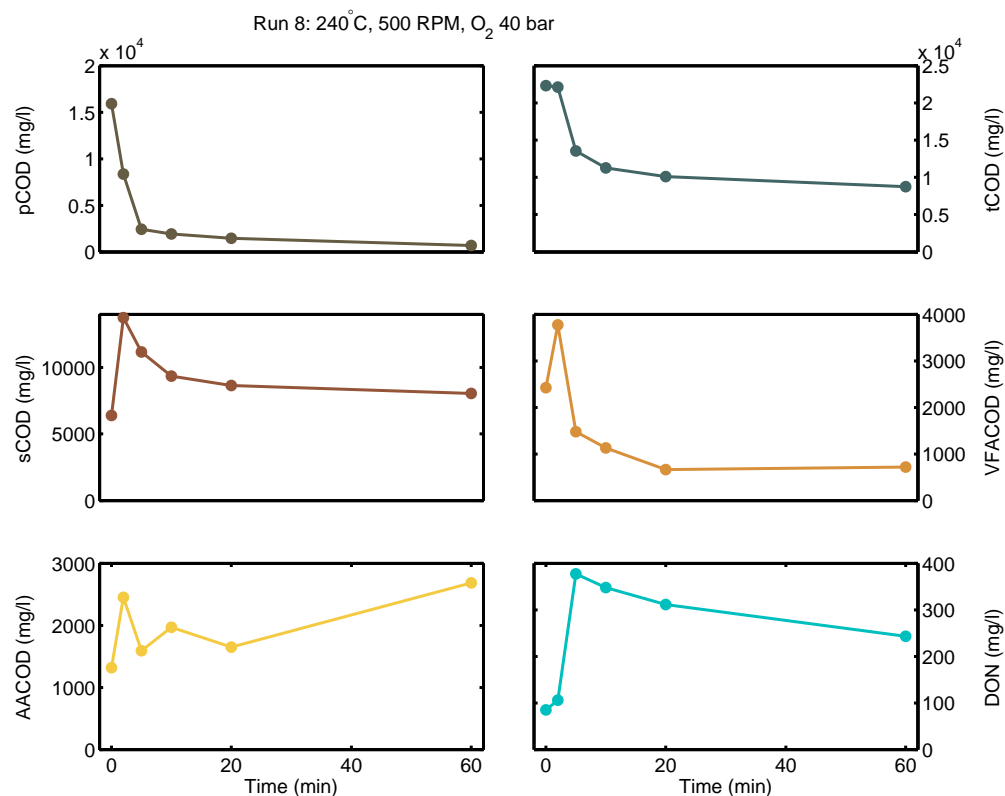


Figure B.8: Experimental results for the compounds of interest from the Set 1 experiments for Run 8.

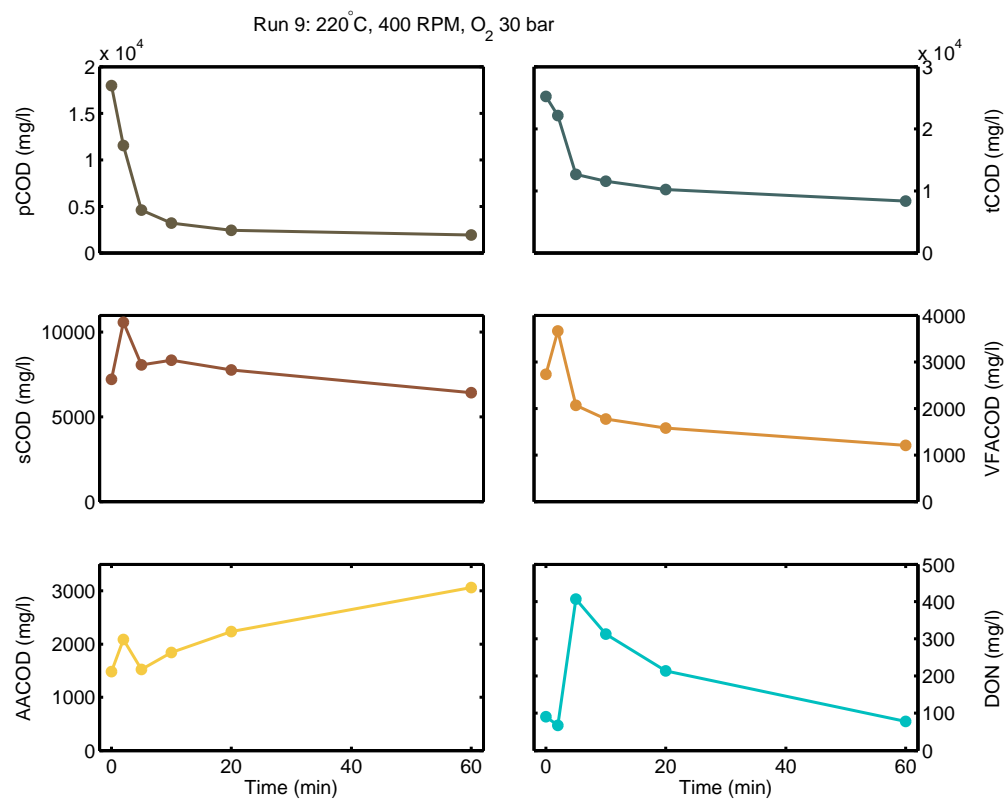


Figure B.9: Experimental results for the compounds of interest from the Set 1 experiments for Run 9.

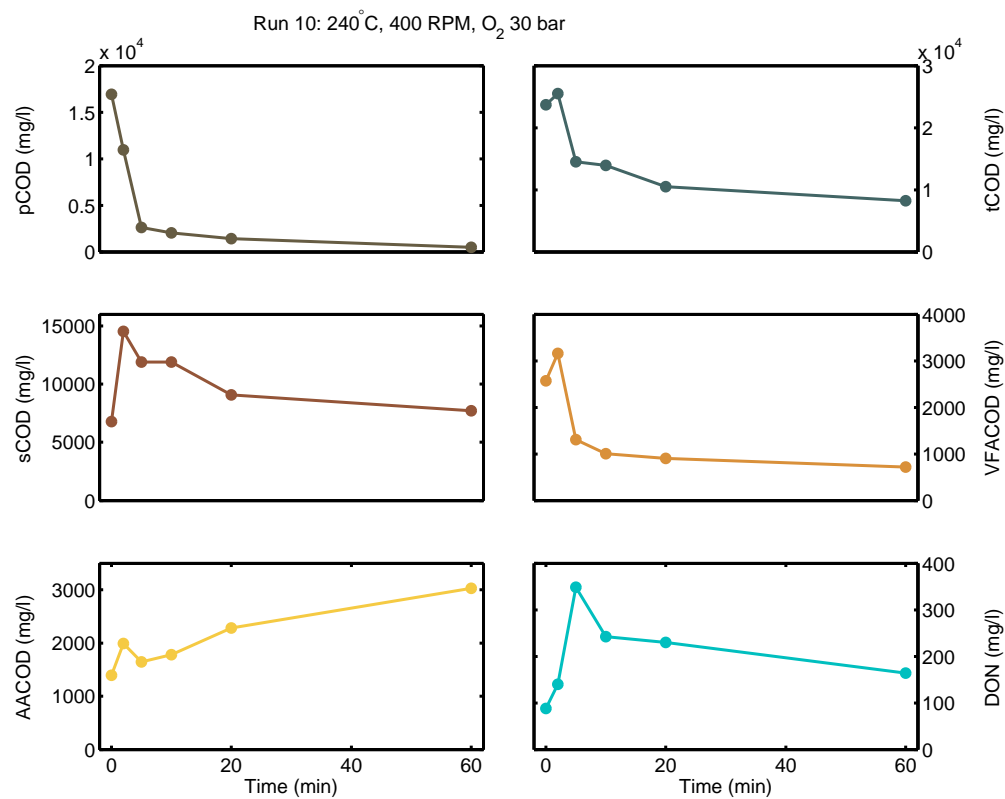


Figure B.10: Experimental results for the compounds of interest from the Set 1 experiments for Run 10.

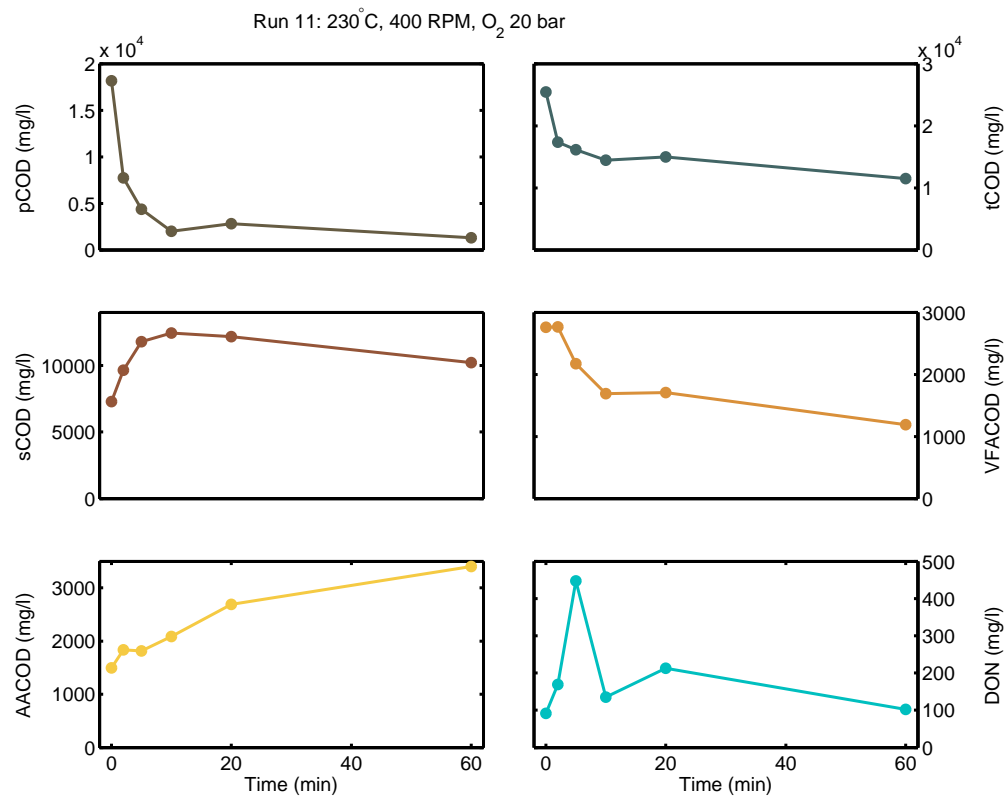


Figure B.11: Experimental results for the compounds of interest from the Set 1 experiments for Run 11.

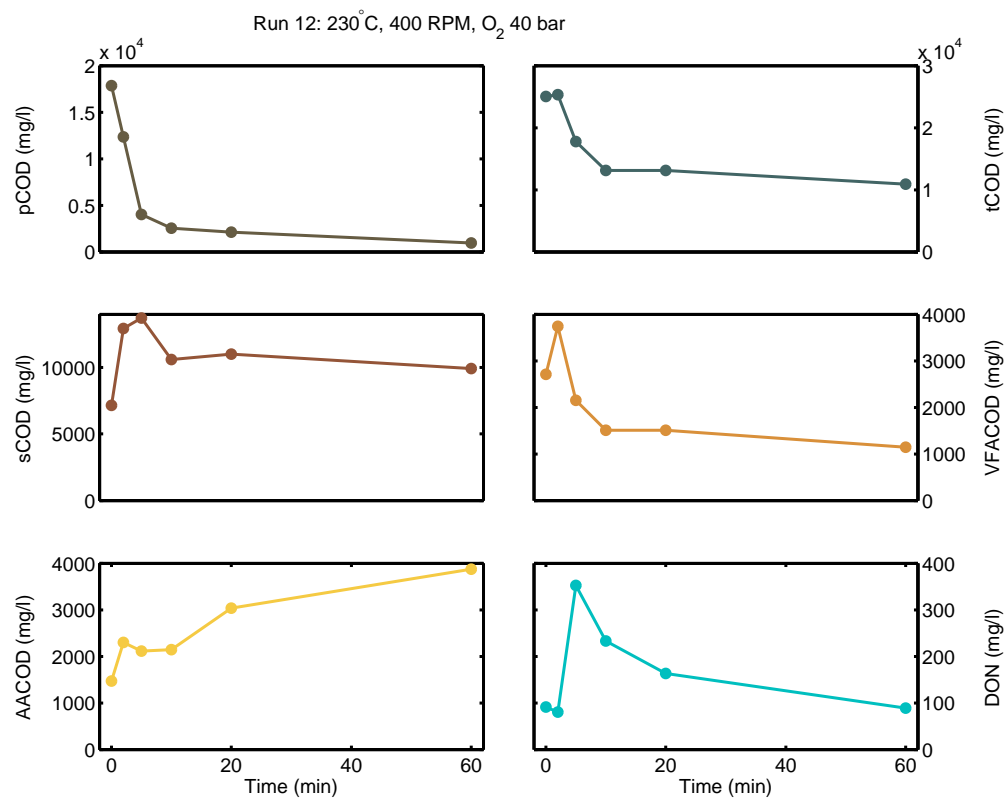


Figure B.12: Experimental results for the compounds of interest from the Set 1 experiments for Run 12.

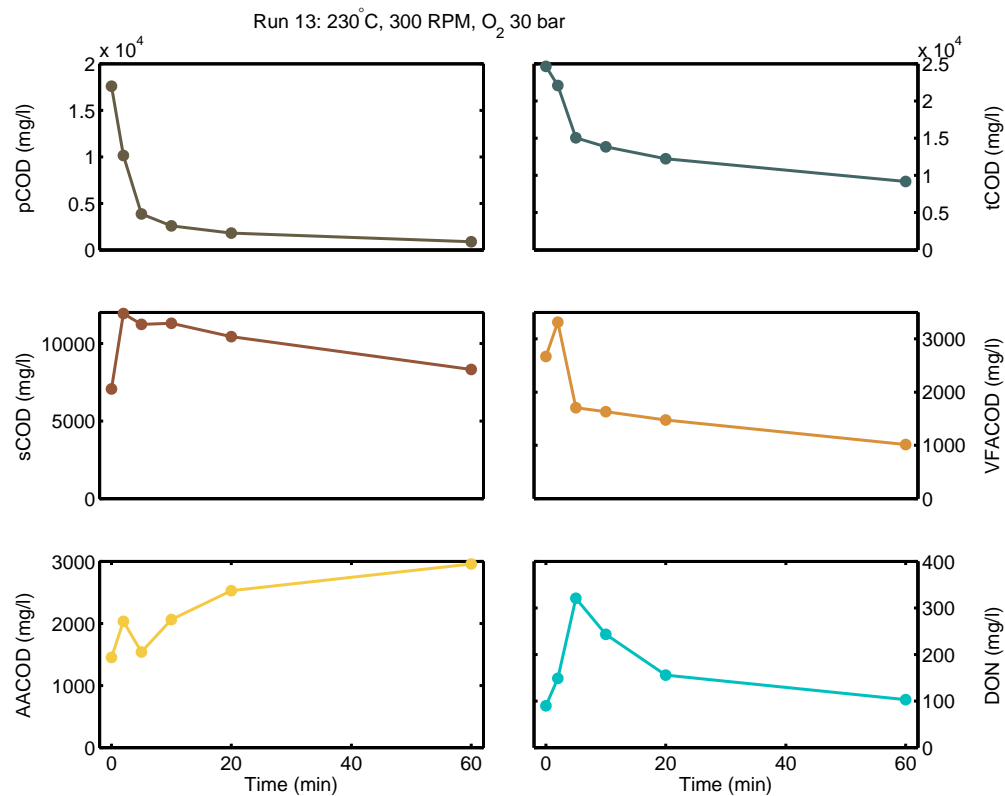


Figure B.13: Experimental results for the compounds of interest from the Set 1 experiments for Run 13.

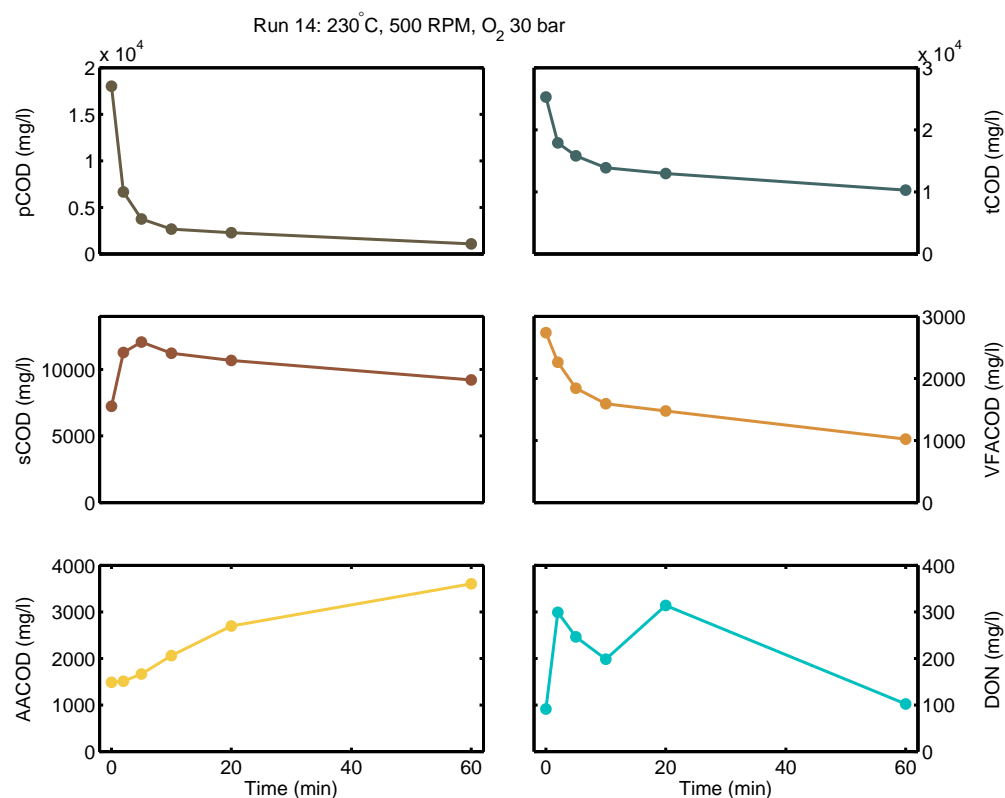


Figure B.14: Experimental results for the compounds of interest from the Set 1 experiments for Run 14.

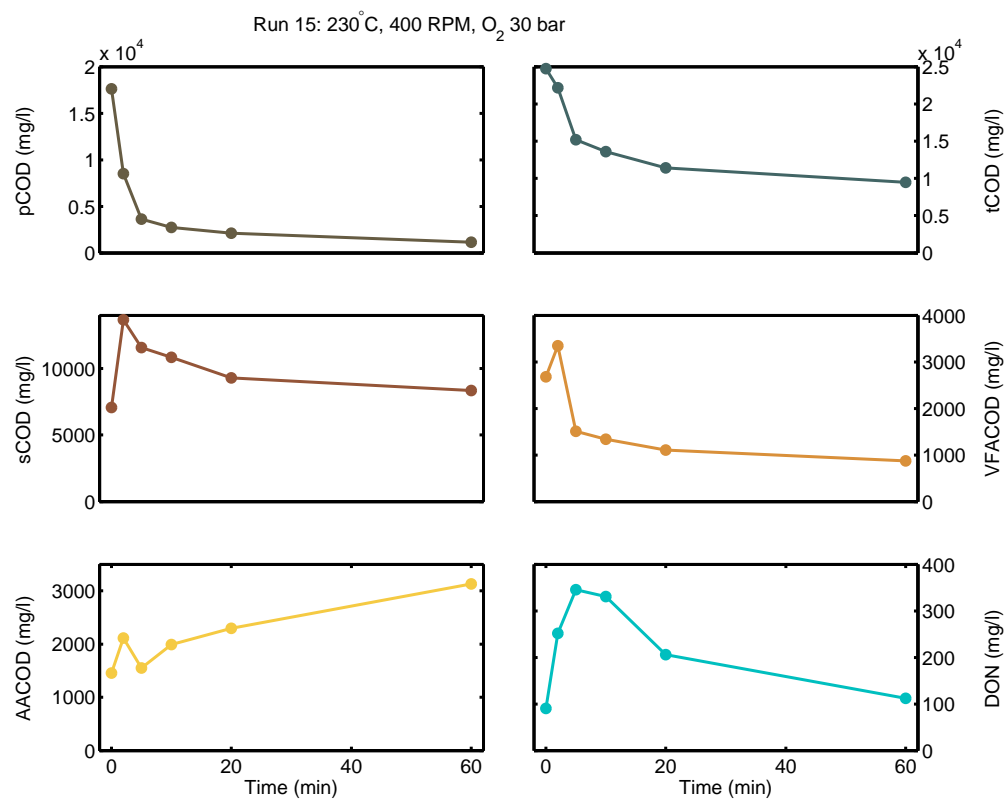


Figure B.15: Experimental results for the compounds of interest from the Set 1 experiments for Run 15.

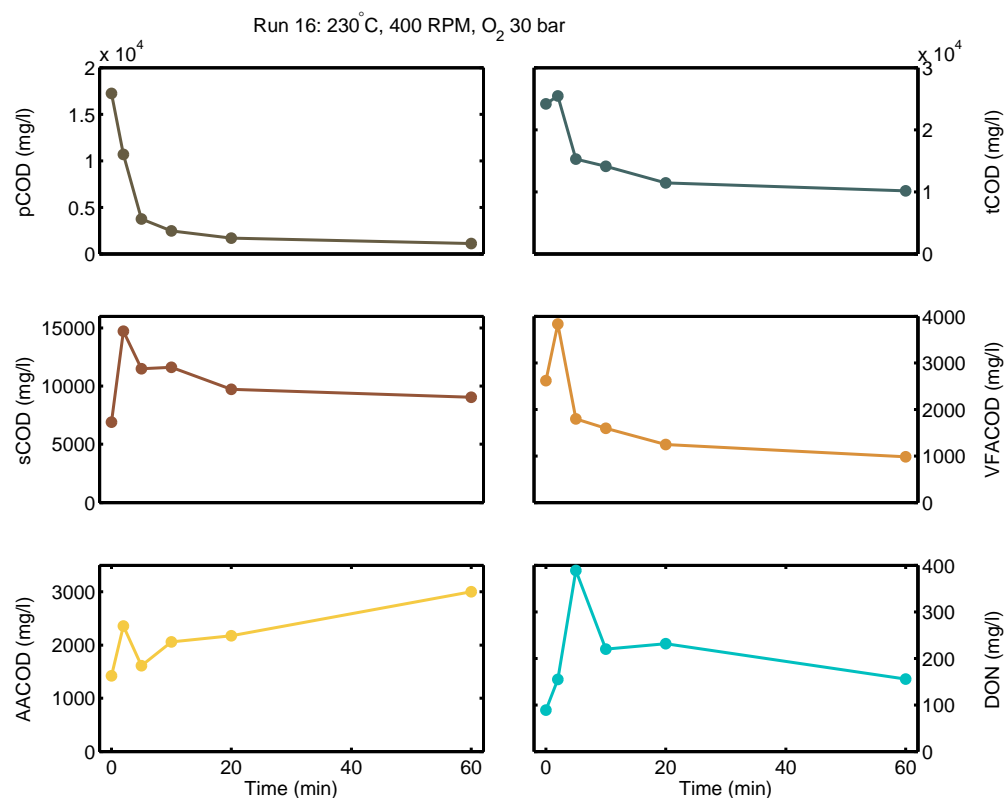


Figure B.16: Experimental results for the compounds of interest from the Set 1 experiments for Run 16.

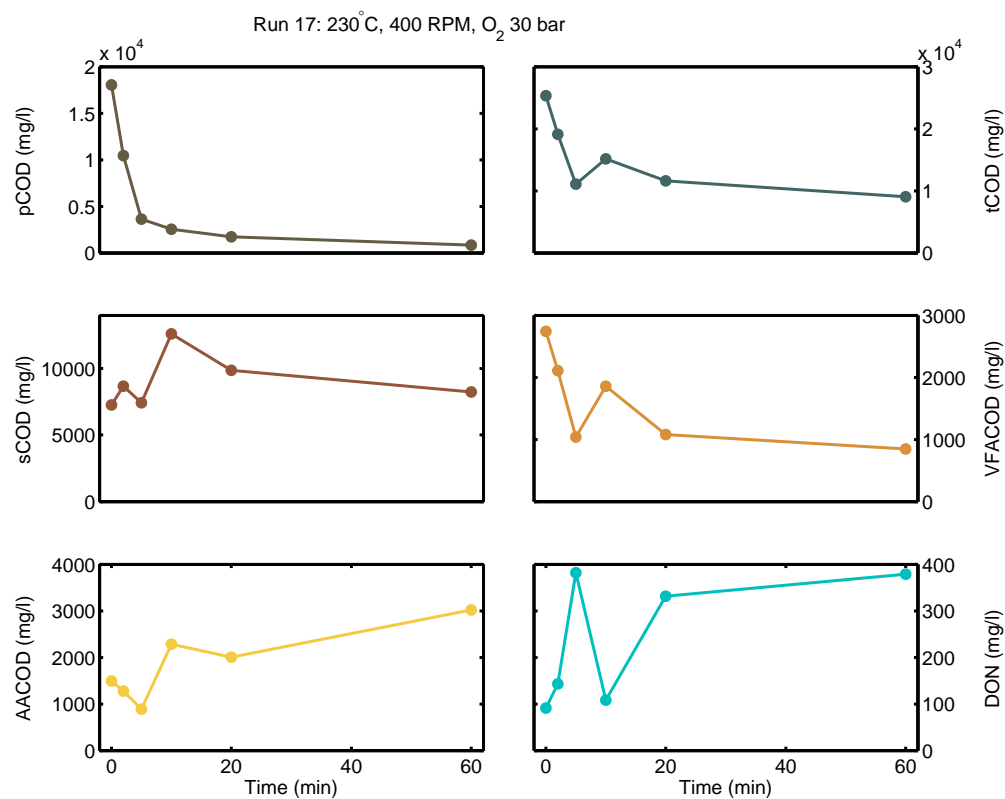


Figure B.17: Experimental results for the compounds of interest from the Set 1 experiments for Run 17.

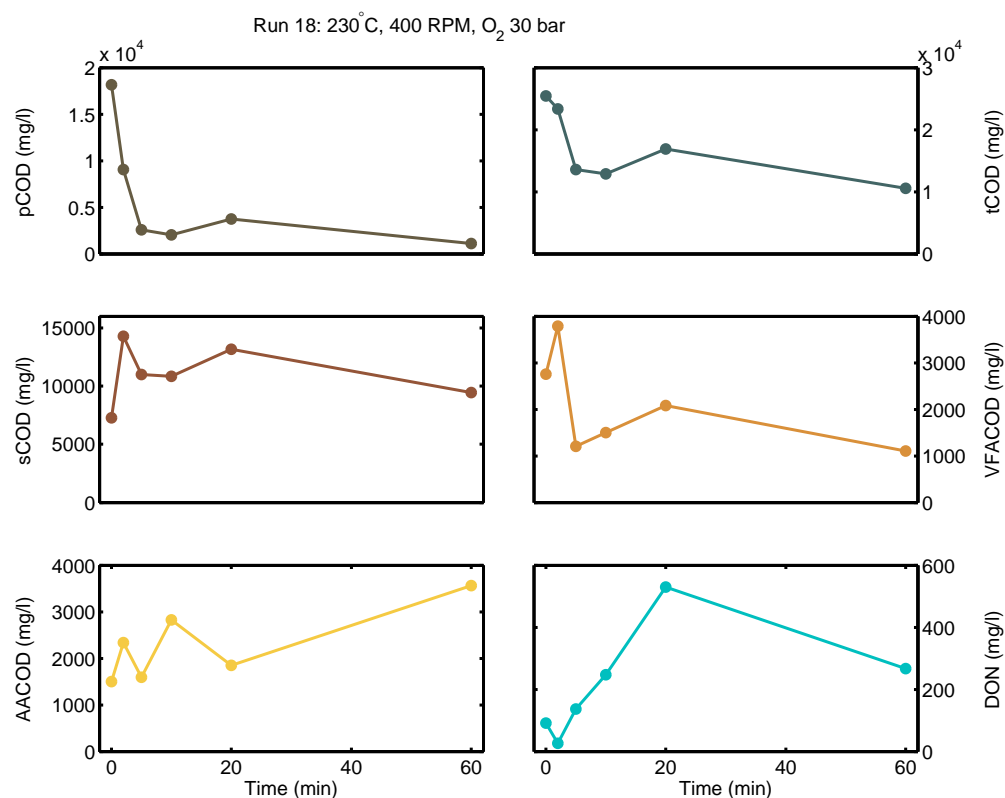


Figure B.18: Experimental results for the compounds of interest from the Set 1 experiments for Run 18.

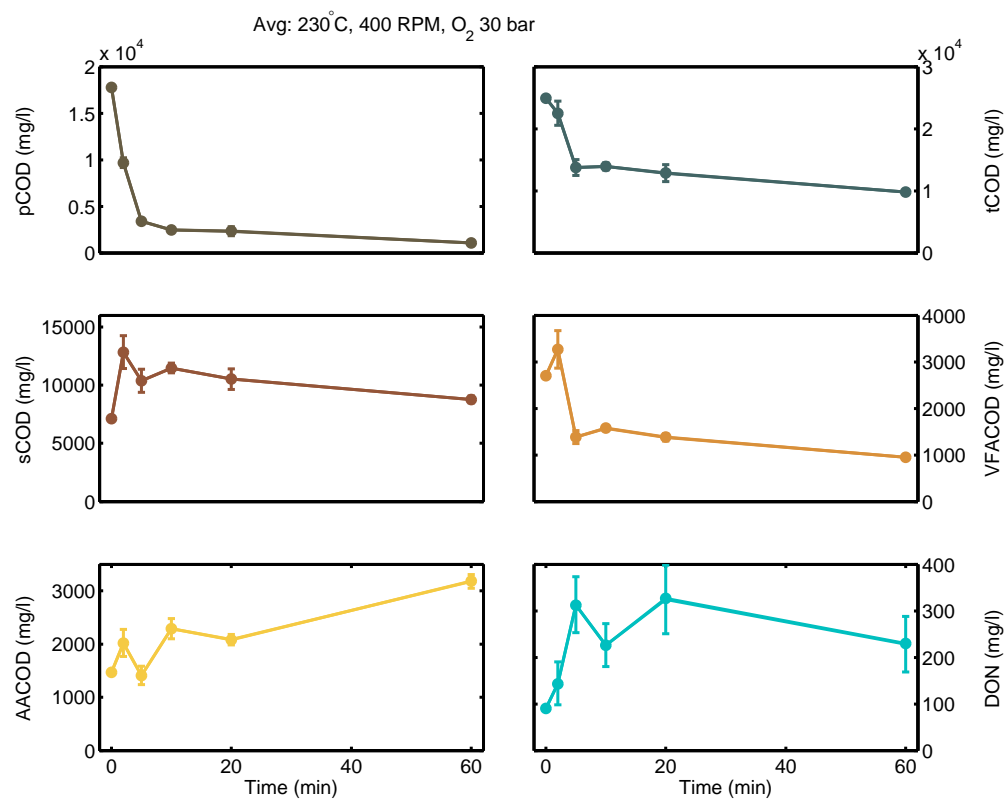


Figure B.19: Experimental results for the compounds of interest from the average of experiment Runs 15 to 18.

# Appendix C

## Model Results

This section presents the comparison of the experimental results with the simulated results produced by the extended kinetic model.

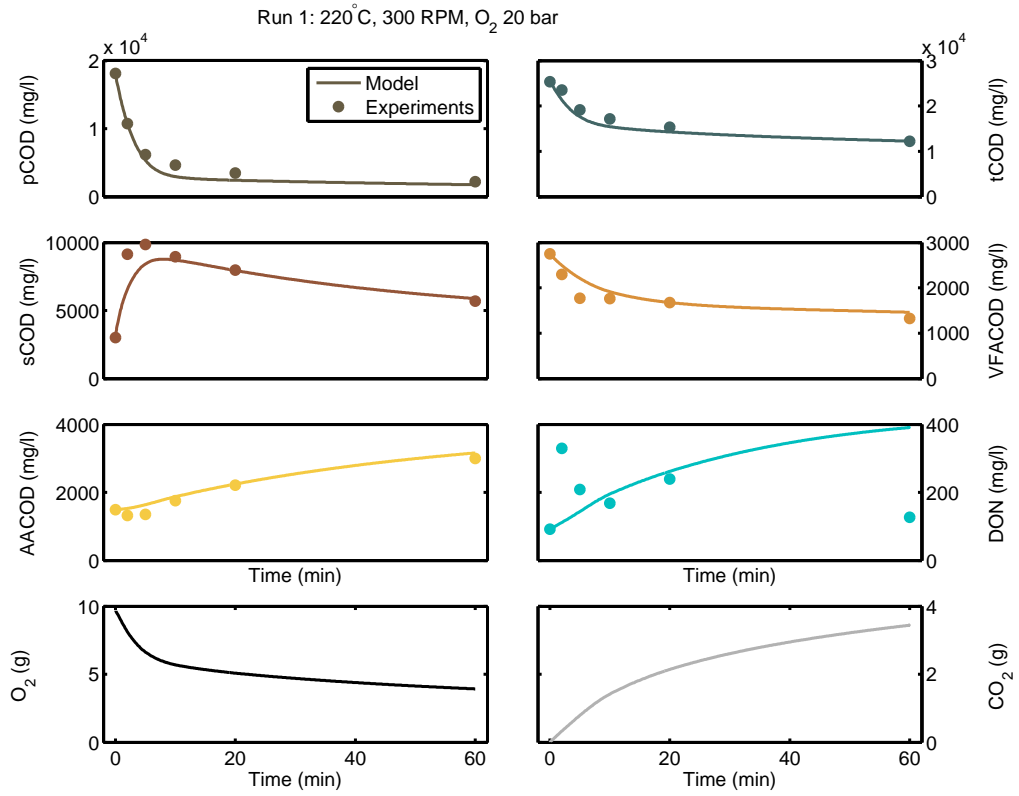


Figure C.1: The extended kinetic model results compared with the experimental results for Run 1.

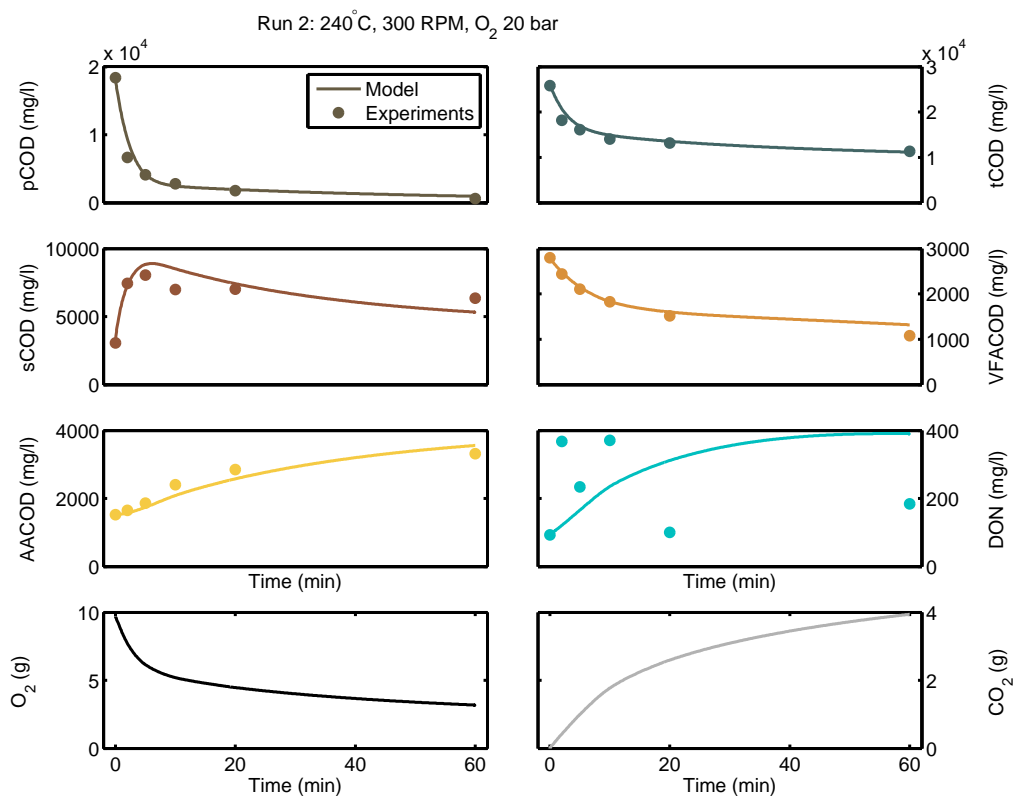


Figure C.2: The extended kinetic model results compared with the experimental results for Run 2.

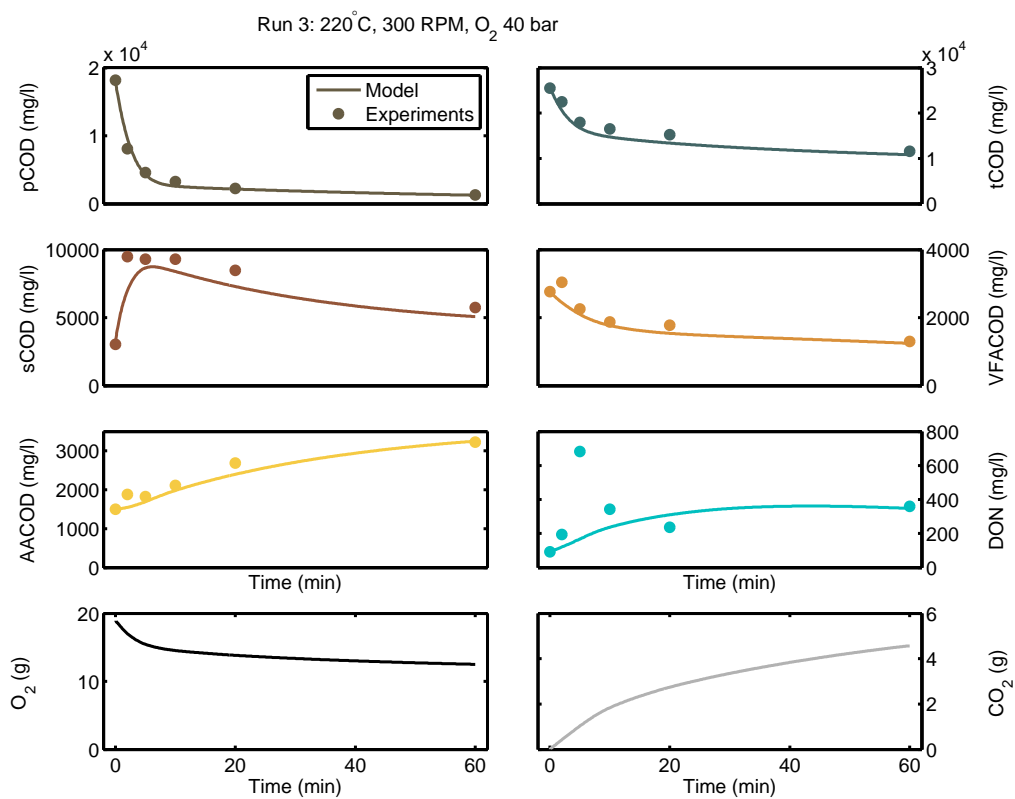


Figure C.3: The extended kinetic model results compared with the experimental results for Run 3.



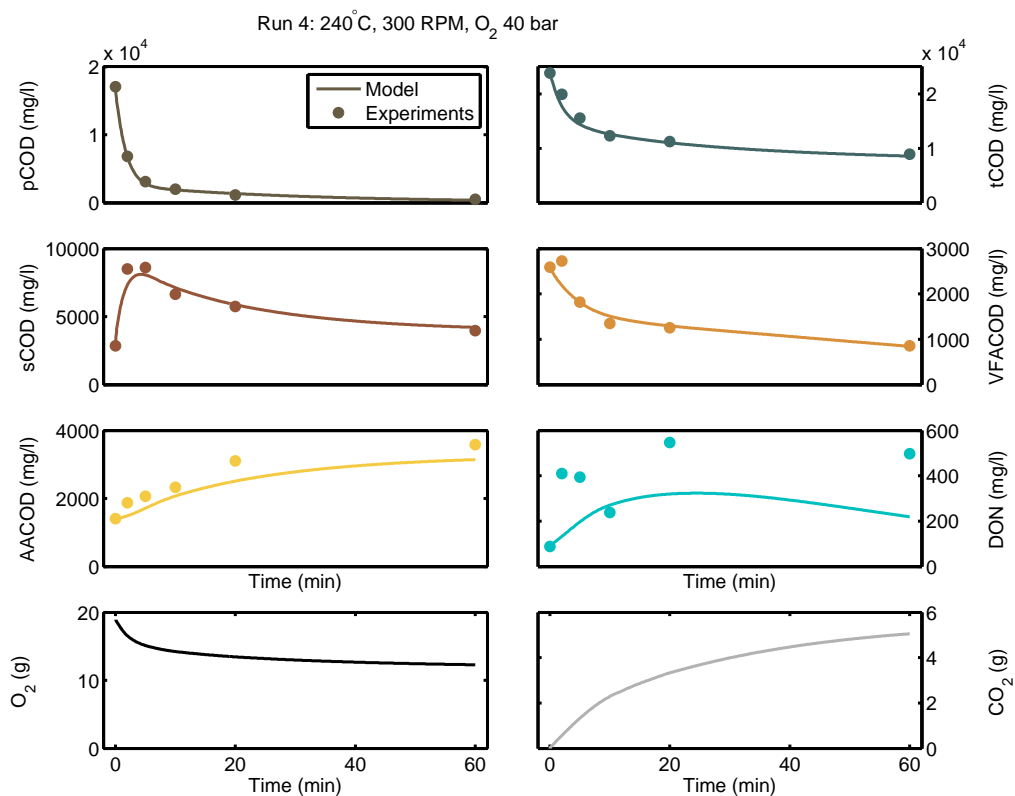


Figure C.4: The extended kinetic model results compared with the experimental results for Run 4.

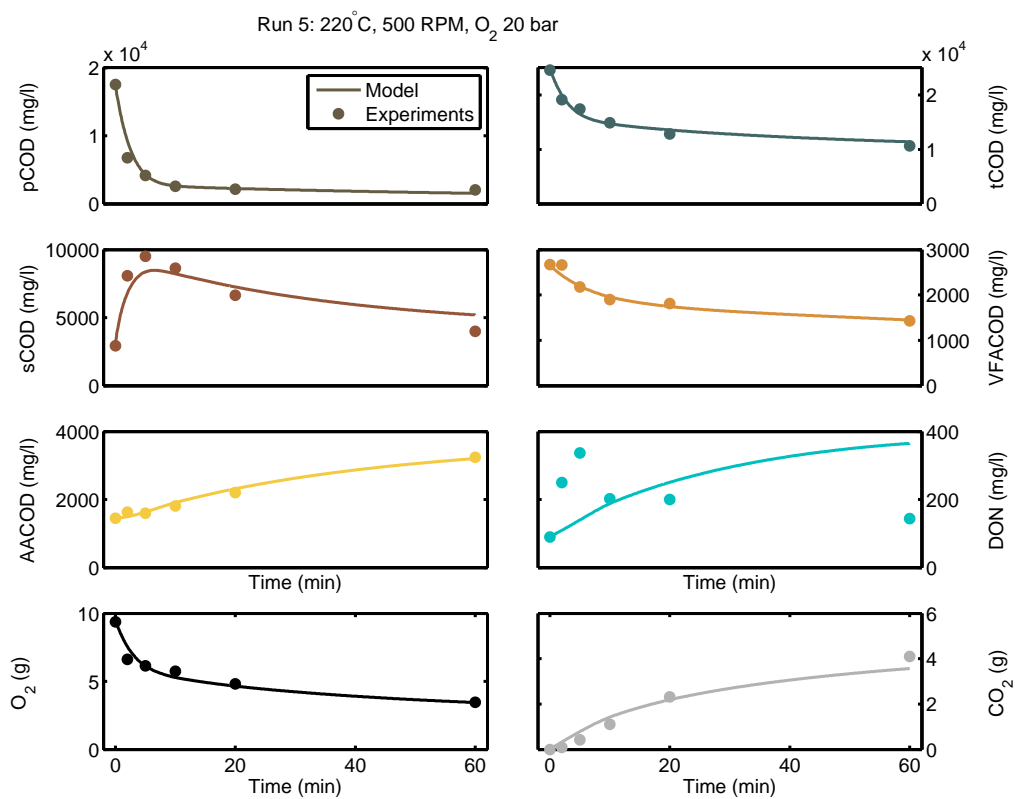


Figure C.5: The extended kinetic model results compared with the experimental results for Run 5.

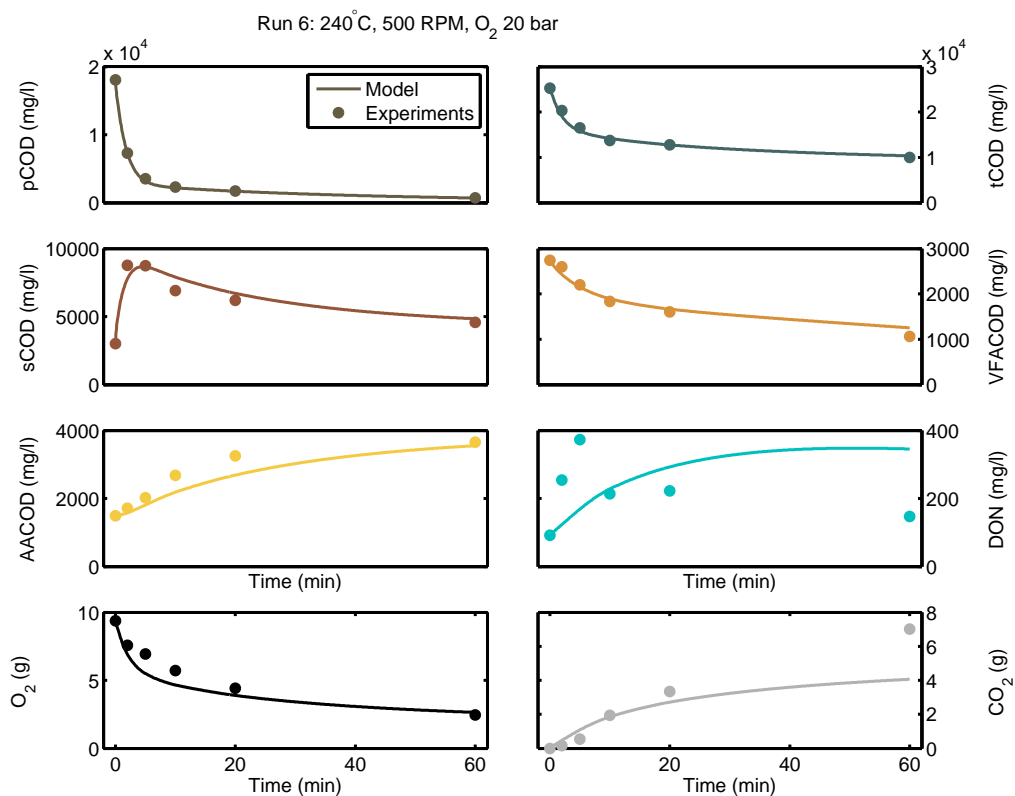


Figure C.6: The extended kinetic model results compared with the experimental results for Run 6.

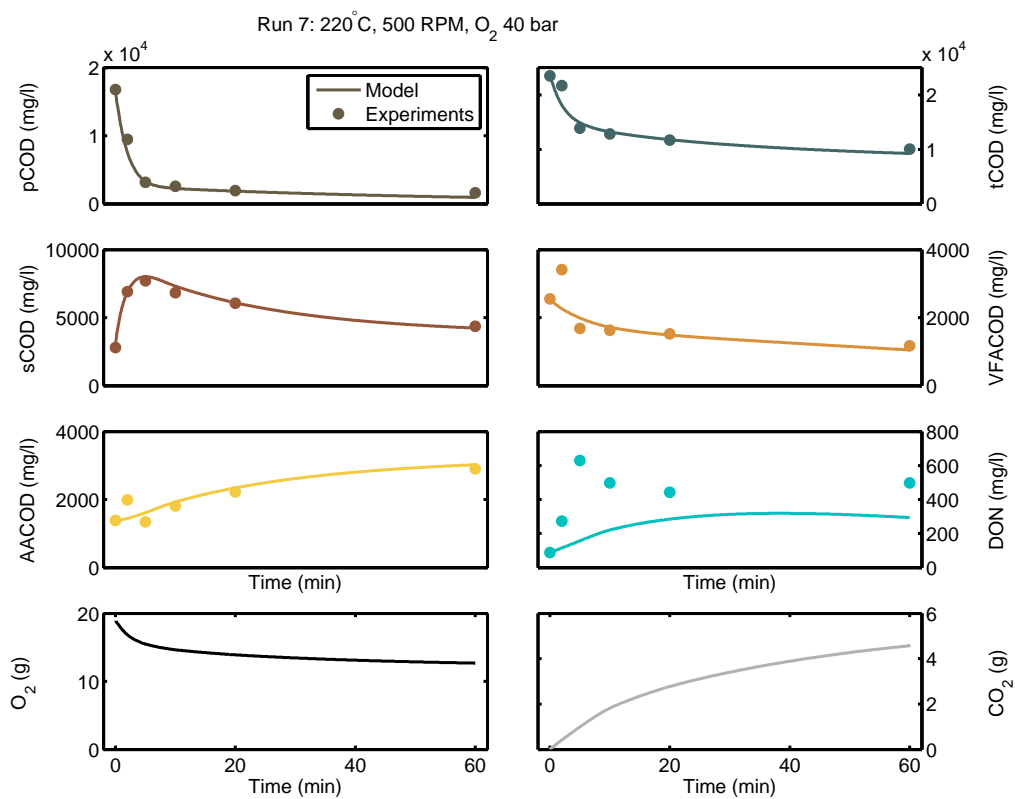


Figure C.7: The extended kinetic model results compared with the experimental results for Run 7.

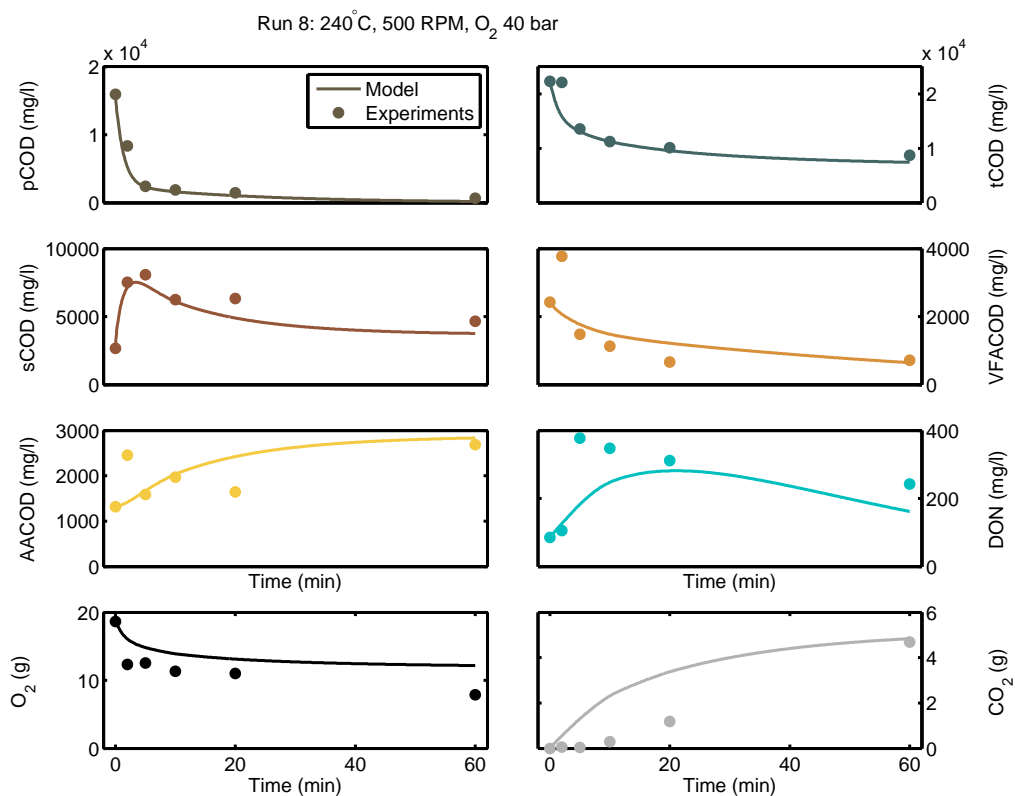


Figure C.8: The extended kinetic model results compared with the experimental results for Run 8.

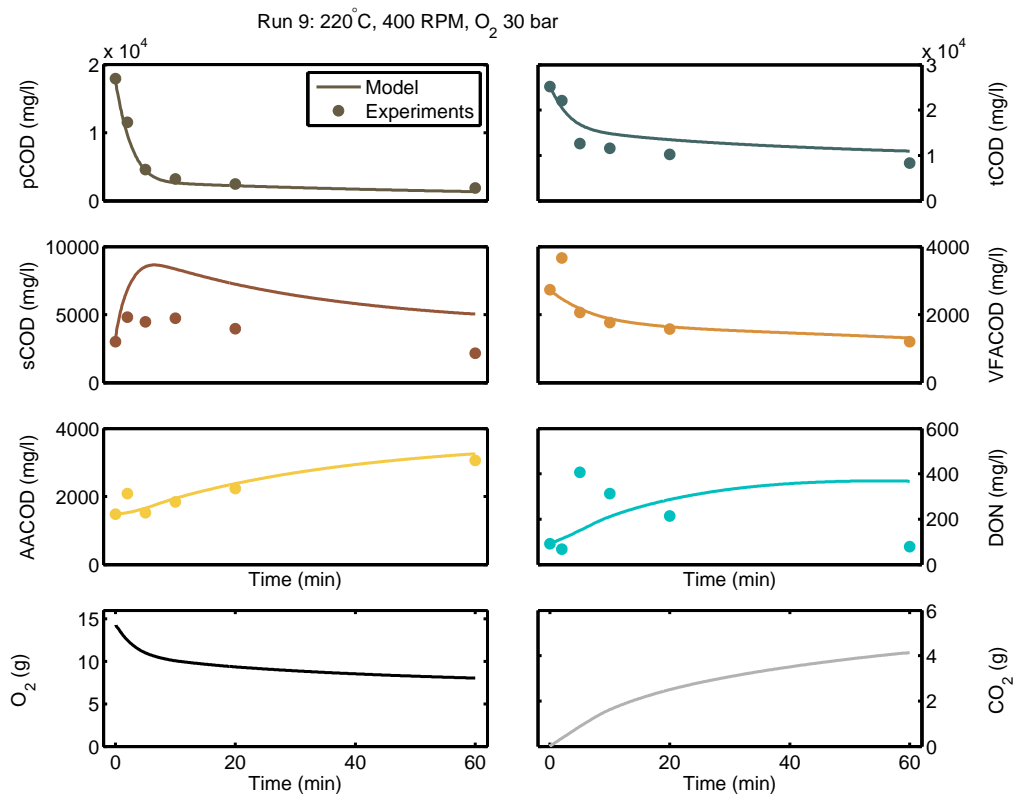


Figure C.9: The extended kinetic model results compared with the experimental results for Run 9.

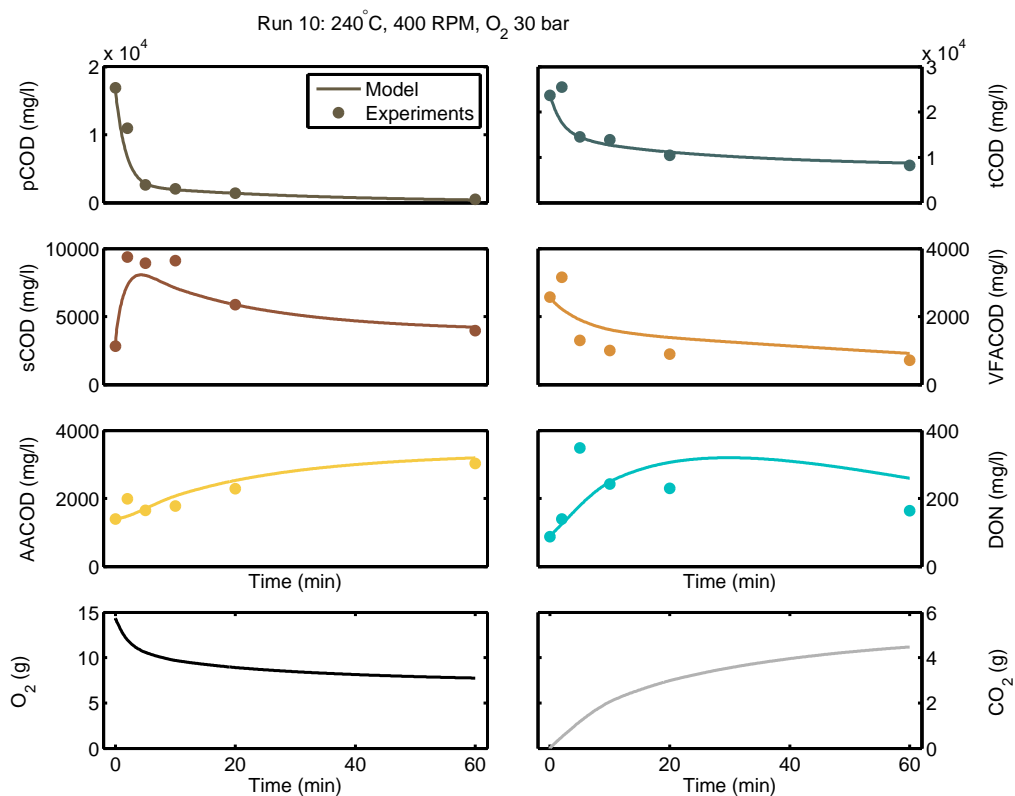


Figure C.10: The extended kinetic model results compared with the experimental results for Run 10.

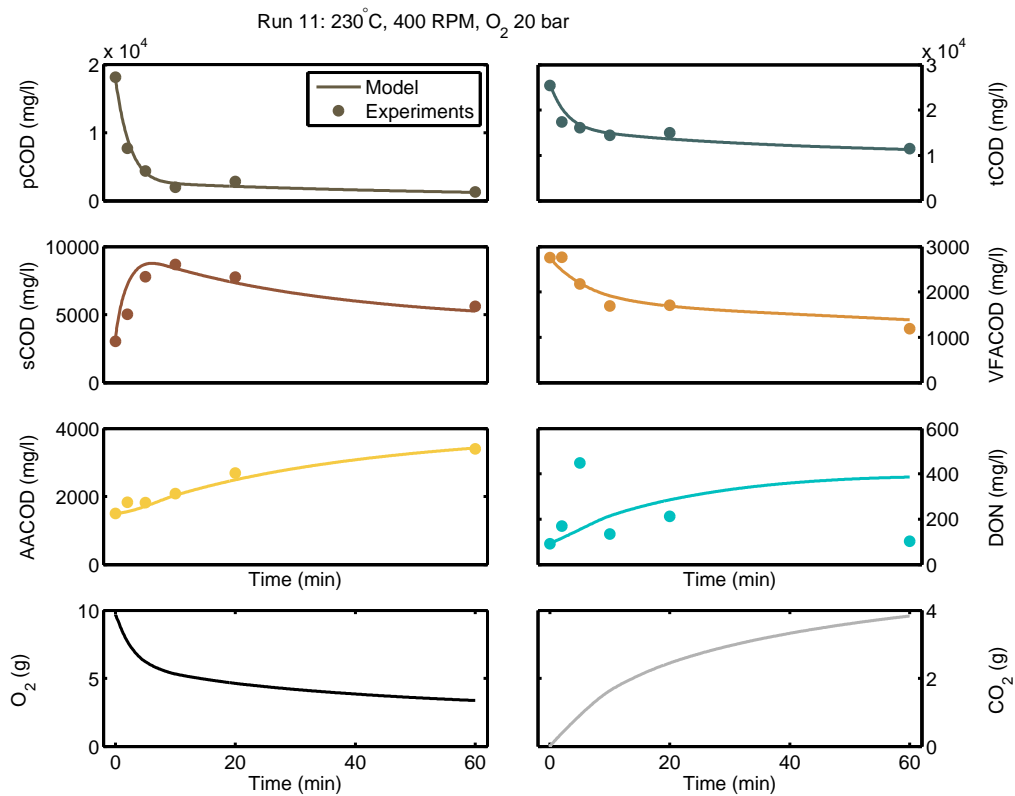


Figure C.11: The extended kinetic model results compared with the experimental results for Run 11.

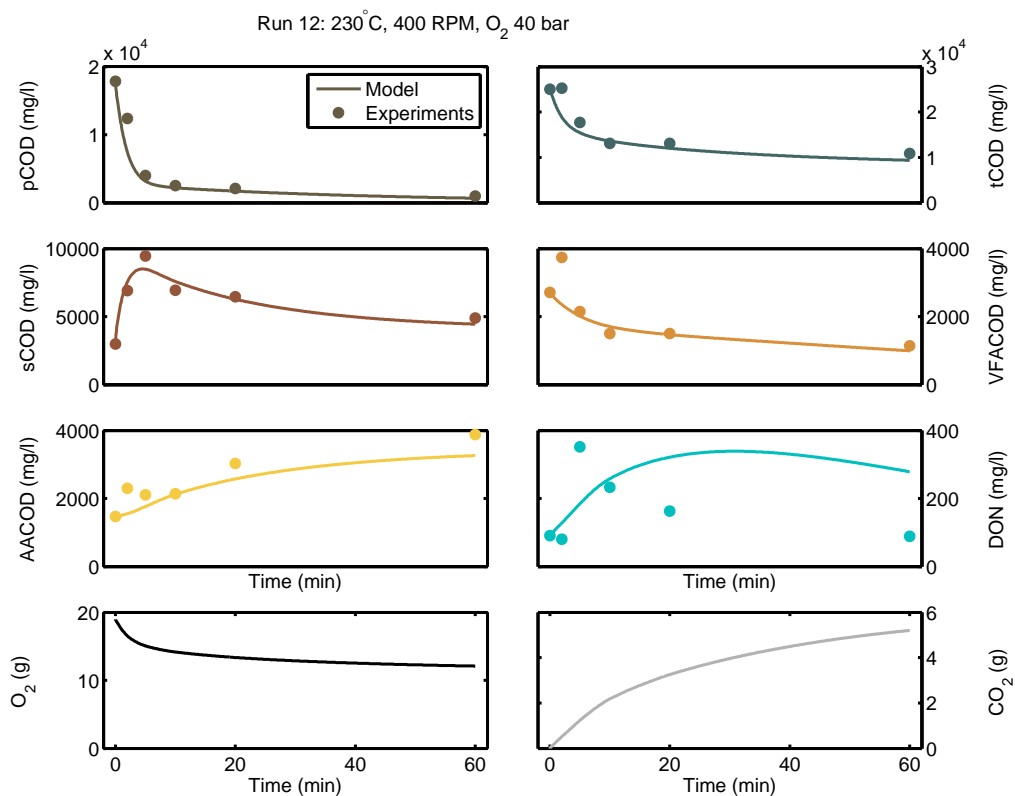


Figure C.12: The extended kinetic model results compared with the experimental results for Run 12.

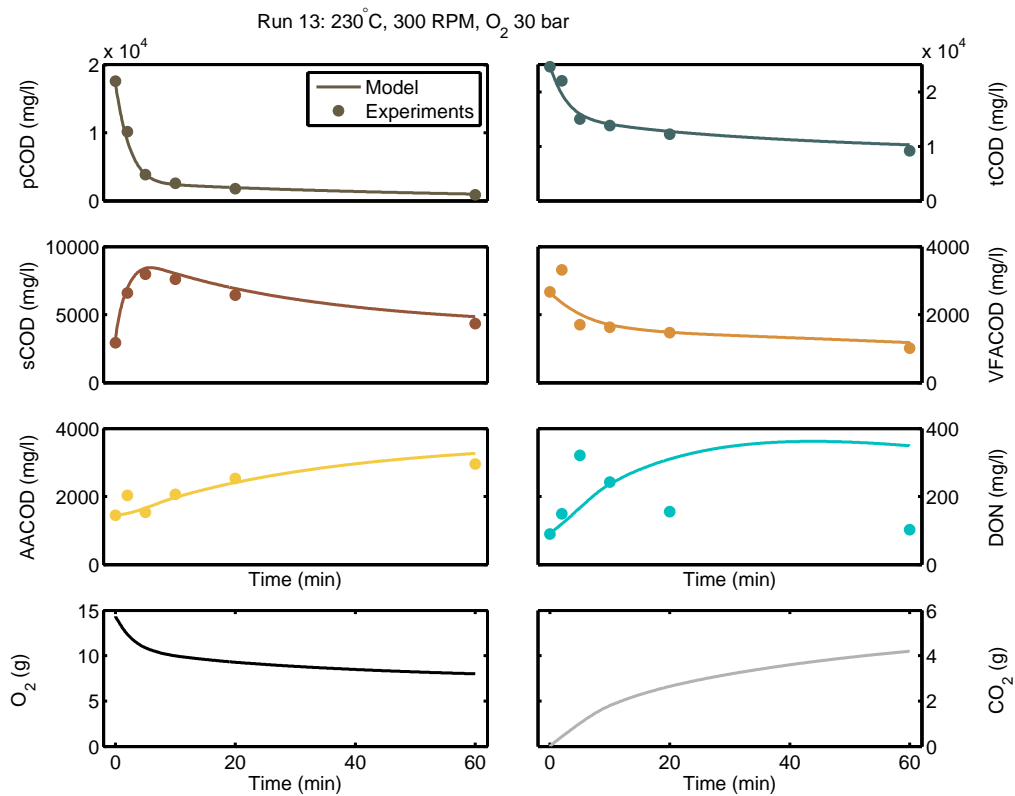


Figure C.13: The extended kinetic model results compared with the experimental results for Run 13.

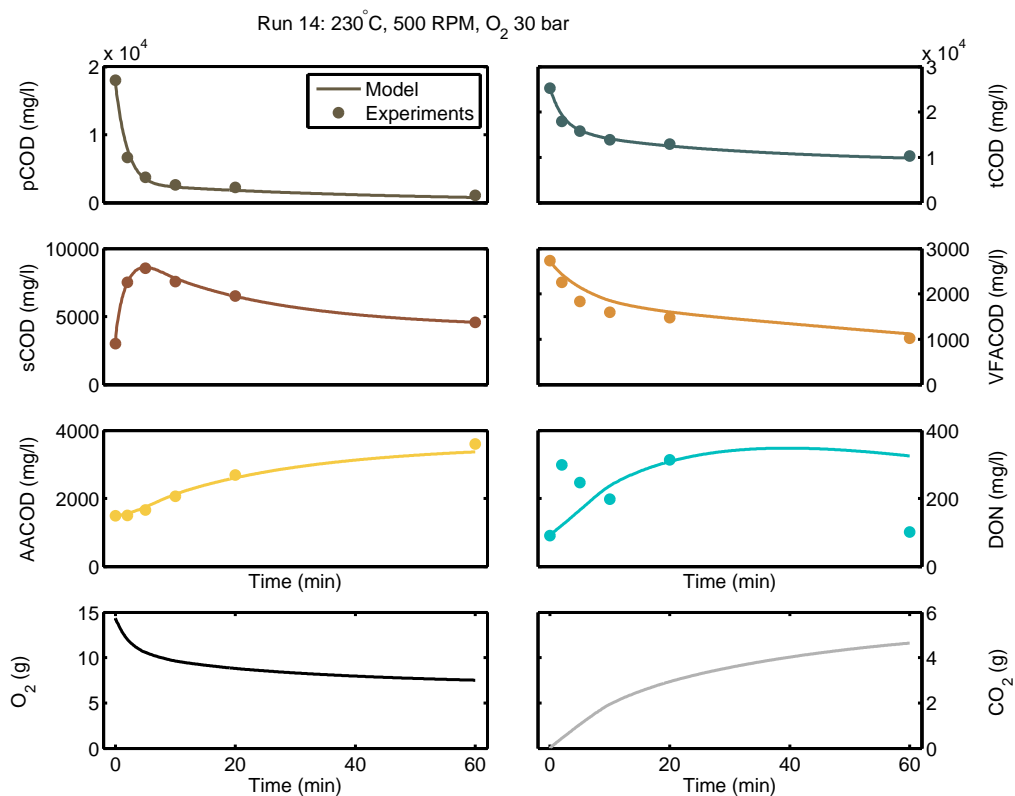


Figure C.14: The extended kinetic model results compared with the experimental results for Run 14.

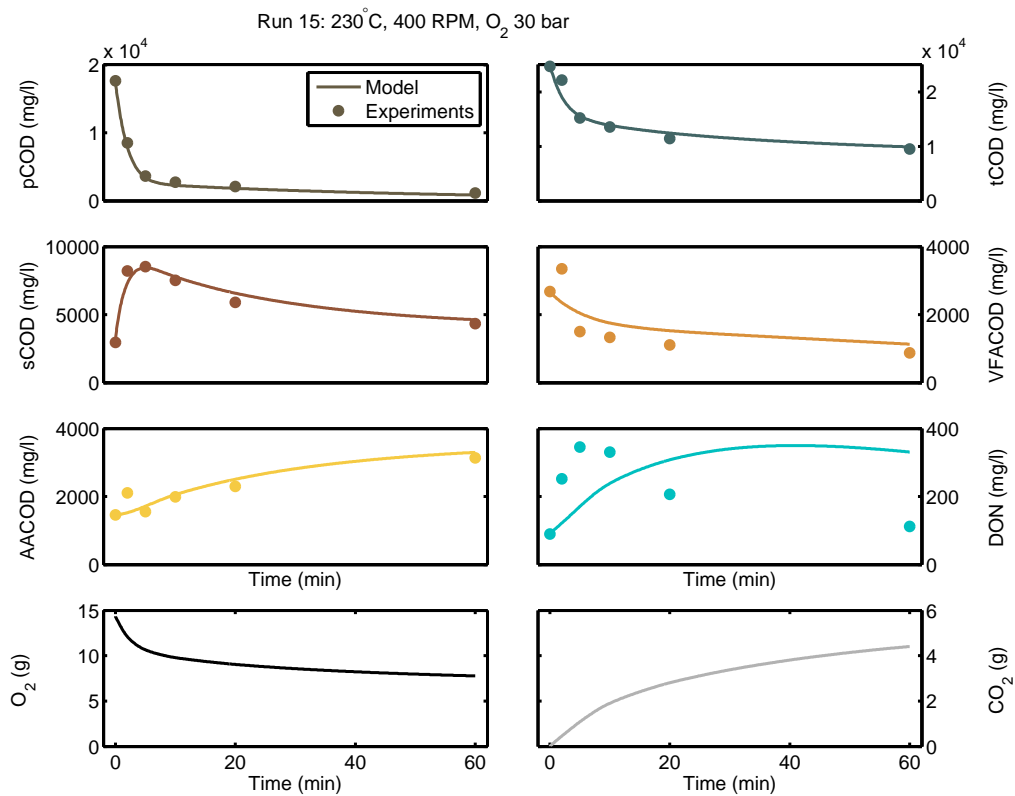


Figure C.15: The extended kinetic model results compared with the experimental results for Run 15.

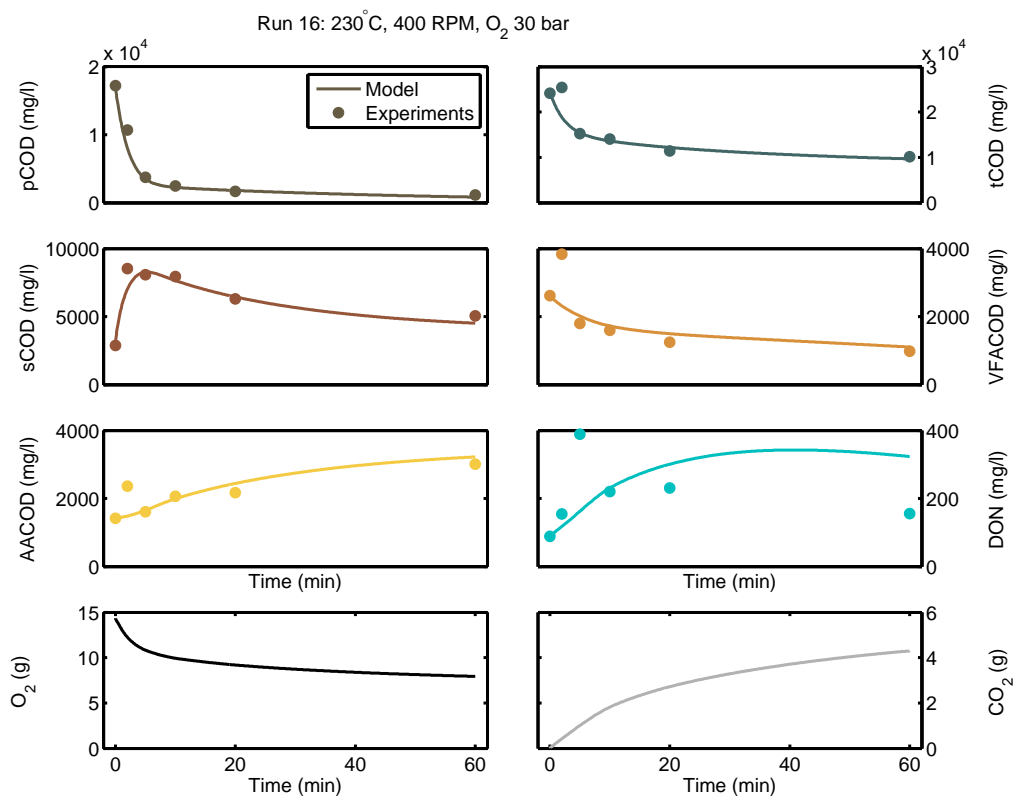


Figure C.16: The extended kinetic model results compared with the experimental results for Run 16.

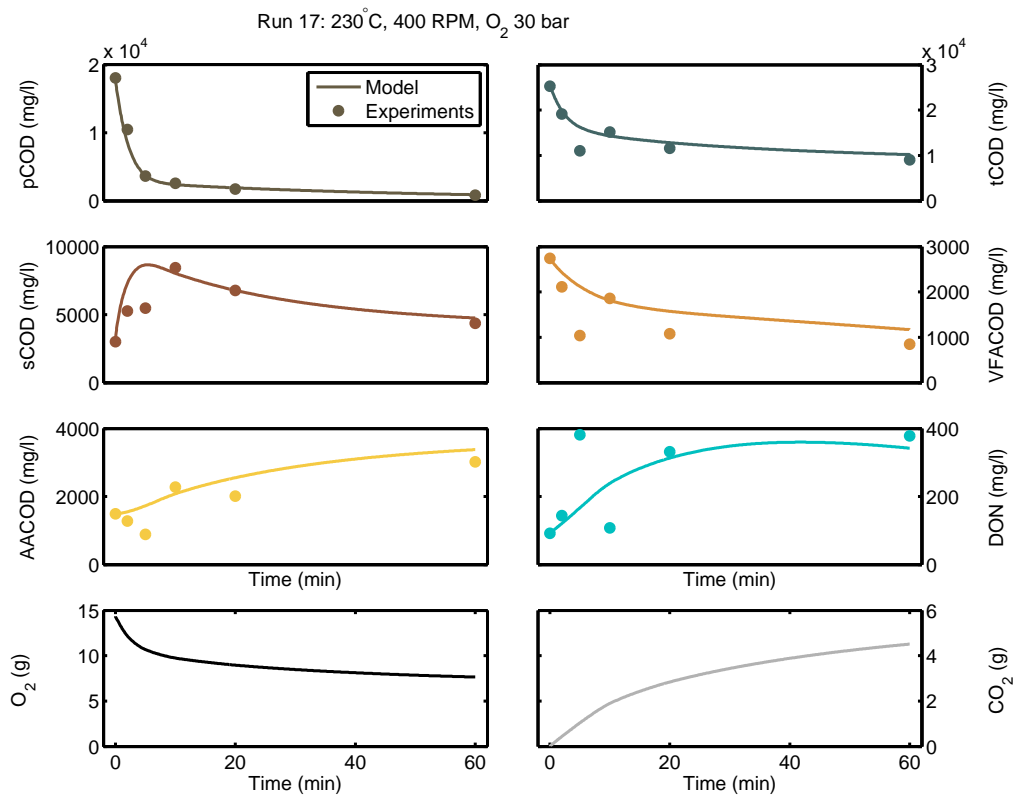


Figure C.17: The extended kinetic model results compared with the experimental results for Run 17.

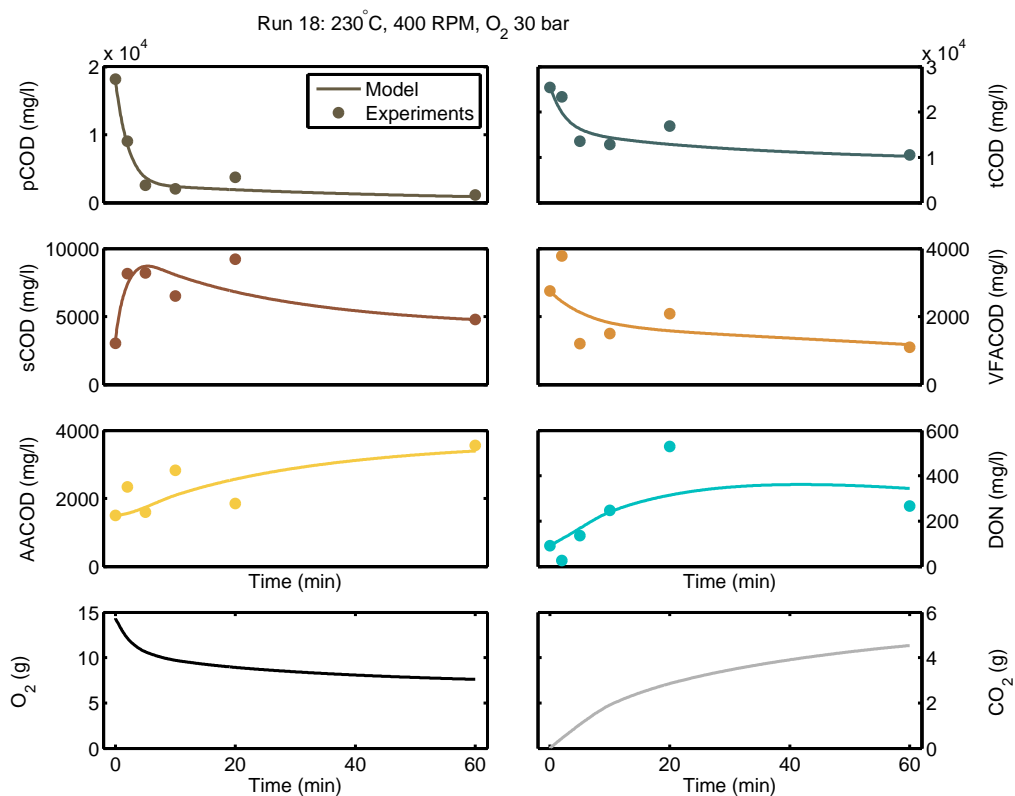


Figure C.18: The extended kinetic model results compared with the experimental results for Run 18.

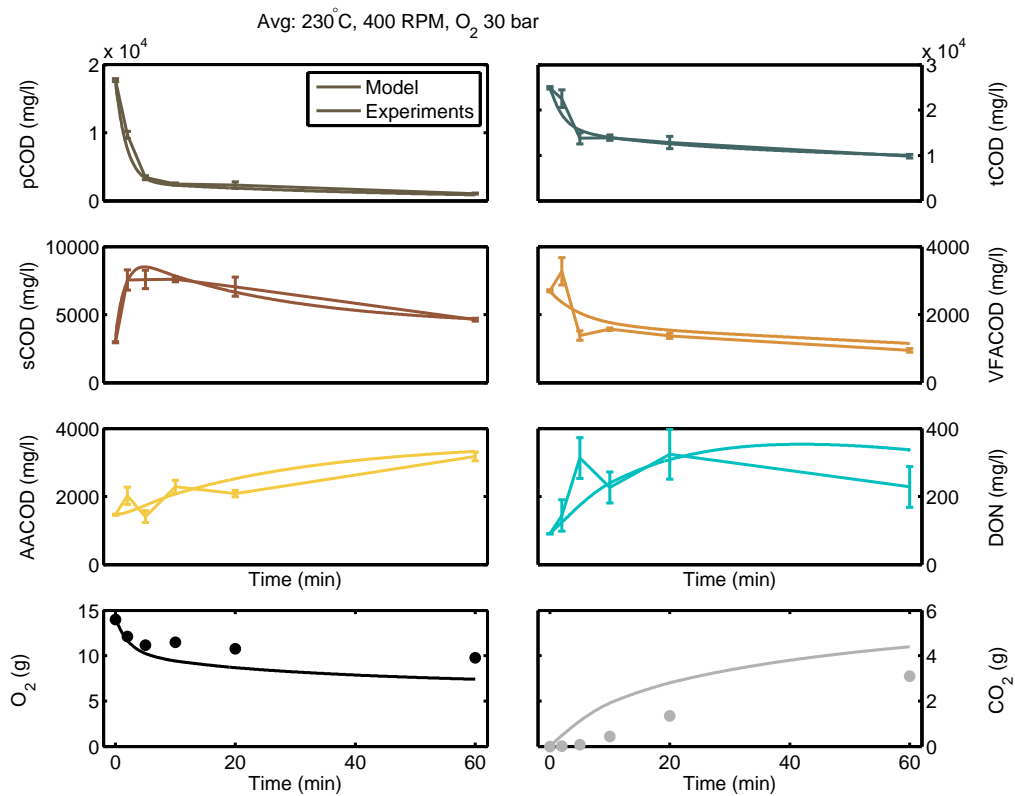


Figure C.19: The extended kinetic model results compared with the average of Runs 15 to 18.